The mitochondrial stress response and its impact on prohibitin-mediated aging phenotypes

Blanca Hernando Rodríguez

The mitochondrial stress response and its impact on prohibitin-mediated aging phenotypes

BY

BLANCA HERNANDO RODRÍGUEZ

Centro Andaluz de Biología del Desarrollo

Universidad Pablo de Olavide

Seville, Spain

September 2018

CERTIFICATE

This is to certify that the thesis entitled “The mitochondrial stress response and its impact on prohibitin-mediated aging phenotypes”, submitted by Blanca Hernando Rodríguez, is her original work carried out under my supervision. This thesis meets the conditions of originality and scientific quality necessary to qualify for the degree of Doctor by the Universidad Pablo de Olavide.

This is also to certify that neither this thesis nor the original work contained therein, has been previously submitted for the award of any degree to this or any other institution.

Dr. Marta Artal Sanz

Index

ABSTRACT

Aging is a natural progression that affects all living organisms from birth, through maturity, to old age. It is characterized by a decline of the physiological integrity and it is accompanied by a higher incidence of age-related diseases, which represent nowadays the most common reason of death. Understanding the aging process has always been of interest. Initially it was thought to be the result of stochastic degradation but, nowadays, it is widely acknowledged that aging is controlled, at least in part, by genetic pathways and biochemical mechanisms. In this work, we focus in mitochondrial dysfunction as one of the most important processes regulating aging. Proper mitochondrial activity is preserved through regulation of mitochondrial dynamics and mitophagy and through proper maintenance of mitochondrial homeostasis. Under proteotoxic conditions the mitochondrial unfolded protein response, UPR^{mt}, is activated to maintain mitochondrial proteostasis by inducing the expression of mitochondrial chaperones and proteases that control protein folding, assembly and degradation.

The mitochondrial prohibitin, PHB, complex is a ring-like structure sitting in the inner mitochondrial membrane. It is composed of two subunits, PHB-1 and PHB-2, that are highly evolutionary conserved. PHBs have been related with many different functions: maintenance of nucleoids organization and stability, protection of newly synthesized mitochondrial proteins, assistance in folding and formation of the respiration super-complexes or acting as scaffold protein. Lack of PHB results in embryonic lethality in *Caenorhabditis elegans*, while homozygous PHB deletion mutants develop into sterile adults due to maternal contribution. In addition, deletion of PHB induces a very strong mitochondrial stress response.

In this work, we show that inducting the UPR^{mt} by PHB deletion does not require the canonical components of the stress response, suggesting an alternative signaling mechanism. We present a sorting strategy capable

of selecting homozygous mutants carrying the UPR^{mt}-GFP stress reporter from GFP-balanced animals at the second larval stage. Because sorting is not completely error-free, we develop an automated high-throughput image analysis protocol that identifies and discards animals carrying the chromosome balancer. This method allows the study of balanced lethal mutations in a high-throughput manner. It can be easily adapted depending on the user's requirements and should serve as a useful resource for the *C. elegans* community for probing new biological aspects of essential nematode genes as well as the generation of more comprehensive genetic networks. In a chromosome-wide RNAi screen for *C. elegans* genes having human orthologues, we uncovered both known and new PHB genetic interactors affecting the UPR^{mt} and growth.

Interestingly, depletion of PHB shows an opposite effect on aging: it shortens lifespan in wild-type worms while it dramatically extends the longevity of the already long-lived insulin/IGF-1 signaling (IIS) pathway mutants. Moreover, the strong mitochondrial stress response elicited upon PHB depletion is remarkably reduced in IIS mutants. We aim at identifying new pathways involved in the regulation of the PHB-mediated mitochondrial stress response, as well as mechanisms responsible for the opposite longevity outcomes of PHB depletion. Towards this aim, we carry out genome-wide RNAi screens in PHB-depleted wild type animals and PHB-depleted IIS mutants.

By performing GO term enrichment analysis, we identify inhibition of protein degradation, disruption of mitochondrial integrity and impairment of ATP synthesis as processes increasing the mitochondrial stress response. Moreover, we report a boost in the mitochondrial stress response as a mechanism to cope with the inhibition of other stress responses, such as nutrient sensing or defense response. Besides, inhibition of processes that

are very energy consuming, such as protein biogenesis or ATP hydrolysis, reduced the mitochondrial stress response.

In particular, we describe two new regulators of the mitochondrial stress response, two transcription factors, C16A3.4 and TLF-1. Furthermore, a new role for chromatin organization emerge in the regulation of the UPR^{mt} and lifespan in an insulin dependent manner. We identify USP-48, a deubiquitinase, as an important factor for the enhanced lifespan of *daf-2* mutants. Additionally, we establish a histone H2A, HIS-65, as a modulator of the mitochondrial stress response and aging in PHB-depleted *daf-2* mutants.

In this work thus, we pinpoint new players involved in the regulation of the mitochondrial stress response. These results will unveil the molecular pathways regulating mitochondrial quality control mechanisms and shed some light on the processes contributing to the differential effect in aging of PHB depletion in wild type and metabolically compromised animals.

INTRODUCTION

1. *Caenorhabditis elegans*

Caenorhabditis elegans is a tiny and transparent, free-living nematode that was first recognized as a model organism for neurobiology, genetics and molecular biology by Ellsworth Dougherty in 1948 (Dougherty and Calhoun 1948). Later, in 1963 Sydney Brenner consolidated the idea of using nematodes as model organisms, expanding their features to new research areas like development. Finally, in 1974, Brenner presented his breakthroughs with the nematode and reported hundreds of mutants (long, rolling, dumpy, uncoordinated and others) (Brenner 1974). Since then, *C. elegans* has become a model system widely used in diverse fields of research.

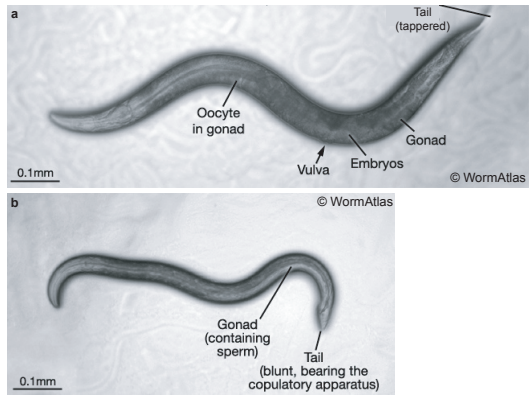

Figure 1. Anatomy of *Caenorhabditis elegans*. Differential interference contrast (DIC) images of an adult hermaphrodite (**a**) and an adult male (**b**), left lateral side. Scale bar 0.1 mm. Adapted from WormAtlas.

Adult nematodes measure about 1 mm and are transparent, which allows easy visualization and differentiation of individual cells and subcellular compartments under a stereoscope (figure 1). Moreover, being transparent enables *in vivo* studies using fluorescent protein reporters. Martin Chalfie won a Nobel Prize in Chemistry in 2008, together with Osamu Shimomura and Roger Y. Tsien, for his work with the green fluorescent protein (GFP)

in *C. elegans*. Another advantage of the nematode is its easiness to be cultivated in agar plates seeded with bacteria as food source and the possibility to be long term cryopreserved and revived when needed.

The nematode exits in two sexes, self-fertilizing hermaphrodites and males (figure 1), and has an invariable number of somatic cells, 959 in hermaphrodites and 1031 in males (Sulston and Horvitz 1977, Sulston, Schierenberg et al. 1983). Despite its morphological simplicity, *C. elegans* has fully defined systems: cuticle, hypodermis, excretory system, neurons, muscles, pharynx, intestine and, in adult stage, gonads. Strikingly, the nervous system is the most complex tissue with 302 neurons and 56 glial cells (which correspond to 32% of the somatic cells in hermaphrodites) and 118 morphologically distinct neuron classes. Both sexes are diploid for the five autosomes (I-V) and the number of X chromosome determines the sex; while hermaphrodites have two, males have a single X chromosome. Males represent only 0.1-0.2% of the population, however under adverse conditions this frequency greatly increases. Mating with males boosts the genetic variability and in laboratories allows to cross mutant strains and to map alleles.

In addition of being self-fertilizing hermaphrodites, another quality of *C. elegans* that facilitates its use in research is its short life cycle, which is less than 3 days (about 65 hours) from egg to gravid adult, at 20ºC. Under favorable conditions, after egg hatching, animals develop through 4 larval stages (L1-L4) in which different organs and structures acquire their final morphology (Byerly, Cassada et al. 1976). Adult hermaphrodites can lay about 300 eggs in a period of 2 to 3 days. Curiously, if a L2 larva encounters stressful conditions it will enter an alternative developmental stage called dauer that can resume development and develop into L4 when the animal experiences favorable conditions (figure 2).

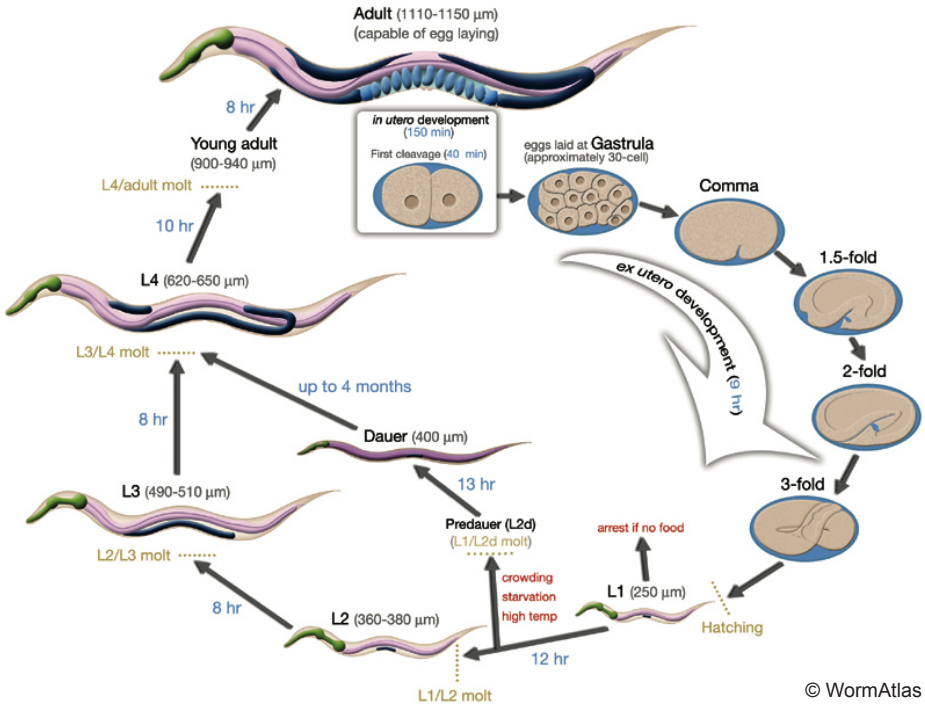

Figure 2. Life cycle of *C. elegans* at 22ºC. The time the animal spends at a certain stage is shown in blue. 0 min is fertilization (not shown). Eggs are laid outside at about 150 min post fertilization during gastrula. The red and yellow dashed lines indicate the larval molt and hatching time respectively. Adapted from WormAtlas.

An important feature of *C. elegans* is that it was the first multicellular organism to have its genome completely sequenced, favoring efficient forward and reverse genetics. Approximately 60–80% of human genes have an orthologue in the *C. elegans* genome (Kaletta and Hengartner 2006), and 40% of genes known to be associated with human diseases have clear orthologues in the *C. elegans* genome (Culetto and Sattelle 2000), making this model organism very powerful for the study of human health.

Furthermore, different techniques for genetic modifications have been developed in *C. elegans*. In particular RNA interference (RNAi) is a potent, specific, rapid and simple method for depleting genetic expression. It allows to describe loss of function phenotypes of genes as well as to examine

genetic interactions in the organism, as RNA can spread from one tissue to another (Tijsterman, May et al. 2004, Conte, MacNeil et al. 2015). In 2006, Andrew Fire and Craig C. Mello received the Nobel prize in physiology or medicine for establishing the RNAi technique in *C. elegans* (Fire, Xu et al. 1998). RNAi can be induced by delivering double stranded RNA (dsRNA) by microinjection, by soaking or by feeding worms with *E. coli* that expresses the dsRNA (Tabara, Grishok et al. 1998, Timmons, Court et al. 2001). RNAi can also be induced by *in vivo* transcription of dsRNA from hairpin or co-injected sense and antisense transgenes (promoter-driven RNAi) (Tavernarakis, Wang et al. 2000).

The microinjection protocol, in which *in vitro* preparations of dsRNA are injected directly into the gonad, provides very reliable gene inhibition, although it is more labor intensive than other methods. In the soaking protocol the dsRNA is passively distributed into the worm, which is very useful for treating a large number of animals at any developmental stage. In the feeding protocols, dsRNA is transcribed in *E. coli* and ingested by animals. This is the method that has been used throughout this work. Similar to soaking, with the feeding technique worms of any stage can be subjected to RNAi and is the least labor intensive and most inexpensive method. It is very suitable for high throughput screenings, using the so-called “feeding RNAi libraries”. Julie Ahringer first generated a library covering most of the genome of *C. elegans* and opened the opportunity to perform high-throughput reverse genetic studies on a model organism and provided the first systematic functional analysis performed in *C. elegans* (Kamath, Fraser et al. 2003).

Multiple genome-wide loss of function screens have been performed to identify genetic interactions, based on different phenotypes such as fluorescent protein reporters expression, dyes, stress resistance, embryo

survival or even lifespan. The feeding protocol is under continuous improvement for high-content screenings, in solid or liquid culture, in 96-wells or 384-wells plates format (Nollen, Garcia et al. 2004, van Haaften, Vastenhouw et al. 2004, Lehner, Crombie et al. 2006). Even protocols using combinatorial RNAi have been designed for genetic interactions studies, either by combining two bacteria population (Lehner, Tischler et al. 2006) or using a bacterial strain expressing dsRNA for two genes (Min, Kang et al. 2010). In these cases, the use of RNAi-hypersensitive strains is recommended.

Last but not least, the community of *C. elegans* researchers has a very open attitude to share information, techniques, supplies, etc. This has been central to the success of *C. elegans* research. Reviews on many topics of *C. elegans* biology are provided as Open Access in WormBook (www.wormbook.org), WormAtlas (www.wormatlas.org) and Wormbase (www.wormbase.org).

Since 1970, *C. elegans* has been used as a model organism for studying aging (Gershon 1970). In 1977, Klass established a method to consistently measure lifespan in *C. elegans* (Klass 1977) and in 1983 he identified eight mutants with altered lifespan (Klass 1983) mapping five of them to the same locus, named *age*-1 (Friedman and Johnson 1988). Later, another gene was identified as modulator of aging, the insulin receptor *daf-2* (Kenyon, Chang et al. 1993). Since then, countless works have been published studying aging and its regulation in the nematode due to its relatively short (mean lifespan about 16 days at 20ºC) and invariant lifespan, apart from all the previously mentioned advantages. More than 200 genes and regimens have been identified and revealed evolutionarily conserved pathways that modulate lifespan (Tissenbaum 2015).

2. Aging

Aging is characterized by a progressive decline of the physiological integrity accompanied by impairment of certain functions of the organism and increased vulnerability to environmental stresses. This deterioration is accompanied by a higher incidence of pathologies known as age-related diseases, such as cancer, diabetes, autoimmune syndromes, cardiovascular disorders and neurodegenerative diseases.

Since aging affects all living organisms, the understanding of the aging process has always aroused curiosity. At the beginning, it was thought that aging was the result of stochastic degradation due to natural entropy on cells, tissues and organs (DiLoreto and Murphy 2015). Importantly, in 1983 Michael R. Klass isolated the first long-lived strain in *C. elegans* (Klass 1983) and opened up a wide range of new possibilities and hopes for the aging research. Nowadays, it is widely acknowledged that aging is a process characterized by loss of homeostasis due to the accumulation of damage in macromolecules. Importantly, the rate of aging is controlled, at least in part, by genetic pathways and biochemical mechanisms. The genes regulating aging are often involved in major signaling pathways that link the rate of aging with environmental inputs. The emerging picture shows a signaling network that is sensitive to nutritional status and controls growth, stress resistance and aging. The majority of the processes modulating aging have been discovered in short-lived model organisms such as yeast, worms and flies. Nevertheless, the same pathways are observed in mammals, suggesting a strong conservation across evolution of the mechanisms governing the process of aging.

Among the most important processes regulating aging we find: genomic instability, telomere attrition, epigenetic alteration, loss of proteostasis,

deregulation of nutrient sensing and mitochondrial dysfunction (Gems and Partridge 2013, Lopez-Otin, Blasco et al. 2013, Uno and Nishida 2016) (figure 3).

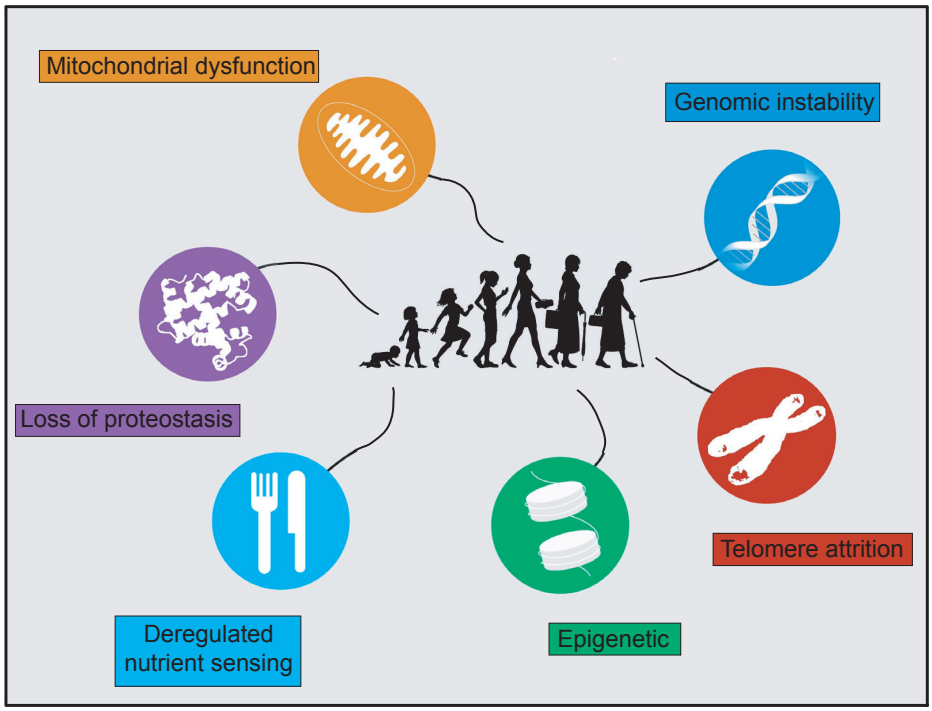

Figure 3. Hallmarks of aging. Scheme of the 6 hallmarks of aging listed in the text: genomic instability, telomere attrition, epigenetic modifications, deregulated nutrient sensing, loss of proteostasis and mitochondrial dysfunction. Adapted from (Lopez-Otin, Blasco et al. 2013).

Genomic instability:

Physical, chemical and biological agents from the environment are continuously challenging the integrity of DNA, causing an accumulation of genetic damage characteristic of aged organisms. In addition, endogenous threats, such as DNA replication errors, spontaneous hydrolytic reactions and reactive oxygen species (ROS) are also menacing genetic stability. During evolution, organisms have developed diverse DNA repair mechanisms in order to minimize and resolve all possible damages inflicted to DNA (Lord and Ashworth 2012).

Telomere attrition:

In addition to the general genomic instability, the regions at the end of each chromosome, telomeres, are particularly susceptible to age-related deterioration (Bernardes de Jesus and Blasco 2012). DNA polymerases do not have the capacity to replicate the ends of linear DNA molecules, which results in the progressive and cumulative loss of chromosomal ends. Progressive shortening of telomeres leads to senescence, apoptosis and affects the pace of aging (Shammas 2011).

Epigenetic mechanisms:

Epigenetic mechanisms, such as DNA methylation, histone post-translational modifications and chromatin remodeling, regulate the interpretation of genetic information and are linked to numerous biological processes. Aging is accompanied by epigenetic changes and perturbations, however, the significance of epigenetics in regulating the rate of aging is not well understood (Pal and Tyler 2016). Nevertheless, an epigenetic trend in aging cells from yeast to humans is the general loss of histones (Sen, Shah et al. 2016). In yeast, overexpression of histones extends lifespan (Feser, Truong et al. 2010). Changes in histones modification affect the rate of aging as well. Histone acetylation levels increase with age and supplementation of spermidine, that generate hypoacetylated chromatin state, enhances lifespan from yeast to human (Eisenberg, Knauer et al. 2009). In addition, histone methylation levels regulates aging (Han and Brunet 2012) (Jin, Li et al. 2011, Maures, Greer et al. 2011). Gain of activating marks (H3K4me3) and loss of repressive marks (H3K27me3) are progressively being considered as hallmarks of aging in worms, while in flies it seems to be the contrary. However, studies in flies suggest a more focused mechanism, modulating expression of genes related with stress

resistance and caloric restriction pathways (Sen, Shah et al. 2016). Last, the relation between histone ubiquitination and sumoylation with aging is less clear due to the big number of targeted substrates.

Loss of proteostasis:

Loss of proteostasis, protein homeostasis, results in the deterioration of cellular functions and is often involved in protein aggregation, a cellular process associated with many age-related disorders (Koga, Kaushik et al. 2011). Proteostasis is maintained by a complex interplay among protein synthesis, folding, degradation and quality controls.

Inhibiting protein translation (Hansen, Taubert et al. 2007), as well as increasing protein degradation via the ubiquitin-proteasome system (UPS) (Li, Gao et al. 2007, Kruegel, Robison et al. 2011), have been shown to increase lifespan. Protein degradation via autophagy plays also an important role in lifespan regulation as it has been shown to be necessary for many long-lived mutants (Melendez, Talloczy et al. 2003, Hansen, Chandra et al. 2008).

Proteostasis relays also in protein quality control systems such as the heat-shock response (HSR), the unfolded protein response (UPR) of the endoplasmic reticulum (ER) (UPR^{ER}) and the mitochondrial UPR (UPR^{mt}) (Labbadia and Morimoto 2014). In particular, the HSR and the UPR^{ER} have been shown to decline with age in different model systems (Blake, Udelsman et al. 1991, Taylor and Dillin 2013) supporting the transcriptional dysregulation of stress responses in adulthood as a conserved event in metazoans.

Deregulated nutrient sensing:

Cells sense their energy status and the availability of nutrients, and communicate with other cells to coordinately regulate whole body metabolic homeostasis. Metabolic homeostasis declines throughout life and is an important determinant of aging, as a number of interventions affecting metabolic pathways also affect the rate of aging.

Since 1935, when McCay first published that restricting food intake in rats dramatically increased lifespan (McCay, Crowell et al. 1989), dietary restriction (DR) has been considered as a "true mechanism of lifespan extension" as it extends lifespan in a wide range of species, from invertebrates to vertebrates (Mair and Dillin 2008). In 1983, Klass reported a method for isolating longevity mutants in *C. elegans* and described five mutants in which the increased longevity was most likely due to reduced caloric intake (Klass 1983). Later these mutants were identified as mutants of the Insulin/IGF-1 signaling (IIS) pathway, *age*-1 mutants (Friedman and Johnson 1988). Indeed, the IIS pathway modulates lifespan in a variety of organisms by multiple mechanisms, some of which overlap with those affected under DR conditions (Iser and Wolkow 2007). IIS is a critical coordinator of nutrient availability with energy homeostasis and metabolic processes. It influences many biological processes, such as determining reproductive status and somatic tissue maintenance with age.

In addition to the IIS pathway, three additional pathways are described as interconnected nutrient-sensing systems: the mechanistic target of rapamycin (mTOR), that senses high amino acid concentrations; AMP-activated protein kinase (AMPK), which senses low energy states by detecting high AMP levels; and sirtuins, that detects NAD^+ levels.

The mTOR kinase plays an integral role in regulating growth and metabolism in response to nutrient levels such as growth factors, amino acid or oxygen levels (Laplante and Sabatini 2012, Johnson, Rabinovitch et al. 2013). mTOR acts in two multiprotein complexes, mTOR complex 1 (mTORC1) and mTOR complex 2 (mTORC2), which are differentiated by the type of the accessory protein, Raptor and Rictor respectively (Saxton and Sabatini 2017). mTORC1 regulates cell growth and metabolism inducing synthesis of proteins, lipids and nucleotides and inhibiting autophagy. mTORC2 controls proliferation and survival by phosphorylation of members of AGC family, such as AKT (Sarbassov, Guertin et al. 2005) and SGK1 (Garcia-Martinez and Alessi 2008), key effectors of the IIS pathway. Inhibition of mTOR activity increases longevity and confers protections against many age-related diseases in yeast (Kaeberlein, Powers et al. 2005), in worms (Vellai, Takacs-Vellai et al. 2003, Jia, Chen et al. 2004), in flies (Kapahi, Zid et al. 2004) and even in mice (Lamming, Ye et al. 2012, Wu, Liu et al. 2013). In the same direction, treatment with the mTOR inhibitor rapamycin extends lifespan in all of these model organisms.

AMPK and sirtuins act contrary to IIS and mTOR, meaning that they signal in response to nutrient deficiency instead of nutrient abundance. AMPK restores energy homeostasis by stimulating catabolic processes and blocking energy-consuming processes. Loss of *aak-2*, the gene encoding the *C. elegans* AMPK protein, decreases lifespan, and over-expression of *aak-2* enhances lifespan (Apfeld, O'Connor et al. 2004). Metformin is an indirect AMPK agonist that also extends lifespan in *C. elegans* (Onken and Driscoll 2010) and in mice (Anisimov, Berstein et al. 2011, Mair, Morantte et al. 2011).

Sirtuins, a class of proteins with diverse enzymatic activities, have evolved to respond to the availability of NAD^+ and convert this

information in longevity control. Overexpression of *Sir2* was first shown to extend replicative lifespan in *Saccharomyces cerevisiae* (Kaeberlein et al., 1999), and subsequent reports indicated that enhanced expression of *sir-2.1* in worms and *dSir2* in flies extended lifespan (Rogina and Helfand, 2004; Tissenbaum and Guarente, 2001). Interestingly, sirtuins and AMPK act together for increasing mitochondrial biogenesis and mitochondrial function (Price, Gomes et al. 2012).

Mitochondrial dysfunction:

Mitochondria are essential organelles characterized by their role in energy metabolism like the tricarboxylic acid (TCA) cycle and oxidative phosphorylation (OXPHOS). A decline in mitochondrial quality and activity is associated with normal aging and correlates with development of a wide range of age-related diseases (Lopez-Otin, Blasco et al. 2013). Mitochondrial functions are key for organisms' survival, playing a central role in metabolic homeostasis, however the link between mitochondrial dysfunctions and aging is more complicated than initially thought, since many mitochondrial mutations have been shown to extend lifespan. Many studies demonstrate that a modest impairment in mitochondrial function leads to lifespan increment, in a wide range of organisms (Lee, Lee et al. 2003, Liu, Jiang et al. 2005, Owusu-Ansah, Song et al. 2013). Intriguingly, worms lacking the nuclear-encoded cytochrome C oxidase subunit (CCO-1), in addition of being long-lived, present activation of the mitochondrial unfolded protein response (UPR^{mt}), a nuclear transcriptomic response that increases expression of mitochondrial chaperones (Durieux, Wolff et al. 2011). In the same direction, an imbalance between mitochondrial and nuclear proteins, due to knock-down of mitochondrial ribosomal proteins, increases lifespan and induces the UPR^{mt}. In addition, the stress response is required for the lifespan extension (Houtkooper, Mouchiroud et al. 2013).

Similarly, depletion of the monooxygenase CLK-1, increases lifespan in a stress response-dependent manner, from worms to mice (Wong, Boutis et al. 1995, Liu, Jiang et al. 2005, Monaghan, Barnes et al. 2015). The UPR^{mt} regulates a large set of genes involved in protein folding, ROS defenses, metabolism and innate immune response (Nargund, Fiorese et al. 2015) (see below). Nevertheless, while a number of mitochondrial perturbations induce the UPR^{mt} and increase lifespan, there are also evidences that the mitochondrial stress response may not be sufficient by itself to extend lifespan (Bennett, Vander Wende et al. 2014).

Mitochondria are also a major source of ROS, what have been determined as the primary cause of damage in macromolecules such as DNA, proteins and lipids. The mitochondrial free radical theory of aging states that aging is the result of accumulation of oxidative damage caused by free radicals generated as by-products of normal metabolism, mainly from mitochondria (Balaban, Nemoto et al. 2005). Nevertheless, this theory is in continuous re-evaluation during the last decade due to new insights that suggest a more complex relation between free radicals and aging (Hekimi, Lapointe et al. 2011). Knockout of the mitochondrial superoxide dismutase SOD-2 in *C. elegans* increases oxidative stress and prolongs lifespan (Van Raamsdonk and Hekimi 2009). The very long-lived mole rats, living up to 30 years, while exhibiting higher levels of ROS generation (Labinskyy, Csiszar et al. 2006), they have higher resistance to oxidative damage to proteins (Perez, Buffenstein et al. 2009). The new proposal is that ROS generation, instead of being the initial prompt of the aging process, represents a stress signal in response to age-dependent damage, initiating different molecular mechanisms in order to alleviate damage. However, ROS accumulation reaches a level at which it becomes toxic and starts to contribute to damage (Hekimi, Lapointe et al. 2011).

3. Cellular compartment stress responses

As previously mentioned, proteostasis is ensured by the coordination of protein translation, folding, trafficking and degradation. Misfolded proteins are detected by compartment-specific stress responses that will adjust different pathways to restore the protein load (Taylor, Berendzen et al. 2014). Mainly three stress responses are responsible for cellular homeostasis., the heat shock response, the unfolded protein response of the endoplasmic reticulum and the mitochondrial unfolded protein response.

The cytoplasmic heat shock response (HSR) (figure 4a) is regulated by the heat shock factor (HSF) transcription factor family, which responds to numerous proteotoxic insults (Akerfelt, Morimoto et al. 2010). Under basal conditions, HSF1, the main heat shock transcription factor, is bound to heat shock protein 90 (HSP90) and inactive. Under stress conditions, HSP90 is displaced, the transcription factor trimerizes and binds to heat response elements in the genome to up-regulate gene expression, including many cytosolic chaperones and proteasome subunits in order to improve protein folding, to increase protein trafficking efficiency and to enhance protein degradation.

The unfolded protein response of the endoplasmic reticulum (UPR^{ER}) (figure 4b) is induced when the charge of unfolded proteins inside the ER is imbalanced with its capacity of proteostasis (Ron and Walter 2007). Three signaling pathways are then activated, each one having a 'detector' component: the inositol-requiring protein 1 (IRE1), the activating transcription factor 6 (ATF6) and the protein kinase RNA-like ER kinase (PERK). Normally the detectors bind the molecular chaperone binding immunoglobulin protein (BiP) and are inactive. When they bind misfolded proteins, they release BiP and induce a transcriptional program

to restore homeostasis: increased folding, trafficking and degradation mechanisms (such as ER-associated protein degradation (ERAD)) or cell death. In addition, translation is reduced through phosphorylation of the eukaryotic translation initiation factor 2α (eIF2α) by PERK. In addition, ER-localized transcripts are degraded through regulated mRNA decay by IRE1.

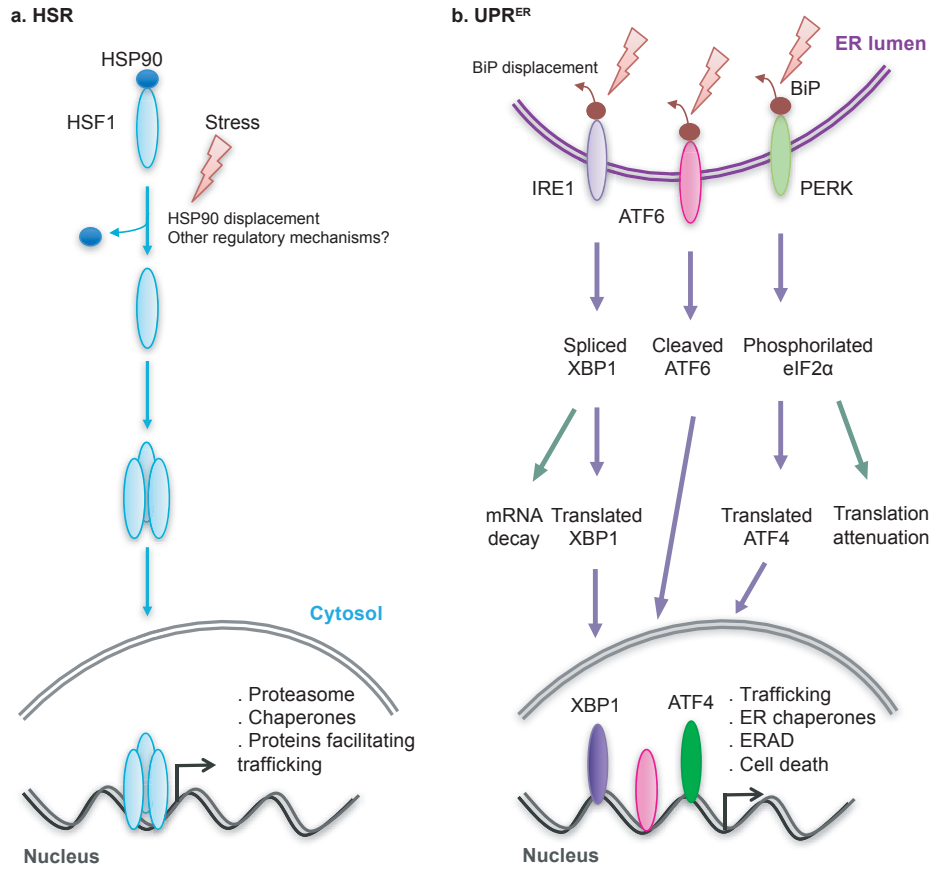

Figure 4. Cellular stress responses. Protein misfolding and/or aggregation is detected by compartment-specific stress responses, which adjust different mechanisms of proteostasis to control the load of proteins in each cellular compartment. Direct detection of misfolded or unfolded proteins allows an autonomous regulation of compartment-specific stress responses. **a.** The heat shock response (HSR) is regulated by the heat shock factor (HSF) transcription factor family, primarily HSF1. Under basal conditions, HSF1 is bound to HSP90 and inhibited. Under stress, HSF1 is released, it trimerizes and binds to heat response elements in the genome to induce expression of

multiple cytosolic chaperone families and proteasome subunits, which culminates in the improvement of protein folding, increased efficiency of protein trafficking pathways and increased protein degradation. **b.** Proteostasis surveillance in the endoplasmic reticulum (ER) is mediated by the unfolded protein response of the ER (UPR^{ER}), which is activated by an imbalance between unfolded proteins inside the ER and the capacity of the ER proteostasis machinery. Three signaling pathways are activated upon protein unbalance. Each of them have an upstream detector component: inositol-requiring protein 1 (IRE1), activating transcription factor 6 (ATF6) and protein kinase RNA-like ER kinase (PERK), which are activated by direct binding to misfolded proteins and released from the inhibition by the chaperone binding immunoglobulin protein (BiP). Each detector is linked to a transcriptional response that induces chaperone expression, membrane expansion, increased efficiency of membrane trafficking, degradation mechanisms (such as ER-associated protein degradation (ERAD)) or cell death. In addition, translation is reduced through phosphorylation of eukaryotic translation initiation factor 2α (eIF2α) by PERK in order to decrease the load of proteins entering the ER. However, preferential translation of specific mRNAs also occurs, including the UPR^{ER} transcription factor ATF4. In addition, ER-localized transcripts are degraded through regulated mRNA decay (RIDD) by IRE1. Adapted from (Taylor, Berendzen et al. 2014).

The mitochondrial unfolded protein response (UPR^{mt}) is activated to recover mitochondrial homeostasis. Under stress conditions like depletion of mtDNA, loss of mitochondrial membrane potential, imbalance between nuclear encoded proteins and mitochondrial encoded proteins or accumulation of unfolded proteins within the mitochondria, there is activation of a retrograde signaling whereby the nucleus is informed to induce a transcriptional program aimed at restoring mitochondrial function.

For the purpose of this work we provide more information on mitochondrial dysfunction and mitochondrial stress response in the next section.

4. Mitochondrial stress response

Proper mitochondrial activity is preserved through regulation of mitochondrial dynamics, fusion and fission, modulation of mitophagy and maintenance of mitochondrial homeostasis through activation of the UPR^{mt}.

To repair damaged components of the mitochondria, these organelles are subjected to fission, which allows segregation of damaged mitochondria, and fusion, for the exchange of material. To counteract the accumulation of defective mitochondria, cells activate mitophagy, a mechanism by which defective mitochondria are selectively detected and degraded (Ni, Williams et al. 2015). Under basal conditions, the serine/threonine protein kinase PINK1 is rapidly cleaved and degraded by mitochondrial proteases, whereas when mitochondria are depolarized, PINK1 is not cleaved and accumulates in the outer mitochondrial membrane. The accumulation of PINK1 facilitates the recruitment of Parkin to the mitochondria and induces Parkin's E3 ubiquitin ligase activity. Once active, Parkin ubiquitinates outer mitochondrial membrane proteins, recruiting autophagy adapter proteins to mitochondria and targeting mitochondria to selective autophagy. Nevertheless, increasing evidences support the idea of a Parkin-independent mitophagy since different autophagy receptors have been shown to localize to mitochondria and recruit autophagosomes without need of Parkin, such as BNIP3, NIX and FUNDC1 (Schweers, Zhang et al. 2007, Liu, Feng et al. 2012, Murakawa, Yamaguchi et al. 2015).

Under proteotoxic conditions the UPR^{mt} is activated to maintain mitochondrial proteostasis by inducing the expression of mitochondrial chaperones and proteases that control protein folding, assembly and degradation (figure 5). While the UPR^{mt} was initially discovered in mammalian cells, the UPR^{mt} signaling pathway has been most extensively studied in the nematode *C. elegans*. Accumulated unfolded and/or unassembled proteins in the mitochondrial matrix are cleaved by the mitochondrial protease, ClpP (Haynes, Petrova et al. 2007) and the resulting peptides are exported to the cytoplasm through the mitochondrial ATP-binding cassette (ABC) transporter, HAF-1 (Haynes, Yang et al. 2010). The

accumulation of the peptides in the cytosol leads to the nuclear import of the transcription factors ATFS-1 (Nargund, Pellegrino et al. 2012). Once in the nucleus, ATFS-1 together with DVE-1 and UBL-5, (Benedetti, Haynes et al. 2006, Haynes, Petrova et al. 2007) induce the expression of genes involved in restoring the mitochondrial homeostasis such as mitochondrial chaperones (*hsp-6* and *hsp-60)*, proteases (*clpp-1*, *lonp-1*, *spg-7* and *ymel-1)*, the fission factor *drp-1* and mitochondrial transporters (*tim-23* and *tim-17)* (Nargund, Pellegrino et al. 2012, Nargund, Fiorese et al. 2015). Moreover, ATFS-1 induces the expression of glycolysis related genes, promoting an alternative form of ATP production, and negatively regulates the expression of multiple tricarboxylic acid (TCA) cycle and oxidative phosphorylation (OXPHOS) genes. Interestingly, in addition to the nuclear localization signal (NLS), ATFS-1 presents a mitochondrial targeting sequence (MTS) and is normally imported to the mitochondria where it is degraded by the Lon protease. During stress, even though the majority of ATFS-1 is translocated to the nucleus due to the defective mitochondrial import, a percentage of ATFS-1 also accumulates inside the mitochondria and binds mitochondrial DNA (mtDNA) where it limits mitochondria-encoded mRNA accumulation (Nargund, Fiorese et al. 2015). Thus, in addition to promote mitochondrial protein homeostasis, the transcription factor ATFS-1 has been proposed to act as a metabolic regulator and to assist in the complete recovery from mitochondrial dysfunction.

Besides changes in the genetic expression, mitochondrial stress causes wide-spread changes in chromatin structure (Merkwirth, Jovaisaite et al. 2016, Tian, Garcia et al. 2016). In particular, mitochondrial stress induces the histone methylase MET-2 and the nuclear co-factor LIN-65 for the di-methylation of the histone H3K9. Although those changes globally cause condensation of the chromatin, it is needed for ATFS-1 and DVE-1 to

bind to the opened free regions (Tian, Garcia et al. 2016). In addition, two conserved demethylases, the jumonji family proteins JMJD-1.2 and JMJD-3.1, have been shown necessary for the induction of the UPR^{mt}, probably by removing the repressive H3K27 methylation marks from coding regions in UPR^{mt}-related genes (Merkwirth, Jovaisaite et al. 2016). Interestingly, the two demethylases are also required for the UPR^{mt} mediated enhancement of lifespan. This suggests that mitochondrial perturbation early in life establishes an epigenetic memory that ensures the protection from future insults and maintains the beneficial effects throughout lifespan.

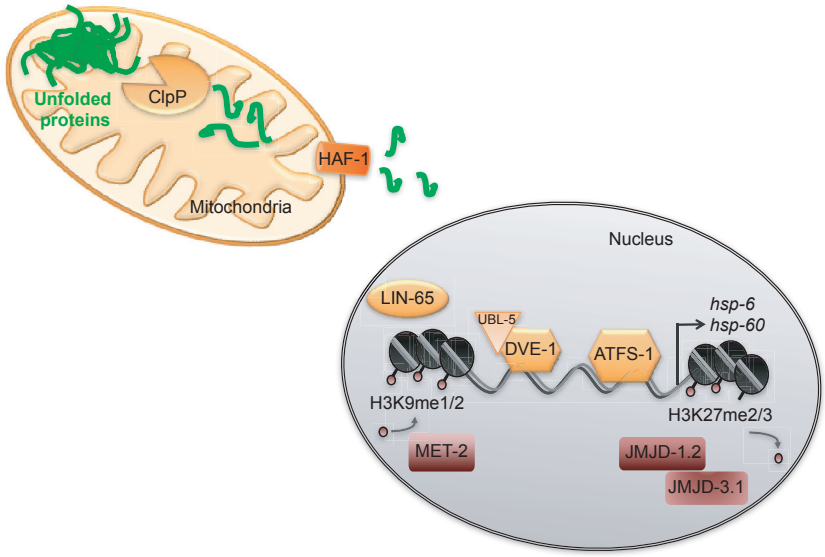

Figure 5. The mitochondrial unfolded protein responses, UPR^{mt}. In order to maintain the mitochondrial proteostasis, the UPR^{mt} is activated and induces the expression of mitochondrial chaperones and proteases. In *Caenorhabditis elegans*, unfolded proteins within the mitochondrial matrix are cleaved by the mitochondrial protease, ClpP, and the resulting peptides are exported to the cytoplasm through the mitochondrial ATP-binding cassette (ABC) transporter, HAF-1. The accumulation of the peptides in the cytosol leads to the nuclear import of the transcription factors ATFS-1, that together with DVE-1 and UBL-5, induce the expression of genes involved in restoring mitochondrial homeostasis. In addition, mitochondrial stress causes changes in chromatin structure. In particular, mitochondrial stress induces the histone methylase MET-2 and the nuclear co-factor LIN-65 for the di-methylation of the histone H3K9. Moreover, two demethylases, JMJD-1.2 and JMJD-3.1, have been shown necessary for the induction of the UPR^{mt}.

Strikingly, the mitochondrial stress response can be activated in a cell non-autonomous manner: perturbing mitochondrial function in the nervous system induces the UPR^{mt} in distinct and non-innervated tissues (Durieux, Wolff et al. 2011, Berendzen, Durieux et al. 2016, Shao, Niu et al. 2016). In addition of being necessary functional components of the UPR^{mt}, the neuropeptide FLP-2 has been reported as a possible mediator of this non-autonomous mechanism, as revealed by performing a large scale CRISPR-Cas9 screen (Shao, Niu et al. 2016). Moreover, Berendzen *et al*. (Berendzen, Durieux et al. 2016) reported serotonin to be necessary for the communication between the affected neurons and the peripheral tissues.

In addition to the UPR^{mt}, which acts mainly at a transcriptional level via ATFS-1, recent studies have identified different cytosolic responses to restore proteostasis and to reduce the proteotoxic effect; these include the mitochondrial to cytosol stress response (MCSR) (Kim, Grant et al. 2016), the mitochondrial precursor over-accumulation stress (mPOS) (Wang and Chen 2015) and the UPR activated by mistargeting of proteins (UPR^{am}) (Wrobel, Topf et al. 2015). The MCSR causes a shift in fat metabolism triggering an accumulation of lipids and cardiolipins and inhibiting ceramide synthesis. This restructuring of fat metabolism facilitates crosstalk between mitochondria and cytosol in order to improve cytosolic protein homeostasis and needs the cooperation of DVE-1 and HSF-1 to induce the cytosolic response upon mitochondrial perturbations (Kim, Grant et al. 2016). The mPOS and the UPR^{am} result in a simultaneous inhibition of translation and an increment of proteosomal activity (Wang and Chen 2015, Wrobel, Topf et al. 2015). The two responses coordinate the inhibition of cap-dependent translation by down-regulating ribosomal proteins, the mTOR pathway and mRNA turnover. However, further investigation is required to decipher the exact mechanism. In worms, it has been shown that under mitochondrial

stress, the kinase GCN-2 phosphorylates the translation initiation factor eIF2a in order to reduce protein translation. Interestingly, this cytosolic response acts in parallel to the ATFS-1 and is required for lifespan extension (Baker, Nargund et al. 2012).

Importantly, the majority of these pathways for restoring mitochondrial homeostasis and resolving mitochondrial stress have been described in many different models, ranging from yeast to human cells.

Interestingly, many mitochondrial perturbations that induce the UPR^{mt} have been shown to extend lifespan in yeast, worms, flies and mice (Jovaisaite and Auwerx 2015). The exact link between UPR^{mt} activation and longevity remains unclear. Nevertheless, it has been demonstrated through RNAi dilution experiments that mild knockdown of ETC genes extends lifespan while too strong knockdown reduces lifespan (Rea, Ventura et al. 2007). Moreover, there are specific spatio-temporal restrictions for an induced UPR^{mt} to enhance lifespan (Dillin, Hsu et al. 2002, Durieux, Wolff et al. 2011). It seems that when the mitochondrial stress is too high, the protective effects of UPR^{mt} are insufficient to counteract the damage, thus the beneficial adaptive response becomes maladaptive.

5. Prohibitin (PHB) complex

Prohibitins are strongly evolutionarily conserved mitochondrial proteins whose true biochemical function still remains unknown (Artal-Sanz and Tavernarakis 2009, Merkwirth and Langer 2009). The prohibitin (PHB) family is composed of two subunits PHB-1 (32 KDa) and PHB-2 (34 KDa), that physically associate with each other to form a large multimeric complex of approximately 1 MDa (Back, Sanz et al. 2002)Sanz et al. 2002 (figure 6a). PHB-2 has a N-terminal trans-membrane domain and the N-terminal

of PHB-1 is expected to be membrane associated. Both proteins contain the conserved PHB domain, common to other scaffolds proteins such as stomatin and flotillin, and a coil-coiled C-terminal domain responsible for the interaction between PHB-1 and PHB-2 (Winter, Kamarainen et al. 2007). 14 heterodimers become associated and form a ring like structure in the inner mitochondrial membrane (IMM), projected into the mitochondrial intermembrane space (Tatsuta, Model et al. 2005) (figure 6a). Loss of either of the subunits leads to the absence of the whole complex, both in unicellular and multicellular eukaryotes (Berger and Yaffe 1998, Artal-Sanz, Tsang et al. 2003).

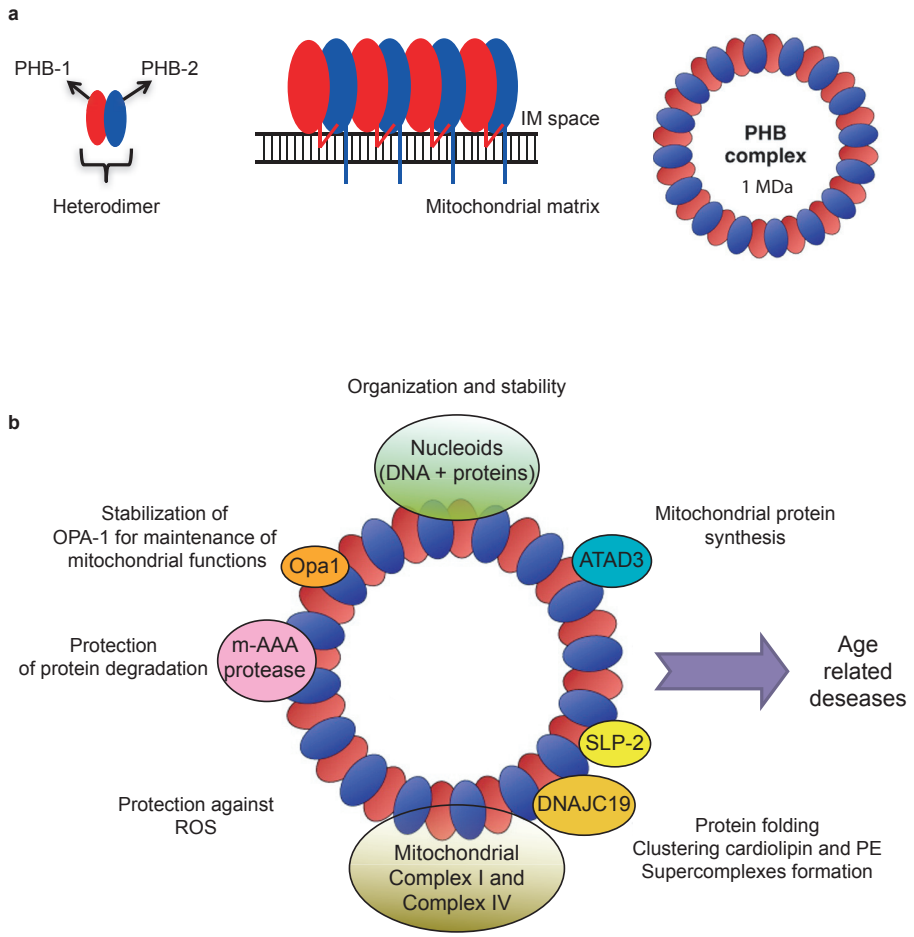

Figure 6. The mitochondrial prohibitin (PHB) complex. a. The PHB complex is composed of two subunits, PHB-1 and PHB-2, that physically associate with each other. PHB-2 has a N-terminal trans-membrane domain and the N-terminal of PHB-1 is expected to be membrane associated. 14 heterodimers become associated and form a ring like structure of approximately 1 MDa sitting in the inner mitochondrial membrane (IMM) projected into the mitochondrial intermembrane space. **b.** Functions of the PHB complex. By interacting with nucleoids, the PHB complex maintains their organization and stability, it protects newly synthesized proteins from degradation by m-AAA protease and promotes mitochondrial protein synthesis acting together with ATAD3. In addition, PHB have been proposed to act as scaffold proteins by stabilizing OPA1 and to act as a holdase-unfoldase type of chaperone by directly binding to newly synthesized mitochondrial translation products, like complex I and complex IV subunits, and to assist in the formation of respiratory super-complexes together with SLP-2 and DNAJC19.

Its high degree of conservation suggests an important cellular function; however, prohibitin deletion does not cause any observable growth phenotype in the unicellular yeast *S. cerevisiae* (Osman, Haag et al. 2009). By contrast, prohibitins are required for embryonic development in *C. elegans* (Artal-Sanz, Tsang et al. 2003) and in mice (Merkwirth, Dargazanli et al. 2008), while their postembryonic depletion by RNAi in *C. elegans* causes severe germline defects (Artal-Sanz, Tsang et al. 2003).

Despite the fact that their exact molecular function is yet to be deciphered, many different roles have been attributed to the PHB complex (figure 6b). They have been involved in cell proliferation (Artal-Sanz, Tsang et al. 2003, Merkwirth, Dargazanli et al. 2008), in maintenance of mitochondrial function (Merkwirth, Dargazanli et al. 2008, Schleicher, Shepherd et al. 2008, Han, Yu et al. 2014) and in the organization and stability of mitochondrial nucleoids (Bogenhagen, Wang et al. 2003, Kasashima, Sumitani et al. 2008). Lack of PHB induces a very strong UPR^{mt} (Yoneda, Benedetti et al. 2004, Bennett, Vander Wende et al. 2014, Gatsi, Schulze et al. 2014, Hernando-Rodriguez, Erinjeri et al. 2018). Moreover, PHBs have been involved in promoting mitochondrial protein synthesis, acting

together with ATAD3 in human cells (He, Cooper et al. 2012), as well as in protecting newly imported proteins from degradation by m-AAA protease in yeast (Steglich, Neupert et al. 1999). Prohibitins have been proposed to directly bind to newly synthesized mitochondrial translation products in order to assist with protein folding, acting as a holdase-unfoldase type of chaperone (Nijtmans, de Jong et al. 2000). In particular, PHB has been suggested as assistant for incompletely assembled complex I (Miwa, Jow et al. 2014) and complex IV (Nijtmans, de Jong et al. 2000, Strub, Paillard et al. 2011) subunits of the electron transport chain (ETC) and also to be responsible for the formation of respiratory super-complexes together with stomatin-like protein 2 (SLP-2) (Mitsopoulos, Chang et al. 2015, Jian, Xu et al. 2017).

Lipid composition of the mitochondrial inner membrane has been shown to be important for respiratory super-complexes formation (Lenaz, Baracca et al. 2010), with cardiolipin playing an essential role in the arrangement and the stabilization of complexes and super-complexes (Pfeiffer, Gohil et al. 2003). Recent studies described a large mitochondrial cardiolipin synthesis complex in human cells that interacts with many cardiolipin-dependent mitochondrial membrane-organizing proteins, like PHB and SLP-2 (Serricchio, Vissa et al. 2018). Osman and colleagues elaborated a synthetic genetic array in yeast looking for new genetic interactors of prohibitins (Osman, Haag et al. 2009). They described a functional relationship of PHB with the lipid composition of the mitochondrial membrane and suggested PHB as a membrane organizer affecting the distribution of cardiolipin and phosphatidyltanolamine by clustering them at distinct sites of the inner mitochondrial membrane. Subsequent studies in cells described DNAJC19 (Richter-Dennerlein, Korwitz et al. 2014) and SLP2 (Da Cruz, Parone et al. 2008, Christie, Lemke et al. 2011) as PHB interacting proteins involved in

cardiolipin remodeling. In sum, prohibitins provide phospholipid platforms for the assembly and stability of the electron transport chain complexes. In agreement with the stabilizing function, prohibitins have been described as scaffold proteins, being in charge of formation of mitochondrial cristae by stabilizing OPA1, an essential component of the mitochondrial fusion machinery (Merkwirth, Dargazanli et al. 2008).

Recently, in mammalian cells, PHB-2 has been reported as a mitochondrial receptor essential for Parkin mediated mitophagy (Wei, Chiang et al. 2017). Upon mitochondrial depolarization and proteasome-dependent outer membrane rupture, PHB-2 binds to LC3, the autophagosomal membrane-associated protein trough a canonical LC3-interacting region.

Furthermore, depletion of PHB in different cell types increases mitochondrial ROS levels (Schleicher, Shepherd et al. 2008, Kathiria, Butcher et al. 2012), whereas its overexpression protects against oxidative stress (Liu, Ren et al. 2009) and reduces ROS production from different injury modalities (Zhou, Qian et al. 2012).

In addition to all the previously mentioned roles in mitochondria, PHBs have been reported to be localized in other cellular compartments such as the plasma membrane (Chowdhury, Thompson et al. 2013), the nucleus (Fusaro, Dasgupta et al. 2003) and the nucleolus (Zhou, Ai et al. 2018). PHBs integrate signals from many pathways like Akt, Raf-MEK-ERK, CaMK and PKC, coordinating diverse aspects of cell physiology (Thuaud, Ribeiro et al. 2013). Specifically, PHBs exert repression of estrogen-receptor activity (He, Feng et al. 2008), of p53 transcriptional activity (Chander, Halpern et al. 2010, Chander, Halpern et al. 2011) and of E2F by recruiting histone deacetylases and co-repressors (Wang, Nath et al. 1999, Wang, Fusaro et al. 2002). In addition, PHB have been shown to associate

with a histone H3.3 chaperone, HIRA, to control genetic expression in human embryonic stem cells (Zhu, Li et al. 2017).

PHBs have been related to several age-related diseases like cancer, neurodegenerative and metabolic disorders (Nijtmans, Artal et al. 2002, Merkwirth, Martinelli et al. 2012, Thuaud, Ribeiro et al. 2013, Mishra and Nyomba 2017, Tortelli, de Godoy et al. 2017, Zi Xu, Ande et al. 2018). Loss of PHB decreases resistance to apoptosis (Merkwirth, Dargazanli et al. 2008) and accelerates aging in yeast (Piper, Jones et al. 2002) and mammalian cells (Kasashima, Ohta et al. 2006, Schleicher, Shepherd et al. 2008, Chowdhury, Kumar et al. 2017). Strikingly, in response to caloric restriction PHB depletion causes lifespan extension in *S. cerevisiae* (Schleit, Johnson et al. 2013). This opposing effect on lifespan is conserved in *C. elegans*: PHB depletion decreases the lifespan of wild type animals, whereas it extends lifespan in a variety of compromised conditions such as in mitochondrial mutants, in dietary restricted mutants and in mutants defective in either of the two diapause signaling pathways, TGF-β signaling and insulin/IGF-1 signaling (Artal-Sanz and Tavernarakis 2009, Gatsi, Schulze et al. 2014). Interestingly, PHB depletion induces the UPR^{mt} in a background dependent manner. While the UPR^{mt} induction upon PHB depletion in otherwise wild type animals is very strong, in the insulin mutants *daf-2(e1370)* and *sgk-1(ok538)* the PHB-mediated induction is suppressed (Gatsi, Schulze et al. 2014).

6. The insulin/IGF-1 signaling (IIS) pathway

The Insulin/IGF-1 signaling (IIS) pathway is a highly-conserved pathway that coordinates growth, differentiation, reproduction and metabolism in response to changing environmental conditions and nutrient availability.

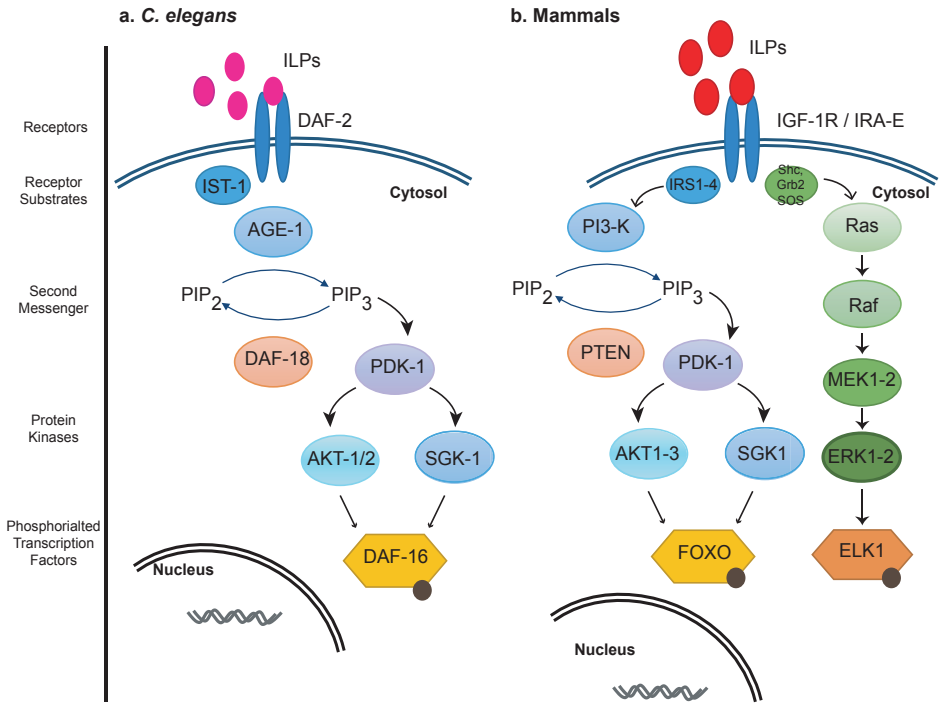

Figure 7. The Insulin/IGF-1 signaling pathway. The Insulin/IGF-1 signaling (IIS) pathway is conserved from invertebrates to mammals. The figure shows the components of the pathway in *Caenorhabditis elegans* (**a**) and in mammals (**b**). Under favourable conditions, the IIS pathway is activated. **a.** Insulin-like peptides (ILPs) bind to the insulin/IGF-1 receptor, DAF-2, and activate it, which leads to the recruitment of insulin/IGF-1 receptor substrate, IST-1. Then, the phosphatidylinositol-3-OH kinase, AGE-1, is activated and triggers an increase in the levels of the second messenger phosphatidylinositol (3,4,5)-triphosphate (PIP3). Levels of the second messenger are controlled by the PTEN phosphatase, DAF-18, that converts PIP3 in phosphatidylinositol (4,5)-biphosphate (PIP2). High levels of PIP3 activates the downstream kinase cascade composed of 3-phosphoinositide-dependent protein kinase 1, PDK-1, the protein kinase B, AKT-1/2, and the Serum- and Glucocorticoid-inducible Kinase 1, SGK-1. Finally, the serine/threonine kinases phosphorylate the fork-head transcription factor, DAF-16, recruiting it in the cytoplasm. **b.** In mammals, the network is more complex, with several insulin/IGF-1 receptors and insulin/IGF-1 receptor substrates. There is activation of two major kinases cascades, the PI3K-PKB/AKT pathway as in invertebrates and the Ras-MAPK pathway, the last being more involved in the mitogenic effects of IIS. Conversely, under unfavourable conditions, the IIS pathway is down-regulated leading to the nuclear translocation of the transcription factors and subsequent activation of the transcriptional program.

Under favourable conditions (figure 7), the IIS pathway is activated and triggers a normal developmental rate and adult lifespan. Insulin-like peptides bind to the insulin/IGF-1 receptor activating it, which leads to the recruitment of an insulin/IGF-1 receptor substrate. Then, the phosphatidylinositol-3-OH kinase (PI3K) is activated and there is an increase in the levels of the second messenger phosphatidylinositol (3,4,5)-triphosphate (PIP_3). Levels of the second messenger are controlled by the PTEN phosphatase that converts PIP_3 in phosphatidylinositol (4,5)-biphosphate (PIP_2). High levels of PIP_3 activates the downstream kinase cascade composed of 3-phosphoinositide-dependent protein kinase 1 (PDK1), the protein kinase B (AKT1-3) and the Serum- and Glucocorticoid-inducible Kinase 1 (SGK1). Finally, the serine/threonine kinases phosphorylate the fork-head transcription factor, FOXO, recruiting it in the cytoplasm (Altintas, Park et al. 2016). Compared to invertebrates, in mammals the network is more complex, with several insulin/IGF-1 receptors and insulin/IGF-1 receptor substrates. There is activation of two major kinases cascades, the PI3K-PKB/AKT pathway and the Ras-MAPK pathway, the last being more involved in the mitogenic effects of IIS (van Heemst 2010).

Conversely, under unfavourable conditions, the IIS pathway is down-regulated leading to the nuclear translocation of FOXO and subsequent activation of the transcriptional program.

Studies in nematodes, first showed that the IIS pathway regulates aging. Loss of function of the sole *C. elegans* insulin/IGF-1 receptor, *daf-2*, increases lifespan up to 250% and this extension is dependent on the transcription factor *daf-16*, the FOXO homologue (Kenyon, Chang et al. 1993, Larsen, Albert et al. 1995). In the fruit fly *Drosophila melanogaster*, IIS regulates as well lifespan, stress responses, growth and development. Inhibition of the insulin receptor (Tatar, Kopelman et al. 2001) or the insulin receptor

substrate (Clancy, Gems et al. 2001) extends lifespan in flies. FIRKO mice, lacking the insulin receptor specifically in fat tissue, are long-lived and have reduced fat mass (Bluher, Michael et al. 2002, Bluher, Kahn et al. 2003). Even in humans, common polymorphisms in several of the IIS genes have been associated with lifespan across diverse cohorts (van Heemst 2010).

Interestingly, in *C. elegans*, reduced IIS, in addition of extending lifespan, alters metabolism (Ruzanov, Riddle et al. 2007), increases resistance to environmental stress such as heat stress (Lithgow, White et al. 1995), oxidative stress (Honda and Honda 1999), heavy metals (Barsyte, Lovejoy et al. 2001), hypoxic conditions (Scott, Avidan et al. 2002) and pathogens (Garsin, Villanueva et al. 2003). Moreover, knockout of *daf-2* helps to maintain better internal homeostasis against cytosolic and ER proteotoxic stress (Henis-Korenblit, Zhang et al. 2010). In addition, *daf-2* mutants have slower development, constitutive dauer formation and reduced brood size (Gems, Sutton et al. 1998). In addition to DAF-16, IIS modulates the activity of two other transcription factors, HSF-1 and SKN-1. These three transcription factors have been shown to act together and in parallel to regulate lifespan and stress resistance. Thus, proper regulation of IIS is crucial for protection from internal and external stresses as well as for long and healthy life in *C. elegans*.

daf-2(e1370) mutants are characterized by general alterations in genes expression (Murphy, McCarroll et al. 2003, Halaschek-Wiener, Khattra et al. 2005, Ruzanov, Riddle et al. 2007), specifically changes in ETC gene expression, increased expression of glyoxylate shunt genes, and reduced expression of genes encoding for TCA cycle components. This leads to changes in proteomic profiles (Stout, Stigter et al. 2013, Narayan, Ly et al. 2016), having reduced mRNA processing and transport and reduced translational machinery. Furthermore, *daf-2* profiles suggest a reorganization

of intermediary metabolism, tuning it down for maximal survival (Artal-Sanz and Tavernarakis 2008).

As previously mention, PHB depletion, while it shortens lifespan of wild type worms, it increases the lifespan of *daf-2* mutants. By using gas chromatography coupled to a flame ionization detector (GC/FID) and ^{1}H NMR spectroscopy, Lourenço *et al.* concluded that PHB depletion leads to broad metabolic changes in wild type as well as in *daf-2* mutants (Lourenco, Munoz-Jimenez et al. 2015). Lack of PHB has an impact on fatty acid composition, amino acid and carbohydrate metabolism on both wild type and *daf-2* mutants, although the effects are more pronounced in wild type worms than in the IIS mutants. They suggested that *daf*-2 mutants suffer metabolic reorganizations that make them more robust to changes induced by PHB depletion and these changes have beneficial and synergistic effects on worm longevity. In particular, PHB depleted *daf-2* mutants, with reorganized metabolic networks, show increased fermentative metabolism and consequently would be expected to be more efficient in energy management.

In order to characterize better the role of PHB in the IIS pathway we analyzed the kinases acting downstream of DAF-2 (Gatsi, Schulze et al. 2014). We showed that only loss of function of SGK-1 recapitulates the enhanced longevity and the reduced UPR^{mt} activation phenotypes observed upon PHB depletion. In addition, the data suggest that SGK-1 is acting in a parallel pathway to the IIS in the regulation of aging and the UPR^{mt}, since the double mutant *daf-2;sgk-1* shows a further enhancement of both phenotypes upon PHB depletion. We established that, in addition to the IIS pathway, SGK-1 acts as part of mTORC2, downstream of RICT-1, in the regulation of the mitochondrial stress response.

OBJECTIVES

OBJECTIVE 1:

To develop a methodology to screen for PHB interactors modulating the mitochondrial stress response

OBJECTIVE 2:

To identify new genetic interactors of PHB involved in the regulation of the UPR^{mt}

OBJECTIVE 3:

To assess the role of the Insulin/IGF-1 signaling pathway in mitochondrial protection

RESULTS AND DISCUSSION

Chapter I:

Combined flow cytometry and high-throughput image analysis to identify prohibitin genetic interactors in *Caenorhabditis elegans*

Modified from the article "Combined flow cytometry and high-throughput image analysis for the study of essential genes in *Caenorhabditis elegans*" published in BMC Biology, January 2018

Blanca Hernando-Rodríguez[1,2*], Annmary Paul Erinjeri[1,2*], María Jesús Rodríguez-Palero[1,2], Val Millar[3,4], Sara González-Hernández[1,2,5], María Olmedo[1,2,6], Bettina Schulze[7], Ralf Baumeister[7], Manuel J. Muñoz[1,2], Peter Askjaer[1] and Marta Artal-Sanz[1,2]

[1] Andalusian Center for Developmental Biology, Consejo Superior de Investigaciones Científicas/Junta de Andalucía/Universidad Pablo de Olavide, Seville, Spain

[2] Department of Molecular Biology and Biochemical Engineering, Universidad Pablo de Olavide, Seville, Spain

[3] GE Healthcare Life Sciences, Maynard Centre, Forest Farm, Whitchurch, Cardiff, United Kingdom

[4] Current address: Target Discovery Institute, Nuffield Department of Medicine, University of Oxford, Oxford, United Kingdom

[5] Current address: Cell and Developmental Biology Area; Centro Nacional de Investigaciones Cardiovasculares Carlos III (CNIC), Madrid, Spain

[6] Current address: Department of Genetics, University of Seville, Seville, Spain

[7] Centre for Biological Signalling Studies (BIOSS), Laboratory for Bioinformatics and Molecular Genetics, Faculty of Biology, and ZBMZ Center for Biochemistry and Molecular Cell Biology (Faculty of Medicine), Albert Ludwigs University of Freiburg, Freiburg, Germany

* Equal contribution

1. PHB deletion induces the UPR^{mt} by a non-canonical mechanism

In *C. elegans*, homozygous *phb-1* and *phb-2* deletion mutants coming from heterozygous mothers develop into adults due to maternal contribution but are sterile (Artal-Sanz and Tavernarakis 2009) and need to be maintained as balanced heterozygous. The *phb-2(tm2998)* deletion was balanced using an inversion on chromosome II, *mIn1,* which carries an integrated pharyngeal GFP element, while for the *phb-1(tm2571)* deletion we used a reciprocal translocation between chromosomes I and III*, hT2,* also accompanied by an integrated pharyngeal GFP element. PHB-1 and PHB-2 are interdependent for protein complex formation and stability (Artal-Sanz, Tsang et al. 2003), thus *phb-1* and *phb-2* mutants showed identical phenotypes: PHB deletion mutants lived shorter than wild type and exhibited a delayed development compared to wild type, with the third larval stage being more than two-fold increased (Hernando-Rodriguez, Erinjeri et al. 2018). PHB complex sits in the inner mitochondrial membrane (Tatsuta, Model et al. 2005) and depletion of the complex induces a strong mitochondrial stress (Yoneda, Benedetti et al. 2004, Bennett, Vander Wende et al. 2014, Gatsi, Schulze et al. 2014).

Mitochondrial stress triggers the expression of the conserved mitochondrial chaperones HSP-6 and HSP-60, which have been used to screen for components of the UPR^{mt} signal transduction pathway (Yoneda, Benedetti et al. 2004, Benedetti, Haynes et al. 2006, Haynes, Petrova et al. 2007, Haynes, Yang et al. 2010). Nuclear genes encoding UPR^{mt} components required for HSP-6 and HSP-60 expression include the putative mitochondrial inner membrane ATP-binding cassette (ABC) transporter protein HAF-1, that exports the peptides resulting from the cleavage of unfolded proteins to

the cytosol (Haynes, Petrova et al. 2007, Haynes, Yang et al. 2010). These peptides trigger an unknown signaling cascade that results in the nuclear localization of the bZIP transcription factor ATFS-1 (Haynes, Yang et al. 2010, Nargund, Pellegrino et al. 2012). Additional transcriptional regulators of the UPR^{mt} are the transcription factor DVE-1 (Haynes, Petrova et al. 2007) and the ubiquitin-like protein UBL-5, that physically interact with each other (Benedetti, Haynes et al. 2006).

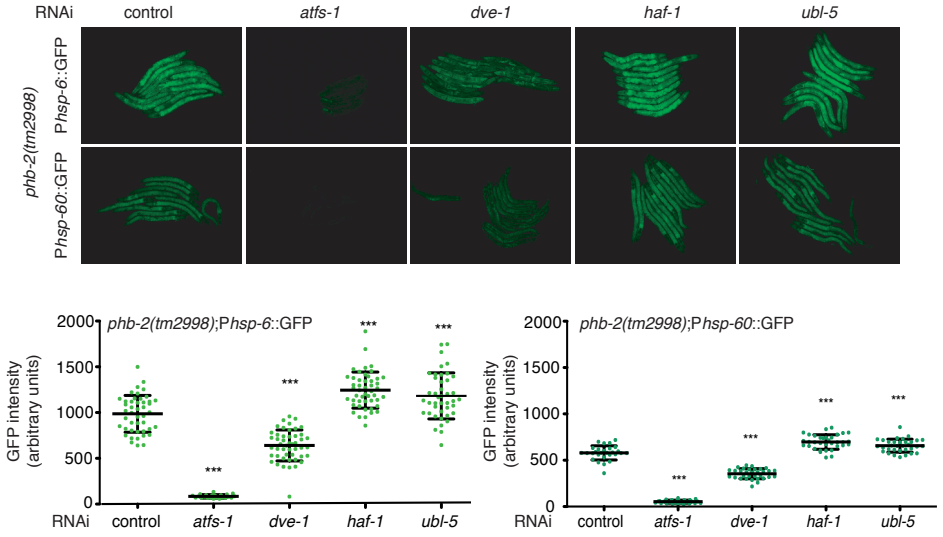

Figure 8: Background dependent induction of UPR^{mt} reporters in PHB deletion mutants. Fluorescent microscopy images of transgenic animals *phb-2(tm2998)*;P*hsp-6*::GFP and *phb-2(tm2998)*;P*hsp-60*::GFP treated with RNAi against the UPR^{mt} components ATFS-1, DVE-1, HAF-1 and UBL-5. Graphical representation of quantification of P*hsp-6*::GFP (bottom panel, left) and P*hsp-60*::GFP (bottom panel, right). The induced UPR^{mt} in prohibitin deletion mutants was suppressed upon depletion of ATFS-1 and DVE-1, whereas the expression of both UPR^{mt} reporters was further increased upon depletion of HAF-1 and UBL-5. (Mean ± SD; *** p value < 0.001; ANOVA test. One representative replica out of three independent replicas is shown. n > 30 in all conditions).

To monitor the UPR^{mt} in PHB deletion mutants, we incorporated the UPR^{mt} reporters, P*hsp-6*::GFP and P*hsp-60*::GFP (Yoneda, Benedetti et al. 2004) and quantified their expression in *phb-2(tm2998)* mutants subjected to RNAi

against the UPR^{mt} components. We observed that the transcription factors ATFS-1 and DVE-1 appeared to be required for full induction of the UPR^{mt} in *phb-2* mutants, since the signal was abolished under *atfs-1(RNAi)* and *dve-1(RNAi)* (figure 8). However, HAF-1 and UBL-5 were not necessary for the PHB-mediated activation of the UPR^{mt}; instead, their depletion further increased the expression of both UPR^{mt} reporters (figure 8). This suggests that HAF-1 and UBL-5 not only are dispensable for signaling the UPR^{mt} upon prohibitin depletion, but blocking peptide transport through HAF-1 increases mitochondrial stress when depleting either subunit of the PHB complex. Our data are in agreement with a previous report showing that *haf-1* is not required for induction of the UPR^{mt} caused by RNAi knockdown of *phb-2* (Bennett, Vander Wende et al. 2014).

Together, these data indicate that PHBs are potentially involved in an alternative mitochondria-to-nucleus signaling mechanism. We therefore aimed to identify PHB genetic interactors and regulators by performing an RNAi screen on PHB mutants and to assess their effects on the UPR^{mt}. Since PHB are essential, deletion mutants are maintained with a balancer that contains a GFP reporter. Therefore, in order to isolate and further investigate PHB mutants we developed an automated method that consists of combined automated worm sorting and high-content image analysis (figure 9). The approach can be adapted and applied to any strain carrying a fluorescently labelled balancer.

2. Sorting homozygous prohibitin deletion mutants

COPAS is a convenient approach for high throughput analysis involving balanced strains as it facilitates a task that manually would be impracticable. For balanced strains in the absence of a gene reporter or when the

reporter carries a different fluorophore, the sorting of the populations is straightforward. However, in our case we needed to sort homozygous *phb-2(tm2998)* deletion mutants from a mixed population of *phb-2(tm2998)/mIn1* balanced animals carrying the UPR^{mt} stress reporter P*hsp-6*::GFP (figure 9).

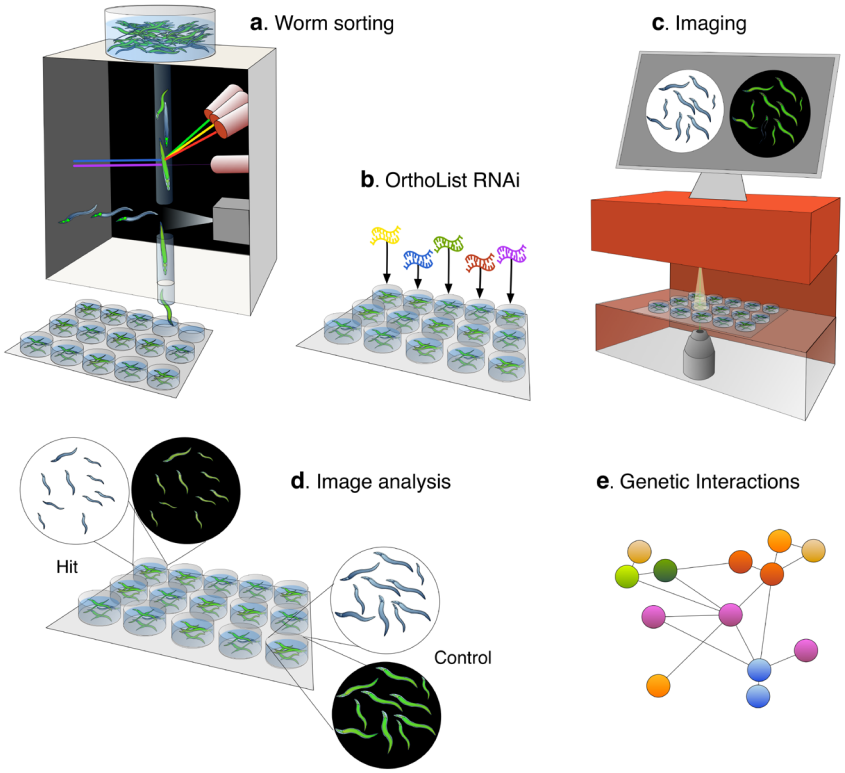

Figure 9: Overview of the screening strategy for the study of essential genes. a. Homozygous *phb-2(tm2998)*;P*hsp-6*::GFP mutants are sorted at the L2 stage from a mixed population of balanced heterozygous *phb-2(tm2998)/mIn1* animals into multiwell plates using the COPAS Biosort, "worm sorting". **b.** Bacteria expressing the OrthoList RNAi sub-library is added to the wells and worms are incubated at 20°C. **c.** At the desired stage, worms are imaged in brightfield and fluorescent channels using an automated microscope. **d.** Employing a user-defined image segmentation protocol, hits can be defined based on different measurements, like reporter expression or worm size, in comparison with the control. **e.** Finally, hits can be analyzed by building genetic networks based on predicted and described protein interactions in different organisms. Image courtesy of Liesbeth de Jong.

We sorted homozygous *phb-2(tm2998)* deletion mutants at the second larval (L2) stage, to allow RNAi treatment during early development. This is more challenging than what has been accomplished earlier as we attempted to sort relatively small homozygous *phb-2(tm2998)* worms expressing P*hsp-6*::GFP all along their body from the population carrying the balancer *mIn1* and hence, expressing a pharyngeal GFP element but not the reporter P*hsp-6*::GFP.

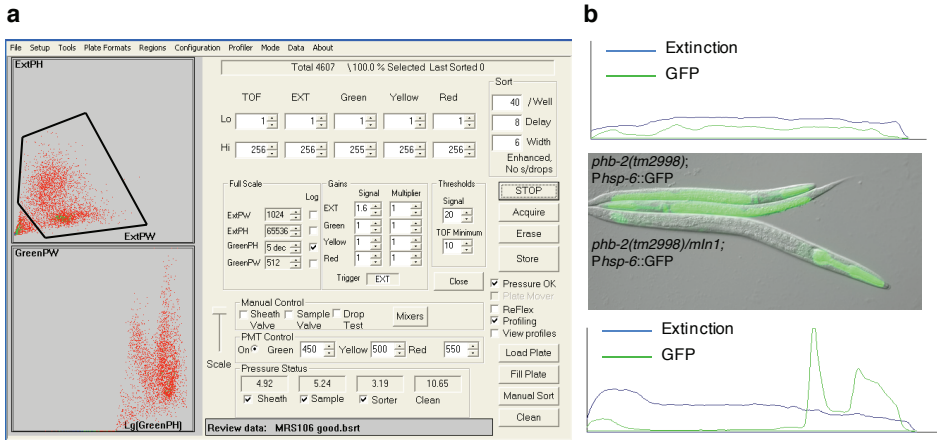

Figure 10: Worm sorting settings based on gating region and Profiler feature. a. COPAS Biosort conditions optimised for sorting homozygous *phb-2(tm2998)*;P*hsp-6*::GFP at the L2 stage. The upper panel reflects the gating region based on the extinction peak height (ExtPH) and the extinction peak width (ExtPW) selecting the worm population. The lower panel shows the worm distribution based on green peak height (green PH) and green peak width (green PW). **b.** Utilising the Profiler II software to distinguish between heterozygous *phb-2(tm2998)/mIn1*;P*hsp-6*::GFP and homozygous *phb-2(tm2998)*;P*hsp-6*::GFP larvae using green parameters. The *phb-2(tm2998)/mIn1*;P*hsp-6*::GFP worms showed two peaks in the green profile corresponding to the two lobes of the pharynx, had a green PH above 10,000 and were excluded (bottom panel). The *phb-2(tm2998)*;P*hsp-6*::GFP larvae showed a profile without pronounced peaks, with a green PH ranging from 700-10,000 and green PW above 120, and were accepted and sorted (top panel). The picture includes a balanced heterozygous *phb-2(tm2998)/mIn1*;P*hsp-6*::GFP expressing P*myo-2*::GFP in the pharynx and two *phb-2(tm2998)*;P*hsp-6*::GFP homozygous deletion mutants with induced P*hsp-6*::GFP expression. They were imaged at the moment of sorting, approximately 48 hours after synchronisation.

The COPAS instrument measures the optical density of the object (extinction), the size of the object, as well as fluorescence intensity in three channels: green, yellow and red (figure 10a). Based on these parameters, the user can define criteria for sorting and dispensing the population of interest into microtiter plates. In order to make the sorting more accurate, the standard COPAS system is implemented with the Profiler II software. Instead of making a single integrated measurement of a signal, the Profiler gives a list of successive point measurements along the object passing through the flow cell, and builds a fluorescence profile. Based on these measurements, it can detect fluorescence intensity peaks along the length of the object (figure 10b).

In our case, in order to remove small particles and possible debris and select specifically worms, we defined a gating region based on the extinction peak height (ExtPH) and the extinction peak width (ExtPW) (figure 10a). Next, we used the green channel (500-520 nm wavelength) to select animals with green body from the rest of the population. As the green signal coming from the pharynx is more intense than the signal coming from the stress reporter, we accepted a signal range between 700-10,000. These numbers refer to the highest value measured along the object. Nevertheless, in some cases, the signal coming from the pharynx is lower, thus we added a width criterion. To measure the width, the program integrates the widths of all the areas of the profile that exceed the value set up as the lower limit of peak height (700). We accepted widths above 120, excluding signals from the pharynx, which do not have the same extent as the body of the worm. All these numbers can be adjusted depending on the user requirements.

Most gene expression reporters in *C. elegans* consist of a given promoter fused to GFP (e.g. the *C. elegans* promoterome (Dupuy, Bertin et al. 2007) or numerous metabolic and stress reporters (Benedetti, Haynes et al. 2006,

Watson, MacNeil et al. 2013)). By exploiting the Profiler II software feature of the worm sorter, we successfully optimised a protocol for sorting homozygous L2 larvae with efficiency greater than 95%. We first attempted to sort L1 larvae in order to expose the animals to RNAi from the beginning of larval development. However, the pharynx of the animals occupies approximately one third of the body length at the L1 stage, complicating the profiling.

Once animals were sorted into 96-well plates, bacteria producing double stranded RNA (dsRNA), prepared in parallel (table 1 and appendix 1), were added to the worms to start the RNAi screen.

Table 1: Day-by-day description of the experimental procedure.

	Preparation of the worms	Preparation of the bacteria
Day 1	Bleaching *phb-2(tm2998)/mIn1*;P*hsp-6*::GFP	Inoculate RNAi library in LB agar O/N 37°C
Day 2	Place starved L1s in liquid OP50 20°C, 120 rpm	
Day 3		Replicate RNAi library in deep well plates O/N 37°C, 180 rpm
Day 4	Sorting L2s *phb-2(tm2998)*;P*hsp-6*::GFP	Bacterial culture and resuspend in complete S medium
Day 5	Incubate 20°C, 120 rpm	

3. Functional genomic analysis of chromosome I using the OrthoList RNAi library

C. elegans has long been an important invertebrate model for elucidating the mechanisms of conserved pathways relevant to human biology and disease. In *C. elegans*, RNAi can be applied by feeding the worms with bacteria expressing dsRNA against distinct genes (Timmons and Fire

1998). This feature has been extensively exploited in *C. elegans* resulting in the generation of various "feeding libraries" covering most of the predicted protein-coding genes in the genome (Kamath, Fraser et al. 2003, Rual, Ceron et al. 2004). Of the ~20,000 predicted protein-coding genes in *C. elegans* (Gerstein, Lu et al. 2010), 7,663 genes have been included in the "OrthoList" (Shaye and Greenwald 2011), a compilation of *C. elegans* genes sharing a human orthologue. About 80% (6,329 clones) of those clones are present in the Ahringer RNAi feeding library (Kamath, Fraser et al. 2003).

In order to streamline the identification of relevant PHB interactors for human health, we assembled the OrthoList RNAi sub-library, maintaining the original name of the published compendium of *C. elegans* genes having human orthologues (Shaye and Greenwald 2011). The generated "OrthoList RNAi sub-library" contains a total of 6,315 RNAi clones, since 14 clones from the Ahringer RNAi library did not grow during the preparation of the sub-library. The 6,315 bacterial clones, that correspond to 6,179 different genes, were organized into 72 96-well plates, leaving empty the last column of the plates for adding the pertinent controls.

As a quality control for the OrthoList RNAi library, we sequenced 144 wide spread clones, of which 131 were identified correctly, corresponding to 91% of the bacterial clones being reliable. In 2011, Qu *et al.* performed an evaluation of the Ahringer *C. elegans* library (Qu, Ren et al. 2011), carrying out a bioinformatics analysis and resolved that 98.3% of the clones are trustworthy, even though 17.5% of the clones needed to be re-annotated. Taking into account these numbers, we concluded that the OrthoList RNAi sub-library that we generated represents a high-quality tool.

The resultant OrthoList RNAi library will be of considerable advantage for

C. elegans researchers to streamline RNAi screens by focusing on genes with translational potential to human health and reducing screening efforts by 60%.

Here, we present a functional genomic analysis of chromosome I using the OrthoList RNAi library. Chromosome I has 1,207 orthologous genes annotated, which correspond to 14 96-well plates. RNAi was initiated at the second larval stage and animals were imaged two days later, at the young adult stage.

4. High throughput image acquisition and analysis

After RNAi treatment, once worms reached the desired stage, we anesthetized the animals and washed off the bacteria from microtiter plates before imaging. Whole-well brightfield and green fluorescence images were taken sequentially using the IN Cell Analyzer 2000, an automated microscope designed for cell based high-content screening that we adapted for worm imaging using a 2x objective (figure 11a). Image analysis was performed with a user-defined protocol within the Developer Toolbox software (version 1.9.2) (GE healthcare), accompanying the IN Cell Analyzer 2000 that enables direct upload and analysis of image stacks. In this protocol, we defined four individual targets; a well edge (used to subtract out any well debris), a worm, a dilated worm (used to calculate intensity of the background adjacent to the worm) and a worm with green head (so these can be eliminated from the dataset downstream of image analysis) (figure 11 and appendix 2). In order to obtain all the required measurement regions in one target, individual targets were linked together. For two targets to be linked there must be at least one pixel overlap to achieve a linkage.

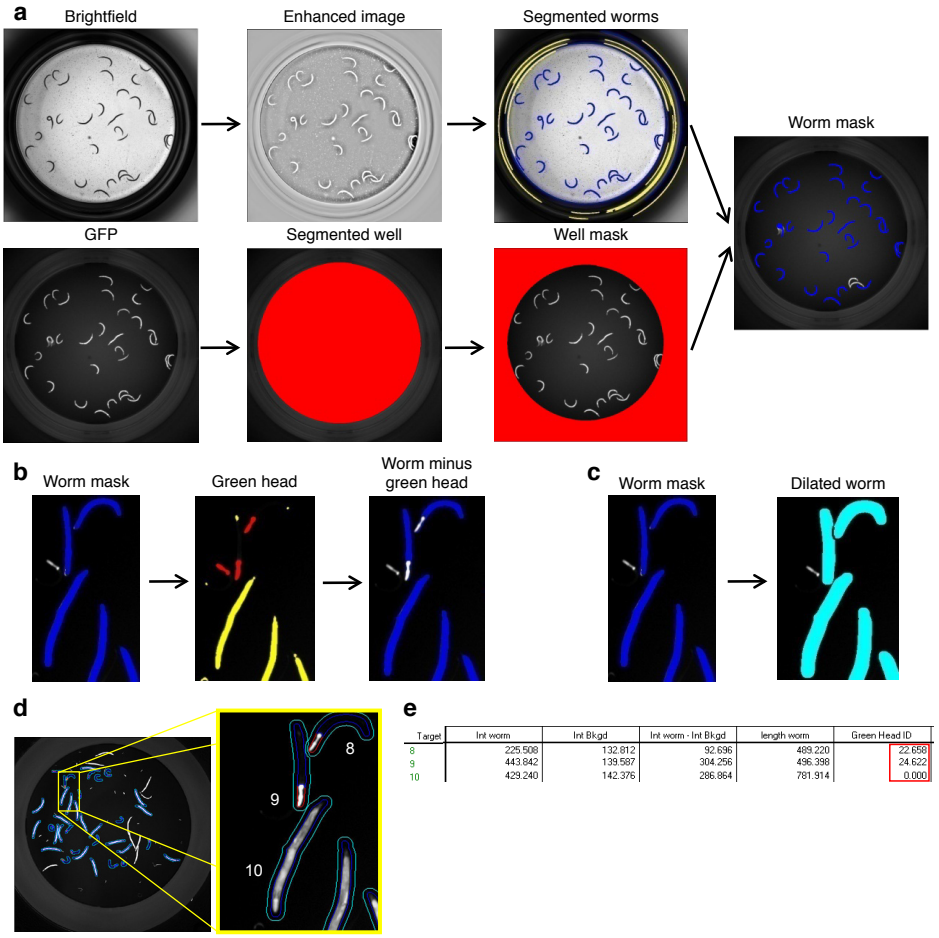

Figure 11: Outline of the image segmentation protocol for balanced mutants. a. Representative images acquired in brightfield and green channels. First, we segmented the well based on intensity in the green channel and we inverted the image (bottom). We subjected the brightfield image to pre-processing to enhance the contrast for ease of segmentation. The segmented worms are tagged in blue and excluded objects in yellow (top). Exclusion criteria are specified in Appendix 2. By subtracting the well mask from the segmented worms, we obtained the worm mask. **b.** Identification of heterozygous animals (green head ID). Once we defined the worm mask, we segmented green heads, tagged in red and in yellow are the excluded objects. Exclusion is based on area and intensity levels. The next step subtracted the identified green heads from the worm bodies. As a result, segmented worms appear blue without the green heads, "worm minus green head". **c.** Background subtraction. Segmented worms were dilated in order to facilitate measurement of the intensity of the immediate background. **d.** Target linking to compose one final target. Worm mask, dilated worm and worm minus green head targets were linked together. The final target shows the three measurement regions: worm in blue, immediate background in cyan and green head in red.

e. Identified targets with the corresponding measurements. Intensity of the worm (Int worm), intensity of the immediate background (Int Bkgd), background subtraction (Int worm – Int Bkgd), worm length and identification of green head (Green Head ID). Targets 8 and 9 correspond to heterozygous worms with a green head ID greater than 0. Additional measures like area, major axis length, X/Y position, form factor can be added as per user requirement.

Each target was created stepwise: First, we applied a pre-process if required, for example to enhance image contrast prior to segmentation; second, the target was segmented in order to generate a mask; and last, we used a sequence of post-processing operations to clean up the mask. Once we defined, optimized and linked together the targets, we acquired, on a per worm basis, measurements such as size, shape or intensity in the different channels.

In more detail, we first segmented the well mask using the auto fluorescence of the well edge in the green channel, and after post-processing refinement steps, we inverted the resultant segmentation mask to obtain the well edge (figure 11a, bottom). Next, we segmented the worms using the brightfield image; again, we applied a pre-process to create an enhanced image from which we segmented the worms (figure 11a, top). After post-processing refinement of the segmented worms, we subtracted the well mask to remove well artefacts. Finally, in order to remove unwanted objects such as long fibers, air bubbles or overlapping worms, we applied acceptance criteria (based on morphological parameters) and created the worm mask (figure 11a). Even though the sorting protocol was largely efficient, some heterozygous worms could still be present in the well. Due to the longer developmental time of *phb-2(tm2998)* homozygous mutants (Hernando-Rodriguez, Erinjeri et al. 2018), the heterozygous worms lay progeny before the mutants reach the young adult stage, and several larvae with green pharynx could be found in the wells. To eliminate these heterozygous

worms, we implemented the segmentation protocol by adding a step that identified worms with green pharynx. Once worms were well delineated, we segmented green heads in the green channel image and used acceptance criteria based in area and intensity to better define them (figure 11b). In order to measure the intensity of the immediate background of each worm, the worm mask was dilated creating a dilated worm (figure 11c). Eventually, we linked targets to get all regions together. The resultant target included all three measurement regions: a worm mask, a dilated worm mask and a worm minus green head mask (figure 11d). We identified worms with a green head by the green head ID value (see appendix 2_Break down of the image analysis protocol); a value greater than 0 indicates that a green head is present. A comprehensive list of measures, morphological and intensity based, for each worm was collected (figure 11e).

With this, we have developed the first automated segmentation protocol for balanced strains in *C. elegans*. High throughput imaging strategies specific to *C. elegans* have been developed using various microscopy platforms (Moy, Conery et al. 2009, Gosai, Kwak et al. 2010, Wahlby, Kamentsky et al. 2012, Maia, Tanenbaum et al. 2015). Like others, the IN Cell Analyzer (GE Healthcare) combines brightfield- and fluorescent-based imaging. We optimized image acquisition to include an entire well of a 96-well plate in a single image, ensuring even brightfield illumination by sealing the 96-well plate with a transparent seal. We ensured the acquisition of an entire 96-well in 2 channels in less than 10 minutes due to the optimized autofocus and scanning times of the IN Cell Analyzer. We built a user-defined, user-friendly image analysis protocol using the Developer Toolbox (GE Healthcare) software. Our segmentation protocol allows intensity-based measurements apart from other measures defined by the user like area, length, curvature, etc., and can be used for any strain

without the need of transgenesis as segmentation is done in the brightfield image. One novelty of this segmentation protocol is the measurement of the background surrounding each target. By dilating the targeted worm, we can easily measure and subtract the intensity of the immediate background. This is very appropriate in the cases of dyes that stain plastic or accumulate at the edges of the wells and can cause different background intensities depending on the area of the well. Another strong point of our image analysis protocol is the successful identification of worms carrying a pharyngeal GFP element. As COPAS sorting is not 100% efficient, heterozygous worms will develop into fertile adults and lay progeny in the wells. Hence, the need of distinguishing worms carrying the GFP-balancer from homozygous mutants. However, this identification strategy can be used for other purposes, like differentiating two populations in the same well.

It is interesting to point out that the COPAS can serve as an alternative to microscopy-based measurements as it can measure length, optical density and fluorescence emission of single worms (Squiban, Belougne et al. 2012{Zugasti, 2016 #79). However, image based microscopy platforms have several advantages: they are faster and images are stored, making them accessible for re-analysis. Also, much smaller number of animals is needed for image based assays as compared to the COPAS and thus, allows for exploration of a large number of different treatments in parallel, such as RNAi or drug screens. Another advantage of image-based screens is that multiple outputs can be examined from the image; fluorescent intensities in different channels, size and shape measurements.

5. Open sourcing of the segmentation protocol through CellProfiler

The segmentation protocol presented above is only compatible with the Developer Toolbox software and hence its usage is limited to researchers with access to the GE platform. To circumvent this, we implemented the protocol in the free and open source CellProfiler software (Carpenter, Jones et al. 2006, Wahlby, Kamentsky et al. 2012), providing an analysis pipeline identifying green head worms, and measuring fluorescence intensities.

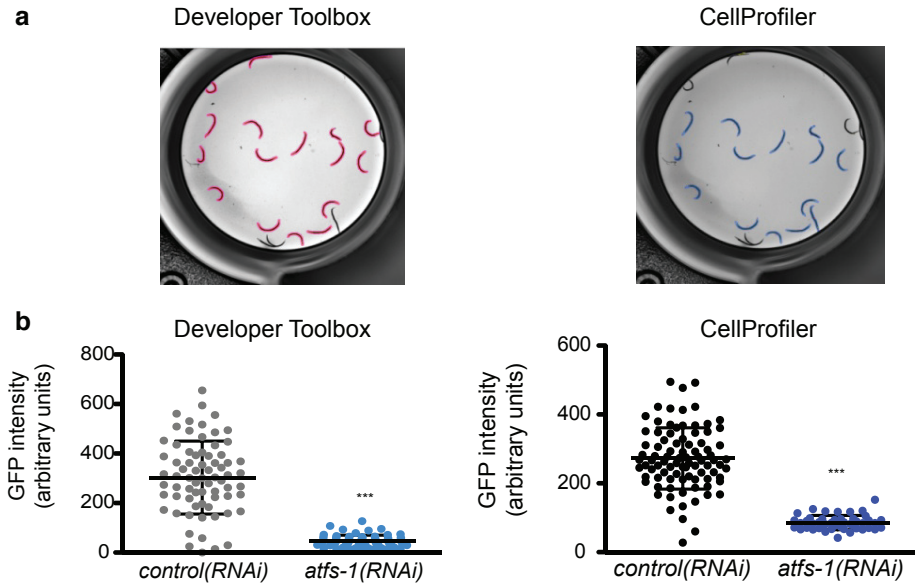

Figure 12: Open sourced segmentation protocol (CellProfiler). a. Comparison of the image segmentation output for *phb-2(tm2998)* mutants generated from Developer toolbox (GE Healthcare) versus CellProfiler. **b.** Comparison of the UPR^{mt} reporter signal after image analysis from Developer toolbox (GE Heathcare) versus CellProfiler. By comparing both dot plots we concluded that results from the different segmentation protocol are highly similar. (Mean ± SD; *** p value < 0.001; t-test). The complete breakdown of the CellProfiler protocol can be found in Appendix 3.

We compared worm segmentation outputs obtained from the Developer Toolbox and the CellProfiler and found them comparable (figure 12a). We also compared the intensity measures obtained from the Developer Toolbox and the CellProfiler by in *phb-2*;P*hsp-6*::GFP mutants in control(RNAi) and subjected to atfs-1(RNAi). Irrespective of the software used for segmentation and quantification, depletion of atfs-1 reduces drastically the mitochondrial stress reporter expression (figure 12b), thus, validating the method.

The image analysis protocol generated through the CellProfiler software can be visualized in appendix 3_Break down of the CellProfiler protocol, and is easily adaptable to the user's needs in terms of different fluorescent markers, image formats and image resolutions.

6. PHB interactors affecting the UPR^{mt}

In order to evaluate changes in GFP expression, a pipeline analysis consisting of several filtering steps, quality control and statistical test was computerized (see methods section). According to the results presented in figure 13a, the intensities measured in the negative (empty vector) and the positive (*atfs-1(RNAi)*) controls were clearly separable. Our RNAi screen was based on *C. elegans* genes annotated to chromosome I sharing orthologues with humans. We found 208 clones to be necessary for the PHB-mediated induction of the mitochondrial stress response, while only the inactivation of one gene, *acd-1,* induced the reporter signal to a greater extent (figure 13b). *acd-1* is an orthologue of members of the human SCNN (Sodium channels epithelial) family, which is involved in the response to acidic pH and is predicted to have sodium channel activity, based on its protein domain information.

Under our experimental conditions, we identified 45.5% of previously described genes required for the activation of the UPR^{mt} (Benedetti, Haynes et al. 2006, Haynes, Petrova et al. 2007, Haynes, Yang et al. 2010, Shore, Carr et al. 2012, Runkel, Liu et al. 2013). Moreover, based on the results from the functional annotation cluster analysis we identified genes, never described to be involved in the regulation of the UPR^{mt}, but belonging to pathways already established to suppress the mitochondrial stress response (figure 13c and table 2). We described a large group of genes encoding proteins of the two ribosomal subunits, genes encoding proteins associated with protein transport including nuclear importins, genes encoding proteasomal subunits and genes involved in mRNA processing.

Interestingly, many of these processes are related to proteostasis. Certainly, inhibition of translation can reduce the expression of any GFP reporter without having a direct effect on the mitochondrial stress response and one should investigate in more detail how silencing ribosomal subunits affects the UPR^{mt}. Nevertheless, it has been previously described that attenuating cytosolic protein synthesis strongly suppresses age-related mitochondrial degeneration in yeast models, including the pro-aging prohibitin mutants (Wang, Zuo et al. 2008). In agreement with this, studies in flies and worms support the hypothesis that inhibition of cytosolic translation is protective during mitochondrial dysfunction (Haynes, Yang et al. 2010, Liu and Lu 2010, Baker, Nargund et al. 2012, Nargund, Pellegrino et al. 2012, Shore, Carr et al. 2012, Houtkooper, Mouchiroud et al. 2013, Runkel, Liu et al. 2013).

Table 2: Candidates reducing the UPR^{mt} in *phb-2* deletion mutants and annotated to pathways previously involved in UPR^{mt} regulation

Ribonucleoproteins	
rps-15	40S ribosomal protein S15
rps-19	40S ribosomal protein S19
rla-0	60S acidic ribosomal protein P0
C37A2.7	60S acidic ribosomal protein P2
rpl-1	60S ribosomal protein L10a
rpl-13	60S ribosomal protein L13
rpl-17	60S ribosomal protein L17
rpl-7	60S ribosomal protein L7
mrpl-24	Probable 39S ribosomal protein L24, mitochondrial
snr-7	Probable small nuclear ribonucleoprotein G
snr-2	Probable small nuclear ribonucleoprotein-associated
rpl-14	Ribosomal protein, large subunit
rpl-30	Ribosomal protein, large subunit
rps-10	Ribosomal protein, small subunit
rps-20	Ribosomal protein, small subunit
Protein Transport	
apg-1	AdaPtin, Gamma chain (clathrin associated complex 1)
sec-8	Exocyst complex component 4
ran-4	Probable nuclear transport factor 2
bbs-9	Protein pthb1 homolog
rab-11.1	Ras-related protein rab-11.1
nsf-1	Vesicle-fusing ATPase
apb-3	Hypothetical protein
xpo-2/imb-5	Importin-beta-like protein
imb-3	Importin-beta-like protein
Proteasome	
rpn-10	26S proteasome non-ATPase regulatory subunit 4
pas-3	Proteasome subunit alpha type-4
pas-4	Proteasome subunit alpha type-7
pbs-5	Proteasome subunit beta type
rpt-5	Proteasome regulatory particle, ATPase-like
mRNA processing/splicing	
snr-7	Probable small nuclear ribonucleoprotein G
snr-2	Probable small nuclear ribonucleoprotein associated
cel-1	mRNA Capping Enzyme Like

In addition to genes already described to be regulators the UPR^{mt}, in this study we found new PHB interactors regulating the mitochondrial stress response such as the histone modifiers *pcaf-1* (histone acetyltransferases) and *met-1* (histone methyltransferase). Given the already described role of epigenetic modifications in regulating the UPR^{mt} (Merkwirth, Jovaisaite et al. 2016, Tian, Garcia et al. 2016), studying in more detail the involvement of these epigenetic markers would shed light in the molecular mechanism underlying the mitochondrial stress response and its impact on aging.

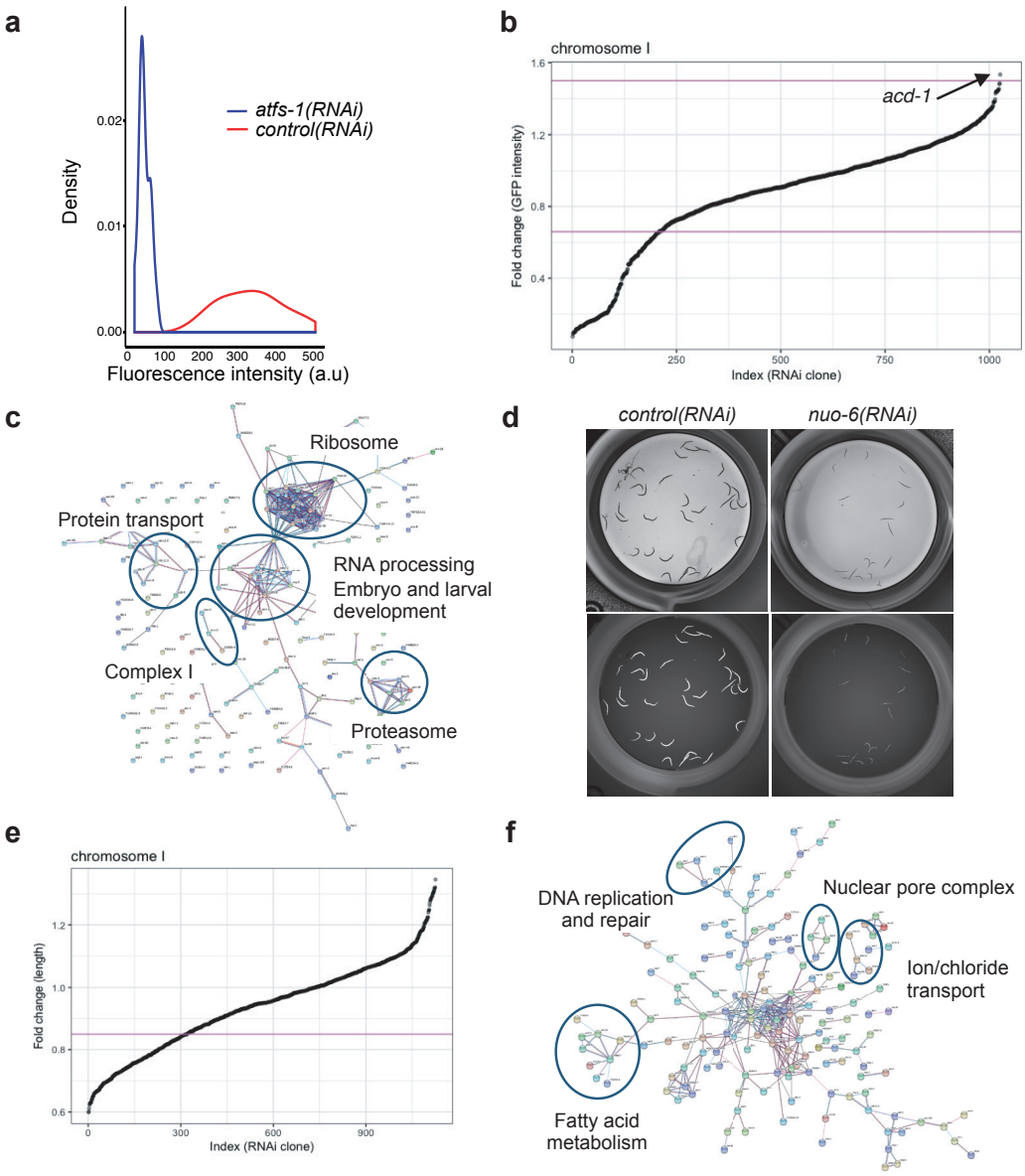

Figure 13: Analysis of the screening data. a. Frequency distribution of the negative (*control(RNAi)*) and positive controls (*atfs-1(RNAi)*) based on the GFP intensities. **b.** Fold change (FC) of GFP intensity of the 1,207 tested RNAi clones against the ordered index. Genes with a p value < 0.001 and a FC < 0.66 or FC > 1.5 were considered as candidates. Depletion of 208 RNAi clones down regulated P*hsp-6*::GFP signal whereas only one candidate triggered a further induction of the reporter. **c.** Interaction network of the 208 genes whose depletion reduced the UPR^{mt}. Networks were built using STRING: nodes are proteins and the edges represent the associations between nodes. Clusters showed genes involved in processes previously described to be

involved in the regulation of the UPR^{mt} such as ribosome, proteasome, RNA processing, protein transport and complex I of the mitochondrial electron transport chain (ETC). **d.** Brightfield and green images of *control(RNAi)* and *nuo-6(RNAi)*. Depletion of NUO-6 triggered a developmental delay in addition to the reduction in the UPR^{mt} reporter expression. **e.** Fold change of worm length of the 1,207 tested RNAi clones against the ordered index. Genes with a FC < 0.85 were considered as clones affecting development. Depletion of 303 genes reduced size of the worms. **f.** Interaction network of the 303 genes whose depletion reduced the worm size. Networks were built using STRING, nodes are proteins and the edges represent the associations between nodes. Clusters showed genes involved in DNA replication and repair, fatty acid metabolism, ion channels and nuclear pore complex.

In comparison with previous screens, we found a big number of additional candidates, possibly due to the quantitative nature of our protocol. Moreover, this could be attributed to the differences in experimental conditions: chemical treatments or a temperature-sensitive mutant versus a mutant of the mitochondrial PHB complex, which might trigger the mitochondrial stress response through an alternative pathway.

We encountered as well a large number of genes involved in embryonic and larval development, as well as three genes encoding for subunits of the mitochondrial NADH dehydrogenase complex (Complex I), *nuo-2*, *nuo-6* and D2030.4 (figure 13c). A closer examination of these worms revealed that they had developmental defects (figure 13d).

7. PHB interactors affecting development

In addition to the quantification of P*hsp-6*::GFP expression, the image analysis allowed us to obtain many other measurements. In order to identify genetic interactors of PHB-2, we analyzed the size of the worms in the same manner as described for the expression of the *hsp-6* reporter but filtering only based on the exclusion of green pharynx (green head

ID > 0), maintaining the rest of the worms irrespective of their size. In this case, we set up a threshold of fold change (FC) < 0.85 to obtain the clones affecting size. We found 303 RNAi clones whose depletion led to smaller size, probably due to developmental delays (figure 13e). The fact that chromosome I is particularly enriched in essential genes partially explains this high number of identified interactions (Chu, Chua et al. 2014). The Ahringer laboratory has performed multiple RNAi screens and assigned biological functions to many genes (Fraser, Kamath et al. 2000, Kamath, Fraser et al. 2003). In addition, Ahringer and colleagues have described many phenotypes, such as embryonic lethality or developmental delay associated with RNAi depletion of individual genes in wild type worms. 31% of the described RNAi clones that caused a developmental delay in wild type animals also affected development of *phb-2* mutants. As mentioned before, experimental procedures and strains were different and could explain the non-complete replicability. The *phb-2* mutants have *per se* a developmental delay and RNAi treatment was performed from the L2 stage instead of from eggs. Therefore, L1 acting genes could have been missed. As expected, among the genes affecting development we found genes encoding ribosomal subunits, proteasome subunits and genes involved in protein transport. Moreover, we identified many genes implicated in fatty acid metabolism, such as *lbp-5, acox-1.3 (F08A8.3), F10G8.9, acdh-3, acdh-4* and *ech-1.2 (T08B2.7)*. By performing protein-protein interaction analysis (figure 13f) we described a cluster of genes encoding for nuclear pore complex proteins (*npp-2, npp-4, npp-6, npp-7*), as well as a cluster of genes involved in DNA replication/repair (*cdt-1, crn-1, msh-6* and *rpa-4*) and meiotic spindle organization (*aspm-1*) and chromosome segregation (*icp-1*). Interestingly, genes implicated in DNA replication/repair and chromosome segregation seem to be PHB specific, as no developmental phenotypes have been previously described for these

genes in other RNAi screens. It would be highly relevant to study in more detail why genes involved in these processes affect the development of prohibitin mutants.

Chapter II:

Genome-wide RNAi screen to identify UPR^{mt} modulators upon PHB depletion in wild type animals and insulin signaling mutants

1. The UPR^{mt} is required for the enhanced longevity of *daf-2* mutants and PHB-depleted *daf-2* mutants

PHB depletion has a differential effect in lifespan as well as in the induction of the mitochondrial stress response depending on the genetic background: Lack of PHB shortens longevity and triggers a very strong induction of the UPR^{mt} in otherwise wild type worms while in the long-lived *daf-2(e1370)* mutants, the induction of the UPR^{mt} is reduced and lifespan is extended (Artal-Sanz and Tavernarakis 2009, Gatsi, Schulze et al. 2014). Since the link between the UPR^{mt} and longevity remains unclear, we analyzed whether the UPR^{mt} was necessary for the enhanced lifespan of *daf-2* mutants upon PHB depletion.

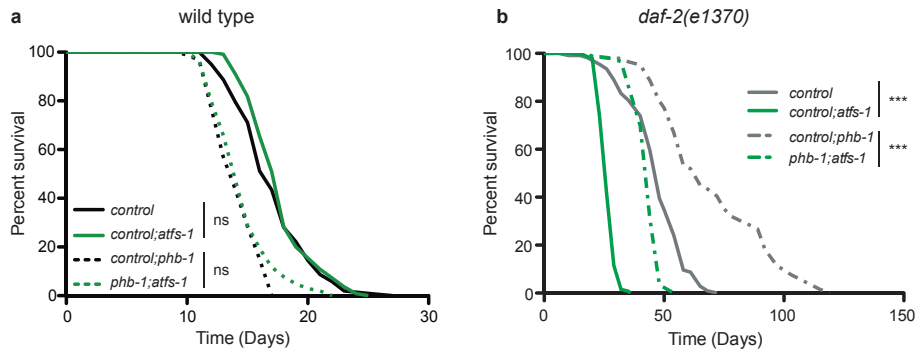

Figure 14: The mitochondrial stress response is required for *daf-2* mutants' lifespan. a. Depletion of ATFS-1 did not affect lifespan of wild type worms nor lifespan of *phb-1(RNAi)*. **b.** Depletion of ATFS-1 shortened lifespan of *daf-2(e1370)* mutants as well as *daf-2;phb-1(RNAi)* mutants. One representative replica out of minimum two independent replicas is shown, each with n > 120.

Depletion of *atfs-1* by RNAi did not affect the lifespan of wild type or PHB-depleted worms (figure 14a), whereas lack of ATFS-1 fully suppressed the extension conferred by *phb-1* depletion to *daf-2* mutants. Moreover, ATFS-1 depletion drastically reduced the lifespan of *daf-2* mutants (figure 14b).

This result shows that the UPR^{mt} is required for the enhanced lifespan of *daf-2* mutants, indicating that two mitochondrial quality controls, mitophagy and UPR^{mt}, play an important role in IIS mutants' longevity. In addition, it suggests that UPR^{mt} is fully responsible for the increment of lifespan upon PHB depletion in *daf*-2 mutants.

Our objective was then to identify new genetic interactors of PHB, to shed light in the molecular mechanisms of the mitochondrial stress response, both in wild type and in IIS mutants, to assess the role of the IIS pathway in mitochondrial protection. To achieve this, we aimed to complete a genome-wide RNAi screen in two genetic backgrounds, PHB deletion mutants and PHB;IIS double mutants, and in duplicate. Although the above described technique (Hernando-Rodriguez, Erinjeri et al. 2018) is efficient in selecting and sorting homozygous PHB mutants inducing the UPR^{mt} reporter, sorting animals posed a bottleneck and we decided to try a double RNAi strategy.

Double RNAi strategies have been already described to be efficient in knocking down two genes simultaneously. Some studies suggest that feeding worms with bacteria that expresses the two dsRNA in the same plasmid is more efficient than mixing two bacterial cultures (Gouda, Matsunaga et al. 2010, Min, Kang et al. 2010). Nevertheless, the mixture of bacterial cultures has been successfully used in many others studies (Lehner, Tischler et al. 2006, Tischler, Lehner et al. 2006, Jadiya and Nazir 2014). We tried to accomplish our objective by mixing the bacterial cultures of the Ortholist RNAi sub-library with *phb-1(RNAi)* bacteria, due to the impossibility of re-designing the whole library with bacteria containing two dsRNA in the same plasmid. Because double RNAi has never been used for screening purposes, in the following sections we provide evidence that double RNAi is suitable for genome-wide studies.

2. Validation of double RNAi strategy

We first ensured that the phenotypes previously observed upon PHB depletion were reproducible when diluting *phb-1(RNAi)* with *control(RNAi)*. Western blot analysis showed that *control(RNAi);phb-1(RNAi)* reduced expression of PHB in both, wild type and *daf-2(e1370)* mutants (figure 15a). When assayed for longevity, diluted *phb-1(RNAi)* recapitulated the already described lifespan phenotypes, i.e. it caused lifespan shortening in wild type worms and lifespan enhancement in the already long-lived *daf-2(e1370)* mutants (figure 15b) (Artal-Sanz and Tavernarakis 2009). As previously mentioned, depletion of PHB induces the UPR^{mt} to a different extent depending on the genetic background; while in wild type worms lack of prohibitin induces a very strong mitochondrial stress response, in the IIS mutants *daf-2(e1370)* this activation is partially reduced (Gatsi, Schulze et al. 2014). Treating worms with *control(RNAi);phb-1(RNAi)* induced the UPR^{mt} in wild type and in *daf-2(e1370)* mutants, recreating the background-dependent induction of the UPR^{mt} upon PHB depletion, with a stronger activation in otherwise wild type worms than in *daf-2(e1370)* mutants (figure 15c). In both cases the induction of the mitochondrial stress response was completely abolished upon *atfs-1(RNAi)* (figure 15c). These results confirm that diluting *phb-1(RNAi)* with *control(RNAi)* is efficient in silencing gene expression and leads to the already described phenotypes upon PHB depletion.

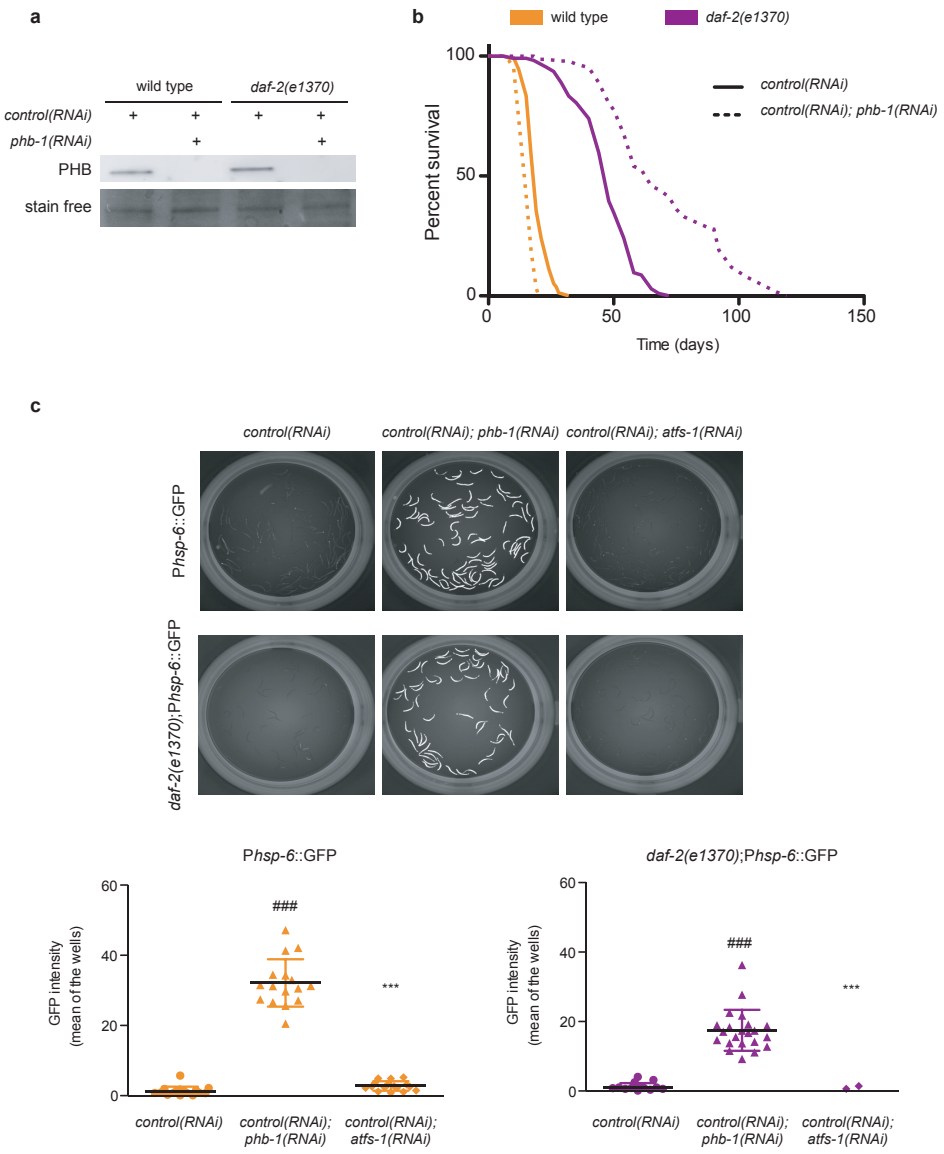

Figure 15: Double RNAi recapitulates de PHB depletion phenotypes. a. Western blot showing PHB protein levels. By combining *phb-1(RNAi)* with *control(RNAi)* PHB protein levels were undetectable both in otherwise wid type worms and in *daf-2* mutants. **b.** Lifespan of *phb-1(RNAi);control(RNAi)* was significantly shorter than wild type. Lifespan of *daf-2(e1370)* mutants was enhanced under *phb-1(RNAi);control(RNAi)*. One representative replica out of two is shown, each with > 120 worms. **c.** Fluorescent microscopy images of transgenic animals P*hsp-6*::GFP and *daf-2(e1370)*;P*hsp-6*::GFP treated with *control(RNAi)*, *phb-1(RNAi);control(RNAi)* and *phb-1(RNAi);atfs-1(RNAi)*. Graphical representation of quantification of P*hsp-6*::GFP (left panel) and *daf-2(e1370)*;P*hsp-6*::GFP (right panel). The dilution of *phb-1(RNAi)* with *control(RNAi)* induced the UPR^{mt} in both genetic backgrounds and the induction was suppressed

upon depletion of ATFS-1. (Mean ± SD; ### *p* value < 0.001 against *control(RNAi)*, *** *p* value < 0.001 against *control(RNAi);phb-1(RNAi)*, ANOVA test. One representative replica out of four independent replica is shown. Dots represent the mean intensities of all the worms in the well. n > 5 wells with more than 20 worms/ well in each condition).

In order to improve the accuracy of the screening, we optimized the different steps. Most of the RNAi screens are performed growing bacteria overnight in 96-wells and inducing the expression of the dsRNA by adding IPTG the next day, without monitoring the actual growth of the bacterial population (Fraser, Kamath et al. 2000, Kamath, Martinez-Campos et al. 2001, Lehner, Tischler et al. 2006). Nevertheless, one important issue of diluting RNAi is to do it in equal proportions and different bacteria expressing dsRNA might have different growth rates. For this reason, we analyzed the bacterial growth in the 96-well plates after overnight culture by measuring the OD_{600}. We observed that bacterial cultures were in stationary phase after the overnight incubation, with a reduced growth rate and an increased accumulation of metabolic waste products. The OD_{600} measured in the wells containing different cultures were elevated and differed from each other (figure 16a). On the other hand, dilution of the overnight culture by 1 in 10 refreshed the media, cells resumed growth and in approximately 1 hour they reached the optimal growth rate, exponential phase, and appeared to be at the healthiest state (figure 16b). We allowed the culture to grow for 3 hours in order to have a high number of cells and we induced the expression of dsRNA for 2 hours. At this moment, except H11, most of the wells showed a similar OD_{600}, corresponding approximatively to the same number of cells (figure 16b). In parallel, we grew *phb-1(RNAi)* following the same procedure in a flask.

We optimized as well the worm growing conditions, such us number of worms (we dispense 60 worms per well), amount of bacteria (40 µl of *phb-1(RNAi)* and 40 µl of the RNAi clone) and speed of shaking (120 rpm).

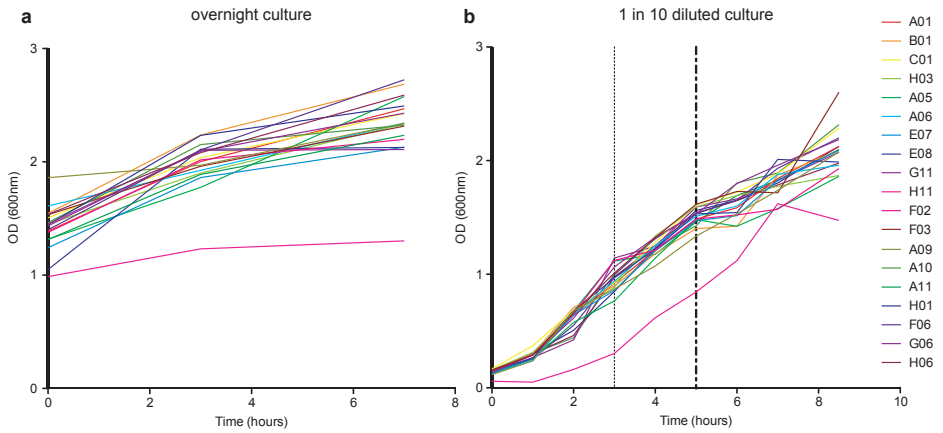

Figure 16: Optimization of bacterial growth in 96-wells plate format. a. Bacterial growth (OD600) curves of 19 random clones in a 96-well plate after an overnight incubation. Bacteria populations were in stationary phase and showed different OD600 between different clones. **b.** Bacterial growth curves of the same 19 clones in a 96-well plate after a 1:10 dilution from the overnight culture. Bacteria started to recover and after 1 hour on incubation they initiated the exponential phase. Moreover, different clones showed a similar OD600 during the first 5 hours of incubation, except one specific clone, H11. Dashed line at 3 hours represents the moment we induced the expression of the dsRNA and dashed line at 5 hours when we stoped the culture.

3. Quality controls of the genome-wide double RNAi screens

After verifying that *phb-1(RNAi)* diluted with *control(RNAi)* triggers the same lifespan and UPR^{mt} induction phenotypes we ascertained whether the strategy is suitable for a high-content studies. In order to give more strength to the data we carried out two biological replicates of the wide-genome screen using the Ortholist RNAi library in the two backgrounds; P*hsp-6*::GFP on *control(RNAi);phb-1(RNAi)* (hereinafter referred as *phb-1(RNAi)*) and *daf-2(e1370)*;P*hsp-6*::GFP on *control(RNAi);phb-1(RNAi)* (hereinafter referred as *daf-2; phb-1(RNAi)*). We dispensed starved L1s in

the 96 well-plates, we added the bacterial mix and we imaged them when they reach the young adult stage, 3 days after for *phb-1(RNAi)* and 4 days after for *daf-2;phb-1(RNAi)*.

Being the first genome-wide screen using double RNAi, we evaluated the quality of the assay. We observed that in the majority of the wells of the two backgrounds in both replicas, the number of worms was between 20 and 40 (figure 17a), even though we aimed at dispensing 60 worms per well. During the different steps, mostly washing and image analysis, some worms are lost. We analyzed more in details the positive controls (*atfs-1(RNAi)*) and the negative controls (empty vector) and we found that the distribution of the populations under the two treatments was separable (figures 17b and 17c). Having properly separated controls ensured that our screen set up is suitable for the detection of differences in expression level in a 96-well plate format. To assess how well positive and negative controls were separated we calculated the Strictly Standardized Mean Difference (SSMD) (Zhang 2007), which evaluates the magnitude of the differences between positive and negative controls per plate and gives solid statistical interpretation. All the screened plates (72 plates x 2 backgrounds x 2 biological replicates) showed a SSMDú ³ 3 (figure 17d), which is an indicator of good quality. We calculated the Pearson correlation coefficient to assess the reproducibility between replicates (figure 17e). We detected that in *phb-1(RNAi)* animals the reproducibility was very high, while in *daf-2;phb-1(RNAi)* mutants the variability increased.

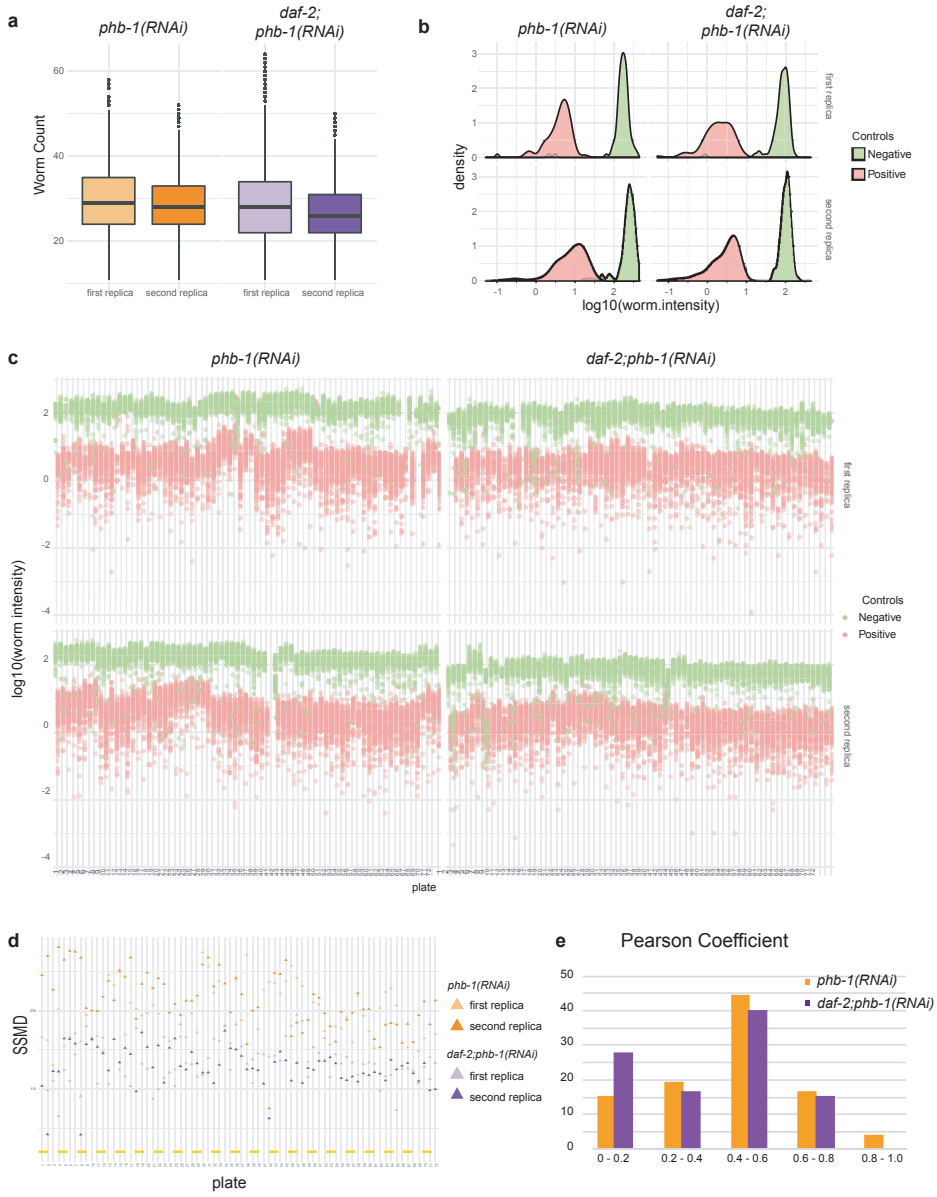

Figure 17: Quality controls of the double RNAi screens. a. Number of worms per well in all the screened plates in each of the replicas in both genetic backgrounds. By dispensing approximately 60 worms, after the complete process, we obtained in the majority of the wells between 20 and 40 worms. **b.** Frequency distribution of the negative (empty vector, green) and positive (*atfs-1(RNAi)*, red) controls based on GFP intensity. Data from one plate assayed in two independent replicas and in the two genetic backgrounds (*phb-1(RNAi)* and *daf-2;phb-1(RNAi)*) is shown. The controls were easily separable in this plate, in the 4 screens. **c.** GFP intensities in negative (empty vector) and positive (*atfs-1(RNAi)*)

control wells in all the screened plates. The controls were easily separable, being the intensity in the positive controls lower than the negative controls. **d.** Strictly Standardized Mean Difference (SSMD) of all the screened plates. Dashed yellow line marks an SSMD of 3, above which it indicates a good quality of the experiment. **e.** Pearson correlation coefficient between the 2 replicas in both backgrounds. In *phb-1(RNAi)* animals the reproducibility was very high, while *daf-2;phb-1(RNAi)* mutants showed a slightly increased variability.

All together, these results suggest that the double RNAi strategy by mixing bacterial culture in equal proportions is suitable for large scale screens. Different studies mentioned the advantages of working with RNAi-hypersensitive strain, such as *rrf-3* (Simmer, Tijsterman et al. 2002), *eri-1* (Kennedy, Wang et al. 2004) or *eri-1;lin-15B* (Wang, Kennedy et al. 2005), for the completion of a genome-wide study, even more when mixing two bacterial cultures. In our case, it was not necessary as we were able to reproduce the PHB depletion phenotypes. We described that in all the plates and both cases the controls were easily separable, confirming that the RNAi is being efficient. Nevertheless, we cannot ensure that the efficiency in silencing will not vary from gene to gene, and will be 100% efficient for all the genes from the library. By calculating the Pearson coefficient, we observed that *daf-2* mutants show a higher variability than wild type worms. This might be explained by the temperature sensitivity and t the developmental phenotypes of the *daf-2(e1370)* allele (Gems, Sutton et al. 1998), higher number of worms presenting dauer arrest as well as a higher percentage of embryonic or L1 arrest. Even so the reproducibility was adequate for the accomplishment of the genome-wide screen.

4. Overlap of the two different strategies: *phb-2* mutants vs *phb-1(RNAi)*

Next, we assessed the efficiency of the double RNAi screen by a functional analysis of 1,207 orthologue genes annotated to chromosome I present in

the Ortholist RNAi library. We compared the hits obtained when treating worms with *phb-1(RNAi)* and the Ortholist RNAi to those obtained by sorting *phb-2(tm2998)* mutants and treating them with single RNAi from the same Ortholist library. In order to make candidates comparable we used the data analysis described in Chapter I (Hernando-Rodriguez, Erinjeri et al. 2018). Briefly, worms with green pharynx (when needed) and worms with a length smaller than 550 μm were discarded. Wells with less than five worms were removed from the analysis. The normalization was by diving the GFP value of each worm by the mean of the GFP of the four negative control wells. Candidates were defined based on the adjusted *p* value coming from ANOVA test and the fold change (FC) (*p* value < 0.001 and FC < 0.66 or FC > 1.5).

We identified 208 RNAi clones, corresponding to 195 genes, that reduced the UPR^{mt} and only one gene, *acd-1*, whose depletion enhanced the mitochondrial stress response in *phb-2* mutants (figures 18a and 13b). When applying the same analytical pipeline, we found 126 RNAi clones reducing the UPR^{mt} and 10 clones that further increased the response in *phb-1(RNAi)* worms (figure 18b).

Among the genes whose depletion increased the response we did not find common clones between the two techniques. In contrast, we detected 50 genes whose depletion reduced the mitochondrial stress response in *phb-2* mutants as well as in *phb-1(RNAi)* (figure 18c). The overlap corresponds to the 25.6% of the candidates found with *phb-2* mutants and to the 39.7% of the candidates found upon *phb-1(RNAi)*. By performing double RNAi, we reduced the number of candidates that suppressed the mitochondrial stress response probably because *phb-2* mutants are more sensible than wild type worms subjected to double RNAi. Still, we were able to identify many of the already known interactors of PHB, such as *apg-1*, *ran-4*, *nsf-1* and

imb-3, annotated to protein transport or *snr-2* and *snr-7*, involved in mRNA processing, beside several ribosomal proteins (Hernando-Rodriguez, Erinjeri et al. 2018).

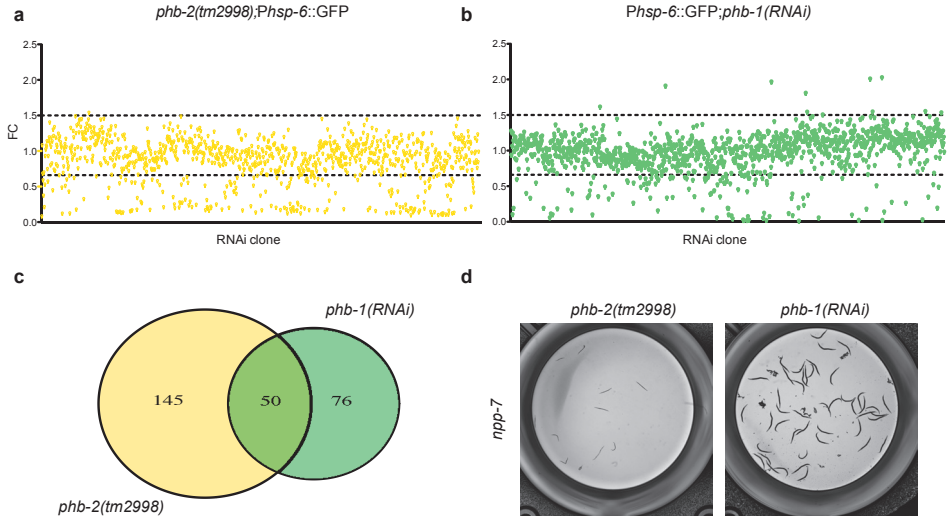

Figure 18: Comparing candidates from *phb-2(tm2998)* and *phb-1(RNAi)* screening. **a.** Fold change (FC) of GFP intensity of the 1,207 tested RNAi clones in *phb-2(tm1998)* mutants against the ordered index. **b.** Fold change (FC) of GFP intensity of the 1,207 tested RNAi clones in *phb-1(RNAi)* worms against the ordered index. Genes with a FC < 0.66 or FC > 1.5 were considered as candidates. Depletion of 208 RNAi clones (corresponding to 195 genes) down regulated P*hsp-6*::GFP expression whereas only one candidate triggered a further induction in *phb-2(tm1998)* mutants. In *phb-1(RNAi)* animals, 126 RNAi clones reduced P*hsp-6*::GFP expression and 10 clones triggered a further induction. **c.** Overlap between the clones down regulating the signal in *phb-2(tm1998)* mutants and in *phb-1(RNAi)* worms. **d.** Example of a gene *(npp-7)* whose depletion caused developmental arrest in *phb-2* deletion mutants and not in *phb-1(RNAi)* worms.

Moreover, we identified 76 new interactors, genes that were not detected when using *phb-2* deletion mutants. Among those we found genes encoding for Nuclear Pore complex Proteins, such as *npp-6* and *npp-7*, that caused developmental defects in *phb-2* mutants, and were excluded from the analysis, but not in *phb-1(RNAi)* (figure 18d). In addition, we found 10 new clones whose depletion induced the UPR^{mt} in *phb-1(RNAi)* worms. Among

those we identified *nuo-6* (NADH ubiquinone oxidoreductase), which in *phb-2* mutants appeared to reduce the mitochondrial stress response due to a delay in development (figure 13d).

Collectively we conclude that, even though we could be losing possible PHB interactors that would only appear using homozygous *phb-2* mutants, the less severe phenotype caused by the double RNAi strategy allowed the identification of new PHB interactors that would not be uncovered when using *phb-2* mutants.

5. PHB interactors affecting the UPR^{mt}: Data analysis using RNAither

The pipeline we used for the functional analysis of genes annotated to chromosome I, both using *phb-2* mutants and *phb-1(RNAi)* was not a completely automated pipeline. In addition, it only allowed the visualization of the data in a per plate manner instead of a global visualization of the results. For these reasons, for the analysis of the genome-wide screens in *phb-1(RNAi)* worms and in *daf-2;phb-1(RNAi)* mutants, we first used RNAither, a statistical pipeline designed to give a list of significant genes from raw signal intensity data (Rieber, Knapp et al. 2009). We took the median intensity of each well as signal intensity.

Data coming from a low number of worms cannot be reliable, so we set up a lowest threshold in order to exclude wells with the 5% lowest worm count in the entire screen ($n < 12$). We applied the Z-score normalization, assuming that most of the RNAi clones in the plate would not have an effect on the signal intensity given that it is a genome-wide screen. The Z-score represents how many standard deviations from the mean the sample is and it

is calculated following the formula Z-score = (x - m) / s, being x the median of the sample, m the mean of the screen and s the standard deviation of the screen. RNAither has the possibility of performing lowess normalization, locally weighted polynomial regression, which is used when two data channels (signal intensity and worm count in this case) that are independent of each other show a tendency to be dependent. Even though this tendency has been shown in many screens, we did not observe such tendency in our case (data not shown).

We selected candidates based on the Z-score (Z score <-2 or Z-score > 2) and we observed that in *phb-1(RNAi)* worms, 454 RNAi clones reduced the UPR^{mt} and 156 RNAi clones further enhanced it. In *daf-2;phb-1(RNAi)* mutants, 467 RNAi clones decreased the signal and 179 RNAi clones increased it (figures 19a and 19b). We didn't find a big difference in the number of genes regulating the mitochondrial stress response depending on the background and in both cases the number of RNAi clones reducing the UPR^{mt} was higher than the number of candidates inducing it. The Venn Diagram shows the overlapping candidates between the two backgrounds, figure 19c. We found genes whose depletion regulated the UPR^{mt} in a background specific manner as well as genes whose depletion modulated the stress response in both backgrounds. It is worth noting that among the candidates reducing the UPR^{mt} in the two backgrounds there was a big overlap; 306 candidates corresponding to 67% of the candidates of *phb-1(RNAi)* and 65% of the candidates from *daf-2;phb-1(RNAi)* were common candidates. These candidates, reducing the mitochondrial stress response in a background independent manner, would be expected to be essential genes for the full activation of the response.

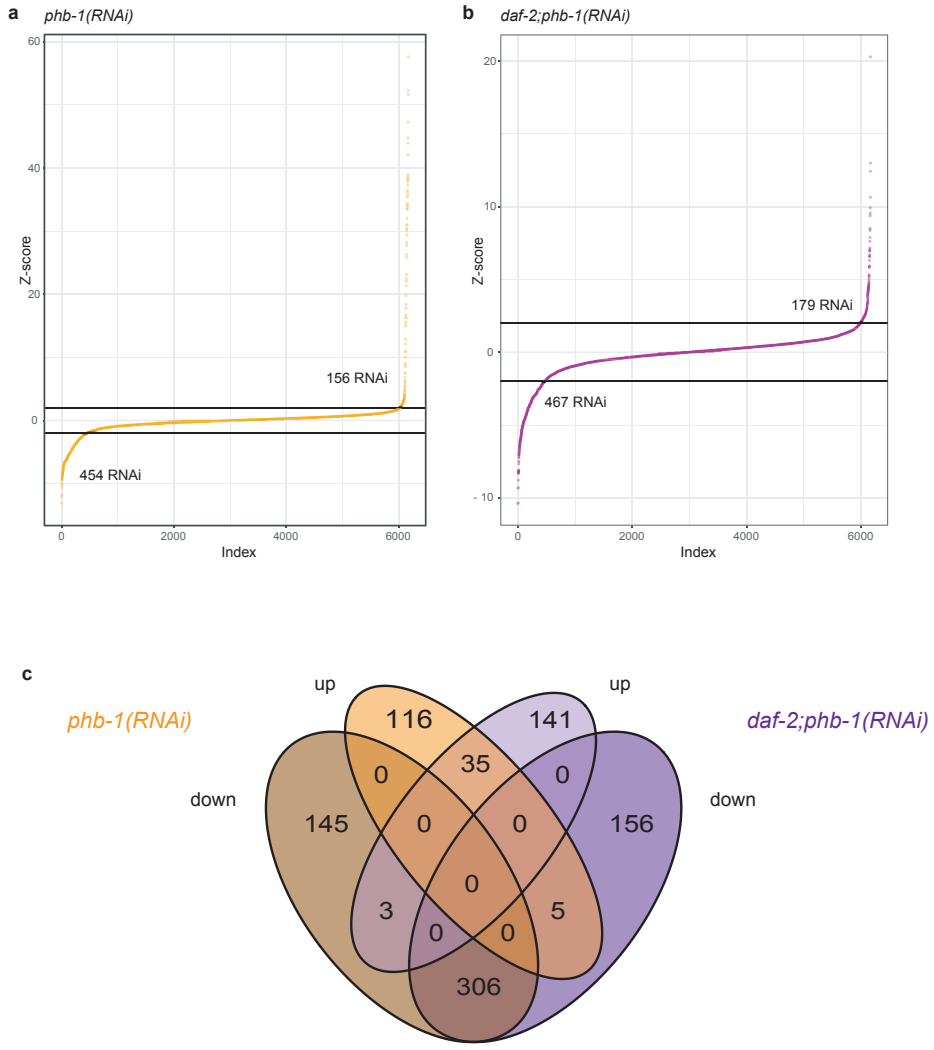

Figure 19: Analysis of GFP values using RNAither. a. Ordered Z-score of GFP intensity of all tested RNAi clones in *phb-1(RNAi)* animals. b. Ordered Z-score of GFP intensity of all the tested RNAi clones in *daf-2;phb-1(RNAi)* mutants. Genes with a Z-score < -2 or Z-score > 2 were considered as candidates. Depletion of 454 genes reduced P*hsp-6*::GFP signal and 156 RNAi clones further enhanced it in *phb-1(RNAi)* worms. Depletion of 467 genes reduced P*hsp-6*::GFP signal and 179 RNAi clones further enhanced it in *daf-2;phb-1(RNAi)* mutants. **c.** Venn Diagram showing the common and specific candidates of each background.

In addition, depletion of 8 clones showed opposing effect on the UPR^{mt} depending on the background; 3 RNAi inhibited the mitochondrial stress in *phb-1(RNAi)* worms while they activated it in *daf-2;phb-1(RNAi)* mutants

and 5 RNAi enhanced the UPR^{mt} in *phb-1(RNAi)* while they reduced it in *daf-2;phb-1(RNAi)* mutants (figure 19c). For a brief description see Box 1.

Box 1: Brief description of candidates with opposing effect:

1. Reducing in *phb-1(RNAi)* worms and increasing in *daf-2;phb-1(RNAi)* mutants

• *max-1* encodes a PH/MyTH4/FERM domain-containing protein that is required for proper motor axon projections (Huang et al. 2002). Depletion of *max-1* increases lifespan in a DAF-16 dependent manner (Hamilton et al. 2005) and results in a synthetic severe growth defect in *ire-1* mutants (Sakaki et al. 2012).

• *haf-9* encodes an ATP-binding cassette (ABC) transporter homologue to the lysosomal peptide transporter associated with antigen processing-like, ABCB9 (TAPL). Together with HAF-4, it localizes in the membrane of intestinal organelles, distinct to lipid droplets but associated with endocytic pathway (Tanji et al. 2016). *haf-4(RNAi)* reduced UPR^{mt} in *phb-1(RNAi)* while did not affect *daf-2;phb-1(RNAi)*.

• *rde-12* encodes a conserved Vasa ATPase-related protein. It functions in production of siRNA involved in RNA interference and is involved in response to exogenous dsRNA (Shirayama et al. 2014).

2. Increasing in *phb-1(RNAi)* worms and reducing in *daf-2;phb-1(RNAi)* mutants

• *sti-1* encodes the orthologue of the Sti1/Hop family of heat shock co-chaperones and plays a role in stress response. Lack of STI-1 shortens lifespan and decreased fertility and thermo-tolerance, possibly acting together with DAF-16 (Gaiser et al. 2009, Song et al. 2009).

• *hrpu-1* is a heterogeneous nuclear RibonucleoProtein U. It has been described as a splicing mediator, regulating a significant part of the alternative splicing and required for the caloric restriction- mediated longevity (Tabrez et al. 2017).

• *gbf-1* is an orthologue of human golgi brefeldin A resistant guanine nucleotide exchange factor 1 (GBF1). It is involved in endoplasmic reticulum organization, endosomal transport and mitochondrial organization (Ackema et al. 2013, Ackema et al. 2014).

• *dhs-28* encodes an orthologue of 17-beta-hydroxisteroid dehydrogenase 4. Lack of *dhs-28* alters lipid composition (Zhang et al. 2010) and content (Butcher et al. 2009). In addition, *dhs-28(RNAi)* suppresses the lengthened defecation cycle of mitochondrial mutants *ckl-1(qm30)* (Liu et al. 2012).

• *dld-1* encodes an orthologue of the dihydrolipoamide dehydrogenase (DLD). Its depletion by RNAi results in induction of P*gst-4*::GFP, P*hsp-4*::GFP and P*hsp-6*::GFP (Melo and Ruvkun 2012) and shortens lifespan (Butler et al. 2013).

Based in bibliography, some candidates appeared particularly interesting: depletion of *max-1* (in our hands, reducing UPR^{mt} in *phb-1(RNAi)* and increasing UPR^{mt} in *daf-2;phb-1(RNAi)*) has been described to regulate lifespan in a DAF-16 dependent manner (Hamilton, Dong et al. 2005) and to cause development defects in *ire-1* mutants (Sakaki, Yoshina et al. 2012); lack of *sti-1* (in our hands increasing UPR^{mt} in *phb-1(RNAi)* and reducing UPR^{mt} in *daf-2;phb-1(RNAi)*) shortens lifespan and decreased fertility and thermo-tolerance, possibly acting together with DAF-16 (Gaiser, Brandt et al. 2009, Song, Lee et al. 2009); depletion of *hrpu-1* (in our hands increasing UPR^{mt} in *phb-1(RNAi)* and reducing UPR^{mt} in *daf-2;phb-1(RNAi)*) suppressed the caloric restriction- mediated longevity (Tabrez, Sharma et al. 2017); and suppression of dld-1 (in our hands increasing UPR^{mt} in *phb-1(RNAi)* and reducing UPR^{mt} in *daf-2;phb-1(RNAi)*) induces different stress responses (Melo and Ruvkun 2012) and shortens lifespan (Butler, Mishur et al. 2013).

a. GO term enrichment analysis

Next, we performed on both backgrounds a Gene Ontology (GO) term analysis for identifying enrichment of biological processes, molecular functions, and cellular compartments, incorporating the RNAi clones that down-regulated and up-regulated the UPR^{mt}, using the Database for Annotation, Visualization and Integrated Discovery (DAVID, (Huang da, Sherman et al. 2009)) (appendix 4_GO terms enrichment). Fold enrichment of GO terms are plotted against the –log of the FDR adjusted *p* value (figure 20). Development and reproduction were the most significantly enriched pathways in both backgrounds. Pathways related to protein synthesis, like translation, ribosome and RNA splicing, also appeared enriched in both backgrounds. Interestingly, U4snRNP, one of the five major components of the spliceosome, was in both cases the cellular component with the highest

fold enrichment. In addition, we found enrichment in both backgrounds of the proteasome complex, which is involved in protein degradation.

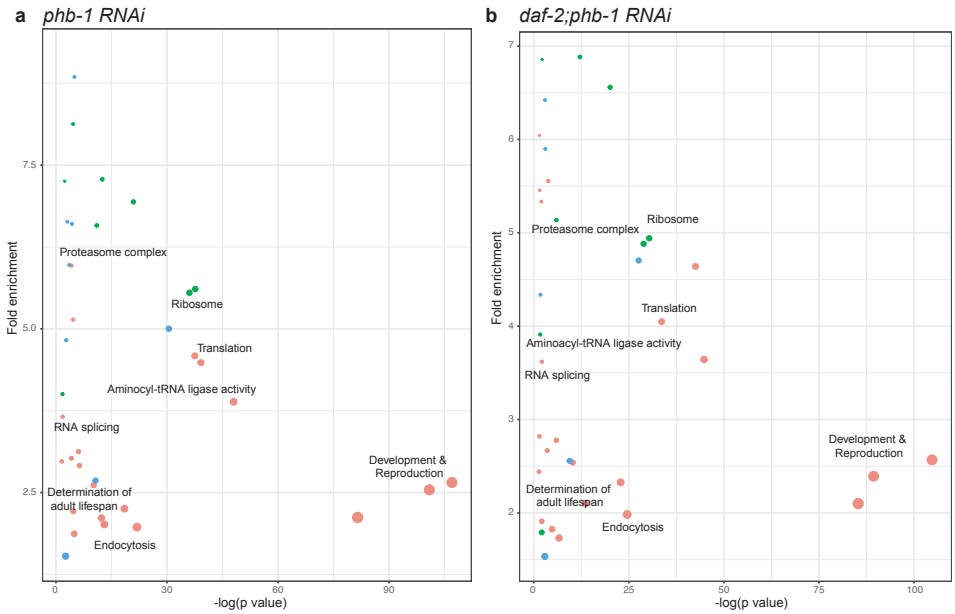

Figure 20: GO term enrichment analysis. Fold enrichment of Gene Ontology (GO) term against the –log10 *p* value in *phb-1(RNAi)* worms (left panel) and in *daf-2;phb-1(RNAi)* mutants (right panel). The enrichment analysis was performed taking together genes whose depletion reduced and increased the mitochondrial stress response. Each bubble represents a GO term, blue represent molecular functions, red biological processes and green cellular compartments. The size of the bubbles displays the number of genes annotated to each GO term that are present in the study. Development and reproduction were the most significantly enriched pathways in both backgrounds. Pathways related to protein synthesis, like translation, ribosome and RNA splicing, also appeared enriched in both backgrounds.
In Appendix 4 we find the complete list of enriched GO terms in *phb-1(RNAi)* animals and in *daf-2;phb-1(RNAi)* mutants. GO terms are classified in Biological Processes (BP), Molecular Functions (MF) and Cellular Compartments (CC). "Count" represents the number of genes annotated to the GO term present in the study.

In general, we observed GO terms related to proteostasis, a process that has already been described to be regulating the mitochondrial stress response (Haynes, Yang et al. 2010, Liu and Lu 2010, Baker, Nargund et al. 2012, Nargund, Pellegrino et al. 2012, Shore, Carr et al. 2012, Houtkooper,

Mouchiroud et al. 2013, Runkel, Liu et al. 2013), thus supporting the validity of our screen. In addition, we uncovered that those processes are involved in the regulation of the UPR^{mt} in a IIS independent manner.

b. KEGG pathway enrichment analysis

The GO term analysis did not reveal any mechanism to explain the mitochondrial protection in the IIS pathway mutants, that could shed light on the differential aging phenotype caused by PHB depletion. Thus, we performed a new enrichment analysis based on the Kyoto Encyclopedia of Genes and Genomes (KEGG) pathway database (Kanehisa, Sato et al. 2016) in both backgrounds, taking together the RNAi clones that down-regulated and up-regulated the UPR^{mt} (appendix 5_KEGG enrichment). In order to make the scale more visually friendly we divided the heat map in three, from the most enriched pathways to the less enriched ones. Figure 21a shows the most enriched common pathways. As previously described for wild type worms (Runkel, Liu et al. 2013), inhibition of ribosomal proteins affected the UPR^{mt} in both backgrounds, as well as depletion of genes related with oxidative phosphorylation. Other pathways involved in proteostasis like spliceosome and proteasome appeared to be regulating the mitochondrial stress response in a background independent manner. We also found RNA transport and phagosome.

Figure 21b shows many other pathways involved in the regulation of the UPR^{mt} in *phb-1(RNAi)* worms as well as in *daf-2(e1370);phb-1(RNAi)* mutants. Among them we found pathways involved in amino sugar metabolism, nucleotide metabolism, DNA replication and repair, DNA transcription, translation, protein folding and degradation, and finally, pathways implicated in signal transduction like MAPK, Wnt, Notch and TGF-β signaling pathways.

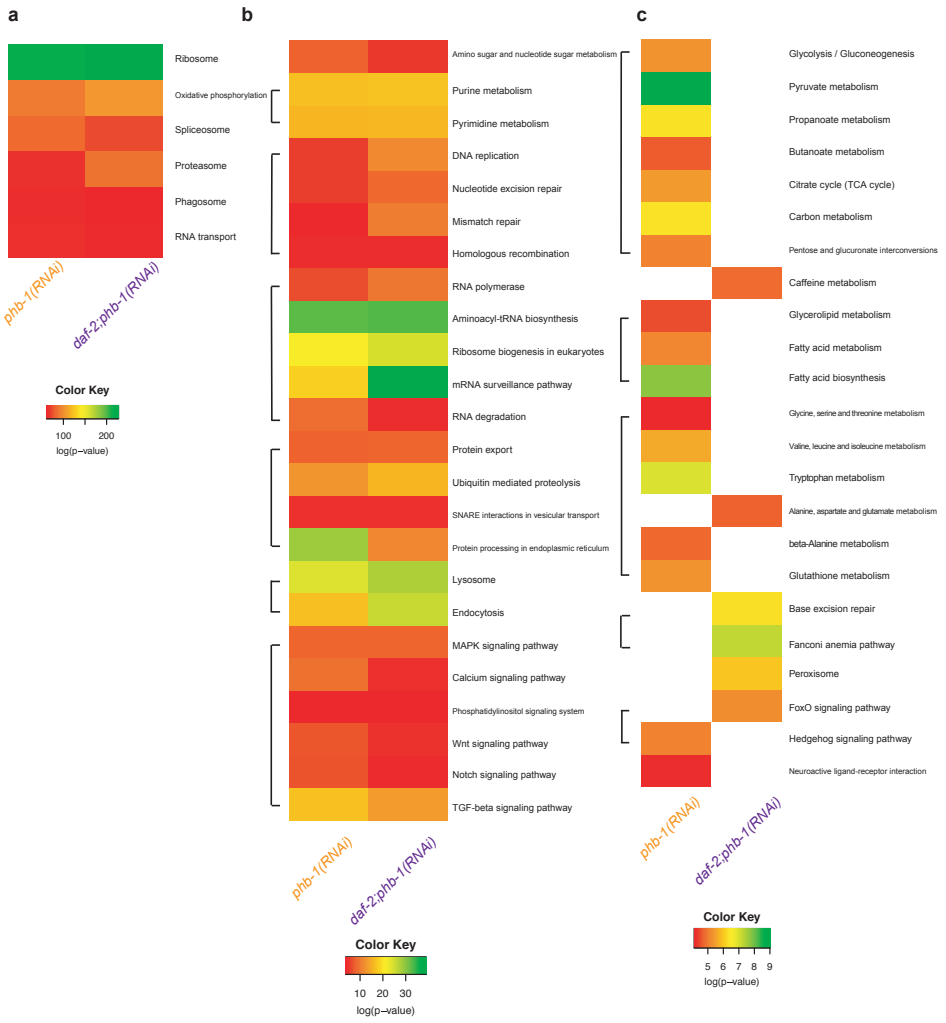

Figure 21: KEGG pathway enrichment analysis. Heat map representing the Kyoto Encyclopedia of Genes and Genomes (KEGG) pathway enrichment analysis in both backgrounds. In order to facilitate visualization, the heat map has been divided in three, based in the –log *p* value scale: the most enriched pathways (**a**), moderate enriched pathways (**b**) and pathways enriched specifically in each of the backgrounds (**c**). Ribosome, oxidative phosphorylation, spliceosome, proteasome, phagosome and RNA transport are the most strongly enriched pathways in an IIS independent manner. Pathways related with carbohydrate and lipids were enriched specifically in *phb-1(RNAi)* worms whereas peroxisome was specifically enriched in *daf-2;phb-1(RNAi)* mutants.

In Appendix 5 we find the complete list of enriched KEGG pathways in *phb-1(RNAi)* animals and in *daf-2;phb-1(RNAi)* mutants. "Proteins" represents the number of genes annotated to the KEGG pathway and "hits" the number of genes present in the study.

A general role in mitochondrial homeostasis and function has been already described for Wnt signaling pathway (Yoon, Ng et al. 2010, Brown, Yang et al. 2017), Notch signaling (Perumalsamy, Nagala et al. 2010, Basak, Roy et al. 2014, Xu, Chi et al. 2015) and TGF-β (Jain, Rivera et al. 2013, Liu and Desai 2015). MAPK signaling has been identified to be activated under ER stress (Hung, Su et al. 2004, Li and Holbrook 2004, Darling and Cook 2014), as well as in some cell lines, inhibition of JNK reduces UPR^{ER} (Verma and Datta 2010, Li, Xu et al. 2013). In addition, mitochondrial oxidative stress induces the MAPK signaling. Recently, Wnt signaling has been described as necessary for the cell non-autonomous UPR^{mt} induction (Zhang, Wu et al. 2018). Moreover, it has been suggested a dual role for PHB as a determinant of TGF-β induced apoptosis and MAPK survival signaling in early stages of tumorigenesis (Zhu, Zhai et al. 2010), as well as a role in aging in *C. elegans* as PHB depletion increases lifespan of animals defective in TGF-β signaling (Artal-Sanz and Tavernarakis 2009). In general, we conclude that evolutionary conserved signaling pathways are involved in the regulation of the mitochondrial stress response, in an IIS pathway independent manner. This suggests that none of these signaling pathways are responsible for the protection against mitochondrial stress observed in *daf-2* mutants.

Last, we identified pathways enriched specifically in only one of the backgrounds (figure 21c). Interestingly in *phb-1(RNAi)* worms we found mostly pathways related with carbohydrate, lipid and amino acid metabolism while those pathways did not appear as regulators of the mitochondrial stress response in *daf-2;phb-1(RNAi)* mutants. Previous work from our group (Lourenco, Munoz-Jimenez et al. 2015) showed that prohibitin depletion altered fatty acid composition leading to an increment in the content of short chain and saturated fatty acids. It is important to

note that the effect in the fatty acid composition upon prohibitin depletion was stronger in wild type worms than in *daf-2(e1370)* mutants. In a similar manner, metabolism of amino acid and carbohydrates was affected more by lack of prohibitin in wild type worms than in *daf-2(e1370)* mutants. Those observations suggest that IIS mutants are more robust and resistant to energy metabolism modifications triggered by PHB depletion. In addition, it has been reported that *daf-2(e1370)* mutants show a shift in metabolism, relying more in the glyoxylate cycle and therefore reducing the expression of the TCA cycle components (Ruzanov, Riddle et al. 2007, Depuydt, Xie et al. 2014). In agreement, we observed that the TCA cycle, Pyruvate metabolism and Glycolysis/Gluconeogenesis specifically enriched within the genes affecting the UPR^{mt} in *phb-1* depleted worms and not in *daf-2* mutants as these processes are differentially expressed in these worms (Dong, Venable et al. 2007).

On the other hand we observed that depletion of genes related with peroxisome affected specifically *daf-2;phb-1(RNAi)* mutants. Peroxisomes are organelles involved in metabolism and required for normal development (Thieringer, Moellers et al. 2003). They carry out the b-oxidation of very long chain fatty acids, the α-oxidation of branched chain fatty acids and synthesis of ether-linked phospholipids. They also generate reactive oxygen species and reactive nitrogen species and possess protective mechanisms to counteract oxidative stress. They are considered as potential regulators of oxidative stress-mediated signaling pathways and thus involved with age-related diseases (Fransen, Nordgren et al. 2012, Nordgren and Fransen 2014). The peroxisomal transport mechanism is essential for peroxisomal functions, import of substrate for b-oxidation, import of CoA for acyl-CoA synthesis, as well as export of the products of peroxisomal metabolism (Rottensteiner and Theodoulou 2006). Due to their overlapping functions,

peroxisomes and mitochondria appear to be intimately linked and the interplay between the two organelles could be important in the context of aging (Ivashchenko, Van Veldhoven et al. 2011). Narayan *et al*. (Narayan, Ly et al. 2016) performed a deep proteome analysis to identify age-related processes. They showed a reduction in about 30 proteins during aging that were involved in peroxisomal protein import and function, indicating an impairment in peroxisomal import during aging in wild type worms. Besides, they showed that F55B11.1 (*xdh-1*), a peroxisomal gene involved in purine metabolism, was more highly expressed in *daf-2* mutants compared to wild type worms during aging, even though its tendency was to decrease throughout aging. Finally, it has been shown that lack of peroxisomal b-oxidation in ASK neurons induces the UPR^{ER} and interrupts the pheromone induced dauer development (Park and Paik 2017). Moreover, by quantitative proteomics of the interactome of Pex14p, Oeljeklaus and colleagues identified both, PHB1 and PHB2, as transient interaction partners of the peroxisomal importomer (Oeljeklaus, Reinartz et al. 2012).

6. Assaying the role of peroxisomes in the UPR^{mt}

All together, these results led us to the question of whether the reduced UPR^{mt} and the increased lifespan of IIS mutants is, at least in part, linked to peroxisomal function.

Therefore, we searched for genes annotated to peroxisome present in our screen, and found that depletion of *prx-12*, *xdh-1* and F18F11.1 induced the UPR^{mt} in *daf-2;phb-1(RNAi)*, without having an effect in *phb-1(RNAi)*. Besides, depletion of *prx-19* further reduced the response in *daf-2;phb-1(RNAi)* mutants but did not affect *phb-1(RNAi)* (table 3).

Table 3: Candidates annotated to peroxisome

RNAi	Z score in *phb-1(RNAi)*	Z score in *daf-2;phb-1(RNAi)*	gene description
prx-12	-0,850	5,314	orthologue to human Pex12, peroxisomal biogenesis factor
xdh-1	0,632	2,420	orthologue of the human xantine dehydrogenase, XDH
F18F11.1	0,827	2,013	orthologue of peroxisomal membrane, PXMP4
prx-19	0,167	-2,157	orthologue to the human peroxisomal farnesylated protein, PXF

prx-12 and *prx-19* encode for two of the 11 *C. elegans* homologs of the 13 human peroxins. They are involved in peroxisome biogenesis and organization, mediating the import of proteins to the peroxisome. In the Ortholist RNAi library, there are others genes encoding for peroxins (*prx-2, prx-3, prx-5, prx-11, prx-13* and *prx-14*), whose depletion did not modulate the UPR^{mt} in the genome-wide screen. *xdh-1* encodes one orthologue of the human xanthine dehydrogenase involved in purine metabolism. *C. elegans* has several homologues of the xanthine dehydrogenase, including F15E6.6 and *gad-3* that are present in the Ortholist library, but did not show any effect on the screen. Finally, F18F11.1 is an orthologue of the human peroxisomal membrane protein 4, PXMP4.

In order to validate our candidates and to analyze more in depth the possible role of peroxisomes in the regulation of the mitochondrial stress response, we re-tested the effect of depleting the candidates, as well as the related genes, in *phb-1(RNAi)* worms and in *daf-2;phb-1(RNAi)* mutants (figure 22). We observed that, opposing to the screening results, depletion of *prx-12, prx-19, prx-3, prx-11* and *prx-14* increased the mitochondrial stress response in *phb-1(RNAi)* (figure 22a). On the contrary, we confirmed that *prx-12(RNAi)* increased the response in *daf-2;phb-1(RNAi)* mutants while depletion of *prx-5* and *prx-13* reduced it; *prx-19(RNAi)* did not affect the response (figure 22b). Moreover, we observed that depletion of one of the xanthine dehydrogenases, *gad-3*, increased the GFP expression levels in *phb-1(RNAi)*, while the orthologue of PXMP4, F18F11.1, increased the signal in both backgrounds (figures 22c and 22d).

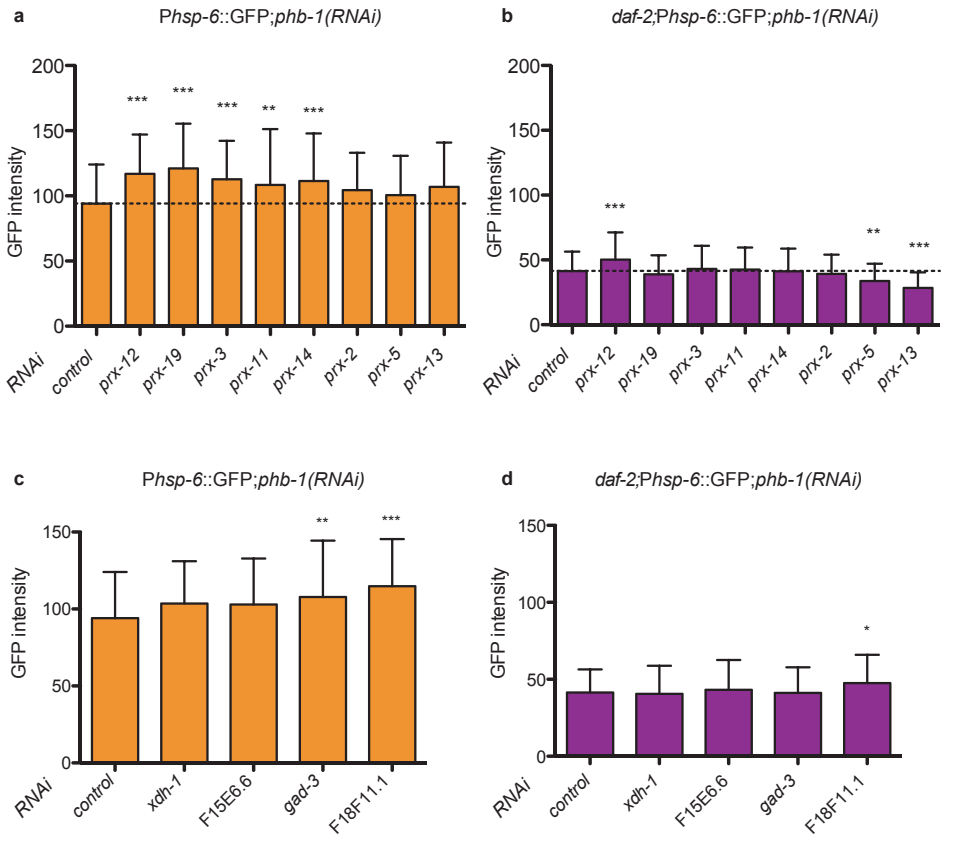

Figure 22: Assaying the role of peroxisomes in the UPR^{mt}. Effect of depleting genes involved in peroxisome biogenesis in P*hsp-6*::GFP expression in *phb-1(RNAi)* worms (**a**) and in *daf-2;phb-1(RNAi)* mutants (**b**). Effect of depleting genes involved in xanthine metabolism in P*hsp-6*::GFP expression in *phb-1(RNAi)* worms (**c**) and in *daf-2;phb-1(RNAi)* mutants (**d**). (Mean ± SD, * p value < 0.1, ** p value < 0.01, *** p value < 0.001; ANOVA test. Combination of three independent replicas is shown. n > 50 in each). Thanks to Aitor Jarit Cabanillas, Estudiante de Grado en Biotecnología, UPO, for this work as part of his Bachelor Thesis.

These results shed some doubts regarding the screen analysis as they were not confirming the specific role of peroxisomes in *daf-2* mutants. We decided to look more in details into the raw data of the screens: single worm quantification, intensities distribution, and the data analysis. RNAither uses the median of the intensities for each well and assumes a normal distribution of the median values in each plate. Looking more

closely, only 9 plates passed the Shapiro-Wilk normality test. Thus, we decided to change the data analysis and design a more personalized but still high throughput pipeline analysis.

7. PHB interactors affecting development

RNAither is a pipeline that has been developed for analysis of cells based screens and does not have in consideration morphological aspects like size. In organism models this is important, particularly it has been published that *hsp-6* expression increases during development and activation of the mitochondrial stress reporters is strongest at L4 and young adult stages (Yoneda, Benedetti et al. 2004). Thus, for the new analysis we decided to consider worm size and set up a criterion to remove worms with a length shorter than 660 μm (figure 23a). In figure 23b we have an example of worms with a size smaller than 660 μm.

We discarded a total of 135 wells in *phb-1(RNAi)* screens and 1,525 wells in the *daf-2;phb-1(RNAi)*. Apart from the RNAi effect on development, this observed reduction in worm size could be due to different reasons, one of them being well contamination. To ensure that the reduced size corresponded to a developmental defect caused by the genetic depletion, we considered only the wells in which the developmental delay was reproducible in both biological repeats. We described 88 genes whose depletion caused developmental defects in *phb-1(RNAi)* and 194 genes whose depletion caused developmental defects in *daf-2;phb-1(RNAi)*. By performing protein-protein interaction analysis of these genes (figure 23c) we described in both cases a cluster of genes encoding for ribonucleoproteins, a cluster of genes involved in protein degradation by proteasome as well as a cluster of genes involved in protein transport. In addition in *daf-2;phb-*

1(RNAi) we found as well a cluster of genes involved in splicing and in ATP biosynthesis. Among of the genes that caused a developmental arrest, we found 46 genes affecting development in both of the backgrounds. By performing functional annotation clusters we found mostly genes belonging to processes involved in protein homeostasis such as proteasome, protein transport and ribosome (table 4).

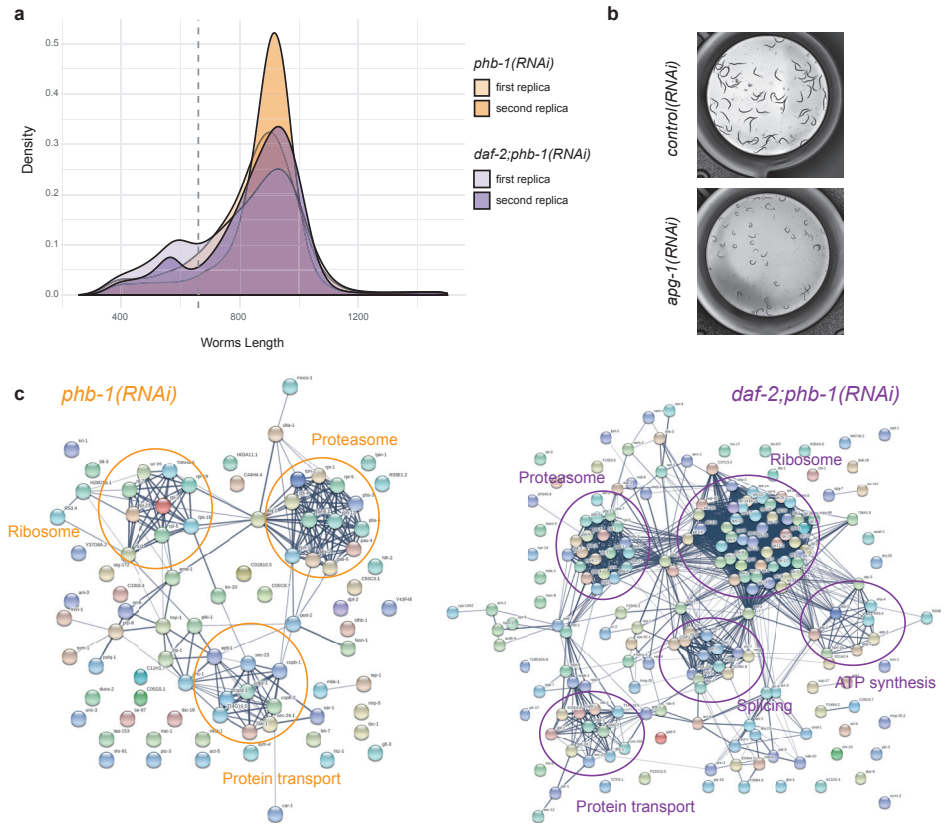

Figure 23: Analysis of the effect of RNAi treatments in worm length. a. Density plot of the worm length in each replica of each background upon depletion of all the tested RNAi clones. The dashed line shows the size limit (660 µm) used. Genes whose depletion reduced the length of the worm below this limit were discarded. **b.** Representative picture of normal sized worms (upper panel) and small worms due to RNAi treatment (lower panel). **c.** Interaction network of genes whose depletion reduced the size in *phb-1(RNAi)* worms. Clusters show genes involved in ribosome, proteasome and protein transport. **d.** Interaction network of genes whose depletion reduced the size in *daf-2;phb-1(RNAi)* worms. Clusters show genes involved in spliceosome and ATP

synthesis in addition to the clusters described for *phb-1(RNAi)* worms. Networks were built using STRING, based on predicted and described interactions in different organisms. Nodes are proteins and the edges represent the associations between nodes.

Table 4: Candidates reducing the size of the worms in a background independent manner

Proteasome	
pbs-5	Proteasome subunit beta type(pbs-5)
pbs-3	Proteasome subunit beta type-3
pas-4	Proteasome subunit alpha type-7
rpt-4	Probable 26S protease regulatory subunit 10B
pbs-2	Proteasome subunit beta type
pas-6	Proteasome subunit alpha type-1
rpt-5	proteasome Regulatory Particle, ATPase-like
rpn-6.1	Probable 26S proteasome regulatory subunit
rpn-2	26S proteasome non-ATPase regulatory subunit 1
rpt-1	26S protease regulatory subunit 7
rpn-1	proteasome Regulatory Particle, Non-ATPase-like
rpn-11	26S proteasome non-ATPase regulatory subunit 14
Protein Transport	
copb-1	Coatomer subunit beta
copb-2	Probable coatomer subunit beta
T14G10.5	Coatomer subunit gamma
sar-1	GTP-binding protein SAR1
copz-1	Probable coatomer subunit zeta(copz-1)
sec-24.1	yeast SEC homolog
apb-1	AP complex subunit beta
sec-23	yeast SEC homolog
Ribosome	
rpl-2	60S ribosomal protein L8
rpl-19	60S ribosomal protein L19
rpl-5	60S ribosomal protein L5
rpl-16	40S ribosomal protein S16
rpl-26	60S ribosomal protein L26
rpl-7	60S ribosomal protein L7
prp-8	Pre-mRNA-splicing factor 8 homolog
rla-0	60S acidic ribosomal protein P0

It is remarkable that the number of RNAi clones affecting development in *daf-2;phb-1(RNAi)* animals is bigger than the number of RNAi clones affecting development in *phb-1(RNAi)* worms, probably because genetic interactors affecting *daf-2;phb-1(RNAi)* include synthetic interactors of *daf-2* mutants. As previously mentioned, *daf-2(e1370)* mutants has several developmental defects (Gems, Sutton et al. 1998) which can explain the big number of RNAi clones affecting development. In addition, IIS mutants, *age-1* and *daf-2*, are more sensitive to RNAi, having a more intense response (Wang and Ruvkun 2004). This also explains why in *daf-2;phb-1(RNAi)* the number of genes affecting development when depleted is higher than in *phb-1(RNAi)*.

Interestingly, ATP synthesis and spliceosome appeared affecting development only in *daf-2;phb-1(RNAi)* mutants. It is known that, even if ATP levels are increased in *daf-2(e1370)* mutants compared to wild type worms (Houthoofd, Braeckman et al. 2005, Artal-Sanz and Tavernarakis 2009), *daf-2(e1370)* mutants express lower levels of ATP synthesis related genes (Halaschek-Wiener, Khattra et al. 2005). Even tough inhibiting ATP synthesis during adulthood increases lifespan (Dillin, Hsu et al. 2002, Chen, Pan et al. 2007) it seems to be required for larval development in *daf-2;phb-1(RNAi)* mutants. Further investigation will be needed to explore the possible mechanisms. Furthermore, elevated levels of alternative splicing have been related with the caloric restriction enhancement of lifespan {Tabrez, 2017 #417. Even though caloric restriction and insulin mutants have different mechanisms, it would be interesting to see whether *daf-2* mutants and *daf-2;phb-1(RNAi)* mutants have also an increment in the alternative splicing and if this increase is required for development.

8. PHB interactors affecting the UPR^{mt}

To identify UPR^{mt} modulators in wild type and IIS mutants upon PHB depletion, we decided to compare the distribution of GFP intensities in every well with the distribution of the values in the control wells of the respective plate, as we detected that not all the plates follow a normal distribution of the GFP expression. Like this we gained statistical power, if the intensity values have a narrow distribution, even if the difference of intensities (Z score) is small, we will have a significant candidate. In the same direction, if the distributions are broad, even if the Z score is big, it will not be a significant candidate. In addition, we filtered the data by discarding worms with a length smaller than 660 μm as worm developmental stage affects *hsp-6* expression (see section above). Then, P*hsp-6*::GFP expression data was normalized by dividing the GFP mean intensity of a given well by the mean GFP intensity of the four negative control wells and we assessed significance by running a t-test comparing the distributions of the data in each well with the distribution in the negative control wells.

Based on the *p* value and the log fold change (LFC) (*p* value < 0.05 and LFC < - 0.58 or LFC > 0.58) we found a big number of genes whose depletion reduced the UPR^{mt}: 355 RNAi clones (5.7%) in *phb-1(RNAi)* worms (figure 24a) and 419 RNAi clones (6.8%) in *daf-2;phb-1(RNAi)* mutants (figure 24b). Additionally, we identified 102 genes (1.7%) in *phb-1(RNAi)* worms (figure 24a) and 286 genes (4.6%) in *daf-2,phb-1(RNAi)* mutants whose depletion further increased the UPR^{mt} (figure 24b). The number of RNAi clones that reduced the mitochondrial stress response was higher than the number of clones that increased it. It is worth to mention that the number of clones affecting the UPR^{mt} was larger in *daf-2;phb-1(RNAi)* than in *phb-1(RNAi),* particularly in the number of candidates that increased the UPR^{mt}, since these mutants have the mitochondrial stress response suppressed.

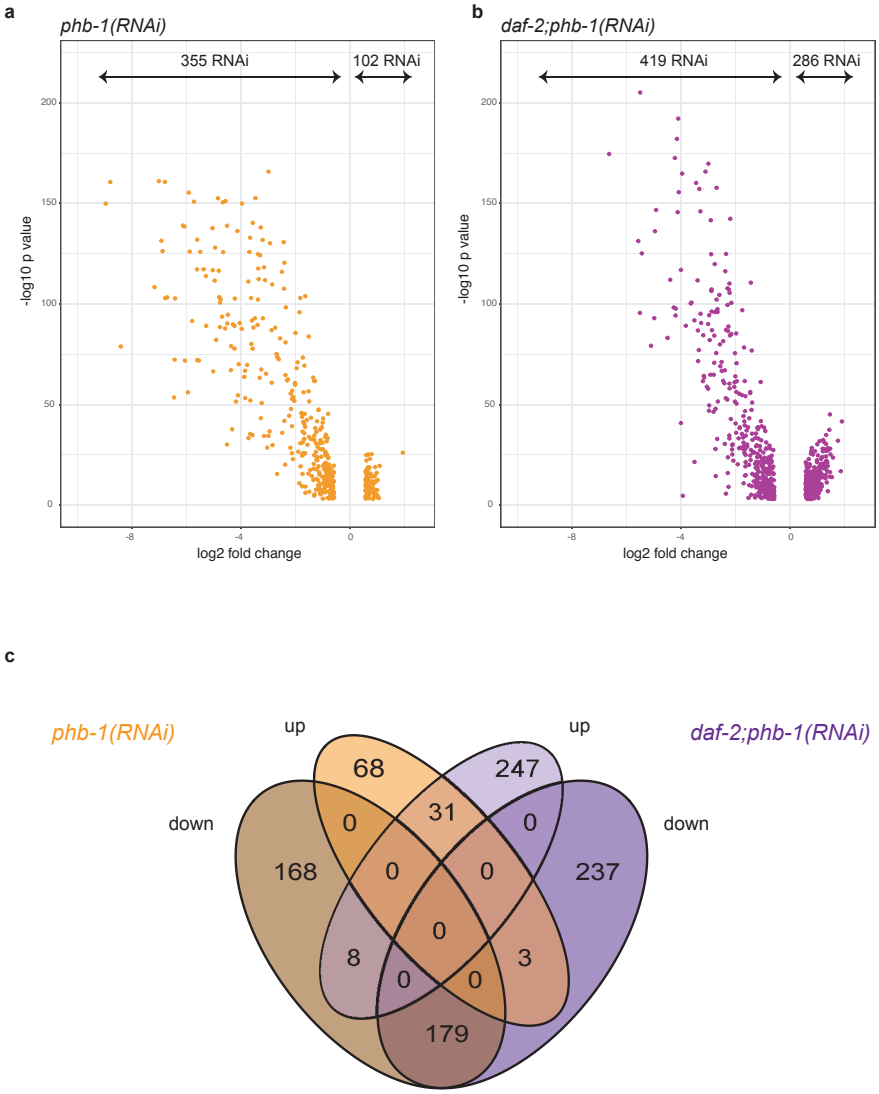

Figure 24: Analysis of GFP intensities using a more personalized pipeline.
a. - log10 *p* value against the log2 fold change (LFC) of GFP intensity of all the tested RNAi clones in *phb-1(RNAi)* worms. **b.** - log10 *p* value against the log2 fold change (LFC) of GFP intensity of all the tested RNAi clones in *daf-2;phb-1(RNAi)* worms. Genes with *p* value < 0.05 and LFC < - 0.58 or LFC > 0.58 were considered as candidates. In *phb-1(RNAi)* animals, depletion of 355 genes down-regulated the P*hsp-6*::GFP signal and depletion of 102 genes further enhanced it. In *daf-2;phb-1(RNAi)* mutants, depletion of 419 genes down-regulated the P*hsp-6*::GFP signal and depletion of 286 genes further enhanced it. **c.** Venn Diagram showing the overlap of candidates between the two backgrounds. Thanks to Ildefonso Cases (REDgen Bioinformatics).

These numbers suggest that *daf-2* mutants are more sensitive to any genetic modification than wild type worms. By looking at the overlap of the identified clones between the two backgrounds, we observed that some candidates were common in both backgrounds and others specifically affected one of the two backgrounds (figure 24c). Among the clones reducing the UPR^{mt}, about half of those that reduced it in *phb-1(RNAi)* also reduced it in *daf-2;phb-1(RNAi)*, while in *daf-2;phb-1(RNAi)* mutants most of the identified clones were specific to this particular genetic background. Among the genes whose depletion increased mitochondrial stress, we found that most of these affected specifically the *daf-2;phb-1(RNAi)* animals. We also identified candidates that had opposing effects: 8 RNAi clones reduced the signal in *phb-1(RNAi),* while increased it in *daf-2;phb-1(RNAi),* and 3 genes whose depletion increased the signal in *phb-1(RNAi)* while reduced it in *daf-2;phb-1(RNAi)* (see below).

a. GO term enrichment analysis, candidates up-regulating the UPR^{mt}

Next, we performed a GO term enrichment analysis using the topGO package in R. This algorithm considers the hierarchical structure of GO and eliminates local similarities and dependencies between GO terms {Alexa, 2006 #126}. We separately examined the genes whose depletion up-regulated and down-regulated the mitochondrial stress response. For the visualization of the enrichment results we used ReviGO, a Web server that takes long lists of GO terms, summarizes them and plots them in scatterplots based in semantic similarity (Supek, Bosnjak et al. 2011) (figure 25 and figure 26 and appendix 6).

Among the processes enriched within the genes whose depletion enhanced the stress signal (figure 25), we described general pathways such as embryo and larval development, determination of adult lifespan, and behavior.

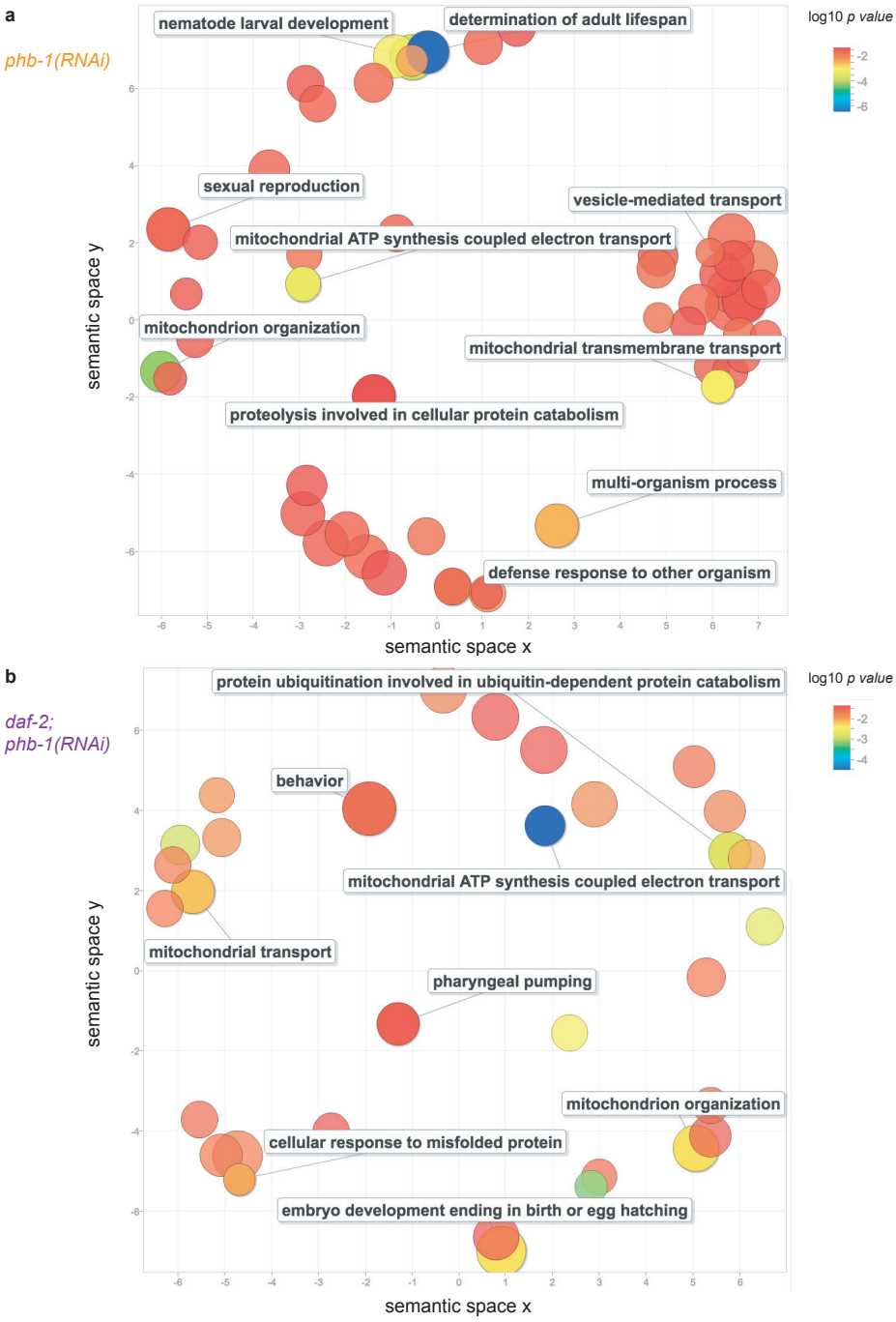
a
phb-1(RNAi)
nematode larval development
determination of adult lifespan
sexual reproduction
vesicle-mediated transport
mitochondrial ATP synthesis coupled electron transport
mitochondrion organization
mitochondrial transmembrane transport
proteolysis involved in cellular protein catabolism
multi-organism process
defense response to other organism
semantic space y
semantic space x
log10 p value
b
daf-2;
phb-1(RNAi)
protein ubiquitination involved in ubiquitin-dependent protein catabolism
behavior
mitochondrial ATP synthesis coupled electron transport
mitochondrial transport
pharyngeal pumping
mitochondrion organization
cellular response to misfolded protein
embryo development ending in birth or egg hatching
semantic space y
semantic space x
log10 p value

Figure 25: GO term enrichment analysis of candidates inducing the mitochondrial stress response. Scatterplot based in semantic similarity showing the GO terms enriched among the candidates inducing the UPR^{mt} in *phb-1(RNAi)* worms (**a**) and in *daf-2;phb-1(RNAi)* mutants (**b**). For the enrichment analysis, we used TopGO algorithm that takes into account the hierarchical structure of GO and eliminates local similarities and dependencies between GO terms. For the visualization of the enrichment results we used ReviGO, a web server that takes long lists of GO terms, summarizes them and plots them in scatterplots based in semantic similarity. For the design of the plots we selected: "Allowed similarity: SMALL" and "Semantic similarity measure: SimRel". In general, we observed that disruption of mitochondrial integrity, impairment of ATP synthesis coupled to electron transport, inhibition of catabolic processes and inhibition of stress responses increased the UPR^{mt} in both backgrounds.
In Appendix 6 we find the complete list of enriched GO terms in *phb-1(RNAi)* animals and in *daf-2;phb-1(RNAi)* mutants using the TopGo algorithm. "Annotated" represents the number of genes annotated to the GO terms and "Significant" the number of genes present in the study.

In both genetic backgrounds, disrupting mitochondrial organization, mitochondrial transmembrane transport and mitochondrial ATP synthesis coupled to electron transport induces a further mitochondrial stress response in both backgrounds. It is expected that disrupting mitochondrial organization and import as well as depleting ETC components involved in the synthesis of ATP induce the mitochondrial stress response (Lee, Lee et al. 2003, Durieux, Wolff et al. 2011, Baker, Nargund et al. 2012, Bennett, Vander Wende et al. 2014, Munkacsy, Khan et al. 2016) (figure 25).

Moreover, depletion of genes related with cellular response to different stresses, (defense response against other organisms in *phb-1(RNAi)* and response to misfolded proteins in *daf-2;phb-1(RNAi)*) increased the mitochondrial stress signal. Under stress conditions, cells activate different protective mechanisms and inhibiting one of them can cause induction of the others as a compensatory mechanism to maintain cellular homeostasis.

Interestingly, in *phb-1(RNAi)*, response to alterations in nutrient levels

and defense response to other organisms appeared enriched (figure 25a and appendix 6). Many studies support the crosstalk between nutrient deprivation and mitochondrial dynamics in order to maintain metabolic homeostasis. During starvation, mitochondrial hyper-fusion (Guedouari, Daigle et al. 2017) and induction of antioxidant genes expression promote survival (Tao, Wu et al. 2017). In addition, PHB depletion has been shown to increase lifespan under caloric restriction both in yeast (Schleit, Johnson et al. 2013) and in worms (Artal-Sanz and Tavernarakis 2009). Two major energy and nutrient sensors, AMPK and mTOR have been involved in mitochondrial dynamics (Li, Wang et al. 2015, Toyama, Herzig et al. 2016). Furthermore, IIS is a critical coordinator of nutrient availability and *daf-2* mutants show a restructured metabolism, which allows a more efficient utilization of nutrient reserves and makes them less sensitive to external nutrient changes (Depuydt, Xie et al. 2014). This restructuring can explain that depletion of genes involved in nutrient sensing does not affect *daf-2;phb-1(RNAi)* mitochondrial stress response.

Similarly, studies from different labs have shown protective roles for mitophagy and the UPR^{mt} during bacterial infection (Dunbar, Yan et al. 2012, Melo and Ruvkun 2012). Exposure to *Pseudomonas aeruginosa* induces an innate immune response similar to the response induced by mitochondrial dysfunction, i.e. induction of transcription of mitochondrial chaperones and secreted lysozymes. Interestingly, ATFS-1 appears as a key regulator of the protective innate immunity (Liu, Samuel et al. 2014, Pellegrino, Nargund et al. 2014). In addition, it has been described that *daf-2* mutants are more resistant to bacterial pathogens, like *Staphylococcus aureus* and *Pseudomonas aeruginosa* (Garsin, Villanueva et al. 2003, Evans, Chen et al. 2008), and have an increased ability to resist bacterial colonization (Podshivalova, Kerr et al. 2017). Being less sensitive to pathogens may

be an explanation why inhibition of the defense response did not further induce the UPR^{mt} in *daf-2* mutants.

Finally, we observed that inhibition of protein catabolism is enriched in both backgrounds, proteolysis involved in cellular catabolism in *phb-1(RNAi)* and ubiquitin mediated catabolism in *daf-2;phb-1(RNAi)*. By decreasing protein catabolism, we increase the load of proteins which will lead to accumulation of damaged or misfolded proteins and induce the mitochondrial stress response. Furthermore, it has described that IIS mutants have increased proteasome activity, which promotes proteostasis and longevity (Matilainen, Arpalahti et al. 2013). Taking into account that the levels of proteins are diminished in *daf-2* mutants, increasing the dose of protein by inhibiting catabolic processes implies a further stress and can have a negative effect on aging. In addition, lifespan of *daf-2* mutants depends directly in the ubiquitination levels of DAF-16 (Li, Gao et al. 2007, Heimbucher, Liu et al. 2015).

b. GO term enrichment analysis, candidates down-regulating the UPR^{mt}

Among the RNAi clones that decreased the mitochondrial stress response (figure 26), we again detected enrichment in general pathways such as gonad development, reproduction, molting, body morphogenesis, growth and locomotion, in both genetic backgrounds. The most enriched processes in both backgrounds are related with protein synthesis such as translation, ribosomal assembly and mRNA processing. Inhibition of pathways related to protein homeostasis have been already described to reduce the mitochondrial unfolded protein response (Haynes, Yang et al. 2010, Nargund, Pellegrino et al. 2012, Shore, Carr et al. 2012, Houtkooper, Mouchiroud et al. 2013, Runkel, Liu et al. 2013, Hernando-Rodriguez,

Erinjeri et al. 2018).

Figure 26: GO term enrichment analysis of the candidates reducing the mitochondrial stress response. Scatterplot based in semantic similarity showing the GO terms enriched among the candidates reducing the UPR^{mt} in *phb-1(RNAi)* worms (**a**) and in *daf-2;phb-1(RNAi)* mutants (**b**). For the enrichment analysis, we used TopGO algorithm that takes into account the hierarchical structure of GO and eliminates local similarities and dependencies between GO terms. For the visualization of the enrichment results we used ReviGO, a web server that takes long lists of GO terms, summarizes them and plots them in scatterplots based in semantic similarity. For the design of the plots we selected: "Allowed similarity: SMALL" and "Semantic similarity measure: SimRel". In general, we observed processes related with protein synthesis and folding or ATP hydrolysis coupled to proton transport reducing the UPR^{mt} in both backgrounds.
In appendix 6 we find the complete list of enriched GO terms in *phb-1(RNAi)* animals and in *daf-2;phb-1(RNAi)* mutants using the TopGo algorithm. "Annotated" represents the number of genes annotated to the GO terms and "Significant" the number of genes present in the study.

Interestingly, we found as well mRNA splicing genes only in *phb-1(RNAi),* in *daf-2;phb-1(RNAi)* those genes caused developmental defects (figure 23c) and are not included in the analysis. Remarkably, *phb-1(RNAi)* worms subjected to RNAi against genes involved in splicing showed a smaller size compared to control worms. In this case, reduced size is, at least in part, responsible for the reduced UPR^{mt} reporter expression. In the same direction, inhibition of protein folding reduced the mitochondrial stress response in both backgrounds. By looking closer to the images, we observed that those worms were smaller than control worms. Looking to the genes annotated to the process, we found mostly Chaperonin Containing TCP-1 (CCT) genes. CCT are responsible for the folding of a significant proportion of newly synthesized proteins. Those genes are essential for viability in yeasts (Stoldt, Rademacher et al. 1996)and in *C. elegans* (Fraser, Kamath et al. 2000, Kamath, Fraser et al. 2003). Thus, in this case, the reduction of the UPR^{mt} reporter expression is due to a delay in development.

Moreover, depletion of genes related with intracellular pH reduction and ATP hydrolysis coupled to proton transport reduced the mitochondrial

stress response in both backgrounds. By looking at the genes annotated to those processes, we identified mainly vacuolar proton ATPase subunits (*vhas*), as previously reported (Runkel, Liu et al. 2013) (figure 26). Different studies in diverse model organisms as *Saccharomyces cerevisiae*, *Candida glabrata* and *Kluyveromyces lactis* assigned protective roles to v-ATPase (Eide, Bridgham et al. 1993, Hamilton, Good et al. 2001, Milgrom, Diab et al. 2007, Nishikawa, Miyazaki et al. 2016). It has been described that vacuolar acidity declines during aging (Hughes and Gottschling 2012), and reduced vacuolar acidity in aged cells cause mitochondrial dysfunction. Overexpression of v-ATPase enhanced lifespan in *S. cerevisiae* (Ruckenstuhl, Netzberger et al. 2014) and vacuolar acidification seems to be critical for lifespan extension under caloric restriction (Hughes and Gottschling 2012, Molin and Demir 2014) and methionine restriction (Ruckenstuhl, Netzberger et al. 2014). Studies in higher systems showed that loss of v-ATPase activity leads to neurodegeneration (Williamson, Wang et al. 2010, Korvatska, Strand et al. 2013). Once again, worm size in these cases was reduced compared to control worms and the lower expression of the reporter might not correspond to a lower mitochondrial stress response.

In general, our results suggest that, in a background independent manner, inhibition of protein degradation, disruption of mitochondrial integrity and impairment of ATP synthesis increases the mitochondrial stress response. Moreover, organisms are able to cope with the inhibition of other stress responses, such as nutrient sensing or defense response, by boosting the mitochondrial stress response. Interestingly, *daf-2* mutants are more resistant to these stresses and do not shown an induction of the mitochondrial stress response. On the other hand, inhibition of protein biogenesis reduces the mitochondrial stress response.

By performing Gene Ontology enrichment analysis, we did not find any process that explain the opposing lifespan phenotypes occurring upon PHB depletion, as the same processes appeared in both backgrounds.

9. Selection of candidates for further analysis

In order to select interesting candidates, we carefully looked at the top candidates as well as into the literature. We used a computer tool for easy visualization of the data (APP) in which we could analyze in a gene-wise manner the mean intensity of the two replicates for each background (figure 27a), together with the mean adj. *p* value, and the distribution of the intensities in both of the replicates (figure 27b). This enabled us to select more robust candidates. In addition, many RNAi clones, despite passing the threshold of accepted worm size, showed a clear reduction of the size. Thus, in the APP we included the distribution of worm length (figure 27c), which allowed us to differentiate effects due to small size of the worms from real effects on P*hsp-6*::GFP expression. Among the top candidates, those that were not consistent in both replicates or had only been tested in one biological repeat, even if they looked interesting based on bibliography, were not selected.

We started by looking at the candidates with opposing effect. By exploring the 8 RNAi clones that reduced the signal in *phb-1(RNAi)* and increased it in *daf-2;phb-1(RNAi)*, we observed that *mrpl-54(RNAi)* and *mel-26(RNAi)* had only one replicate in *daf-2;phb-1(RNAi)* and affected size in *phb-1(RNAi)*, so we did not re-test them. The rest of RNAi clones having opposing effect were re-tested (*rad-54, aph-1, uggt-2, max-1, clec-53, hlh-34*) (table 5, group 1). From the 3 genes whose depletion increased the signal in *phb-1(RNAi)* and reduced the signal in *daf-2;phb-1(RNAi)*, we only re-tested

hif-1, the orthologue of the mammalian hypoxia-induced factor (table 5, group 2). This transcription factor is required for survival under hypoxic conditions and has been shown to modulate the UPR^{ER} (Chen, Thomas et al. 2009) while induction of the UPR^{mt} by Paraquat did not require it (Runkel, Liu et al. 2013). The other 2 clones, *rsp-3*, an splicing factor, and *hrpu-1,* a heterogeneous nuclear ribonucleoprotein U, had only one replicate and showed reduced size of *daf-2;phb-1(RNAi)* worms.

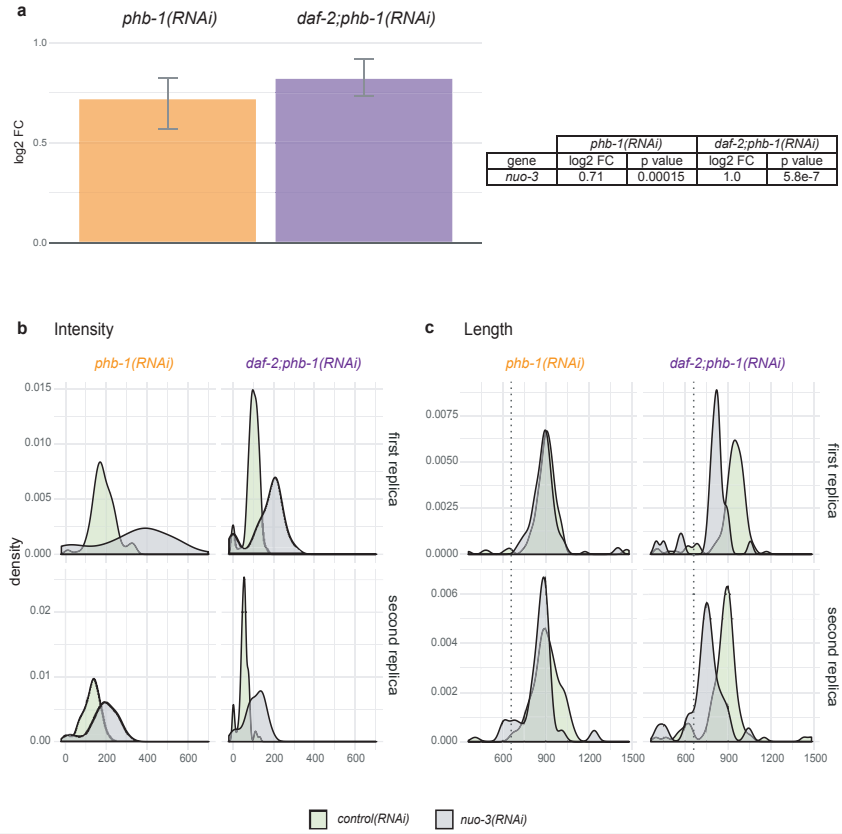

	phb-1(RNAi)		daf-2;phb-1(RNAi)	
gene	log2 FC	p value	log2 FC	p value
nuo-3	0.71	0.00015	1.0	5.8e-7

Figure 27: Computer tool (APP) designed for easy visualization of the data. As a representative example the effect of depleting *nuo-3* (complex I subunit of the ETC) is shown **a.** log2 FC of GFP intensity in *phb-1(RNAi)* animals and in *daf-2;phb1(RNAi)* mutants upon *nuo-3(RNAi)*. Mean ± SD of the two replicas is depicted in the bar graph. In the table, mean log2 FC and *p* value are shown. **b.** Density plots of GFP values of each replica in both backgrounds. In green are values from the negative controls (empty vector) and in grey values from the chosen candidate. **c.** Density plots of worm length values of each replica in both backgrounds. In green are values from the negative controls (empty vector) and in grey values from the chosen candidate. Dashed line represents the limit length (660 µm).

Then we looked at general regulators of the mitochondrial stress response. Among the 179 genes whose depletion reduced the mitochondrial stress response in a background independent manner, we found numerous genes involved in the maintenance of proteostasis as previously described (Runkel, Liu et al. 2013) and already discussed above. These included both small and large ribosomal subunits, tRNA aminoacylation proteins, several subunits of the cytosolic chaperonin complex (CCT), proteins involved in protein transport, many proteasomal regulatory subunits as well as many vacuolar H^+ ATPases. Consequently, their depletion may have an indirect effect in the regulation of the UPR^{mt}. With the aim of identifying direct UPR^{mt} regulators we chose to re-test 3 transcription factors, C16A3.4, *tlf-1* and *pha-4* (table 5, group 3).

Among the 31 genes whose depletion increased the signal in a background independent manner, we mainly detected mitochondrial genes such us *nuo-3, nuo-5, nuo-6, cco-1, cox-4, tomm-22* and mitochondrial ribosomal subunits, *mrpl-17* and *mrpl-46*. It seems very straight-forward that depletion of genes encoding subunit of the ETC complexes and involved in mitochondrial biogenesis induces additional mitochondrial stress and most of those have been already described (Bennett, Vander Wende et al. 2014, Munkacsy, Khan et al. 2016). Interestingly, we found *daf-16(RNAi)* increasing the stress response in both backgrounds, as already shown upon PQ treatment (Runkel, Liu et al. 2013). DAF-16 is involved in longevity and resistance to various stresses such as heat stress and ER stress (Kenyon, Chang et al. 1993, Lithgow, White et al. 1995, Liang, Moussaif et al. 2006, Henis-Korenblit, Zhang et al. 2010) and has been shown to be necessary for long-lived mitochondrial mutants (Senchuk, Dues et al. 2018). Apart from DAF-16, we did not find any interesting strong candidate whose depletion increased in both backgrounds within the RNAi screen to re-test.

Table 5: Selection and re-test of the candidates

		genome-wide screen *phb-1(RNAi)*		validation *phb-1(RNAi)*		genome-wide screen *daf-2;phb-1(RNAi)*		validation *daf-2;phb-1(RNAi)*	
	Gene	**LFC**	**adj. *p value***	**LFC**	**adj. *p value***	**LFC**	**adj. *p value***	**LFC**	**adj. *p value***
Group 1	**rad-54**	**-0,65**	**0,00**	-0,01	0,69	**0,87**	**0,03**	0,10	0,22
	aph-1	**-0,82**	**0,03**	-0,09	0,17	**1,06**	**0,00**	-0,05	0,42
	uggt-2	**-0,64**	**0,01**	-0,10	0,55	**1,04**	**0,00**	0,01	0,83
	max-1	**-0,71**	**0,00**	-0,10	0,47	**0,60**	**0,00**	0,05	0,56
	clec-53	**-0,64**	**0,00**	-0,14	0,43	**1,20**	**0,00**	-0,02	0,61
	hlh-34	**-0,76**	**0,00**	-0,08	0,52	**0,65**	**0,05**	0,06	0,40
Group 2	**hif-1**	**0,66**	**0,00**	0,01	0,27	**-0,91**	**0,01**	0,05	0,49
Group 3	**C16A3.4**	**-2,00**	**0,00**	**-1,10**	**0,00**	**-1,25**	**0,00**	**-1,54**	**0,00**
	tlf-1	**-0,72**	**0,00**	**-0,85**	**0,00**	**-1,71**	**0,00**	**-0,83**	**0,00**
	pha-4	**-0,66**	**0,00**	-0,23	0,22	**-1,20**	**0,00**	-0,15	0,38
Group 4	**bag-1**	**-0,84**	**0,00**	-0,09	0,45	0,28	0,19	-0,01	0,83
	F26A3.1	**-1,17**	**0,00**	-0,04	0,51	0,41	0,30	-0,01	0,50
	hpk-1	**-0,97**	**0,00**	-0,52	0,00	-0,07	0,17	-0,19	0,03
	eef-1B.1	**-1,74**	**0,00**	**-0,86**	**0,00**	-0,69	0,22	-0,20	0,21
	skr-1	**-0,92**	**0,00**	**-0,69**	**0,00**	-0,80	0,44	**-0,92**	**0,00**
	blmp-1	**-1,75**	**0,00**	**-0,84**	**0,00**	-0,57	0,02	**-0,74**	**0,05**
	sams-4	**-0,65**	**0,00**	-0,11	0,38	0,25	0,19	0,12	0,15
Group 5	**ptr-3**	0,00	0,00	-0,16	0,26	**0,88**	**0,01**	0,07	0,48
	trak-1	0,05	0,77	0,03	0,11	**1,12**	**0,00**	0,25	0,12
	mef-2	0,11	0,00	-0,02	0,53	**1,17**	**0,00**	0,10	0,47
	tat-5	-0,07	0,01	-0,03	0,42	**0,96**	**0,00**	0,06	0,55
	nmat-2	0,08	0,03	-0,05	0,67	**0,88**	**0,00**	0,06	0,49
	M04C9.1	0,25	0,08	-0,37	0,38	**1,20**	**0,00**	0,06	0,39
	skr-2	-0,18	0,17	-0,11	0,56	**0,81**	**0,00**	-0,12	0,49
	stl-1	0,30	0,23	-0,07	0,34	**1,35**	**0,00**	0,09	0,51
	usp-48	0,37	0,02	0,07	0,44	**1,76**	**0,00**	0,37	0,03
	smn-1	0,10	0,50	-0,11	0,39	**0,93**	**0,00**	-0,01	0,46
	cri-1	0,18	0,33	-0,08	0,39	**1,06**	**0,00**	0,09	0,48
	his-65	0,46	0,00	0,06	0,55	**0,81**	**0,00**	**0,60**	**0,00**
	lem-3	-0,85	0,36	-0,03	0,75	**0,91**	**0,00**	-0,03	0,44
	ceh-28	-0,25	0,12	-0,14	0,43	**0,63**	**0,00**	-0,02	0,28
	irx-1	-0,10	0,50	-0,14	0,45	**0,69**	**0,00**	-0,07	0,52
	nhr-69	0,15	0,34	-0,01	0,32	**0,77**	**0,00**	0,13	0,24
	ifo-1	0,61	0,07	0,01	0,48	**0,60**	**0,00**	-0,01	0,71
	his-59	0,81	0,42	-0,25	0,07	**0,74**	**0,00**	0,00	0,59
	hmg-5	0,88	0,39	-0,12	0,44	**1,01**	**0,00**	0,11	0,39
	klo-1	0,82	0,46	-0,10	0,60	**0,79**	**0,01**	0,01	0,80
	F32H5.1	0,29	0,01	-0,20	0,50	**0,73**	**0,01**	0,04	0,55
Group 6	**hpl-2**	-0,07	0,52	0,05	0,47	0,48	0,14	0,49	0,01
	tag-260	-0,09	0,58	-0,34	0,10	0,42	0,00	-0,06	0,53

Next, we considered UPR^{mt} regulators acting in a background-dependent manner. Under the scope of the opposing aging phenotype caused by prohibitin depletion, we focused on RNAi clones reducing the UPR^{mt} in *phb-1(RNAi)* (table 5, group 4) and RNAi clones increasing the response in *daf-2;phb-1(RNAi)* (table 5, group 5). We selected genes that were strong candidates in the screen, not reducing size and having a good distribution of the intensity data, and related to stress responses or lifespan based on bibliography. In addition, we re-tested two more genes that, even though did not appear as candidates, were close to it (being clear candidates in one replica) and, based on bibliography, looked interesting (table 5, group 6).

10. Re-testing of candidates

In total we chose 38 candidates to re-test (table 5): 6 clones whose depletion reduced the response in *phb-1(RNAi)* but increased the response in *daf-2;phb-1(RNAi)*, 1 clone whose depletion increased the response in *phb-1(RNAi)* but reduced the response in *daf-2;phb-1(RNAi),* 3 clones whose depletion reduced the response in both backgrounds, 7 clones whose depletion reduced specifically the UPR^{mt} in *phb-1(RNAi)* and 21 clones whose depletion increased the UPR^{mt} specifically in *daf-2;phb-1(RNAi)*. In addition, even though based on the *p* value and the LFC they were not candidates, we re-tested two more RNAi clones that were close to be candidates and were interesting based on bibliography. We re-tested those 40 clones in liquid following the same experimental procedure as the one used in the genome-wide screen, except that parents subjected to synchronization by bleaching were grown on solid media instead of in liquid. To give more strength, and remove possible positional effect, we customized the plate by randomizing the positions of the negative

and positive controls and by duplicating each clone. We performed two independent biological replicates. The data analysis was identical to the one carried out for the wide-genome screen, candidates were determined based on the mean of the adjusted *p* value and the mean of the log of the fold change (LFC): *p* value < 0.05 and LFC < -0.58 or LFC > 0.58. From the 40 re-tested clones only 6 were validated (figure 28 and table 5).

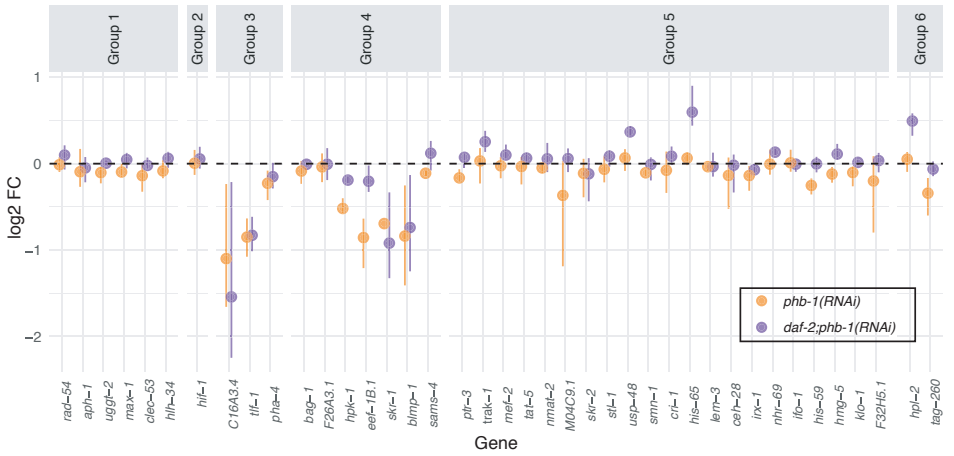

Figure 28: Analysis of GFP values of the 38 clones re-tested in liquid. log2 fold change (FC) of GFP expression of the 38 clones re-tested in liquid in both backgrounds. Mean ± SD of the two replicas is depicted. Genes are clustered based on the phenotype observed in the screen. Group 1; reduced UPR^{mt} in *phb-1(RNAi)* and increased UPR^{mt} in *daf-2;phb-1(RNAi)*. Group 2; increased UPR^{mt} in *phb-1(RNAi)* and reduced UPR^{mt} in *daf-2;phb-1(RNAi)*. Group 3; reduced UPR^{mt} in both backgrounds. Group 4; reduced specifically in *phb-1(RNAi)*. Group 5; increased specifically in *daf-2;phb-1(RNAi)*. Group 6; others. Based on the *p* value and the log2 FC (*p* value < 0.05 and LFC < -0.58 or LFC > 0.58), we obtained 4 candidates reducing the mitochondrial stress response in a IIS independent manner (C16A3.4, *tlf-1, skr-1* and *blmp-1*), 1 candidate that suppressed the signal specifically in *phb-1(RNAi)* (*eef-1B.1*), 1 candidate that induced specifically the UPR^{mt} in *daf-2;phb-1(RNAi)* mutants (*his-65*) and two candidates that showed a clear tendency to increase the signal specifically in *daf-2;phb-1(RNAi)* mutants (*usp-48* and *hpl-2*).

None of the clones with opposing effects reproduced the phenotype (figure 28 and table 5, groups 1 and 2). From the 3 candidates whose depletion reduced the UPR^{mt} in both backgrounds (figure 28 and table 5, group 3),

C16A3.4 and *tlf-1* confirmed the phenotype, while *pha-4* did not have any effect; from the 7 clones that reduced the signal specifically in *phb-1(RNAi)* (figure 28 and table 5, group 4), *eef-1B.1* recapitulated the phenotype by reducing significantly *hsp-6* expression only in *phb-1(RNAi)*; *skr-1* and *blmp-1* appeared to reduce the signal in both backgrounds; from the 21 genes whose depletion increased the response in *daf-2;phb-1(RNAi)* (figure 28 and table 5, group 5), only *his-65* was confirmed.

Particularly surprising was the reduction in the number of candidates whose depletion further enhanced the mitochondrial stress response in *daf-2;phb-1(RNAi)*. One possible explanation is that, as mentioned above, for the wide-genome screen mothers were grown in liquid while for the validation they were grown on plate. Growing worms in liquid culture introduces changes in metabolic rates, they appear somewhat starved and can affect the mitochondrial stress response (Lewis and Fleming 1995, Van Voorhies and Ward 1999). We conclude that metabolism and stress is substantially altered depending on the growing conditions. Due to lack of time we did not pursue a more exhaustive re-testing but retain those candidates that were statistically significant for being more robust for further analysis.

The objective of this study was to understand why PHB depletion induces the UPR^{mt} to a different extent depending on the genetic background and whether this modulates lifespan, leading to opposing phenotypes. For this reason, we paid more attention to RNAi clones that specifically induced the mitochondrial stress response in *daf-2;phb-1(RNAi)*, which could be responsible for the enhanced lifespan of *daf-2* upon PHB depletion. Looking closer to the re-tested RNAi clones we observed that, although not to such a great degree as in the genome-wide screen, *usp-48* and *hpl-2* increased the response specifically in *daf-2;phb-1(RNAi)* (figure 28 and table 5, group 6) and thus were selected as candidates for further characterization.

Box 2: Brief description of the candidates:

• C16A3.4 is an orthologue of human ZNF622, the C2H2 zinc finger gene 622. It is predicted to have nucleic acid binding activity and zinc ion binding activity based on protein domain. It has been involved in different stress responses (Mabon et al. 2009, Leung et al. 2012, Marza et al. 2015).

• *tlf-1* encodes a TATA binding protein (TBP)-like factor (TLF). It is a functional transcription factor and is required for embryonic RNA polymerase II transcription (Dantonel et al. 2000, Kaltenbach et al. 2000). RNAi against *tlf-1* has been shown to reduce lifespan (Samuelson et al. 2007, Kashyap et al. 2012).

• *eef-1B.1* is one of the two homologues of EEF1B, eukaryotic elongation translation factor 1-β, and it is predicted to have translation elongation activity, based on protein domain information. RNAi against this gene induced the expression of phase II detoxification genes (Wang et al. 2010, Li et al. 2011).

• *skr-1* encodes a homolog of the human Skp1 protein, a member of the SCF complex that targets proteins for ubiquitin-mediated degradation by the proteasome. Depletion of *skr-1* reduces DAF-16 transcriptional activity, shortens lifespan of *daf-2* mutants (Ghazi et al. 2007) and strongly attenuates the induction of SKN-1 dependent genes (Wu et al. 2016).

• *blmp-1* is the homologue of the mammalian PRDM1/BLIMP1 transcriptional repressor and a component of the heterochromatic pathway regulating developmental processes such as germ cell migration or dauer development. In addition, it has been shown to be required for *daf-2* mutants' lifespan (Samuelson et al. 2007) and to regulate hypoxia response (Padmanabha et al. 2015).

• *his-65* encodes an H2A histone. Its depletion induces the expression of the infection response gene *irg-1* (Dunbar et al. 2012).

• *usp-48* is the orthologue of USP48, ubiquitin specific protease 48, and is predicted to have thiol-dependent ubiquitinyl hydrolase activity, based on protein domain information. Recent studies have described new functions of USP-48 related with epigenetics modifications by regulating histone ubiquitination levels (Uckelmann et al. 2018, Velimezi et al. 2018)

• *hpl-2* encodes one of the two *C. elegans* heterochromatin protein 1 homologues. It is required for silencing of transgenes in the germline as well as for somatic development. It has been suggested as a regulator of dauer diapause, longevity and lipid metabolism (Meister et al. 2011). In addition, it has been shown to function in the maintenance of ER homeostasis (Kozlowski et al. 2014)

To wrap up, 4 candidates reduced the mitochondrial stress response in a IIS independent manner, *C16A3.4, tlf-1, skr-1* and *blmp-1*; 1 candidate suppressed the signal specifically in *phb-1(RNAi)*, *eef-1B.1*; and 3 candidate induced specifically the UPR^{mt} in *daf-2;phb-1(RNAi)* mutants, *his-65*, *usp-48* and *hpl-2*. For a brief description of these 8 RNAi clones see Box 2.

11. Validation of candidates modulating the UPR^{mt}

In order to validate the candidates, we evaluated the effect of depleting the 8 selected genes in solid media, under basal conditions as well as under PHB depletion, in wild type and in *daf-2* mutants (figure 29). Depletion of C16A3.4 and *tlf-1* reduced the PHB-mediated mitochondrial stress response in both backgrounds, *phb-1(RNAi)* and *daf-2;phb-1(RNAi)* (figures 29a and 29b). Surprisingly, depletion of *eef-1B.1*, *skr-1* and *blmp-1* appeared to reduce the UPR^{mt} specifically in *daf-2;phb-1(RNAi)* (figures 29c, 29d and 29e), even though in the liquid validation depletion of *eef-1B.1* reduced the expression levels only in *phb-1(RNAi)* and depletion of *skr-1* and *blmp-1* reduced the response in both, *phb-1(RNAi)* and *daf-2;phb-1(RNAi)*. Depletion of *hpl-2* induced the mitochondrial stress response in all the tested conditions, wild type, *daf-2*, *phb-1(RNAi)* and *daf-2;phb-1(RNAi)* (figure 29f). Finally, depletion of *his-65* and *usp-48* increased the signal specifically in *daf-2;phb-1(RNAi)* mutants (figures 29g and 29h). While it is true that *his-65(RNAi)* showed a statistically significant induction the UPR^{mt} in *daf-2* mutants, we did not consider this induction as a real induction of the mitochondrial stress response when looking at the pictures and the GFP values, very low GFP levels, that correspond to autofluorescence.

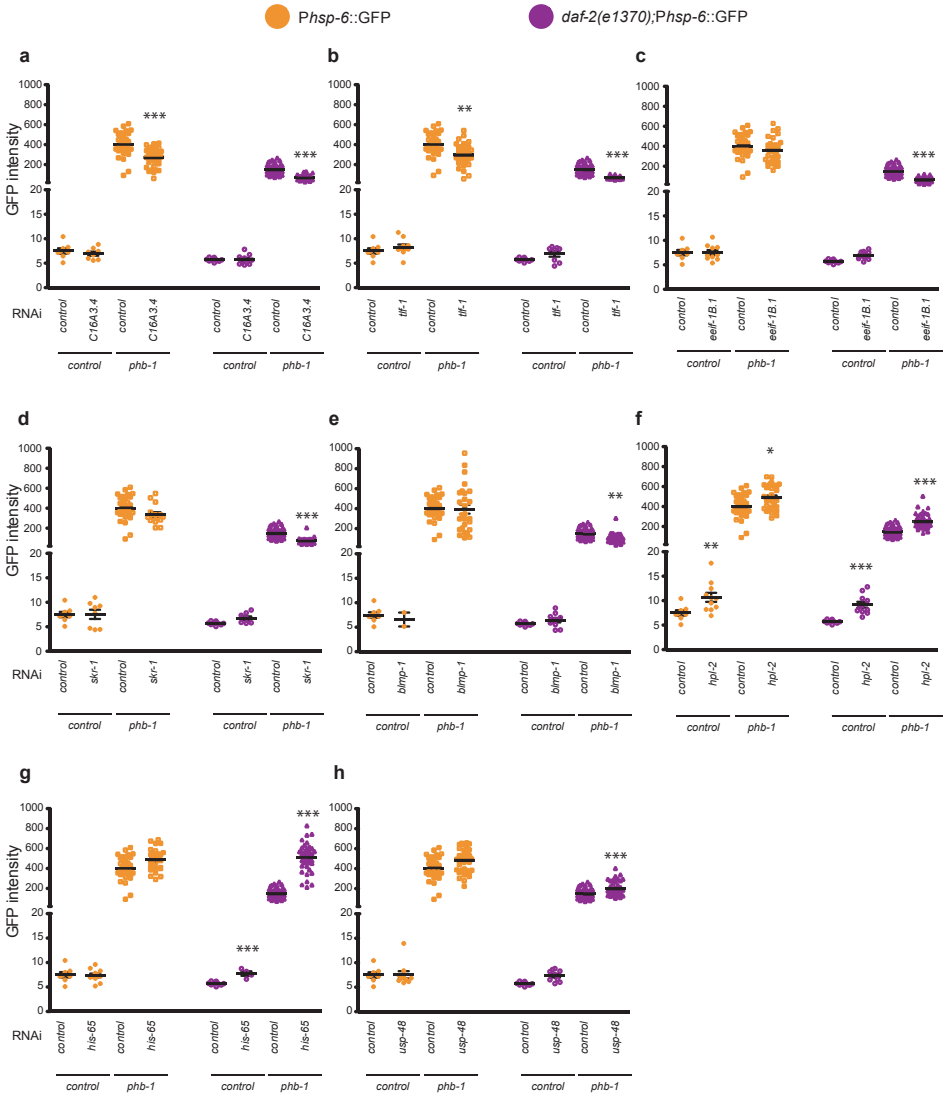

Figure 29: Analysis of P*hsp-6*::GFP expression of the 8 validated RNAi clones tested on plate. Effect of depleting the 8 RNAi clones in wild type animals, *daf-2* mutants, *phb-1(RNAi)* worms and *daf-2;phb-1(RNAi)* mutants in solid media. (Mean ± SD; * p value < 0.1, ** p value < 0.01, *** p value < 0.001; ANOVA comparing the effect of all the tested RNAi in each background against its respective control (control(RNAi)) and assuming normal distribution of the data.

It was particularly unexpected that depletion of *eef-1B.1*, *skr-1* and *blmp-1* had a different phenotype in the genome-wide screen, in the re-test and in the validation. We isolated them first as specific *phb-1(RNAi)* suppressors,

during the re-test we selected them as general regulators of the mitochondrial stress response and in the validation, they appeared to be specific of IIS PHB depleted mutants. We decided not to continue analyzing these genes due to the high variability and inconsistent results.

hpl-2 encodes one of the two *C. elegans* Heterochromatin protein 1 (HP1) homologues. HP1 family proteins are conserved epigenetic regulators that localize to centric heterochromatin, telomeres and specific sites of euchromatin and control gene expression depending on the context (de Wit, Greil et al. 2007). *hpl-2* has been shown to genetically interact with the TGF-β signaling pathway and the IIS pathway and to modulate expression of genes involved in dauer decision. Interestingly, *hpl-2* mutants have extended lifespan, which is dependent on DAF-2 and DAF-16 activity, and show altered lipid metabolism (Meister, Schott et al. 2011). In addition, worms lacking HPL-2 are more resistant to ER stress due to the constitutive activation of UPR^{ER} and autophagy (Kozlowski, Garvis et al. 2014). These studies suggest that HPL-2, as other chromatin modifying proteins, modulate genetic expression in response to environmental conditions. HPL-2 plays a role in dampening the UPR^{ER}, and our result suggests that it may be involved in the general attenuation of stress responses. Further studies will be needed in order to understand the mechanism and its relation with the nutrient sensing pathways, IIS and TGF-β. However, for the aim of this work we decided not to continue studying this gene.

After validation, we had 2 transcription factors whose depletion reduce the mitochondrial stress response in *phb-1(RNAi)* worms and in *daf-2;phb-1(RNAi)* mutants: C16A3.4 and *tlf-1*. We wanted then to study their implication in cellular stress responses and determine whether the two transcription factors are general modulator of cellular stress or they are specific regulators of the UPR^{mt}. Furthermore, we obtained two

epigenetic factors, *his-65* and *usp-48*, whose depletion further induce the mitochondrial stress response specifically in *daf-2;phb-1(RNAi)* mutants. We were interested in analyzing the implication of depleting these two genes in aging.

12. C16A3.4 and *tlf-1*, two new regulators of the mitochondrial stress response

C16A3.4, the orthologue of a human conserved C2H2 zinc finger gene, and *tlf-1*, a TATA binding protein (TBP)-like factor, are two transcription factors whose depletion reduced the mitochondrial stress signal consistently in both backgrounds, *phb-1(RNAi)* and *daf-2;phb-1(RNAi)* without affecting *hsp-6* expression in the absence of mitochondrial stress (figures 29a and 29b). We wanted to assess whether these genes were also regulators of other stress responses, such as the UPR^{ER} or the heat shock response (HSR). For this we tested the effect of depleting C16A3.4 and *tlf-1* on the expression of the UPR^{ER} reporter, P*hsp-4*::GFP, and the HSR reporter, P*hsp-16.2*::GFP.

Treating worms with tunicamycin, an inhibitor of protein N-glycosylation, a critical step for the synthesis of glycoproteins, induced the expression of P*hsp-4*::GFP, which was abolished upon depletion of *ire-1*, a key regulator of the UPR^{ER} (figure 30a). Neither C16A3.4(RNAi) nor *tlf-1(RNAi)* had an effect in the response.

When subjecting worms to heat shock, there was a high induction of the P*hsp-16.2*::GFP reporter, that was reduced upon depletion of the heat shock transcription factor, *hsf-1(RNAi)* (figure 30b). Once again, we observed that depletion of the two candidates did not reduce or increase the response (figure 30b).

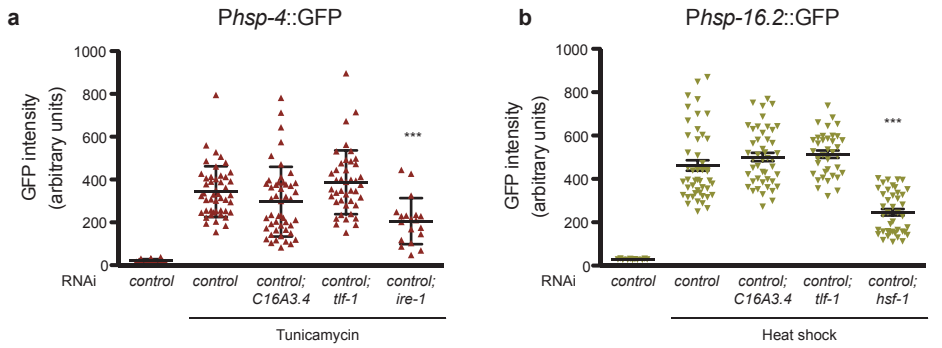

Figure 30: The transcription factors, C16A3.4 and *tlf-1*, are specific modulators of the mitochondrial stress response. a. Depletion of C16A3.4 and *tlf-1* did not reduce the UPR^{ER}. Treatment with Tunicamycin (7.2 μM) induced the expression of P*hsp-4*::GFP. This response was supressed by *ire-1(RNAi)* while it was not affected by depletion of C16A3.4 nor *tlf-1*. **b.** Depletion of C16A3.4 and *tlf-1* did not reduce the cytosolic HSR. Subjecting worm to heat shock induced the expression of P*hsp-16.2*::GFP. This response was supressed by *hsf-1(RNAi)* while it was not affected by depletion of C16A3.4 nor *tlf-1*. (n > 20 in all conditions. Mean ± SD; *** *p* value < 0.001; ANOVA test. Combination of at least two independent replicas is shown, n > 20 in each).

This suggests that these two transcription factors are specifically modulating the mitochondrial stress response, instead of being general stress regulators.

We then asked ourselves whether these two genes were specific regulators of the PHB-elicited mitochondrial stress response or were general regulators of the UPR^{mt}. For this we analyzed the effect of depleting the two transcription factors in worms subjected to other mitochondrial stress inducers, such as lack of SPG-7, a component of the m-AAA protease, or knocking down *cco-1*, the nuclear-encoded cytochrome *c* oxidase-1 subunit Vb/COX4 (figure 31).

SPG-7 regulates proteolytic degradation of mitochondrial proteins and is required for mitochondrial ribosome biogenesis. Depletion of *spg-7* causes slow growth and reduced brood size, increases pathogen resistance

(Pellegrino, Nargund et al. 2014), perturbs mitochondrial morphology, induces of the UPR^{mt} (Benedetti, Haynes et al. 2006, Haynes, Yang et al. 2010, Nargund, Pellegrino et al. 2012, Nargund, Fiorese et al. 2015) and increases lifespan of wild type worms (Curran and Ruvkun 2007, Pellegrino, Nargund et al. 2014). In our case, depletion of SPG-7 strongly induced the UPR^{mt}, which was abolished by *atfs-1(RNAi)*. We observed that both, C16A3.4 and *tlf-1* were necessary for the induction of the UPR^{mt} upon *spg-7(RNAi)* (figure 31a).

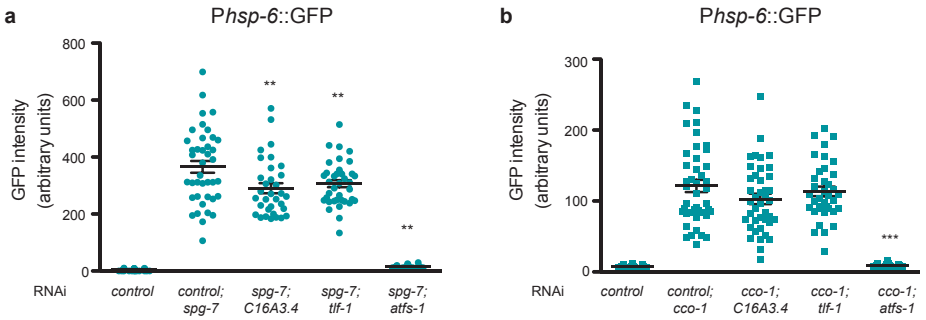

Figure 31: Effect of depleting the two transcriptional factors, C16A3.4 and *tlf-1*, in the UPR^{mt} elicited by other stress. a. Depletion of C16A3.4 and *tlf-1* reduced the UPR^{mt} elicited by lack of SPG-7. Depletion of *spg-7* induced a strong mitochondrial stress response which is abolished by *atfs-1(RNAi)*. Depletion of C16A3.4 and *tlf-1* by RNAi reduced the UPR^{mt} elicited by *spg-7(RNAi)*. **b.** Depletion of C16A3.4 and *tlf-1* did not reduce the UPR^{mt} elicited by lack of CCO-1. Depletion of *cco-1* induced a mild mitochondrial stress response which is abolished by *atfs-1(RNAi)*, while depletion of C16A3.4 and *tlf-1* by RNAi did not affect the UPR^{mt} elicited by *cco-1(RNAi)*. (n > 20 in all conditions. Mean ± SD; ** p value < 0.01; *** p value < 0.001; ANOVA test. Combination of at least two independent replicas is shown, n > 20 in each).

Depletion of *cco-1,* causes also developmental delay, induces the mitochondrial stress response (Bennett, Vander Wende et al. 2014, Tian, Garcia et al. 2016) and increases lifespan (Tullet, Hertweck et al. 2008, Durieux, Wolff et al. 2011). Nevertheless, knockdown of this gene results in intermediate phenotypes as compared the phenotypes caused by knocking-

down other ETC genes (Dillin, Hsu et al. 2002, Lee, Lee et al. 2003, Rea, Ventura et al. 2007). Accordingly, we observed that *cco-1(RNAi)* induced a mild UPR^{mt}, which was again abolished by *atfs-1(RNAi*). Interestingly, depletion of any of the genes, C16A3.4 and *tlf-1*, did not affect the mild induction of the UPR^{mt} caused by *cco-1(RNAi)* (figure 31b).

All together, these results suggest that C16A3.4 and *tlf-1* are two new regulators of mitochondrial stress response caused by a severe mitochondrial defect.

C16A3.4 is an orthologue of a human conserved C2H2 zinc finger gene, ZNF622, but has not been characterized in *C. elegans*. Based on its protein domains it is predicted to have nucleic acid binding activity and zinc ion binding activity. It has been involved in different stress responses, although all the information we have is based on RNAi screens. Mabon *et al.* performed a systematic screen looking for determinants of hypoxic sensitivity in intact organism and identified C16A3.4, since its depletion produced hypoxia resistance (Mabon, Mao et al. 2009). Marza *et al.* performed an RNAi genome-wide screen and found that depletion of C16A3.4 increased the expression of the UPR^{ER} reporter P*ckb-2*::GFP under stress conditions (tunicamycin treatment) (Marza, Taouji et al. 2015). C16A3.4 also shares a high homology with the yeast YBR267W, required for ribosomal large subunit biogenesis. Leung *et al.* investigated the role of the nucleolus in fundamental stress responses and provided evidences that signals initiating from ribosome biogenesis regulate SKN-1 activity. They showed that inhibiting ribosome biogenesis genes, such as C16A3.4, induced the expression of P*gst-4*::GFP (Leung, Empinado et al. 2012).

Although in our hands C16A3.4 seems to be regulating specifically the mitochondrial stress response, in other studies under different conditions,

lack of C16A3.4 induces the expression of *ckb*-2 and *gst-4*. The phase II detoxification gene *gst-4* is a very well characterized target of SKN-1. By looking for ChIP-Seq data from the "Regulatory Elements in *C. elegans*" project in modENCODE, *ckb-2* has a binding site for SKN-1 in its promotor region. Thus, it could be that C16A3.4 is a general regulator of cellular homeostasis, while it is necessary for the induction of the mitochondrial stress response under severe defects, it represses SKN-1 activity, thus inhibiting the phase II detoxification response and the expression of *ckb-2*.

TLF-1 is a component of the core promoter recognition factor TFIID, responsible for initiation of RNA polymerase II transcription. TFIID is composed of a TATA binding protein (TBP), a series of TBP-associated factors (TAFs) and a TBP-like factor, TLF. In *C. elegans*, TLF-1 is expressed and functions in all somatic cells and it is required for early embryonic transcription since it plays a positive role in polymerase II transcription (Dantonel, Quintin et al. 2000, Kaltenbach, Horner et al. 2000). TLF is also involved in embryonic transcription in *Xenopus* and *Zebrafish* (Veenstra, Weeks et al. 2000, Muller, Lakatos et al. 2001), while in mice TLF is required specifically for chromatin reorganization during spermatogenesis (Martianov, Fimia et al. 2001, Martianov, Brancorsini et al. 2002). In addition to embryonic transcription, TLF-1 regulates the lifespan of *daf-2* mutants (Samuelson, Carr et al. 2007) and is required to preserve its mobility (Kashyap, Perera et al. 2012). Finally, RNAi against TLF-1 elicits a loss of neuronal ASE fate (Poole, Bashllari et al. 2011). Moreover, *tlf-1* has been described to be required for the induction of the immune response gene *irg-1* (Estes, Dunbar et al. 2010), which has been shown to be also regulated by *atfs-1* (Pellegrino, Nargund et al. 2014). This suggests that TLF-1 and ATFS-1 might have common target genes and could be cooperating for the induction of their transcriptional targets.

13. HIS-65 and USP-48 reduce the mitochondrial stress response of *daf-2;phb-1(RNAi)* mutants and are required for lifespan

Depletion of *his-65*, a H2A histone, and depletion of *usp-48*, a ubiquitin specific protease, further induced the mitochondrial stress response specifically in *daf-2;phb-1(RNAi)*. We wondered whether this induction of the UPR^{mt} corresponded to a shortening of lifespan (figure 32).

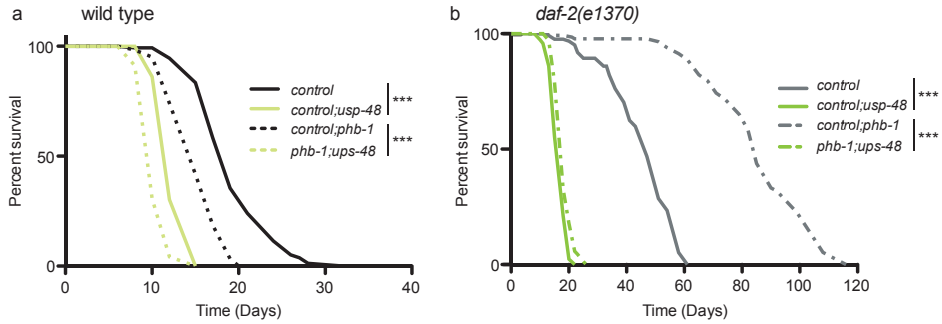

Figure 32: Effect of depleting *usp-48* in the lifespan of wild type and IIS mutants. Depletion of *usp-48* shortened lifespan of wild type animals, *phb-1(RNAi)* worms (**a**), as well as that of *daf-2(e1370)* and *daf-2;phb-1(RNAi)* mutants (**b**). (One representative lifespan experiment out of minimum two independent replicas is shown, n > 120 in each).

We observed that *usp-48(RNAi)* reduced lifespan in all the tested conditions, wild type, *phb-1(RNAi)*, *daf-2* mutants and *daf-2;phb-1(RNAi)* mutants (figures 32a and b). During the completion of the lifespans we observed a lot of exploded worms particularly in the *daf-2* mutant backgrounds and worms were looking sick. Interestingly the shortening of the lifespan is dramatically stronger in *daf-2* mutants (65.5%) and in *daf-2;phb-1(RNAi)* mutants (75.5%) compared to wild type (27.5%) and *phb-1(RNAi)* (26.5%) backgrounds, showing that *daf-2* mutants relay more on *usp-48* function.

USP-48 is the orthologue of human USP48, a deubiquitinating enzyme belonging to the ubiquitin-specific proteases, USPs, family. In *C. elegans*, USP-48 is required for many functions of germline maintenance and suppresses the *Muv* phenotype of *lin-15AB(n765)* (Cui, Kim et al. 2006) and RNAi against *usp-48* has been shown to shorten lifespan in *daf-2* mutants as well as in *daf-2;daf-16* double mutants (Samuelson, Carr et al. 2007).

Deubiquitinating enzymes have emerged as key players in the regulation of genome instability (Kee and Huang 2016). Recent studies in cell lines defined USP48 as a key regulator of DNA repair, tuning the ubiquitination levels of histones H2A (Uckelmann, Densham et al. 2018, Velimezi, Robinson-Garcia et al. 2018). Nevertheless, loss of USP48 increases resistance to camptothecin, a topoisomerase inhibitor, (Uckelmann, Densham et al. 2018), and alleviates increased sensitivity and genomic instability of Fanconi Anemia cells (Velimezi, Robinson-Garcia et al. 2018), both by enhancing homologous recombination markers and histone H2A ubiquitination. Additionally, USP48 has been described as an interactor of ubiquinated nucleosomes (Kalb, Latwiel et al. 2014) and, by ChiP-MS studies on histone marks, USP48 appears to be associated with the active regions in the transcriptional landscape (Engelen, Brandsma et al. 2015, Ji, Dadon et al. 2015). It would be of a high interest to identify the substrates of USP-48 in worms, and thus analyze whether the increase in the mitochondrial stress response upon depletion of *usp-48* is due to a loss of genetic stability or a remodeling in chromatin structure.

In addition, USP48 has been suggested as a new mechanism of crosstalk between NFKB and p53 stress response pathways in a manner independent of its deubiquitinase activity (Schweitzer and Naumann 2015, Cetkovska, Sustova et al. 2017), which opens another possibility of USP-48 mechanism

of action.

While *usp-48(RNAi)* shortens lifespan in all backgrounds, depletion of *his-65* does not affect lifespan of wild type, nor of *phb-1(RNAi)* worms (figure 33a). Interestingly, albeit lifespan of *daf-2* mutants is unaffected by *his-65(RNAi)*, PHB depletion requires HIS-65 for enhancing the lifespan of *daf-2* mutants (figure 33b). While conducting the lifespans we detected that *his-65(RNAi)* caused 100% embryo lethality (gastrula stage) in otherwise wild type animals, in *daf-2* mutants and in *phb-1(RNAi)* worms, where the sterility was attenuated. Interestingly, *daf-2* mutants subjected to *phb-1(RNAi);his-65(RNAi)* had a prolonged larval development and gonad development was completely suppressed.

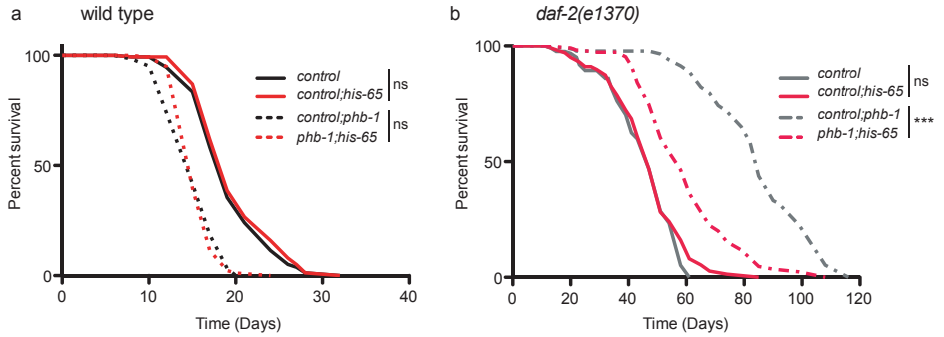

Figure 33: Effect of depleting *his-65* in the lifespan of wild type and IIS mutants. Depletion of *his-65* did not affect lifespan of wild type animals or *phb-1(RNAi)* worms (**a**), nor lifespan of *daf-2* mutants (**b**). However *his-65(RNAi)* shortened lifespan of *daf-2;phb-1(RNAi)* mutants (**b**). (One representative lifespan experiment out of minimum two independent replicas is shown, n > 120 in each).

Histone modifications play important roles in chromatin functions, activation or repression of gene transcription, as well as in DNA repair and genome stability (Bassing, Chua et al. 2002). However, it has been shown that many chromatin regulators have greater effects on gene induction/ repression kinetics than during steady-state growth (Weiner, Chen et al.

2012). In *Arabidopsis thaliana*, histone modifications have been described as necessary for osmotic stress response (Chen, Luo et al. 2010), defense response to *Verticillium dahlia* (Hu, Pei et al. 2014), thermotolerance and oxidative stress (Weng, Yang et al. 2014). Interestingly, in *Saccharomyces cerevisiae*, in addition of being important for osmotic stress (Magraner-Pardo, Pelechano et al. 2014) and heat shock response (Zanton and Pugh 2006), histone modifications play a role in nutritional stress response (Liu, Li et al. 2015, Oh, Suganuma et al. 2018). Oleate stress reduces the expression of ribosome genes and induces the expression of citrate cycle related genes. Htz1, the yeast H2A histone, binding profiles change in response to oleate, suggesting Htz1 is kind of a sensor of oleate stress (Liu, Li et al. 2015). Moreover, in yeast, it has been published that decreased expression of histones or a defect in nucleosome assembly bursts mitochondrial metabolism (Galdieri, Zhang et al. 2016): there is increased mtDNA levels, increased oxygen consumption, increased ATP levels and increased expression of TCA and OXPHOS genes.

In *C. elegans*, the histone variant H3.3 has been shown to be important for heat stress response (Delaney, Mailler et al. 2018) as it was previously shown in *Drosophila* (Schwartz and Ahmad 2005) and human cells (Kim, Heo et al. 2011). In addition, the histone chaperone HIRA is responsible for a correct association and functioning of the histone variant H3.3 (Delaney, Mailler et al. 2018). Curiously, PHB have been described to form protein complexes with HIRA and to modulate H3.3 deposition (Zhu, Li et al. 2017). PHB and HIRA affect chromatin organization and expression of metabolic genes.

IIS plays a central role in the regulation of metabolism, and *daf-2* mutants have a shift in metabolism that is responsible for its enhanced lifespan. Interestingly, metabolic modifications associated with caloric restriction

are, at least partially, caused by TORC1-mediated chromatin remodeling (Chen, Fan et al. 2012, Sen, Shah et al. 2016) and DAF-16 has been shown to physically interact with chromatin remodeler SWI/SNF (Riedel, Dowen et al. 2013). It would be of a great interest to study how depletion of *his-65* affects *daf-2;phb-1(RNAi)* metabolism and mitochondrial homeostasis, to note *his-65(RNAi)* in *daf-2;phb-1(RNAi)* induced P*hsp-6*::GFP expression up to *phb-1(RNAi)* levels, and to investigate whether this is responsible for the lifespan phenotype.

FUTURE PROSPECTS

Prohibitins (PHBs), PHB-1 and PHB-2, are evolutionarily conserved and ubiquitously expressed proteins. They form multimeric ring complexes in the inner mitochondrial membrane and diverse functions have been attributed to them, such as maintenance of mitochondrial morphogenesis acting as scaffolds (Merkwirth, Martinelli et al. 2012) or stabilization of mitochondrial proteins acting as chaperones (Nijtmans, de Jong et al. 2000). Lack of PHB affects lifespan and induces a strong mitochondrial stress response (Artal-Sanz and Tavernarakis 2009, Gatsi, Schulze et al. 2014, Hernando-Rodriguez, Erinjeri et al. 2018). In this work, we reveal new genetic interactors of PHB in order to uncover the molecular mechanisms regulated by PHB involved in the maintenance of mitochondrial homeostasis and its impact on aging.

PHB are essential for embryonic development in *Caenorhabditis elegans* (Artal-Sanz, Tsang et al. 2003), however homozygous PHB deletion mutants develop into sterile adults due to maternal contribution. Therefore, deletion mutants need to be maintained as balanced heterozygous. We developed a successful strategy for automated whole animal image-based RNAi screening that can be adapted and applied to any balanced strain carrying a fluorescently labelled balancer and potentially an additional gene expression reporter (Hernando-Rodriguez, Erinjeri et al. 2018). We optimized a sorting strategy, using flow cytometry, capable of separating homozygous mutant animals expressing a GFP-based stress reporter from a GFP-marked balanced population at an early larval stage (L2). In addition, we established a robust and free available automated imaging protocol where worm segmentation is done in the brightfield image, thus usable for many different purposes. Another strong point of our image analysis protocol is the successful identification of worms carrying a pharyngeal GFP element.

Furthermore, we have created the Ortholist RNAi sub-library, that contains exclusively *C. elegans* genes that present orthologue gene in humans (Shaye and Greenwald 2011). This sub-library streamlines RNAi screens by focusing on genes with translational potential to human health and reducing efforts by 60%. Recently an update of the Ortholist has been published (Kim, Underwood et al. 2018) and showed that from the 7663 genes reported in the original Ortholist, only 151 genes changed, confirming the high quality and giving more strength to our RNAi sub-library.

With this strategy, we were able to identify new genetic interactors of PHB that modulate the mitochondrial unfolded protein response, UPR^{mt}.

A striking phenotype of PHB depletion is its opposing effect on aging: while it shortens lifespan of wild type worms, loss of PHB enhances the lifespan of the already long-lived Insulin/IGF-1 Signaling (IIS) mutants (Artal-Sanz and Tavernarakis 2009, Gatsi, Schulze et al. 2014). Moreover, the mitochondrial stress response induced in those mutants upon PHB depletion is reduced compared to that of wild type worms. In this work, we report that the UPR^{mt} is required for the long lifespan of *daf-2* mutants and inhibition of this response suppresses the enhancement of the lifespan elicited by PHB depletion. It has been described that mitophagy (Palikaras, Lionaki et al. 2015), the UPR^{ER} (Henis-Korenblit, Zhang et al. 2010) and the HSR (Morley and Morimoto 2004) are required for the long lifespan of *daf-2* mutants. Here we add one more signaling pathway that contributes to the enhanced lifespan of these mutants. It would be interesting to study whether these stress responses, together with DAF-16, share, at least partially, a common genetic program that would be responsible for the IIS aging phenotype.

We aimed at performing a systematic study looking for PHB genetic

interactors involved in the regulation of the UPR^{mt} both in wild type and in IIS mutants. Due to the bottle neck that sorting homozygous mutants caused, for the realization of the RNAi screen, in two genetic backgrounds and in duplicate, we changed to a double RNAi strategy after ensuring that it was appropriate for high throughput approaches. It is worth mentioning the relatively small overlap between the candidates from *phb-2* mutants and the candidates from *phb-1(RNAi)*. One possibility could be that the RNAi strategy leads to a less efficient genetic depletion, which could be improved by using a strain hypersensitive to RNAi, such as *rrf-3* or *eri*-1 mutants (Asikainen, Storvik et al. 2007)8. Nevertheless, by comparing with previously published RNAi screens looking for suppressors of the UPR^{mt} (Benedetti, Haynes et al. 2006, Shore, Carr et al. 2012, Runkel, Liu et al. 2013), when using the double RNAi strategy, we replicated the majority of them (12 out of 20 and depletion of 4 of the described genes caused developmental arrest under our conditions). In addition, the less penetrant phenotype conferred us an advantage since it allowed the identification of PHB interactors that caused larval arrest in *phb*-2 mutants. PHB deletion mutants have slower development, are completely sterile and may be more sensible to any genetic modification, which cause developmental arrest. Indeed, we observed that depletion of genes implicated in DNA repair causes larval arrest in *phb*-2 mutants. By using double RNAi, we encountered interesting candidates involved in DNA repair and chromatin modification. It is worth noting that *tlf-1(RNAi)* causes larval arrest in the double mutant *phb-2;daf-2* (data no shown).

One interesting point is the different results depending on the data analysis used. RNAither is a statistical pipeline designed to give a list of significant genes from raw signal intensity data (Rieber, Knapp et al. 2009). We took the median intensity of each well as signal intensity and applied the Z-score

normalization. When taking the median value, we were estimating all the GFP values distributions were normal, which afterwards we realized it was not the case. In addition, we assumed that, since it is a genome-wide RNAi, most of the RNAi clones would not have an effect on the signal intensity. However, we did not take in account the variability between different plates. RNAither is a pipeline developed for cell-based screens, where the variability is lower. When working with a complete organism, such us *C. elegans*, the inherent variability of the system has to be taken in account. When we looked more closely to the plates we understood we should normalize the data to its respective controls (control(RNAi) in each plate). The analysis performed with a more personalized pipeline with the help of REDgen Bioinformatics compared the distribution of the intensities in each well with the distribution of the intensities in the controls wells. This allowed us to gain statistical power. Another thing that we implemented in the second analysis was a size exclusion criteria, since small worms have lower P*hsp-6*::GFP expression levels. When we changed to the second analysis, the number of genes reducing the signal in both backgrounds was extremely reduced. From 306 candidates reducing in both backgrounds in first analysis, 127 have been excluded based on size and 136 appeared as common candidates with the second analysis. Among those common candidates, are the candidates that we validated on plate. Curiously, the number of RNAi clones affecting *daf-2;phb-1(RNAi)* mutants increased drastically, almost doubled, while the number of candidates increasing the UPR^{mt} in *phb-1(RNAi)* diminished to the half. The distribution of the intensities in *daf-2;phb*-1 is quite narrow whereas in *phb-1(RNAi)* the distribution is wider. This might explain the differences in the number of candidates, since in the second analysis the detection of candidates is related with the distribution: the narrower the distribution is, the higher the statistical power is. Another difference

between the two analysis was that with RNAither we did not consider the *p* value, which will also explain why the number of candidates is reduced from the first to the second analysis. When we looked more closely to the genes whose depletion caused opposing effect on the UPR^{mt} depending on the background we observed that the majority of the candidates from the first analysis showed the same tendency when analyzed with the second analysis but without being significant. Again, the second analysis gave us more statistical power. Indeed, by performing two different analysis we were able to identify strong and interesting candidates such as *hrpu-1* or *sti-1*, candidates with the first analysis and clear tendency with the second. It would be interesting to do a more thorough examination of the overlap between the two analysis and further study other possible regulators of the UPR^{mt} elicited by PHB depletion.

It is interesting to note that inhibition of protein synthesis by depleting ribosomal proteins, both small and large subunits, produced developmental arrest in in *phb-1(RNAi)* worms and in *daf-2;phb-1(RNAi)* mutants. Protein synthesis inhibition has been largely described as causing developmental arrest early in life and lifespan extension in adults (Chen, Pan et al. 2007, Curran and Ruvkun 2007, Hansen, Taubert et al. 2007, Pan, Palter et al. 2007, Syntichaki, Troulinaki et al. 2007, Dalton and Curran 2018). Moreover, we observed that inhibition of translation, mostly by depletion of ribosomal proteins and translation initiation factors, alleviated the mitochondrial stress elicited by lack of PHB in both backgrounds. This phenomenon was already described in flies and in worms (Haynes, Yang et al. 2010, Liu and Lu 2010, Baker, Nargund et al. 2012, Nargund, Pellegrino et al. 2012, Shore, Carr et al. 2012, Houtkooper, Mouchiroud et al. 2013, Runkel, Liu et al. 2013). This is a good example of processes that are key regulators of development, reproduction and aging.

Curiously, inhibition of protein folding by depletion of Chaperonin Containing TCP-1 (CCT) genes, and inhibition of ATP hydrolysis coupled to proton transport, mainly by depleting vacuolar proton ATPase (v-ATPase) genes, reduced the mitochondrial stress in both backgrounds. In both cases, this decrease in the stress response was due to a reduction of the worm size. Even though we set a size criterion to exclude worms with developmental defects, this criterion was quite permissive and we were able to identify processes and genes necessary for development. During the L3/L4 larval stage there is an immense mitochondrial proliferation. Furthermore, it has been shown that depletion of ETC genes during this stage has an impact on aging, while depleting of these genes during adulthood does not affect lifespan (Dillin, Hsu et al. 2002, Rea, Ventura et al. 2007). It would be interesting to study the effect of depleting CCT genes, v-ATPAses encoding genes and genes related with splicing after L3/L4 stage and analyze whether they behave similar to ETC genes.

Interestingly, we found two new regulators of the UPR^{mt}, C16A3.4 and TLF-1, not previously involved in maintenance of mitochondrial homeostasis. Strikingly, the two transcription factors appeared to be required for the activation of the UPR^{mt} mainly under a strong mitochondrial defect, like depletion of PHB or SPG-7. Instead, C16A3.4 and TLF-1 are not necessary for dealing with the stress elicited by lack of CCO-1. SPG-7 in *C. elegans* functions as part of a m-AAA metalloprotease and PHB have been described to physically interact with m-AAA protease in yeast (Steglich, Neupert et al. 1999). The m-AAA protease regulates degradation of mitochondrial proteins as well as formation of mitochondrial protein complexes. Depletion of PHB and SPG-7 causes mitochondrial disorganization and accumulation of unfolded/misfolded proteins. However, cco-1encondes the cytochrome c oxidase-1 subunit Vb/COX4, a component of the electron transport chain

whose depletion has been described to cause mild defects (Durieux, Wolff et al. 2011). Depletion of CCO-1, might not cause such as proteotoxic stress as the lack of proteins involved in global protein assembly/degradation. It could be interesting to study whether C16A3.4 and TLF-1 are involved preferentially in promoting a chaperone-mediated program to resolve mitochondrial homeostasis. Furthermore, we should assess whether these two transcription factors are necessary for the enhanced lifespan under mitochondrial stress response. Interestingly, TLF-1 has been described as required for lifespan of *daf-2* mutants (Samuelson, Carr et al. 2007).

In addition, both TLF-1 and ATFS-1 have been described to be necessary for the induction of the immune response gene *irg-1* (Estes, Dunbar et al. 2010{Pellegrino, 2014 #38). This suggests that *tlf-1* and *atfs-1* might have common target genes and could be cooperating for the induction of their transcriptional targets that would be interesting to identify.

Moreover, we encountered two new genes involved in the mitochondrial protection conferred by lack of the IIS pathway: USP-48 and HIS-65. USP48 has been involved in DNA repair in cells, and its depletion confers protection under genomic stress (Uckelmann, Densham et al. 2018) (Velimezi, Robinson-Garcia et al. 2018) and USP48 appears to be associated with the active regions of the chromatin (Engelen, Brandsma et al. 2015, Ji, Dadon et al. 2015). Additionally, USP48 has been suggested as a new mechanism of crosstalk between NFKB and p53 stress response pathways in a manner independent of its deubiquitinase activity (Schweitzer and Naumann 2015, Cetkovska, Sustova et al. 2017). However, it is known that chromatin remodeling affects aging (Sen, Shah et al. 2016) and it is interesting that USP48 modulates ubiquitination levels of H2A in other organisms. Our other candidate is HIS-65, a histone H2A, from which very little is known in *C. elegans*. However, it is described that histones

depletion shifts metabolism from fermentative to mitochondrial (Galdieri, Zhang et al. 2016). Moreover, it has been suggested that *daf-2* mutants undergo a metabolic restructuring which confer them higher metabolic efficiency (McElwee, Schuster et al. 2006, Depuydt, Xie et al. 2014). They show an increase in mitochondrial fermentative malate dismutation, which contributes to their increased longevity (Rea and Johnson 2003, Edwards, Copes et al. 2013). In addition, it is suggested that lack of PHB causes a further increment in fermentative metabolism in these mutants (Lourenco, Munoz-Jimenez et al. 2015). It would be interesting to study whether *daf-2;phb-1(RNAi)* do not have the capacity to burst mitochondrial metabolism and require the fermentative metabolism for the enhanced lifespan in the absence of HIS-65. And whether USP-48 is involved in the process by modulating histones ubiquitination levels.

CONCLUSIONS

1. PHB deletion induces the mitochondrial unfolded protein response by a non-canonical mechanism.

2. PHB deletion results in sterility and null mutations need to be maintained in heterozygosis using chromosome balancers. A semi-automated workflow, combining worm sorting and high-content image analysis, has been set-up for balanced strains carrying a fluorescently labelled balancer and a gene expression reporter. This technique can be applied to the systematic analysis of other essential genes.

3. IIS mutants have a reduced mitochondrial stress response upon PHB depletion compared to wild type worms. However, this reduced mitochondrial stress response is essential for the increased lifespan conferred by PHB depletion. Importantly, *daf-2(e1370)* mutants in the absence of mitochondrial stress require the mitochondrial UPR^{mt} for enhanced longevity.

4. In order to study PHB interactors in two backgrounds, wild type and *daf-2* mutants, we optimized an additional technique. We conclude that a double-RNAi technique is appropriate for high-content approaches.

5. By performing different data analysis, we obtained different results. When analysing high-content data, it is important to look at the distribution of the data, not assuming normal distribution, and to normalize to the respective control. However, the strongest candidates appeared with both analysis.

6. The screening has provided interesting candidates that can be studied in further detail in the future

7. Inhibition of protein degradation, disruption of mitochondrial

integrity and impairment of ATP synthesis coupled to electron transport increases the mitochondrial stress response in *phb-1(RNAi)* worms and in *daf-2;phb-1(RNAi)* mutants.

8. Inhibition of protein biogenesis reduces the mitochondrial stress response in *phb-1(RNAi)* worms and in *daf-2;phb-1(RNAi)* mutants.

9. C16A3.4 and TLF-1 are two new regulators of the mitochondrial stress response elicited by proteotoxic stress or mitochondrial disorganization.

10. USP-48 is needed for normal lifespan in wild type, *phb-1(RNAi)* animals, *daf-2* mutants and PHB-depleted *daf-2* mutants. Nevertheless, its depletion has a stronger effect in IIS mutants.

11. Lack of HIS-65 (H2A) induces the mitochondrial stress response and reduces lifespan specifically in *daf-2;phb-1(RNAi)* mutants

MATERIALS AND METHODS

1. Nematodes strains and maintenance

The *C. elegans* strains used in this study are listed in the next table. Unless otherwise stated, we cultured the worms according to standard methods (Brenner 1974). We maintained nematodes at 20°C on nematode growth media (NGM) agar plates seeded with live *Escherichia coli* OP50, obtained from the Caenorhabditis Genetics Center (CGC).

Strain	Description	Genotype	Original name
N2	wild type, Bristol strain		
BR927	*daf-2* loss of function mutant	*daf-2(e1370)III*	
MRS57	wild type with the mitochondrial stress reporter	*zcIs13[* P*hsp-6::* GFP*]V*	
MRS20	daf-2 los of funtion mutant with the mitochondrial stress reporter	*daf-2(e1370)III;zcIs13[* P*hsp-6::* GFP*]V*	
MRS106	balanced *phb-* 2 loss of function mutant with the mitochondrial stress reporter	*phb-2(tm2998) /mIn1* [*dpy-10(e128) mIs* 14(P*myo-2* ::GFP)]II;*zcIs13* [P*hsp-6::* GFP]V	
MRS104	balanced *phb-2* loss of function mutant with the mitochondrial stress reporter	*phb-2(tm2998) /mIn1* [*dpy-10(e128) mIs* 14(P*myo-2* ::GFP)]II;*zcIs13* [P*hsp-60::* GFP]V	
MRS85	wild type with the ER stress reporter	*zcIs4[* P*hsp-4::* GFP*]V*	SJ4005
MRS178	wild type with the heat shock reporter	*dvIs70 [*P*hsp-16.2::* GFP + *rol-6(su1006]*	CL2070

2. Preparation of bacteria for liquid RNAi assays

OrthoList RNAi sub-library (Hernando-Rodriguez, Erinjeri et al. 2018) plates were replicated in LB agar, and bacteria were grown overnight at 37 °C. The advantage of growing the bacteria in solid media is the ease of visualizing bacterial clones that do not grow. If needed, the samples can be kept at 4 °C for 2 days maximum. Next day, we inoculated the RNAi library in 2.2-ml 96-well plates (VWR). Using the pin replicator, we inoculated the bacteria from the LB agar into 1.2 ml of LB supplemented with ampicillin (100 µg/ml, Sigma-Aldrich) and tetracycline (15 µg/ml, Sigma-Aldrich). Positive and negative controls were added in the last column of the plate. We cultured the bacteria overnight at 37 °C with shaking (180 rpm, New BrunswickTM Innova® 44/44R). In order to have fresh cultures, on the day of sorting, we inoculated 100 µl of the O/N cultures in 900 µl of LB supplemented with ampicillin and tetracycline in deep well plates (VWR)

and incubated for 3 h at 37 °C with shaking. We added isopropylthio-β-galactoside (IPTG, 1 mM, Sigma-Aldrich) to the wells to induce plasmid expression for 2 h at 37 °C with shaking. Then, we harvested the cultures by centrifugation (10 min, 3200 g, 4 °C, Eppendorf 5810R) and re-suspended the pellets in 250 µl of S-medium supplemented with carbenicillin (25 µg/ml, Sigma-Aldrich), IPTG (1 mM, Sigma-Aldrich) and cholesterol (5 µg/ml, Sigma-Aldrich).

3. Worm preparation and worm dispensing

For each round of sorting, we synchronized the worms, obtaining eggs from gravid hermaphrodites by hypo-chlorite treatment. Briefly, 20 ml of liquid culture with worms suspended in S-medium supplemented with OP50 (30 g/L wet weight) was washed with M9 until the supernatant appeared cleared of bacteria. We added bleaching solution and energetically agitated the tubes for 2 min. After centrifugation and removal of the supernatant, we washed the worms with M9. We added a second round of bleaching solution for less than 1 min. We washed the pellets three more times with M9 and filtered them with 40 µm Nylon Cell Strainers (VWR) to remove the possible remains of adult worms. We allowed the embryos to hatch overnight in M9 at 20 °C with shaking (120 rpm, New BrunswickTM Innova® 44/44R). The following day, we placed starved L1s in S-medium with OP50 (30 g/L) for 48 h at 20 °C with shaking (120 rpm). At this point, the population is heterogeneous. Since homozygous *phb-2(tm2998)* mutants show a developmental delay, they are at the second larval stage after 48h. Worms were washed out from the OP50 culture by successive centrifugations until the supernatant was clear. We re-suspended worms in M9 supplemented with 0.01% Triton X-100 (T8787, Sigma-Aldrich) to avoid worms sticking to the plastic. Next, we sorted 40 worms per well

using enhanced mode, with a sort delay (time from analysis of the object to the sort command) of 7 ms and a sort width (drop volume) of 6 ms.

Subsequently, we added to the worms 25 µl of S-medium supplemented with carbenicillin (25 µg/ml, Sigma-Aldrich), IPTG (1 mM, Sigma-Aldrich) and cholesterol (5 µg/ml, Sigma-Aldrich), and then 75 µl of the bacterial culture was added. We incubated the worms for 48 h at 20 °C with shaking (120 rpm, New BrunswickTM Innova® 44/44R) until they reached the young adult stage.

During the sorting, we aimed to keep the sheath flow rate constant at 9.5 ml/min and a worm concentration of 15–20 events per second. At the start of each experiment, a small sample (one single worm in 96 wells) was sorted and visually verified to confirm a correct sorting, that is, correct number of animals and correct selection of the population.

The worm sorter is a pressurized machine, and one should pay attention to any clog that might interfere with the liquid flow from the sample cup to the flow cell.

Every day, before starting, the tubes were cleaned by passing consecutively from the sample cup 10% bleach, water and 70% ethanol, and then rinsing with abundant water. Moreover, all the solutions were passed through a 40 µm Nylon Cell Strainer (VWR) filter.

In the case of P*hsp-6*::GFP and *daf-2(e1370);*P*hsp-6*::GFP, we obtained synchronized L1 larvae by collecting eggs after hypochlorite treatment and allowing them to hatch and arrest overnight in M9 at 20 ºC with agitation (120 rpm). We dispensed 40 µl of worm suspension in order to have 60 L1s per well using a microplate dispenser (EL406 washer dispenser, BioTek).

Subsequently, we added to the worms 25 µl of S medium supplemented with carbenicillin (25 µg/ml – Sigma-Aldrich), IPTG (1 mM – Sigma-Aldrich) and cholesterol (5 µg/l – Sigma-Aldrich). We added 40 µl of *phb-1(RNAi)* and 40 µl of the OrthoList sub-library bacterial culture. We incubated worms at 20ºC with shaking (120 rpm) until they reached the young adult stage.

4. Imaging of multi-well plates

In order to have clear images, we washed the plates by sequential flushes of water, shaking to disaggregate the bacteria, sedimentation of the worms and aspiration of the supernatant (EL406 washer dispenser, Biotek). Prior to this, we added 10 µl of tetramisole hydrochloride (100 mM, Sigma-Aldrich) to each well to paralyze the worms. Each well was filled to the brim and sealed with transparent SealPlate (Sigma-Aldrich) to ensure the horizontal meniscus required to give uniform brightfield illumination across each well. We acquired pictures in brightfield and green channel with the IN Cell Analyzer 2000 (GE Healthcare) using a 2× objective in order to have the entire well in one image. A whole 96-well plate can be imaged in less than 5 minutes in each of the channels.

5. Data analysis

An empty feeding vector, pL4440, was used as negative control (control(RNAi)) and *atfs-1(RNAi)*, that suppresses almost completely the UPR^{mt}, as positive control.

The pipeline used to analyze the *phb-2(tm2998);* P*hsp-6*::GFP mutants screen consists of several filtering steps, quality control and statistical

test. First, based on the green head ID, worms with a green pharynx were discarded, as well as worms with a length smaller than 550 μm. In order to remove outliers, the 5th and the 95th percentiles of the distribution were excluded. After filtering, wells with less than five worms were removed from the analysis. A quality assay was performed in the control wells: only control wells with mean GFP intensity between 200 and 500 arbitrary units (a.u.) and a coefficient of variation < 0.5 were accepted. If less than two control wells remained accepted, the plate was discarded and the process repeated. In order to make data from different plates comparable, the data was normalized by dividing the GFP value of each worm by the mean of the GFP of the four negative control wells. Finally, statistics were assessed by running an analysis of variance (ANOVA) test followed by a Dunnett's test. Candidates were defined based on the adjusted *p* value and the fold change (FC) (*p* value < 0.001 and FC < 0.66 or FC > 1.5).

In the case of the double RNAi screen using the strains P*hsp-6*::GFP and *daf-2(e1370)*;P*hsp-6*::GFP we carried out two independent replicates, we assessed the quality of the screens and we performed three types of analysis.

As quality control, we calculated the Strictly Standardized Mean Difference (SSMD) (Zhang 2007), that evaluates the magnitude of the differences between positive and negative controls, and the Pearson coefficient to calculate the reproducibility between replicates. The SSMD is calculated by the formula $SSMD = (\mu_1 - \mu_2) / (\sqrt{(\sigma_1^2 + \sigma_2^2 - 2\sigma_1\sigma_2)})$, being m the mean and s the variance of a given population. The SSMD reflects the probability of the difference being greater than 0; the larger the absolute value of SSMD, the greater the differentiation between the two populations. $|SSMD| \geq 3$ indicates that the size of the mean difference is at least three times that of the standard deviation of the difference between the two populations and is an indicator of good quality. The Pearson coefficient gives information about

the magnitude of the correlation as well as the direction of the relationship. It ranges from -1 to 1, 1 being a perfect positive relation between the two variables, -1 implies a perfect negative relation and 0 indicates that there is no linear correlation between the variables.

The first analysis was using the same pipeline we used in the screen performed with *phb-2* mutants, we analyzed the plates containing genes annotated to chromosome I completed with *phb-1(RNAi)* worms. We then compared the candidates obtained with *phb-2(tm2998)* mutants and with *phb-1(RNAi)* worms.

The second analysis was using RNAither, a statistical pipeline designed to give a list of significant genes from raw signal intensity data (Rieber, Knapp et al. 2009). We did not set a size criterion and we excluded wells with the 5% lowest worm count in the entire screen ($n < 12$). We took the median intensity of each well as signal intensity. We carried out the Z-score normalization as we were performing a genome-wide screen. The Z-score represents how many standard deviations from the mean the sample is and it is calculated following the formula $Z\text{-score} = (x - m) / s$, being x the median of the sample, m the mean of the screen and s the standard deviation of the screen. We selected candidates based on the Z-score (Z score <-2 or Z-score > 2).

For the third analysis, we designed a more personalized pipeline with the help of REDgene Bioinformatics that consists of filtering and normalizing the data followed by a statistical test. This pipeline can be applied in a high throughput manner. First, worms with a length smaller than 660 μm were discarded and wells with less than 10 worms after the filtering were removed from the analysis. In order to make data from different plates comparable, data were normalized by dividing the GFP mean intensity of

the well by the mean of the GFP of the four negative control wells. Finally, significance of the differences was assessed by running a t-test comparing the distributions of the data in each well with the distribution in the negative control wells. The resulting *p* values were corrected for multiple testing by the Benjamini-Hochberg method (Hochberg and Benjamini 1990). Candidates were defined based on the mean of the adjusted *p* value and mean of the LOG2 of the fold change (LFC) (*p* value < 0.05 and LFC < -0.58 or LFC > 0.58).

Interaction networks were built using STRING (Szklarczyk, Morris et al. 2017), based on predicted and described interactions in different organisms, and functional annotation clustering was performed with DAVID Bioinformatics Resource 6.8 (Huang da, Sherman et al. 2009).

For the first GO term enrichment analysis, we incorporated the RNAi clones that down-regulated and up-regulated the UPR^{mt} and we used the DAVID Bioinformatics Resource 6.8 (Huang da, Sherman et al. 2009) and we plotted the enrichment result using R. For the second GO term enrichment analysis, we used the topGO package in R. This time we separately examined the genes whose depletion up-regulated and down-regulated the mitochondrial stress response. This algorithm considers the hierarchical structure of GO and eliminates local similarities and dependencies between GO terms (Alexa, Rahnenfuhrer et al. 2006). For the visualization of the enrichment results we used ReviGO, a web server that takes long lists of GO terms, summarizes them and plots them in scatterplots based in semantic similarity (Supek, Bosnjak et al. 2011).

For the KEGG pathway enrichment we also took together the RNAi clones that down-regulated and up-regulated the UPR^{mt} and we plotted the enrichment result in a heat map using R.

6. RNAi assays on plate

For RNAi experiments worms were placed on NGM plates, supplemented with 25 µg/ml carbenicillin (Sigma-Aldrich) and 10 µg/ml nystatin (Sigma-Aldrich), seeded with HT115 (DE3) *E. coli* bacteria (deficient for RNase-E) transformed with empty the required dsRNA plasmid. Each bacterial strain was inoculated, from an overnight pre-inoculum, in LB (ampicillin (100 µg/ml) (Sigma-Aldrich) and tetracycline (15 µg/ml) (Sigma-Aldrich). The overnight culture was diluted (1:10) and grown in a shaking incubator at 37°C for 3 hours, until it reached an OD_{600} of around 1.5. Then, in order to induce the dsRNA expression, we added IPTG (final concentration: 1 mM) (Sigma-Aldrich) to the bacterial culture and we harvested the bacterial culture after 2 hours of incubation at 37°C by centrifugation (8 min at 6000×*g,* 4°C). Following, we washed the pellets with S Basal and harvested them again. Finally, we re-suspended bacterial pellets to a final concentration of 30 g/L in complete S Medium. Bacterial stocks were kept at 4°C up to 4 days before being used. For all the double RNAi treatments, bacterial stocks were mixed in a proportion of 1:1 before seeding the plates.

A semi-synchronous embryo population was grown on plates seeded with the appropriate RNAi bacterial clone at 20°C until the desired stage (young adult).

7. Stress assays

To monitor the UPR^{ER} we used the strain expressing the reporter P*hsp-4*::GFP. When worms reached the L4 stage we transferred them to new RNAi plates with 7.2 µM tunicamycin (Sigma-Aldrich) and incubated for 6 hours at 20°C.

For heat shock assays we grew worms expressing P*hsp-16.2*::GFP on RNAi plates until the L4 stage and subjected them to 35°C for 2 hours followed by 4 hours of recovery at 20°C.

8. Imaging

On the day of imaging, 20-30 worms previously anesthetized with 10 mM Levamisole (Sigma-Aldrich), were mounted on 2% agarose pads and imaged using the AxioCam MRm camera on a Zeiss ApoTome Microscope. Image analysis was performed using the ImageJ software. Emission intensity was measured on greyscale images with a pixel depth of 16 bits. At least two independent assays were carried out and data was analyzed by one-way ANOVA using the GraphPad Prism software (version 5.0a).

9. Lifespan Analysis

All lifespans were performed at 20°C. Semi-synchronized eggs were obtained by hypochlorite treatment of adult hermaphrodites and placed on NGM plates seeded with HT115 *E. coli* bacteria. During the course of the lifespan assays, we transferred adult worms to fresh plates every day during their reproductive period and afterwards on alternate days. Worms were scored as dead when they no longer responded to touch, while exploded animals, those exhibiting bagging (embryo hatching inside the worm), or dried out at the edges of the plates were censored.

We used the GraphPad Prism software (version 5.0a) to plot survival curves and to determine significant differences in lifespans (log-rank (Mantel-Cox) test). See Table S1 for lifespan statistics.

10. Western blot

Prohibitin depletion was assessed by immunoblot assay. A semi-synchronized population of worms was grown at 20°C until they reached day 1 of adulthood when we washed them from the plate with M9 and harvested them in 1.5 ml eppendorfs. We washed the pellets at least three times with M9 in order to remove the bacteria. We froze the samples in liquid nitrogen and store them at -80°C. We performed protein determination with an RC DC (reducing agent and detergent compatible) protein assay (Bio-Rad). We loaded 30 μg of protein in a TGX Stain-Free 12% acrylamide gel (Bio-Rad). Following electrophoresis, we used the Trans-Blot Turbo Transfer System (Bio-Rad) to transfer the proteins to a nitrocellulose membrane. We visualized the immunoblots by chemiluminescent detection (Pierce ECL Western Blotting Substrate). We incubated the western blots with Prohibitin_APP-2 antibody (Hernando-Rodriguez, Erinjeri et al. 2018), 1:3000, overnight at 4 °C and we used the stain free system as loading control.

11. Solutions

LB (Luria-Bertani) media, solid and liquid, supplemented with ampicillin 100μg/ml and tetracycline 15 μg/ml, both from Sigma-Aldrich.

M9 buffer:22 mM KH_2PO_4, 33.7 mM Na_2HPO_4, 85.6 mM NaCl, 1 mM $MgSO_4$.

S Basal: 6.6 mM $K_2HPO_4.3H_2O$, 43.4 mM KH_2PO_4, 100 mM NaCl

S medium buffer: 50mM KH_2PO_4 pH6, 10mM $C_6H_5K_3O_7$ pH6, 100mM NaCl, 3mM $CaCl_2$, 3mM $MgSO_4$, 10 ml oftrace metal solution.

Supplemented with carbenicillin 25 μg/ml, IPTG 1 mM and cholesterol 5 μg/ml, all of them from Sigma-Aldrich.

Trace Metal solution: 5 mM Disodium EDTA, 2.5 mM FeSO4 7*H2O, 1mM MnCl2 4*H2O, 1mM ZnSO4 7*H2O, 0.1mM CuSO4 5*H2O

Bleaching solution (2.75 ml H_2O, 2 ml commercial bleach, 0.250 ml 5 M KOH)

APPENDIX

Appendix 1: Detailed experimenal protocol

Screening strain and reagents:

*phb-2(tm2998)/mIn1[dpy-10(e128)mIs14(*P*myo-2*::GFP*)]II;*P*hsp6*::GFP mutants

RNAi library based on the compendium of the *C. elegans* genes sharing homologues in humans.

Last column of the plates reserved for controls: Empty feeding vector, pL4440, as negative control and *atfs-1(RNAi)*, that suppresses almost completely the UPR^{mt}, as positive.

LB (Luria-Bertani) media, solid and liquid, supplemented with ampicillin 100μg/ml and tetracycline 15 μg/ml, both from Sigma-Aldrich.

M9 buffer:22 mM KH_2PO_4, 33.7 mMNa_2HPO_4, 85.6 mMNaCl, 1 mM$MgSO_4$.

S medium buffer (potassium phosphate pH6 50mM, potassium citrate pH6 10mM, NaCl 100mM, $CaCl_2$ 3mM, $MgSO_4$ 3mM, trace metal solution) supplemented with carbenicillin 25 μg/ml, IPTG 1 mM and cholesterol 5 μg/ml, all of them from Sigma-Aldrich.

Bleaching solution (2.75 ml H_2O, 2 ml commercial bleach, 0.250 ml 5 M KOH)

1mM IPTG from Sigma-Aldrich to induce the expression of the dsRNA in the bacteria

Triton X-100 (T8787) from Sigma-Aldrich

Tetramisole hydrochloride (L9756) from Sigma-Aldrich

Day 1:

RNAi library replication: The RNAi library was frozen in glycerol supplemented LB in microtiter plates. The last column of the plates was left free to add the pertinent controls. Using a pin replicator (BOEKEL), we replicated the plate in LB agar supplemented with ampicillin (100μg/ml - Sigma-Aldrich) and tetracycline (15 μg/ml – Sigma-Aldrich). The advantage of growing the bacteria in solid media is the ease to visualize the wells where the bacteria did not grow. Bacteria was grown overnight at 37ºC and then kept at 4ºC.

Synchronization of *phb-2(tm2998)/mIn1;*P*hsp-6*::GFPmutants: The worms were synchronized as previously described [2]. Briefly, 20 ml of liquid culture with worms in OP50 (30 g/l) were washed with M9 until the supernatant appeared clear of bacteria. Bleaching solution was added and tubes were energetically agitated for 2 minutes. After

centrifugation and removal of the supernatant, the worms were washed with M9. A second round of bleaching solution was added for less than 1 minute. The pellet was then washed three more times with M9 and filtered with 40 μm Nylon Cell Strainers (VWR) to remove the possible remains of adult worms. Embryos were allowed to hatch overnight in M9 at 20ºC with shaking (120rpm - New Brunswick™ Innova® 44/44R).

Day 2:

Starved *phb-2(tm2998)/mIn1;*P*hsp-6*::GFP L1s were placed in liquid OP50 (30 g/l) for 48 hours at 20ºC with shaking, (120rpm - New Brunswick™ Innova® 44/44R), until they reached L2 stage.

Day 3:

Inoculation of the RNAi library in 2.2ml 96 well plates: Using the pin replicator (BOEKEL) we inoculated the bacteria from LB agar in 1.2 ml of LB supplemented with ampicillin (100μg/ml - Sigma-Aldrich) and tetracycline (15 μg/ml – Sigma-Aldrich) in deep well plates (VWR). Positive and negative controls were added in the last column of the plate. The bacterial cultures were grown overnight at 37ºC with shaking (180rpm - New Brunswick™ Innova® 44/44R).

Day 4:

Preparation of the bacteria: 100 μl of the O/N cultures were inoculated in 900 μl of LB supplemented with ampicillin (100μg/ml - Sigma-Aldrich) and tetracycline (15 μg/ml – Sigma-Aldrich) in deep well plates (VWR) and incubated for 3 hours at 37ºC with shaking (180rpm - New Brunswick™ Innova® 44/44R). IPTG (1mM– Sigma-Aldrich) was added to the wells in order to induce the expression of the plasmid for 2 hours at 37ºC with shaking (180rpm - New Brunswick™ Innova® 44/44R). The cultures were harvested by centrifugation (3200g during 10 minutes at 4ºC – Eppendorf 5810R) and pellets were resuspended in 250 μl of S-medium supplemented with carbenicillin (25 μg/ml – Sigma-Aldrich), IPTG (1 mM – Sigma-Aldrich) and cholesterol (5 μg/ml – Sigma-Aldrich).

Preparation of the worms: Worms were washed out from the OP50 culture by successive centrifugations until the supernatant was clear. Worms were resuspended in M9 supplemented with Triton X-100 (Sigma-Aldrich) to a final concentration of 0.01% to avoid adherence to the plastic.

Sorting of the worms: 40 homozygous L2s were sorted in each well in a volume of 40 μl, 25 μl of S medium supplemented with carbenicillin (25 μg/ml – Sigma-Aldrich), IPTG(1 mM – Sigma-Aldrich) and cholesterol (5 μg/ml – Sigma-Aldrich) were added to the worms. Finally, 75 μl of the bacterial culture was added.

Worms were incubated for 48 hours at 20ºC with shaking, (120rpm - New Brunswick™ Innova® 44/44R) until they reached young adult stage.

Day 6:

Imaging of the plates: In order to have clear images, the plates were washed by sequential flush of water, shaken to disaggregate the bacteria, sedimentation of the worms and aspiration of the supernatant (EL406 washer dispenser, BioTek). Prior to this, 10 µl of tetramisolehydrochloride (100 mM - Sigma-Aldrich) was added to each well to paralyze the worms. Pictures in brightfield and green channel were acquired using the IN Cell Analyzer 2000 (GE Healthcare). The 2x objective was used in order to have the entire well in one image.

Appendix 2: Break down of the image analysis protocol

Target Sets		
Well_FITC		
Acceptance Criteria	None set	
Channel FITC-FITC		
Preprocessing	**Run Preprocess Macro**	Channel **2** to **6** Information Equilization, then **6** to **6** Histogram Equilization, Smooth
Segmentation	**Intensity Segmentation**	Min threshold 0, max threshold 1982 (of transformed image in channel 6)
Postprocessing	**Sieve (Binary)**	Keep targets with an area > than 9999994 um2
	Fill Holes	
	Erosion (Binary)	Kernel size 51
		Binary Mask copied to channel 7
	Run Postprocess Macro	Channel **7** to Channel **8** Invert
Measures	No measures	

Brightfield-seg worms		
Acceptance Criteria	[Area]>100008.&[Dens - Levels]>1808.&[Form Factor]<0.58.&[Dens - Levels]<2800.&[End Nodes]<58.&[SD - Levels]>100	
Channel TL-Brightfield-DAPI		
Preprocessing	**Run Preprocess Macro**	Channel 1 to 16, Detail Extractor (Gain=1, Kernel=99) then 16 to 16 Smooth (9x9 kernels), Maximise Contrast, Inversion
Segmentation	**Vesicle Segmentation**	min Granule Size 15um, max Granule size 35um, number of scales 3, sensitivity 93, sensitivity range 1.70 (of transformed image in channel 16)
Postprocessing	**Sieve (Binary)**	keep targets with an area > than 12300 um2
	Erosion (Binary)	Kernel size 5
	Sieve (Binary)	keep targets with an area > than 2999.998 um2
	Dilation (Binary)	Kernel size 7
	Erosion (Binary)	Kernel size 9
	Sieve (Binary)	Keep targets with an area > than 4999.99 um2
	Dilation (Binary)	Kernel size 6
		Binary Mask copied to channel 10
Measures	No measures	

Worms-Well Edge		
Acceptance Criteria	[Area]>100008.&[Fiber Length]<15008.&[Branch Nodes]<28.&[Form Factor]>0.088.&[Form Factor]<0.4	
Channel FITC-FITC		
Preprocessing	**Run Preprocess Macro**	Subtraction Channel **10** - Channel**8** to Channel **11**
Segmentation	**Intensity Segmentation**	Min threshold 1, Max threshold 4095 (of binary Image in channel 11)
Postprocessing	**Sieve (Binary)**	Keep targets with an area < than 99999.96 um2
	Sieve (Binary)	Keep targets with an area > than 13409.48 um2
		Binary Mask copied to channel 13
Measures	No measures	

Green Head		
Acceptance Criteria	[Area]<62008.&[SD - Levels]>200	
Channel FITC-FITC		
Preprocessing	None applied	
Segmentation	**Vesicle Segmentation**	Min Granule Size 1um, max Granule size 30um, number of scales 2, sensitivity 56
Postprocessing	**Dilation (Binary)**	Kernel size 3
	Sieve (Binary)	Keep targets with an area > than 449.99 um2
	Erosion (Binary)	Kernel size 3
		Binary Mask copied to channel 14
Measures	No measures	

Final Worm Mask			
Acceptance Criteria	none applied		
Channel FITC-FITC			
Preprocessing	**Run Preprocess Macro**	Channel 13*1	
Segmentation	**Intensity Segmentation**	Min threshold 1, Max threshold 4095 (of binary image in channel 13)	
Postprocessing	None applied		
Measures	No measures		

Dilated Worm		
Acceptance Criteria	none applied	
Channel FITC-FITC		
Preprocessing	**Run Preprocess Macro**	Channel 13*1
Segmentation	**Intensity Segmentation**	Min threshold 1, Max threshold 4095 (of binary image in channel 13)
Postprocessing	**Clump Breaking**	Using second segmentation Final Worm Mask, include secondary targets Radius 6
		Binary Mask copied to channel 9
	Run Postprocess Macro	Channel **9** minus **8** to channel **8**
Measures	No measures	

Worm-Green Head		
Acceptance Criteria	None set	
Channel FITC-FITC		
Preprocessing	**Run Preprocess Macro**	Subraction channel 13 - channel 14 to channel 15
Segmentation	**Intensity Segmentation**	Min threshold 1, Max threshold 4095 (of binary image in channel 15)
Postprocessing	None applied	
Measures	No measures	

Target Linking

Target set Dilated Worm_Final WormMask	**One to One**	
	Primary target set	Dilated Worm
	Secondary target set	Final Worm Mask
	Output target set	Dilated Worm_Final WormMask
	Overlap criteria	Secondary target is 100% witin primary target
Target set Dilated Worm_Worm-GreenHead	**One to One**	
	Primary target set	Dilated Worm
	Secondary target set	Worm-Green Head
	Output target set	Dilated Worm_Worm-green Head
	Overlap criteria	Any intersection
Target set Worm_ Bkgd_GreenHead	**Composed One to One Link**	
	Primary target set	Dilated Worm_Final Worm Mask
	Secondary target set	Dilated Worm_Worm-Green Head
	Output target set	Worm_Bkgd_GreenHead
	Overlap criteria	Any intersection

Measures

Target set Worm_ Bkgd_GreenHead		
Measure	**From Image**	**Equation**
ID Green Head	FITC-FITC (Ch2)	100 - (([Area<\Worm_Bkgd_GreenHead\Worm-Green Head>] / [Area<\Worm_Bkgd_GreenHead\Final worms mask>]) * 100)
Int Worm	FITC-FITC (Ch2)	[Dens - Levels<\Worm_Bkgd_GreenHead\Final worms mask>]
Int Bkgd	FITC-FITC (Ch2)	([DxA<\Worm_Bkgd_GreenHead\Dilated worms>] - [DxA<\Worm_Bkgd_GreenHead\Final worms mask>]) / ([Area<\Worm_Bkgd_GreenHead\Dilated worms>] - [Area<\Worm_Bkgd_GreenHead\Final worms mask>])
Int Worm - Int Bkgd	FITC-FITC (Ch2)	[Int worm] - [Int Bkgd]
Length Worm	FITC-FITC (Ch2)	[Fiber Length<\Worm_Bkgd_GreenHead\Final worms mask>]
Count All Worms	FITC-FITC (Ch2)	[Count<\Worm_Bkgd_GreenHead\Final worms mask>]
Count Worms with Green Head	FITC-FITC (Ch2)	[ID Green Head]>2

Measure Definitions	
Dens - Levels	Mean gray level value of the pixels contained within the target outline. Gray levels is an intensity scale, where black = 0 and white = 4095 (12-bit image).
DxA	Density (in current density unit) multiplied by area of the target (in current spatial unit).
Standard Deviation	A standard deviation (SD) of pixel densities, which measures the pixel density variation within the target, may also be reported. SD values are available for any density unit.
Area	Area of a target.
Length	Maximum distance across a target. Boundaries may be crossed.
Form Factor	Estimate of circularity, expressed as a value between 0 and 1 (1 equals a perfect circle). Perimeter^2/4*TT*Area
Max Chord-straight	This is the maximum straight-line distance across a target, without crossing a boundary.
Max Chord-curved	Maximum center line through target.
Pos X	Position along the X-axis. Value corresponds to the horizontal coordinate of the center of the mass of the target.
Pos Y	Position along the Y-axis. Value corresponds to the vertical coordinate of the center of the mass of the target.
Fiber length	Total length within a single fibrous shape.

Appendix 3: Break down of the CellProfiler protocol

CellProfiler Pipeline: http://www.cellprofiler.org
Version: 3

IMPUT MODULES

Module 1: Images:\'To begin creating your project, use the Images module to compile a list of files and/or folders that you want to analyse. You can also specify a set of rules to include only the desired files in your selected folders

Filter image:? : Images only

Module 2:

Metadata:\'The Metadata module optionally allows you to extract information describing your images (i.e, metadata) which will be stored along with your measurements. This information can be contained in the file name and/or location, or in an external file

Extract metadat:? : No
Metadata data type: Text
Metadata types: {}
Extraction method count: 1
Metadata extraction method: Extract from file/folder names
Metadata source: File name
Regular expression:^(?P<**Plate**>.*)_(?P<**Well**>\x5BA-P\x5D\x5B0-9\x5D{2})_s(?P<**Site**>\x5B0-9\x5D)_w(?P<**ChannelNumber**>\x5B0-9\x5D)
Regular expression:(?P<**Date**>\x5B0-9\x5D{4}_\x5B0-9\x5D{2}_\x5B0-9\x5D{2})$
Extract metadata from: All images
Select the filtering criteria: and (file does contain “”)
Metadata file location:
Match file and image metadata:\x5B\x5D
Use case insensitive matchin:? : No

Module 3:

Names And Types:\'The Names And Types module allows you to assign a meaningful name to each image by which other modules will refer to it

Assign a name to: Images matching rules
Select the image type: Grayscale image
Name to assign these images: DNA
Match metadata:\x5B\x5D
Image set matching method: Order
Set intensity range from: Image metadata
Assignments count: 3
Single images count: 0

Maximum intensity: 255.0
Select the rule criteria: and (file does contain “Cy3”)
Name to assign these images: Cy3
Name to assign these objects: Cell
Select the image type: Grayscale image
Set intensity range from: Image metadata
Retain outlines of loaded object:? : No
Name the outline image: LoadedOutlines
Maximum intensity: 255.0
Select the rule criteria: and (file does contain “FITC”)
Name to assign these images: FITC
Name to assign these objects: Nucleus
Select the image type: Grayscale image
Set intensity range from: Image metadata
Retain outlines of loaded object:? : No
Name the outline image: LoadedOutlines
Maximum intensity: 255.0
Select the rule criteria: and (file does contain “Brightfield”)
Name to assign these images: Brightfield
Name to assign these objects: Cytoplasm
Select the image type: Grayscale image
Set intensity range from: Image metadata
Retain outlines of loaded object:? : No
Name the outline image: LoadedOutlines
Maximum intensity: 255.0

Module 4: Groups:\’The Groups module optionally allows you to split your list of images into image subsets (groups) which will be processed independently of each other. Examples of groupings include screening batches, microtiter plates, time-lapse movies, etc

Do you want to group your image:? : No
grouping metadata count: 1
Metadata category: None

ANALYSIS MODULES

Module 5: Image Math

Operation: Invert
Raise the power of the result by: 1.0
Multiply the result by: 1.0
Add to result: 0.0
Set values less than 0 equal to :? : Yes
Set values greater than 1 equal to :? : Yes
Ignore the image mask:? : No
Name the output image: InvertedFITC

Image or measuremen:? : Image
Select the first image: FITC
Multiply the first image by: 1.0
Measurement:
Image or measuremen:? : Image
Select the second image:
Multiply the second image by: 1.0
Measurement:

Module 6: Identify Primary Objects

Select the input image: InvertedFITC
Name the primary objects to be identified: Well_FITC_small
Typical diameter of objects, in pixel units (Min, Max): 1500,2000
Discard objects outside the diameter rang:? : Yes
Try to merge too small objects with nearby larger object:? : No
Discard objects touching the border of the imag:? : Yes
Method to distinguish clumped objects: None
Method to draw dividing lines between clumped objects: Intensity
Size of smoothing filter: 10
Suppress local maxima that are closer than this minimum allowed distance: 7.0
Speed up by using lower-resolution image to find local maxim:? : Yes
Name the outline image: Primary Outlines
Fill holes in identified objects? : After both thresholding and declumping
Automatically calculate size of smoothing filter for declumping? : Yes
Automatically calculate minimum allowed distance between local maxim:? : Yes
Retain outlines of the identified objects? : No
Automatically calculate the threshold using the Otsu method? : Yes
Enter Laplacian of Gaussian threshold: 0.5
Automatically calculate the size of objects for the Laplacian of Gaussian filter? : Yes
Enter LoG filter diameter: 5.0
Handling of objects if excessive number of objects identified: Continue
Maximum number of objects: 500
Threshold setting version: 1
Threshold strategy: Global
Thresholding method: Otsu
Select the smoothing method for thresholding: No smoothing
Threshold smoothing scale: 1.0
Threshold correction factor: 1.0
Lower and upper bounds on threshold: 0.0, 1.0
Approximate fraction of image covered by objects? : 0.01
Manual threshold: 0.04
Select the measurement to threshold with: None

Select binary image: None
Masking objects: None
Two-class or three-class thresholding? : Three classes
Minimize the weighted variance or the entropy? : Weighted variance
Assign pixels in the middle intensity class to the foreground or the backgroun:? : Background
Method to calculate adaptive window size: Image size
Size of adaptive window: 10
Use default parameters? : Default
Lower outlier fraction: 0.05
Upper outlier fraction: 0.05
Averaging method: Mean
Variance method: Standard deviation
# of deviations: 2.0

Module 7: Expand Or Shrink Objects

Select the input objects: Well_FITC_small
Name the output objects: Well_FITC
Select the operation: Shrink objects by a specified number of pixels
Number of pixels by which to expand or shrink: 5
Fill holes in objects so that all objects shrink to a single point? : No
Retain the outlines of the identified objects? : No
Name the outline image: Shrunken Nuclei Outlines

Module 8: Image Math

Operation: Invert
Raise the power of the result by: 1.0
Multiply the result by: 1.0
Add to result: 0.0
Set values less than 0 equal to 0? : Yes
Set values greater than 1 equal to 1? : Yes
Ignore the image masks? : No
Name the output image: InvertedBF
Image or measurement? : Image
Select the first image: Brightfield
Multiply the first image by: 1.0
Measurement:
Image or measurement? : Image
Select the second image:
Multiply the second image by: 1.0
Measurement:

Module 9: Morph

Select the input image: InvertedBF
Name the output image: BrightfieldBackground

Select the operation to perform: open
Number of times to repeat operation: Once
Repetition number: 2
Diameter: 31.0
Structuring element: Disk
X offset: 1.0
Y offset: 1.0
Angle: 0.0
Width: 3.0
Height: 3.0
Custom: 5,5,1111111111111111111111111
Rescale values from 0 to 1? : Yes

Module 10: Image Math

Operation: Subtract
Raise the power of the result by: 1.0
Multiply the result by: 1.0
Add to result: 0.0
Set values less than 0 equal to 0? : Yes
Set values greater than 1 equal to 1? : Yes
Ignore the image masks? : No
Name the output image: BF_worm_image
Image or measurement? : Image
Select the first image: InvertedBF
Multiply the first image by: 1.0
Measurement:
Image or measurement? : Image
Select the second image: BrightfieldBackground
Multiply the second image by: 1.0
Measurement:

Module 11: Mask Image

Select the input image: BF_worm_image
Name the output image: Masked_BF_worm_image
Use objects or an image as a mask? : Objects
Select object for mask: Well_FITC
Select image for mask: None
Invert the mask? : No

Module 12: Identify Primary Objects

Select the input image: Masked_BF_worm_image
Name the primary objects to be identified: Worm_objects
Typical diameter of objects, in pixel units (Min, Max): 30, 400
Discard objects outside the diameter range? : Yes

Try to merge too small objects with nearby larger objects? : No
Discard objects touching the border of the image? : No
Method to distinguish clumped objects: Intensity
Method to draw dividing lines between clumped objects: None
Size of smoothing filter: 10
Suppress local maxima that are closer than this minimum allowed distance: 7.0
Speed up by using lower-resolution image to find local maxima? : Yes
Name the outline image: PrimaryOutlines
Fill holes in identified objects? : Never
Automatically calculate size of smoothing filter for declumping? : Yes
Automatically calculate minimum allowed distance between local maxima? : Yes
Retain outlines of the identified objects? : No
Automatically calculate the threshold using the Otsu method? : Yes
Enter Laplacian of Gaussian threshold: 0.5
Automatically calculate the size of objects for the Laplacian of Gaussian filte:? : Yes
Enter LoG filter diameter: 5.0
Handling of objects if excessive number of objects identified: Continue
Maximum number of objects: 500
Threshold setting version: 1
Threshold strategy: Automatic
Thresholding method: Otsu
Select the smoothing method for thresholding: Automatic
Threshold smoothing scale: 1.0
Threshold correction factor: 1.0
Lower and upper bounds on threshold: 0.0, 1.0
Approximate fraction of image covered by objects? : 0.01
Manual threshold: 0.0
Select the measurement to threshold with: None
Select binary image: None
Masking objects: None
Two-class or three-class thresholding? : Two classes
Minimize the weighted variance or the entropy? : Weighted variance
Assign pixels in the middle intensity class to the foreground or the background? : Foreground
Method to calculate adaptive window size: Image size
Size of adaptive window: 10
Use default parameter:? : Default
Lower outlier fraction: 0.05
Upper outlier fraction: 0.05
Averaging method: Mean
Variance method: Standard deviation
# of deviations: 2.0

Module 13: Measure Object Size Shape

Select objects to measure: Worm_objects

Calculate the Zernike?features? : No

Module 14: Filter Objects

Name the output objects: Worms

Select the object to filter: Worm_objects

Select the filtering mode: Measurements

Select the filtering method: Limits

Select the objects that contain the filtered objects: None

Retain outlines of the identified objects? : No

Name the outline image: FilteredObjects

Rules file location: Elsewhere...\x7C

Rules file name: rules.txt

Class number: 1

Measurement count: 2

Additional object count: 0

Assign overlapping child to: Both parents

Select the measurement to filter by: AreaShape_Solidity

Filter using a minimum measurement value? : No

Minimum value: 0.7

Filter using a maximum measurement value? : Yes

Maximum value: 0.9

Select the measurement to filter by: AreaShape_MajorAxisLength

Filter using a minimum measurement value? : No

Minimum value: 0.0

Filter using a maximum measurement value? : Yes

Maximum value: 450

Module 15: Identify Secondary Objects

Select the input objects: Worms

Name the objects to be identified: DilatedWorms

Select the method to identify the secondary objects: Distance - N

Select the input image: Brightfield

Number of pixels by which to expand the primary objects: 5

Regularization factor: 0.05

Name the outline image: SecondaryOutlines

Retain outlines of the identified secondary objects? : No

Discard secondary objects touching the border of the image? : No

Discard the associated primary objects? : No

Name the new primary objects: FilteredNuclei

Retain outlines of the new primary objects? : No

Name the new primary object outlines: FilteredNucleiOutlines

Fill holes in identified objects? : No
Threshold setting version: 1
Threshold strategy: Automatic
Thresholding method: Otsu
Select the smoothing method for thresholding: No smoothing
Threshold smoothing scale: 1.0
Threshold correction factor: 1.0
Lower and upper bounds on threshold: 0.0,1.0
Approximate fraction of image covered by objects? : 0.01
Manual threshold: 0.0
Select the measurement to threshold with: None
Select binary image: None
Masking objects: None
Two-class or three-class thresholding? : Two classes
Minimize the weighted variance or the entropy? : Weighted variance
Assign pixels in the middle intensity class to the foreground or the background? : Foreground
Method to calculate adaptive window size: Image size
Size of adaptive window: 10
Use default parameters? : Default
Lower outlier fraction: 0.05
Upper outlier fraction: 0.05
Averaging method: Mean
Variance method: Standard deviation
# of deviations: 2.0

Module 16: IdentifyTertiaryObjects:

Select the larger identified objects: DilatedWorms
Select the smaller identified objects: Worms
Name the tertiary objects to be identified: WormBackground
Name the outline image: CytoplasmOutlines
Retain outlines of the tertiary objects? : No
Shrink smaller object prior to subtraction? : No

Module 17: Mask Image

Select the input image: FITC
Name the output image: MaskedFITC
Use objects or an image as a mask? : Objects
Select object for mask: Well_FITC
Select image for mask: None
Invert the mask? : No

Module 18: Correct Illumination Calculate

Select the input image: MaskedFITC

Name the output image: IllumFITC
Select how the illumination function is calculated: Regular
Dilate objects in the final averaged image? : No
Dilation radius: 1
Block size: 60
Rescale the illumination function? : No
Calculate function for each image individually, or based on all images? : Each
Smoothing method: Fit Polynomial
Method to calculate smoothing filter size: Automatic
Approximate object size: 10
Smoothing filter size: 10
Retain the averaged image? : No
Name the averaged image: IllumBlueAvg
Retain the dilated image? : No
Name the dilated image: IllumBlueDilated
Automatically calculate spline parameters? : Yes
Background mode: auto
Number of spline points: 5
Background threshold: 2.0
Image resampling factor: 2.0
Maximum number of iterations: 40
Residual value for convergence: 0.001

Module 19: Correct Illumination Apply:

Select the input image: MaskedFITC
Name the output image: CorrFITC
Select the illumination function: IllumFITC
Select how the illumination function is applied: Subtract

Module 20: Identify Primary Objects

Select the input image: CorrFITC
Name the primary objects to be identified: Worm_heads
Typical diameter of objects, in pixel units (Min, Max): 5, 10
Discard objects outside the diameter range? : Yes
Try to merge too small objects with nearby larger objects? : No
Discard objects touching the border of the image? : Yes
Method to distinguish clumped objects: Intensity
Method to draw dividing lines between clumped objects: None
Size of smoothing filter: 10
Suppress local maxima that are closer than this minimum allowed distance: 7.0
Speed up by using lower-resolution image to find local maxima? : Yes
Name the outline image: PrimaryOutlines
Fill holes in identified objects? : Never
Automatically calculate size of smoothing filter for declumping? : Yes

Automatically calculate minimum allowed distance between local maxima? : Yes
Retain outlines of the identified objects? : No
Automatically calculate the threshold using the Otsu method? : Yes
Enter Laplacian of Gaussian threshold: 0.5
Automatically calculate the size of objects for the Laplacian of Gaussian filter? : Yes
Enter LoG filter diameter: 5.0
Handling of objects if excessive number of objects identified: Continue
Maximum number of objects: 500
Threshold setting version: 1
Threshold strategy: Global
Thresholding method: Otsu
Select the smoothing method for thresholding: Automatic
Threshold smoothing scale: 1.0
Threshold correction factor: 1.0
Lower and upper bounds on threshold: 0.004,1.0
Approximate fraction of image covered by objects? : 0.01
Manual threshold: 0.0
Select the measurement to threshold with: None
Select binary image: None
Masking objects: None
Two-class or three-class thresholding? : Two classes
Minimize the weighted variance or the entropy? : Weighted variance
Assign pixels in the middle intensity class to the foreground or the background? : Background
Method to calculate adaptive window size: Image size
Size of adaptive window: 10
Use default parameters? : Default
Lower outlier fraction: 0.05
Upper outlier fraction: 0.05
Averaging method: Mean
Variance method: Standard deviation
# of deviations: 2.0

Module 21: Overlay Outlines

Display outlines on a blank image? : No
Select image on which to display outlines: Brightfield
Name the output image: OrigOverlay
Outline display mode: Color
Select method to determine brightness of outlines: Max of image
Width of outlines: 1
Select outlines to display: None
Select outline color: cyan
Load outlines from an image or objects? : Objects

Select objects to display: Worms
Select outlines to display: None
Select outline color: yellow
Load outlines from an image or objects? : Objects
Select objects to display: Worm_heads
Select outlines to display: None
Select outline color: Blue
Load outlines from an image or objects? : Objects
Select objects to display: WormBackground

Module 22: Display Data On Image

Display object or image measurements? : Object
Select the input objects: Worms
Measurement to display: Number_Object_Number
Select the image on which to display the measurements: OrigOverlay
Text color: red
Name the output image that has the measurements displayed: DisplayImage
Font size (points): 12
Number of decimals: 0
Image elements to save: Image
Annotation offset (in pixels): 0
Display mode: Text
Color map: Default
Display background image? : Yes
Color map scale: Use this image\'s measurement range
Color map range: 0.0,1.0

Module 23: Save Images:

Select the type of image to save: Image
Select the image to save: DisplayImage
Select the objects to save: None
Select the module display window to save: None
Select method for constructing file names: From image filename
Select image name for file prefix: Brightfield
Enter single file name: OrigBlue
Number of digits: 4
Append a suffix to the image file name? : Yes
Text to append to the image name: _outlines
Saved file format: png
Output file location: Default Output Folder\x7C
Image bit depth: 8-bit integer
Overwrite existing files without warning? : No
When to save: Every cycle
Rescale the images? : No

Save as grayscale or color image? : Grayscale
Select colormap: Default
Record the file and path information to the saved image? : No
Create subfolders in the output folder? : No
Base image folder: Elsewhere...\x7C
Saved movie format: avi

Module 24: Relate Object

Select the input child objects: Worm_heads
Select the input parent objects: Worms
Calculate child-parent distances? : None
Calculate per-parent means for all child measurements? : No
Calculate distances to other parents? : No
Parent name: None

Module 25: Measure Object Intensity:

Hidden: 2
Select an image to measure: FITC
Select an image to measure: Cy3
Select objects to measure: Worms
Select objects to measure: WormBackground

Module 26: Measure Object Size Shape:

Select objects to measure: Worms
Calculate the Zernike features? : Yes

Module 27: Export To Spread sheet:

Select the column delimiter: Comma (“,”)
Add image metadata columns to your object data file? : No
Limit output to a size that is allowed in Excel? : No
Select the measurements to export: Yes
Calculate the per-image mean values for object measurements? : No
Calculate the per-image median values for object measurements? : No
Calculate the per-image standard deviation values for object measurements? : No
Output file location: Default Output Folder\x7C
Create a GenePattern GCT file? : No
Select source of sample row name: Metadata
Select the image to use as the identifier: None
Select the metadata to use as the identifier: None
Export all measurement types? : Yes
: Image\x7CFileName_Brightfield,Worms\x7CIntensity_MinIntensity_Cy3,Worms\x7CIntensity_MinIntensity_FITC,Worms\x7CIntensity_IntegratedIntensityEdge_FITC,Worms\x7CIntensity_IntegratedIntensityEdge_Cy3,Worms\x7CIntensity_StdIntensity_Cy3,Worms\x7CIntensity_StdIntensity_FITC,Worms\x7CIntensity_MassDisplacement_Cy3,Worms\x7CIntensity_MassDisplacement_FITC,Worms\x7CIntensity_UpperQuartileIntensity_Cy3,Worms\

x7CIntensity_UpperQuartileIntensity_FITC,Worms\x7CIntensity_IntegratedIntensity_FITC,Worms\x7CIntensity_IntegratedIntensity_Cy3,Worms\x7CIntensity_MinIntensityEdge_FITC,Worms\x7CIntensity_MinIntensityEdge_Cy3,Worms\x7CIntensity_MADIntensity_Cy3,Worms\x7CIntensity_MADIntensity_FITC,Worms\x7CIntensity_MeanIntensity_Cy3,Worms\x7CIntensity_MeanIntensity_FITC,Worms\x7CIntensity_MeanIntensityEdge_FITC,Worms\x7CIntensity_MeanIntensityEdge_Cy3,Worms\x7CIntensity_MaxIntensity_Cy3,Worms\x7CIntensity_MaxIntensity_FITC,Worms\x7CIntensity_MedianIntensity_FITC,Worms\x7CIntensity_MedianIntensity_Cy3,Worms\x7CIntensity_LowerQuartileIntensity_Cy3,Worms\x7CIntensity_LowerQuartileIntensity_FITC,Worms\x7CIntensity_MaxIntensityEdge_FITC,Worms\x7CIntensity_MaxIntensityEdge_Cy3,Worms\x7CIntensity_StdIntensityEdge_Cy3,Worms\x7CIntensity_StdIntensityEdge_FITC,Worms\x7CAreaShape_Perimeter,Worms\x7CAreaShape_MinorAxisLength,Worms\x7CAreaShape_Center_Y,Worms\x7CAreaShape_Center_X,Worms\x7CAreaShape_Area,Worms\x7CAreaShape_MinFeretDiameter,Worms\x7CAreaShape_Solidity,Worms\x7CAreaShape_MaxFeretDiameter,Worms\x7CAreaShape_MeanRadius,Worms\x7CAreaShape_EulerNumber,Worms\x7CAreaShape_MedianRadius,Worms\x7CAreaShape_Compactness,Worms\x7CAreaShape_Extent,Worms\x7CAreaShape_Eccentricity,Worms\x7CAreaShape_MaximumRadius,Worms\x7CAreaShape_FormFactor,Worms\x7CAreaShape_Zernike_1_1,Worms\x7CAreaShape_Zernike_0_0,Worms\x7CAreaShape_Zernike_3_1,Worms\x7CAreaShape_Zernike_3_3,Worms\x7CAreaShape_Zernike_2_2,Worms\x7CAreaShape_Zernike_2_0,Worms\x7CAreaShape_Zernike_5_1,Worms\x7CAreaShape_Zernike_5_3,Worms\x7CAreaShape_Zernike_5_5,Worms\x7CAreaShape_Zernike_4_2,Worms\x7CAreaShape_Zernike_4_4,Worms\x7CAreaShape_Zernike_4_0,Worms\x7CAreaShape_Zernike_7_1,Worms\x7CAreaShape_Zernike_7_3,Worms\x7CAreaShape_Zernike_7_5,Worms\x7CAreaShape_Zernike_7_7,Worms\x7CAreaShape_Zernike_6_2,Worms\x7CAreaShape_Zernike_6_0,Worms\x7CAreaShape_Zernike_6_4,Worms\x7CAreaShape_Zernike_6_6,Worms\x7CAreaShape_Zernike_9_1,Worms\x7CAreaShape_Zernike_9_3,Worms\x7CAreaShape_Zernike_9_5,Worms\x7CAreaShape_Zernike_9_7,Worms\x7CAreaShape_Zernike_9_9,Worms\x7CAreaShape_Zernike_8_0,Worms\x7CAreaShape_Zernike_8_2,Worms\x7CAreaShape_Zernike_8_4,Worms\x7CAreaShape_Zernike_8_6,Worms\x7CAreaShape_Zernike_8_8,Worms\x7CAreaShape_MajorAxisLength,Worms\x7CAreaShape_Orientation,Worms\x7CChildren_Worm_heads_Count

Representation of Nan/Inf: NaN
Add a prefix to file names? : Yes
Filename prefix: Worm_Measurements
Overwrite existing files without warning? : No

Data to export: Do not use
Combine these object measurements with those of the previous object? : No
File name: DATA.csv
Use the object name for the file name? : Yes

Appendix 4: GO term enrichment

phb-1(RNAi)

Class	TERM	Description	Count	Fold.Enrichment	logFDR
MF	GO:0004298	threonine-type endopeptidase activity	11	8,85	5,01
CC	GO:0005839	proteasome core complex	11	8,13	4,66
CC	GO:0022627	cytosolic small ribosomal subunit	23	7,28	12,52
CC	GO:0015935	small ribosomal subunit	9	7,26	2,40
CC	GO:0022625	cytosolic large ribosomal subunit	36	6,94	20,94
MF	GO:0015078	hydrogen ion transmembrane transporter activity	11	6,64	3,09
MF	GO:0046961	proton-transporting ATPase activity rotational mechanism	13	6,60	4,32
CC	GO:0000502	proteasome complex	23	6,58	11,04
MF	GO:0019843	rRNA binding	13	5,98	3,64
BP	GO:0015991	ATP hydrolysis coupled proton transport	14	5,97	4,21
CC	GO:0030529	intracellular ribonucleoprotein complex	74	5,61	37,66
CC	GO:0005840	ribosome	72	5,55	36,07
BP	GO:0015992	proton transport	17	5,14	4,65
MF	GO:0003735	structural constituent of ribosome	71	5,00	30,51
MF	GO:0004812	aminoacyl-tRNA ligase activity	14	4,83	2,79
BP	GO:0018996	molting cycle collagen and cuticulin-based cuticle	93	4,59	37,53
BP	GO:0006412	translation	99	4,48	39,20
CC	GO:0005681	spliceosomal complex	14	4,00	1,79
BP	GO:0006915	apoptotic process	138	3,89	48,02
BP	GO:0008380	RNA splicing	16	3,66	1,83
BP	GO:0040039	inductive cell migration	36	3,13	6,09
BP	GO:0016477	cell migration	30	3,02	4,17
BP	GO:0043652	engulfment of apoptotic cell	20	2,98	1,59
BP	GO:0007281	germ cell development	41	2,91	6,34
MF	GO:0003723	RNA binding	67	2,68	10,69
BP	GO:0002119	nematode larval development	381	2,65	107,03
BP	GO:0008406	gonad development	68	2,61	10,20
BP	GO:0000003	reproduction	383	2,54	100,92
BP	GO:0006898	receptor-mediated endocytosis	137	2,25	18,52
BP	GO:0040018	positive regulation of multicellular organism growth	55	2,21	4,69
BP	GO:0009792	embryo development ending in birth or egg hatching	408	2,12	81,53
BP	GO:0040035	hermaphrodite genitalia development	116	2,11	12,29
BP	GO:0008340	determination of adult lifespan	132	2,01	13,10
BP	GO:0040011	locomotion	199	1,97	21,91
BP	GO:0010171	body morphogenesis	83	1,87	4,94
MF	GO:0000166	nucleotide binding	108	1,53	2,61

daf-2;phb-1(RNAi)

Class	TERM	Description	Count	Fold.Enrichment	log.FDR
CC	GO:0022627	cytosolic small ribosomal subunit	23	6,88	12,13
CC	GO:0015935	small ribosomal subunit	9	6,86	2,21
CC	GO:0022625	cytosolic large ribosomal subunit	36	6,56	20,08
MF	GO:0015078	hydrogen ion transmembrane transporter activity	11	6,42	2,96
BP	GO:0000028	ribosomal small subunit assembly	9	6,04	1,48
MF	GO:0046961	proton-transporting ATPase activity rotational mechanism	12	5,90	3,05
BP	GO:0015991	ATP hydrolysis coupled proton transport	14	5,55	3,84
BP	GO:0000027	ribosomal large subunit assembly	10	5,46	1,57
BP	GO:0002181	cytoplasmic translation	11	5,33	1,99
CC	GO:0000502	proteasome complex	19	5,14	5,95
CC	GO:0030529	intracellular ribonucleoprotein complex	69	4,94	30,36
CC	GO:0005840	ribosome	67	4,88	28,89
MF	GO:0003735	structural constituent of ribosome	69	4,70	27,59
BP	GO:0018996	molting cycle collagen and cuticulin-based cuticle	101	4,64	42,52
MF	GO:0004812	aminoacyl-tRNA ligase activity	13	4,34	1,78
BP	GO:0006412	translation	96	4,05	33,61
CC	GO:0071013	catalytic step 2 spliceosome	14	3,91	1,70
BP	GO:0006915	apoptotic process	139	3,64	44,77
BP	GO:0008380	RNA splicing	17	3,62	2,14
BP	GO:0032940	secretion by cell	21	2,82	1,49
BP	GO:0007281	germ cell development	42	2,78	5,96
BP	GO:0040039	inductive cell migration	33	2,67	3,53
BP	GO:0002119	nematode larval development	396	2,57	104,74
MF	GO:0003723	RNA binding	66	2,56	9,44
BP	GO:0008406	gonad development	71	2,54	10,24
BP	GO:0016477	cell migration	26	2,44	1,37
BP	GO:0000003	reproduction	387	2,39	89,36
BP	GO:0006898	receptor-mediated endocytosis	152	2,33	22,85
BP	GO:0040035	hermaphrodite genitalia development	124	2,10	13,60
BP	GO:0009792	embryo development ending in birth or egg hatching	434	2,10	85,31
BP	GO:0040011	locomotion	215	1,98	24,57
BP	GO:0040018	positive regulation of multicellular organism growth	51	1,91	2,10
BP	GO:0010171	body morphogenesis	87	1,83	4,83
CC	GO:0005622	intracellular	59	1,79	2,09
BP	GO:0008340	determination of adult lifespan	122	1,73	6,65
MF	GO:0000166	nucleotide binding	112	1,53	2,90

Appendix 5: KEGG pathway enrichment

phb-1(RNAi)

term_id	proteins	hits	pvalue_fdr	term_description
3010	97	65	1,1E-96	Ribosome
190	70	35	8,0E-45	Oxidative phosphorylation
1100	433	58	4,4E-38	Metabolic pathways
3050	29	23	1,2E-36	Proteasome
3040	82	30	1,5E-33	Spliceosome
3013	82	27	8,9E-29	RNA transport
4145	41	20	1,4E-25	Phagosome
970	24	11	8,2E-14	Aminoacyl-tRNA biosynthesis
4141	80	15	3,4E-12	Protein processing in endoplasmic reticulum
4142	47	11	3,4E-10	Lysosome
3008	46	10	5,3E-09	Ribosome biogenesis in eukaryotes
3015	45	9	7,7E-08	mRNA surveillance pathway
4350	16	6	3,3E-07	TGF-beta signaling pathway
230	54	9	3,3E-07	Purine metabolism
4144	54	9	3,3E-07	Endocytosis
240	44	8	8,4E-07	Pyrimidine metabolism
4120	45	7	1,4E-05	Ubiquitin mediated proteolysis
4020	32	5	3,5E-04	Calcium signaling pathway
3018	35	5	5,2E-04	RNA degradation
620	20	4	6,3E-04	Pyruvate metabolism
4010	42	5	1,1E-03	MAPK signaling pathway
3060	10	3	1,1E-03	Protein export
520	24	4	1,1E-03	Amino sugar and nucleotide sugar metabolism
61	3	2	1,9E-03	Fatty acid biosynthesis
4310	29	4	2,2E-03	Wnt signaling pathway
4330	14	3	2,7E-03	Notch signaling pathway
380	16	3	3,8E-03	Tryptophan metabolism
3020	16	3	3,8E-03	RNA polymerase
1200	67	5	7,0E-03	Carbon metabolism
640	20	3	7,0E-03	Propanoate metabolism

3030	22	3	8,7E-03	DNA replication
3420	22	3	8,7E-03	Nucleotide excision repair
280	26	3	1,4E-02	Valine, leucine and isoleucine degradation
20	28	3	1,6E-02	Citrate cycle (TCA cycle)
10	29	3	1,7E-02	Glycolysis / Gluconeogenesis
480	29	3	1,7E-02	Glutathione metabolism
1212	31	3	2,0E-02	Fatty acid metabolism
40	11	2	2,0E-02	Pentose and glucuronate interconversions
4130	11	2	2,0E-02	SNARE interactions in vesicular transport
4340	11	2	2,0E-02	Hedgehog signaling pathway
3440	12	2	2,3E-02	Homologous recombination
410	13	2	2,6E-02	beta-Alanine metabolism
650	14	2	2,9E-02	Butanoate metabolism
561	15	2	3,2E-02	Glycerolipid metabolism
3430	15	2	3,2E-02	Mismatch repair
4070	18	2	4,4E-02	Phosphatidylinositol signaling system
4080	18	2	4,4E-02	Neuroactive ligand-receptor interaction
260	19	2	4,7E-02	Glycine, serine and threonine metabolism

daf-2;phb-1(RNAi)

term_id	proteins	hits	pvalue_fdr	term_description
3010	97	62	4,2E-91	Ribosome
190	70	31	5,8E-38	Oxidative phosphorylation
3040	82	32	3,5E-37	Spliceosome
1100	433	54	1,2E-34	Metabolic pathways
3013	82	27	3,9E-29	RNA transport
3050	29	19	4,9E-28	Proteasome
4145	41	21	8,2E-28	Phagosome
3015	45	15	1,8E-16	mRNA surveillance pathway
970	24	11	4,7E-14	Aminoacyl-tRNA biosynthesis
4142	47	12	8,9E-12	Lysosome
4144	54	12	4,9E-11	Endocytosis
3008	46	11	1,4E-10	Ribosome biogenesis in eukaryotes

230	54	9	2,7E-07	Purine metabolism
240	44	8	6,9E-07	Pyrimidine metabolism
4120	45	8	7,8E-07	Ubiquitin mediated proteolysis
4350	16	5	8,3E-06	TGF-beta signaling pathway
3030	22	5	4,4E-05	DNA replication
4141	80	8	5,8E-05	Protein processing in endoplasmic reticulum
3430	15	4	1,6E-04	Mismatch repair
3020	16	4	2,0E-04	RNA polymerase
3420	22	4	7,3E-04	Nucleotide excision repair
4010	42	5	8,8E-04	MAPK signaling pathway
3060	10	3	9,1E-04	Protein export
3460	15	3	3,1E-03	Fanconi anemia pathway
3410	6	2	8,0E-03	Base excision repair
4146	47	4	1,1E-02	Peroxisome
520	24	3	1,1E-02	Amino sugar and nucleotide sugar metabolism
4310	29	3	1,9E-02	Wnt signaling pathway
4068	31	3	2,2E-02	FoxO signaling pathway
4020	32	3	2,2E-02	Calcium signaling pathway
4130	11	2	2,2E-02	SNARE interactions in vesicular transport
3440	12	2	2,6E-02	Homologous recombination
3018	35	3	2,7E-02	RNA degradation
232	1	1	3,0E-02	Caffeine metabolism
250	14	2	3,1E-02	Alanine, aspartate and glutamate metabolism
4330	14	2	3,1E-02	Notch signaling pathway
4070	18	2	4,9E-02	Phosphatidylinositol signaling system

Appendix 6: TopGO enrichment

up-regulating in *phb-1(RNAi)*

GO.ID	Term	Annotated	Significant	adj.pvalue
GO:0008340	determination of adult lifespan	565	28	3,40E-07
GO:0007005	mitochondrion organization	57	7	6,60E-05
GO:0002119	nematode larval development	1477	45	2,20E-04
GO:0042775	mitochondrial ATP synthesis coupled elec...	21	4	4,80E-04
GO:0009792	embryo development ending in birth or eg...	1758	47	7,70E-04
GO:1990542	mitochondrial transmembrane transport	11	3	8,60E-04
GO:0051704	multi-organism process	499	18	3,22E-03
GO:0015986	ATP synthesis coupled proton transport	17	3	3,28E-03
GO:0043053	dauer entry	38	4	4,70E-03
GO:0031667	response to nutrient levels	46	4	9,31E-03
GO:1902578	single-organism localization	566	20	1,39E-02
GO:0044070	regulation of anion transport	11	2	1,62E-02
GO:0046467	membrane lipid biosynthetic process	31	3	1,81E-02
GO:0098542	defense response to other organism	56	4	1,83E-02
GO:0015914	phospholipid transport	12	2	1,92E-02
GO:0044743	protein transmembrane import into intrac...	12	2	1,92E-02
GO:0051707	response to other organism	57	4	1,94E-02
GO:0009607	response to biotic stimulus	57	4	1,94E-02
GO:0043207	response to external biotic stimulus	57	4	1,94E-02
GO:0051050	positive regulation of transport	57	4	1,94E-02
GO:1902600	hydrogen ion transmembrane transport	50	6	1,97E-02
GO:0044765	single-organism transport	545	19	2,06E-02
GO:0006897	endocytosis	649	19	2,21E-02
GO:0042594	response to starvation	34	3	2,32E-02
GO:0031669	cellular response to nutrient levels	14	2	2,58E-02
GO:0008355	olfactory learning	14	2	2,58E-02
GO:0009267	cellular response to starvation	14	2	2,58E-02
GO:0015748	organophosphate ester transport	14	2	2,58E-02
GO:0019953	sexual reproduction	439	14	2,59E-02
GO:0033036	macromolecule localization	708	20	2,68E-02
GO:0051241	negative regulation of multicellular org...	199	8	2,73E-02
GO:0033554	cellular response to stress	317	11	2,76E-02
GO:0044703	multi-organism reproductive process	445	14	2,87E-02
GO:0051093	negative regulation of developmental pro...	201	8	2,88E-02
GO:0071495	cellular response to endogenous stimulus	65	4	2,98E-02
GO:0007281	germ cell development	281	10	3,02E-02
GO:0022412	cellular process involved in reproductio...	281	10	3,02E-02
GO:0061064	negative regulation of nematode larval d...	167	7	3,14E-02
GO:0048581	negative regulation of post-embryonic de...	167	7	3,14E-02
GO:0007611	learning or memory	39	3	3,32E-02
GO:0065002	intracellular protein transmembrane tran...	16	2	3,32E-02

GO:0031668	cellular response to extracellular stimu...	16	2	3,32E-02
GO:1905952	regulation of lipid localization	16	2	3,32E-02
GO:0071496	cellular response to external stimulus	16	2	3,32E-02
GO:0071806	protein transmembrane transport	16	2	3,32E-02
GO:0006810	transport	1513	39	3,34E-02
GO:0044708	single-organism behavior	100	5	3,46E-02
GO:0071310	cellular response to organic substance	135	6	3,54E-02
GO:0099131	ATP hydrolysis coupled ion transmembrane...	40	3	3,54E-02
GO:0099132	ATP hydrolysis coupled cation transmembr...	40	3	3,54E-02
GO:0010942	positive regulation of cell death	40	3	3,54E-02
GO:0090662	ATP hydrolysis coupled transmembrane tra...	40	3	3,54E-02
GO:0032940	secretion by cell	136	6	3,65E-02
GO:0006818	hydrogen transport	59	6	3,71E-02
GO:0015992	proton transport	59	6	3,71E-02
GO:0007015	actin filament organization	41	3	3,77E-02
GO:0051445	regulation of meiotic cell cycle	104	5	4,00E-02
GO:0007635	chemosensory behavior	42	3	4,01E-02
GO:0016192	vesicle-mediated transport	786	21	4,01E-02
GO:0008306	associative learning	18	2	4,14E-02
GO:0034613	cellular protein localization	256	9	4,17E-02
GO:0050890	cognition	43	3	4,25E-02
GO:0006869	lipid transport	43	3	4,25E-02
GO:0040020	regulation of meiotic nuclear division	73	4	4,30E-02
GO:0070727	cellular macromolecule localization	258	9	4,35E-02
GO:0046903	secretion	143	6	4,48E-02
GO:0006898	receptor-mediated endocytosis	563	16	4,50E-02
GO:0007617	mating behavior	44	3	4,50E-02
GO:1905037	autophagosome organization	19	2	4,57E-02
GO:0000045	autophagosome assembly	19	2	4,57E-02
GO:0007167	enzyme linked receptor protein signaling...	75	4	4,67E-02
GO:0051603	proteolysis involved in cellular protein...	145	6	4,74E-02
GO:0010171	body morphogenesis	433	13	4,79E-02
GO:0009719	response to endogenous stimulus	76	4	4,87E-02

up-regulating in *daf-2;phb-1(RNAi)*

GO.ID	Term	Annotated	Significant	result1
GO:0042775	mitochondrial ATP synthesis coupled elec...	21	7	0,000
GO:0007413	axonal fasciculation	52	9	0,001
GO:0015696	ammonium transport	19	5	0,001
GO:0042787	protein ubiquitination involved in ubiqu...	39	7	0,002
GO:0043171	peptide catabolic process	21	5	0,002
GO:0032222	regulation of synaptic transmission. cho...	14	4	0,003
GO:0009792	embryo development ending in birth or eg...	1758	102	0,005
GO:0007005	mitochondrion organization	57	8	0,005
GO:0006839	mitochondrial transport	17	4	0,007

GO:0006515	misfolded or incompletely synthesized pr...	10	3	0,010
GO:0071218	cellular response to misfolded protein	10	3	0,010
GO:0006890	retrograde vesicle-mediated transport. G...	11	3	0,013
GO:1990542	mitochondrial transmembrane transport	11	3	0,013
GO:0006486	protein glycosylation	55	7	0,014
GO:0043413	macromolecule glycosylation	55	7	0,014
GO:0016485	protein processing	32	5	0,016
GO:0070085	glycosylation	57	7	0,017
GO:0071407	cellular response to organic cyclic comp...	33	5	0,018
GO:1901699	cellular response to nitrogen compound	34	5	0,020
GO:0009101	glycoprotein biosynthetic process	73	8	0,020
GO:1901374	acetate ester transport	13	3	0,021
GO:0032224	positive regulation of synaptic transmis...	13	3	0,021
GO:0015870	acetylcholine transport	13	3	0,021
GO:0032543	mitochondrial translation	23	4	0,021
GO:0051604	protein maturation	35	5	0,023
GO:0007610	behavior	443	30	0,025
GO:0016358	dendrite development	36	5	0,025
GO:0042493	response to drug	14	3	0,025
GO:0051231	spindle elongation	14	3	0,025
GO:0043050	pharyngeal pumping	52	6	0,034
GO:0010639	negative regulation of organelle organiz...	39	5	0,035
GO:0045132	meiotic chromosome segregation	97	9	0,038
GO:0009100	glycoprotein metabolic process	83	8	0,040
GO:1901657	glycosyl compound metabolic process	41	5	0,042
GO:0009887	animal organ morphogenesis	84	8	0,043
GO:0015985	energy coupled proton transport. down el...	17	3	0,043
GO:0015986	ATP synthesis coupled proton transport	17	3	0,043
GO:0050806	positive regulation of synaptic transmis...	17	3	0,043
GO:0010212	response to ionizing radiation	17	3	0,043
GO:0098813	nuclear chromosome segregation	132	11	0,045
GO:0014070	response to organic cyclic compound	42	5	0,046
GO:0042755	eating behavior	56	6	0,046
GO:1901137	carbohydrate derivative biosynthetic pro...	183	14	0,048
GO:0071417	cellular response to organonitrogen comp...	18	3	0,050

down-regulating in *phb-1(RNAi)*

GO.ID	Term	Annotated	Significant	adj.pvalue
GO:0006412	translation	229	90	1,40E-26
GO:0006898	receptor-mediated endocytosis	563	89	1,10E-15
GO:0040011	locomotion	1180	155	4,80E-14
GO:0040035	hermaphrodite genitalia development	512	77	2,40E-12
GO:0008406	gonad development	673	112	3,20E-12
GO:0015991	ATP hydrolysis coupled proton transport	19	13	9,70E-12
GO:0006418	tRNA aminoacylation for protein translat...	28	15	3,70E-11

GO:0010171	body morphogenesis	433	65	2,10E-10
GO:0007281	germ cell development	281	49	1,90E-08
GO:0040018	positive regulation of multicellular org...	224	37	2,30E-07
GO:0002181	cytoplasmic translation	17	9	4,10E-07
GO:0040039	inductive cell migration	109	23	6,70E-07
GO:0000398	mRNA splicing. via spliceosome	94	21	7,70E-07
GO:0008340	determination of adult lifespan	565	68	8,10E-07
GO:0000028	ribosomal small subunit assembly	14	8	8,70E-07
GO:0006413	translational initiation	31	11	3,00E-06
GO:0000027	ribosomal large subunit assembly	15	7	2,50E-05
GO:0006458	'de novo' protein folding	11	6	3,20E-05
GO:0032940	secretion by cell	136	23	3,40E-05
GO:0051452	intracellular pH reduction	12	6	6,10E-05
GO:0000470	maturation of LSU-rRNA	19	7	1,50E-04
GO:0043652	engulfment of apoptotic cell	70	14	2,00E-04
GO:0006414	translational elongation	20	7	2,20E-04
GO:0016477	cell migration	254	44	3,50E-04
GO:0000910	cytokinesis	50	11	4,00E-04
GO:0045727	positive regulation of translation	11	5	4,60E-04
GO:0042254	ribosome biogenesis	150	42	6,00E-04
GO:0048477	oogenesis	156	22	7,40E-04
GO:0030490	maturation of SSU-rRNA	36	11	1,11E-03
GO:0010608	posttranscriptional regulation of gene e...	167	26	1,51E-03
GO:0071426	ribonucleoprotein complex export from nu...	21	6	2,12E-03
GO:0000462	maturation of SSU-rRNA from tricistronic...	28	7	2,12E-03
GO:0061077	chaperone-mediated protein folding	15	5	2,38E-03
GO:0040007	growth	419	60	2,50E-03
GO:0000122	negative regulation of transcription fro...	63	11	3,01E-03
GO:0030866	cortical actin cytoskeleton organization	10	4	3,15E-03
GO:0022613	ribonucleoprotein complex biogenesis	193	50	3,97E-03
GO:0006405	RNA export from nucleus	27	9	5,11E-03
GO:0051028	mRNA transport	18	5	5,73E-03
GO:0007276	gamete generation	353	63	5,91E-03
GO:0030728	ovulation	26	6	6,73E-03
GO:0071826	ribonucleoprotein complex subunit organi...	84	24	8,42E-03
GO:0034622	cellular macromolecular complex assembly	299	43	8,89E-03
GO:0035188	hatching	36	7	9,38E-03
GO:0040022	feminization of hermaphroditic germ-line	29	6	1,17E-02
GO:0031033	myosin filament organization	96	13	1,22E-02
GO:0042335	cuticle development	86	12	1,25E-02
GO:0022618	ribonucleoprotein complex assembly	78	23	1,29E-02
GO:1990778	protein localization to cell periphery	30	6	1,38E-02
GO:0035194	posttranscriptional gene silencing by RN...	110	14	1,59E-02
GO:0016441	posttranscriptional gene silencing	110	14	1,59E-02
GO:0034504	protein localization to nucleus	40	7	1,66E-02

GO:0090501	RNA phosphodiester bond hydrolysis	50	8	1,81E-02
GO:0031047	gene silencing by RNA	112	14	1,84E-02
GO:0043067	regulation of programmed cell death	70	10	1,87E-02
GO:0016071	mRNA metabolic process	178	32	1,88E-02
GO:0006997	nucleus organization	41	7	1,89E-02
GO:0061640	cytoskeleton-dependent cytokinesis	24	5	2,03E-02
GO:0040002	collagen and cuticulin-based cuticle dev...	82	11	2,17E-02
GO:0007052	mitotic spindle organization	43	7	2,41E-02
GO:1902850	microtubule cytoskeleton organization in...	43	7	2,41E-02
GO:0000478	endonucleolytic cleavage involved in rRN...	10	3	2,60E-02
GO:0006379	mRNA cleavage	10	3	2,60E-02
GO:0031034	myosin filament assembly	95	12	2,60E-02
GO:0071688	striated muscle myosin thick filament as...	95	12	2,60E-02
GO:0007163	establishment or maintenance of cell pol...	64	9	2,75E-02
GO:0015833	peptide transport	260	30	2,82E-02
GO:0035264	multicellular organism growth	252	42	2,89E-02
GO:0030010	establishment of cell polarity	45	7	3,03E-02
GO:0042273	ribosomal large subunit biogenesis	44	17	3,09E-02
GO:0031032	actomyosin structure organization	109	13	3,20E-02
GO:0042886	amide transport	263	30	3,22E-02
GO:0006606	protein import into nucleus	36	6	3,22E-02
GO:1902593	single-organism nuclear import	36	6	3,22E-02
GO:0040021	hermaphrodite germ-line sex determinatio...	36	6	3,22E-02
GO:0044744	protein targeting to nucleus	36	6	3,22E-02
GO:0006888	ER to Golgi vesicle-mediated transport	27	5	3,27E-02
GO:0051146	striated muscle cell differentiation	110	13	3,42E-02
GO:0055001	muscle cell development	110	13	3,42E-02
GO:0006417	regulation of translation	68	13	3,46E-02
GO:0034248	regulation of cellular amide metabolic p...	68	13	3,46E-02
GO:0051254	positive regulation of RNA metabolic pro...	145	16	3,55E-02
GO:0042692	muscle cell differentiation	122	14	3,56E-02
GO:0006754	ATP biosynthetic process	19	4	3,58E-02
GO:0051170	nuclear import	37	6	3,63E-02
GO:0090502	RNA phosphodiester bond hydrolysis. endo...	28	5	3,77E-02
GO:0007275	multicellular organism development	2634	303	3,84E-02
GO:0016246	RNA interference	101	12	3,95E-02
GO:0044265	cellular macromolecule catabolic process	208	21	4,17E-02
GO:0000460	maturation of 5.8S rRNA	20	4	4,25E-02
GO:0071822	protein complex subunit organization	258	25	4,28E-02
GO:0000466	maturation of 5.8S rRNA from tricistroni...	12	3	4,31E-02
GO:0033206	meiotic cytokinesis	12	3	4,31E-02
GO:0000387	spliceosomal snRNP assembly	12	3	4,31E-02
GO:0016458	gene silencing	127	14	4,76E-02
GO:0007051	spindle organization	60	8	4,81E-02
GO:1902582	single-organism intracellular transport	116	13	4,93E-02

GO:0009145	purine nucleoside triphosphate biosynthe...	21	4	4,98E-02
GO:0009206	purine ribonucleoside triphosphate biosy...	21	4	4,98E-02
GO:0010629	negative regulation of gene expression	267	31	4,99E-02

down-regulating in *daf-2;phb-1(RNAi)*

GO.ID	Term	Annotated	Significant	adj.pvalue
GO:0018996	molting cycle. collagen and cuticulin-ba...	195	67	4,9E-28
GO:0040035	hermaphrodite genitalia development	512	113	5,9E-28
GO:0000003	reproduction	1800	285	3,3E-22
GO:0040011	locomotion	1180	188	1,4E-21
GO:0006915	apoptotic process	362	74	6,4E-16
GO:0010171	body morphogenesis	433	78	1,5E-13
GO:0008406	gonad development	673	150	4,9E-13
GO:0007281	germ cell development	281	54	3,1E-10
GO:0015991	ATP hydrolysis coupled proton transport	19	12	1,2E-09
GO:0040039	inductive cell migration	109	28	7,3E-09
GO:0006418	tRNA aminoacylation for protein translat...	28	12	3,9E-07
GO:0006412	translation	229	55	5,9E-07
GO:0040018	positive regulation of multicellular org...	224	39	8,7E-07
GO:0016246	RNA interference	101	23	1,7E-06
GO:0043652	engulfment of apoptotic cell	70	17	1,6E-05
GO:0000470	maturation of LSU-rRNA	19	8	4,3E-05
GO:0022618	ribonucleoprotein complex assembly	78	22	5,4E-05
GO:0000027	ribosomal large subunit assembly	15	7	6,0E-05
GO:0061077	chaperone-mediated protein folding	15	7	6,0E-05
GO:0045727	positive regulation of translation	11	6	6,9E-05
GO:0006458	'de novo' protein folding	11	6	6,9E-05
GO:0007276	gamete generation	353	73	8,7E-05
GO:0030728	ovulation	26	9	8,8E-05
GO:0006998	nuclear envelope organization	16	7	9,9E-05
GO:0051452	intracellular pH reduction	12	6	1,3E-04
GO:0008340	determination of adult lifespan	565	67	1,6E-04
GO:0000398	mRNA splicing. via spliceosome	94	18	2,5E-04
GO:0006379	mRNA cleavage	10	5	5,0E-04
GO:0051301	cell division	183	32	5,9E-04
GO:0000462	maturation of SSU-rRNA from tricistronic...	28	8	9,5E-04
GO:0051302	regulation of cell division	28	8	9,5E-04
GO:0007067	mitotic nuclear division	134	21	1,3E-03
GO:0030104	water homeostasis	12	5	1,4E-03
GO:0030490	maturation of SSU-rRNA	36	12	1,8E-03
GO:0050793	regulation of developmental process	547	77	1,9E-03
GO:0016477	cell migration	254	49	1,9E-03
GO:0006397	mRNA processing	133	27	2,0E-03
GO:0006270	DNA replication initiation	13	5	2,1E-03
GO:0042254	ribosome biogenesis	150	46	2,3E-03

GO:0006357	regulation of transcription from RNA pol...	258	33	2,6E-03
GO:0035194	posttranscriptional gene silencing by RN...	110	27	2,8E-03
GO:0044786	cell cycle DNA replication	14	5	3,0E-03
GO:0048477	oogenesis	156	22	4,1E-03
GO:0071426	ribonucleoprotein complex export from nu...	21	6	4,2E-03
GO:0031167	rRNA methylation	10	4	5,1E-03
GO:0006352	DNA-templated transcription. initiation	29	7	5,6E-03
GO:0000132	establishment of mitotic spindle orienta...	29	7	5,6E-03
GO:0040022	feminization of hermaphroditic germ-line	29	7	5,6E-03
GO:0043628	ncRNA 3'-end processing	16	5	5,8E-03
GO:0007098	centrosome cycle	16	5	5,8E-03
GO:0033365	protein localization to organelle	123	18	6,1E-03
GO:0034622	cellular macromolecular complex assembly	299	49	6,4E-03
GO:0042127	regulation of cell proliferation	96	15	6,5E-03
GO:0045893	positive regulation of transcription. DN...	143	20	6,7E-03
GO:0042273	ribosomal large subunit biogenesis	44	18	6,8E-03
GO:0051445	regulation of meiotic cell cycle	104	19	7,5E-03
GO:0016073	snRNA metabolic process	11	4	7,6E-03
GO:0006364	rRNA processing	102	30	7,9E-03
GO:0006413	translational initiation	31	7	8,2E-03
GO:0040020	regulation of meiotic nuclear division	73	12	9,6E-03
GO:0040002	collagen and cuticulin-based cuticle dev...	82	13	9,7E-03
GO:0000278	mitotic cell cycle	232	37	1,0E-02
GO:0007097	nuclear migration	48	9	1,0E-02
GO:0040023	establishment of nucleus localization	48	9	1,0E-02
GO:0010942	positive regulation of cell death	40	8	1,0E-02
GO:0034504	protein localization to nucleus	40	8	1,0E-02
GO:0010564	regulation of cell cycle process	139	23	1,0E-02
GO:0016071	mRNA metabolic process	178	36	1,1E-02
GO:0035195	gene silencing by miRNA	12	4	1,1E-02
GO:0000387	spliceosomal snRNP assembly	12	4	1,1E-02
GO:0006401	RNA catabolic process	49	9	1,2E-02
GO:0051647	nucleus localization	50	9	1,3E-02
GO:0046903	secretion	143	19	1,4E-02
GO:0006402	mRNA catabolic process	42	8	1,4E-02
GO:0040007	growth	419	62	1,4E-02
GO:0071822	protein complex subunit organization	258	30	1,5E-02
GO:0007051	spindle organization	60	10	1,6E-02
GO:0000460	maturation of 5.8S rRNA	20	5	1,6E-02
GO:0006414	translational elongation	20	5	1,6E-02
GO:0032940	secretion by cell	136	18	1,7E-02
GO:0045787	positive regulation of cell cycle	61	10	1,8E-02
GO:2000113	negative regulation of cellular macromol...	127	17	1,8E-02
GO:0048646	anatomical structure formation involved ...	147	19	1,8E-02
GO:0040025	vulval development	251	29	1,8E-02
GO:0090502	RNA phosphodiester bond hydrolysis. endo...	28	6	1,8E-02
GO:0035188	hatching	36	7	1,9E-02
GO:0071684	organism emergence from protective struc...	36	7	1,9E-02

GO:0090502	RNA phosphodiester bond hydrolysis. endo...	28	6	1,8E-02
GO:0035188	hatching	36	7	1,9E-02
GO:0071684	organism emergence from protective struc...	36	7	1,9E-02
GO:0044770	cell cycle phase transition	36	7	1,9E-02
GO:0000154	rRNA modification	18	7	1,9E-02
GO:0031124	mRNA 3'-end processing	14	4	1,9E-02
GO:0040014	regulation of multicellular organism gro...	239	43	2,0E-02
GO:0010558	negative regulation of macromolecule bio...	129	17	2,1E-02
GO:0006366	transcription from RNA polymerase II pro...	280	38	2,1E-02
GO:0048569	post-embryonic animal organ development	254	29	2,1E-02
GO:0000956	nuclear-transcribed mRNA catabolic proce...	37	7	2,2E-02
GO:0007338	single fertilization	54	9	2,2E-02
GO:0045184	establishment of protein localization	258	33	2,3E-02
GO:0009791	post-embryonic development	1497	278	2,3E-02
GO:0035046	pronuclear migration	46	8	2,3E-02
GO:0010501	RNA secondary structure unwinding	22	5	2,4E-02
GO:0070897	DNA-templated transcriptional preinitiat...	15	4	2,4E-02
GO:0045944	positive regulation of transcription fro...	132	17	2,5E-02
GO:0043623	cellular protein complex assembly	184	22	2,6E-02
GO:0006260	DNA replication	74	18	2,6E-02
GO:0015031	protein transport	251	32	2,8E-02
GO:0040028	regulation of vulval development	196	23	2,8E-02
GO:0048522	positive regulation of cellular process	423	54	2,8E-02
GO:0009201	ribonucleoside triphosphate biosynthetic...	23	5	2,9E-02
GO:0043068	positive regulation of programmed cell d...	31	6	2,9E-02
GO:0022411	cellular component disassembly	66	10	2,9E-02
GO:0031123	RNA 3'-end processing	32	9	3,0E-02
GO:0090501	RNA phosphodiester bond hydrolysis	50	12	3,0E-02
GO:0031034	myosin filament assembly	95	13	3,1E-02
GO:0071688	striated muscle myosin thick filament as...	95	13	3,1E-02
GO:0010941	regulation of cell death	86	12	3,2E-02
GO:0031327	negative regulation of cellular biosynth...	136	17	3,3E-02
GO:0009890	negative regulation of biosynthetic proc...	136	17	3,3E-02
GO:0031033	myosin filament organization	96	13	3,3E-02
GO:0008105	asymmetric protein localization	32	6	3,4E-02
GO:0045935	positive regulation of nucleobase-contai...	153	23	3,5E-02
GO:0040027	negative regulation of vulval developmen...	158	19	3,5E-02
GO:0000910	cytokinesis	50	8	3,7E-02
GO:0006275	regulation of DNA replication	10	3	3,7E-02
GO:0000478	endonucleolytic cleavage involved in rRN...	10	3	3,7E-02
GO:0006360	transcription from RNA polymerase I prom...	10	3	3,7E-02
GO:0010940	positive regulation of necrotic cell dea...	10	3	3,7E-02
GO:0031125	rRNA 3'-end processing	10	3	3,7E-02
GO:0065001	specification of axis polarity	10	3	3,7E-02
GO:0040032	post-embryonic body morphogenesis	10	3	3,7E-02

GO:0007049	cell cycle	456	64	3,8E-02
GO:0000469	cleavage involved in rRNA processing	17	4	3,8E-02
GO:0007040	lysosome organization	17	4	3,8E-02
GO:0002181	cytoplasmic translation	17	4	3,8E-02
GO:0000245	spliceosomal complex assembly	17	4	3,8E-02
GO:0080171	lytic vacuole organization	17	4	3,8E-02
GO:0070482	response to oxygen levels	17	4	3,8E-02
GO:0010629	negative regulation of gene expression	267	45	3,9E-02
GO:0009142	nucleoside triphosphate biosynthetic pro...	25	5	4,0E-02
GO:0009566	fertilization	60	9	4,0E-02
GO:0007346	regulation of mitotic cell cycle	89	12	4,1E-02
GO:0015833	peptide transport	260	32	4,2E-02
GO:0043067	regulation of programmed cell death	70	10	4,2E-02
GO:0045892	negative regulation of transcription. DN...	90	12	4,4E-02
GO:0007052	mitotic spindle organization	43	7	4,5E-02
GO:1902850	microtubule cytoskeleton organization in...	43	7	4,5E-02
GO:0051028	mRNA transport	18	4	4,6E-02
GO:0006367	transcription initiation from RNA polyme...	18	4	4,6E-02
GO:0010453	regulation of cell fate commitment	18	4	4,6E-02
GO:0032508	DNA duplex unwinding	26	5	4,6E-02
GO:0051172	negative regulation of nitrogen compound...	142	17	4,7E-02
GO:0042886	amide transport	263	32	4,8E-02
GO:1903047	mitotic cell cycle process	201	32	4,8E-02
GO:0007506	gonadal mesoderm development	11	3	4,8E-02
GO:0030201	heparan sulfate proteoglycan metabolic p...	11	3	4,8E-02
GO:0010939	regulation of necrotic cell death	11	3	4,8E-02
GO:0006378	mRNA polyadenylation	11	3	4,8E-02
GO:0015012	heparan sulfate proteoglycan biosyntheti...	11	3	4,8E-02
GO:0045930	negative regulation of mitotic cell cycl...	53	8	5,0E-02

Appendix 7: Table S1_Lifespan data

	Median survival	max survival*	# deaths/total	P value, compared to control RNAi	P value, compared to phb-1 (RNAi)
daf-2(e1370)_control	48	58	105 / 115		
daf-2(e1370)_control	47	58	50 / 149		
daf-2(e1370)_control;atfs-1	26	32	135 / 157	< 0.0001 (***)	
daf-2(e1370)_control;his-65	48	65	95 / 106	0.1004 (ns)	
daf-2(e1370)_control;his-65	47	61	79 / 152	0,3448 (ns)	
daf-2(e1370)_control;phb-1	65	103	134 / 158	< 0.0001 (***)	
daf-2(e1370)_control;phb-1	85	108	77 / 142	< 0.0001 (***)	
daf-2(e1370)_control;phb-1	67	87	21 / 153		
daf-2(e1370)_control;usp-48	15	20	61 / 142	< 0.0001 (***)	
daf-2(e1370)_control;usp-48	18	20	53 / 179	< 0.0001 (***)	
daf-2(e1370)_phb-1;atfs-1	44	48	86 / 88		< 0.0001 (***)
daf-2(e1370)_phb-1;atfs-1	58	61	127 / 148		< 0.0001 (***)
daf-2(e1370)_phb-1;his-65	68	92	122 / 137		0,5131 (ns)
daf-2(e1370)_phb-1;his-65	58	82	92 / 149		< 0.0001 (***)
daf-2(e1370)_phb-1;his-65	64	90	30 / 145		0,2067 (ns)
daf-2(e1370)_phb-1;ups-48	18	20	129 / 155		< 0.0001 (***)
daf-2(e1370)_phb-1;ups-48	18	22	160 / 200		< 0.0001 (***)
wild type_control	19	26	89 / 150		
wild type_control	17	24	83 / 149		
wild type_control;atfs-1	18	22	110 / 160	0,3095 (ns)	
wild type_control;atfs-1	17	24	95 / 150	0,5781 (ns)	
wild type_control;his-65	19	26	115 / 150	0,4533 (ns)	
wild type_control;his-65	19	24	125 / 150	0,1386 (ns)	
wild type_control;phb-1	15	19	72 / 150	< 0.0001 (***)	
wild type_control;phb-1	17	19	64 / 150	< 0.0001 (***)	
wild type_control;usp-48	12	15	92 / 191	< 0.0001 (***)	
wild type_control;usp-48	14	17	64 / 150	< 0.0001 (***)	
wild type_phb-1;atfs-1	14	18	107 / 160		0,1535 (ns)
wild type_phb-1;atfs-1	19	26	99 / 150		< 0.0001 (***)
wild type_phb-1;his-65	15	19	91 / 149		0,4726 (ns)
wild type_phb-1;his-65	17	19	101 / 150		0,2067 (ns)
wild type_phb-1;ups-48	10	12	106 / 198		< 0.0001 (***)
wild type_phb-1;ups-48	14	17	84 / 150		< 0.0001 (***)

*max survival represents the day where more than 90% of the population is dead

REFERENCES

Ackema, K. B., J. Hench, S. Bockler, S. C. Wang, U. Sauder, H. Mergentaler, B. Westermann, F. Bard, S. Frank and A. Spang (2014). "The small GTPase Arf1 modulates mitochondrial morphology and function." EMBO J **33**(22): 2659-2675.

Ackema, K. B., U. Sauder, J. A. Solinger and A. Spang (2013). "The ArfGEF GBF-1 Is Required for ER Structure, Secretion and Endocytic Transport in C. elegans." PLoS One **8**(6): e67076.

Akerfelt, M., R. I. Morimoto and L. Sistonen (2010). "Heat shock factors: integrators of cell stress, development and lifespan." Nat Rev Mol Cell Biol **11**(8): 545-555.

Alexa, A., J. Rahnenfuhrer and T. Lengauer (2006). "Improved scoring of functional groups from gene expression data by decorrelating GO graph structure." Bioinformatics **22**(13): 1600-1607.

Altintas, O., S. Park and S. J. Lee (2016). "The role of insulin/IGF-1 signaling in the longevity of model invertebrates, C. elegans and D. melanogaster." BMB Rep **49**(2): 81-92.

Anisimov, V. N., L. M. Berstein, I. G. Popovich, M. A. Zabezhinski, P. A. Egormin, T. S. Piskunova, A. V. Semenchenko, M. L. Tyndyk, M. N. Yurova, I. G. Kovalenko and T. E. Poroshina (2011). "If started early in life, metformin treatment increases life span and postpones tumors in female SHR mice." Aging (Albany NY) **3**(2): 148-157.

Apfeld, J., G. O'Connor, T. McDonagh, P. S. DiStefano and R. Curtis (2004). "The AMP-activated protein kinase AAK-2 links energy levels and insulin-like signals to lifespan in C. elegans." Genes Dev **18**(24): 3004-3009.

Artal-Sanz, M. and N. Tavernarakis (2008). "Mechanisms of aging and energy metabolism in Caenorhabditis elegans." IUBMB Life **60**(5): 315-322.

Artal-Sanz, M. and N. Tavernarakis (2009). "Prohibitin and mitochondrial biology." Trends Endocrinol Metab **20**(8): 394-401.

Artal-Sanz, M. and N. Tavernarakis (2009). "Prohibitin couples diapause signalling to mitochondrial metabolism during ageing in C. elegans." Nature **461**(7265): 793-797.

Artal-Sanz, M., W. Y. Tsang, E. M. Willems, L. A. Grivell, B. D. Lemire, H. van der Spek and L. G. Nijtmans (2003). "The mitochondrial prohibitin complex is essential for embryonic viability and germline function in Caenorhabditis elegans." J Biol Chem **278**(34): 32091-32099.

Asikainen, S., M. Storvik, M. Lakso and G. Wong (2007). "Whole genome microarray analysis of C. elegans rrf-3 and eri-1 mutants." FEBS Lett **581**(26): 5050-5054.

Back, J. W., M. A. Sanz, L. De Jong, L. J. De Koning, L. G. Nijtmans, C. G. De Koster, L. A. Grivell, H. Van Der Spek and A. O. Muijsers (2002). "A structure for the yeast prohibitin complex: Structure prediction and evidence from chemical crosslinking

and mass spectrometry." Protein Sci **11**(10): 2471-2478.

Baker, B. M., A. M. Nargund, T. Sun and C. M. Haynes (2012). "Protective coupling of mitochondrial function and protein synthesis via the eIF2alpha kinase GCN-2." PLoS Genet **8**(6): e1002760.

Balaban, R. S., S. Nemoto and T. Finkel (2005). "Mitochondria, oxidants, and aging." Cell **120**(4): 483-495.

Barsyte, D., D. A. Lovejoy and G. J. Lithgow (2001). "Longevity and heavy metal resistance in daf-2 and age-1 long-lived mutants of Caenorhabditis elegans." FASEB J **15**(3): 627-634.

Basak, N. P., A. Roy and S. Banerjee (2014). "Alteration of mitochondrial proteome due to activation of Notch1 signaling pathway." J Biol Chem **289**(11): 7320-7334.

Bassing, C. H., K. F. Chua, J. Sekiguchi, H. Suh, S. R. Whitlow, J. C. Fleming, B. C. Monroe, D. N. Ciccone, C. Yan, K. Vlasakova, D. M. Livingston, D. O. Ferguson, R. Scully and F. W. Alt (2002). "Increased ionizing radiation sensitivity and genomic instability in the absence of histone H2AX." Proc Natl Acad Sci U S A **99**(12): 8173-8178.

Benedetti, C., C. M. Haynes, Y. Yang, H. P. Harding and D. Ron (2006). "Ubiquitin-like protein 5 positively regulates chaperone gene expression in the mitochondrial unfolded protein response." Genetics **174**(1): 229-239.

Bennett, C. F., H. Vander Wende, M. Simko, S. Klum, S. Barfield, H. Choi, V. V. Pineda and M. Kaeberlein (2014). "Activation of the mitochondrial unfolded protein response does not predict longevity in Caenorhabditis elegans." Nat Commun **5**: 3483.

Berendzen, K. M., J. Durieux, L. W. Shao, Y. Tian, H. E. Kim, S. Wolff, Y. Liu and A. Dillin (2016). "Neuroendocrine Coordination of Mitochondrial Stress Signaling and Proteostasis." Cell **166**(6): 1553-1563 e1510.

Berger, K. H. and M. P. Yaffe (1998). "Prohibitin family members interact genetically with mitochondrial inheritance components in Saccharomyces cerevisiae." Mol Cell Biol **18**(7): 4043-4052.

Bernardes de Jesus, B. and M. A. Blasco (2012). "Potential of telomerase activation in extending health span and longevity." Curr Opin Cell Biol **24**(6): 739-743.

Blake, M. J., R. Udelsman, G. J. Feulner, D. D. Norton and N. J. Holbrook (1991). "Stress-induced heat shock protein 70 expression in adrenal cortex: an adrenocorticotropic hormone-sensitive, age-dependent response." Proc Natl Acad Sci U S A **88**(21): 9873-9877.

Bluher, M., B. B. Kahn and C. R. Kahn (2003). "Extended longevity in mice lacking the insulin receptor in adipose tissue." Science **299**(5606): 572-574.

Bluher, M., M. D. Michael, O. D. Peroni, K. Ueki, N. Carter, B. B. Kahn and C. R. Kahn (2002). "Adipose tissue selective insulin receptor knockout protects against obesity and obesity-related glucose intolerance." Dev Cell **3**(1): 25-38.

Bogenhagen, D. F., Y. Wang, E. L. Shen and R. Kobayashi (2003). "Protein components of mitochondrial DNA nucleoids in higher eukaryotes." Mol Cell Proteomics **2**(11): 1205-1216.

Brenner, S. (1974). "The genetics of Caenorhabditis elegans." Genetics **77**(1): 71-94.

Brown, K., P. Yang, D. Salvador, R. Kulikauskas, H. Ruohola-Baker, A. M. Robitaille, A. J. Chien, R. T. Moon and V. Sherwood (2017). "WNT/beta-catenin signaling regulates mitochondrial activity to alter the oncogenic potential of melanoma in a PTEN-dependent manner." Oncogene **36**(22): 3119-3136.

Butcher, R. A., J. R. Ragains, W. Li, G. Ruvkun, J. Clardy and H. Y. Mak (2009). "Biosynthesis of the Caenorhabditis elegans dauer pheromone." Proc Natl Acad Sci U S A **106**(6): 1875-1879.

Butler, J. A., R. J. Mishur, S. Bhaskaran and S. L. Rea (2013). "A metabolic signature for long life in the Caenorhabditis elegans Mit mutants." Aging Cell **12**(1): 130-138.

Byerly, L., R. C. Cassada and R. L. Russell (1976). "The life cycle of the nematode Caenorhabditis elegans. I. Wild-type growth and reproduction." Dev Biol **51**(1): 23-33.

Carpenter, A. E., T. R. Jones, M. R. Lamprecht, C. Clarke, I. H. Kang, O. Friman, D. A. Guertin, J. H. Chang, R. A. Lindquist, J. Moffat, P. Golland and D. M. Sabatini (2006). "CellProfiler: image analysis software for identifying and quantifying cell phenotypes." Genome Biol **7**(10): R100.

Cetkovska, K., H. Sustova and S. Uldrijan (2017). "Ubiquitin-specific peptidase 48 regulates Mdm2 protein levels independent of its deubiquitinase activity." Sci Rep **7**: 43180.

Chander, H., M. Halpern, L. Resnick-Silverman, J. J. Manfredi and D. Germain (2010). "Skp2B attenuates p53 function by inhibiting prohibitin." EMBO Rep **11**(3): 220-225.

Chander, H., M. Halpern, L. Resnick-Silverman, J. J. Manfredi and D. Germain (2011). "Skp2B overexpression alters a prohibitin-p53 axis and the transcription of PAPP-A, the protease of insulin-like growth factor binding protein 4." PLoS One **6**(8): e22456.

Chen, D., K. Z. Pan, J. E. Palter and P. Kapahi (2007). "Longevity determined by developmental arrest genes in Caenorhabditis elegans." Aging Cell **6**(4): 525-533.

Chen, D., E. L. Thomas and P. Kapahi (2009). "HIF-1 modulates dietary restriction-mediated lifespan extension via IRE-1 in Caenorhabditis elegans." PLoS Genet **5**(5):

e1000486.

Chen, H., M. Fan, L. M. Pfeffer and R. N. Laribee (2012). "The histone H3 lysine 56 acetylation pathway is regulated by target of rapamycin (TOR) signaling and functions directly in ribosomal RNA biogenesis." Nucleic Acids Res **40**(14): 6534-6546.

Chen, L. T., M. Luo, Y. Y. Wang and K. Wu (2010). "Involvement of Arabidopsis histone deacetylase HDA6 in ABA and salt stress response." J Exp Bot **61**(12): 3345-3353.

Chowdhury, D., D. Kumar, U. Bhadra, T. A. Devi and M. P. Bhadra (2017). "Prohibitin confers cytoprotection against ISO-induced hypertrophy in H9c2 cells via attenuation of oxidative stress and modulation of Akt/Gsk-3beta signaling." Mol Cell Biochem **425**(1-2): 155-168.

Chowdhury, I., W. E. Thompson, C. Welch, K. Thomas and R. Matthews (2013). "Prohibitin (PHB) inhibits apoptosis in rat granulosa cells (GCs) through the extracellular signal-regulated kinase 1/2 (ERK1/2) and the Bcl family of proteins." Apoptosis **18**(12): 1513-1525.

Christie, D. A., C. D. Lemke, I. M. Elias, L. A. Chau, M. G. Kirchhof, B. Li, E. H. Ball, S. D. Dunn, G. M. Hatch and J. Madrenas (2011). "Stomatin-like protein 2 binds cardiolipin and regulates mitochondrial biogenesis and function." Mol Cell Biol **31**(18): 3845-3856.

Chu, J. S., S. Y. Chua, K. Wong, A. M. Davison, R. Johnsen, D. L. Baillie and A. M. Rose (2014). "High-throughput capturing and characterization of mutations in essential genes of Caenorhabditis elegans." BMC Genomics **15**: 361.

Clancy, D. J., D. Gems, L. G. Harshman, S. Oldham, H. Stocker, E. Hafen, S. J. Leevers and L. Partridge (2001). "Extension of life-span by loss of CHICO, a Drosophila insulin receptor substrate protein." Science **292**(5514): 104-106.

Conte, D., Jr., L. T. MacNeil, A. J. Walhout and C. C. Mello (2015). "RNA Interference in Caenorhabditis elegans." Curr Protoc Mol Biol **109**: 26 23 21-30.

Cui, M., E. B. Kim and M. Han (2006). "Diverse chromatin remodeling genes antagonize the Rb-involved SynMuv pathways in C. elegans." PLoS Genet **2**(5): e74.

Culetto, E. and D. B. Sattelle (2000). "A role for Caenorhabditis elegans in understanding the function and interactions of human disease genes." Hum Mol Genet **9**(6): 869-877.

Curran, S. P. and G. Ruvkun (2007). "Lifespan regulation by evolutionarily conserved genes essential for viability." PLoS Genet **3**(4): e56.

Da Cruz, S., P. A. Parone, P. Gonzalo, W. V. Bienvenut, D. Tondera, A. Jourdain, M. Quadroni and J. C. Martinou (2008). "SLP-2 interacts with prohibitins in the

mitochondrial inner membrane and contributes to their stability." Biochim Biophys Acta **1783**(5): 904-911.

Dalton, H. M. and S. P. Curran (2018). "Hypodermal responses to protein synthesis inhibition induce systemic developmental arrest and AMPK-dependent survival in Caenorhabditis elegans." PLoS Genet **14**(7): e1007520.

Dantonel, J. C., S. Quintin, L. Lakatos, M. Labouesse and L. Tora (2000). "TBP-like factor is required for embryonic RNA polymerase II transcription in C. elegans." Mol Cell **6**(3): 715-722.

Darling, N. J. and S. J. Cook (2014). "The role of MAPK signalling pathways in the response to endoplasmic reticulum stress." Biochim Biophys Acta **1843**(10): 2150-2163.

de Wit, E., F. Greil and B. van Steensel (2007). "High-resolution mapping reveals links of HP1 with active and inactive chromatin components." PLoS Genet **3**(3): e38.

Delaney, K., J. Mailler, J. M. Wenda, C. Gabus and F. A. Steiner (2018). "Differential Expression of Histone H3.3 Genes and Their Role in Modulating Temperature Stress Response in Caenorhabditis elegans." Genetics **209**(2): 551-565.

Depuydt, G., F. Xie, V. A. Petyuk, A. Smolders, H. M. Brewer, D. G. Camp, 2nd, R. D. Smith and B. P. Braeckman (2014). "LC-MS proteomics analysis of the insulin/IGF-1-deficient Caenorhabditis elegans daf-2(e1370) mutant reveals extensive restructuring of intermediary metabolism." J Proteome Res **13**(4): 1938-1956.

Dillin, A., A. L. Hsu, N. Arantes-Oliveira, J. Lehrer-Graiwer, H. Hsin, A. G. Fraser, R. S. Kamath, J. Ahringer and C. Kenyon (2002). "Rates of behavior and aging specified by mitochondrial function during development." Science **298**(5602): 2398-2401.

DiLoreto, R. and C. T. Murphy (2015). "The cell biology of aging." Mol Biol Cell **26**(25): 4524-4531.

Dong, M. Q., J. D. Venable, N. Au, T. Xu, S. K. Park, D. Cociorva, J. R. Johnson, A. Dillin and J. R. Yates, 3rd (2007). "Quantitative mass spectrometry identifies insulin signaling targets in C. elegans." Science **317**(5838): 660-663.

Dougherty, E. C. and H. G. Calhoun (1948). "Possible significance of free-living nematodes in genetic research." Nature **161**(4079): 29.

Dunbar, T. L., Z. Yan, K. M. Balla, M. G. Smelkinson and E. R. Troemel (2012). "C. elegans detects pathogen-induced translational inhibition to activate immune signaling." Cell Host Microbe **11**(4): 375-386.

Dupuy, D., N. Bertin, C. A. Hidalgo, K. Venkatesan, D. Tu, D. Lee, J. Rosenberg, N. Svrzikapa, A. Blanc, A. Carnec, A. R. Carvunis, R. Pulak, J. Shingles, J. Reece-Hoyes, R. Hunt-Newbury, R. Viveiros, W. A. Mohler, M. Tasan, F. P. Roth, C. Le Peuch, I. A. Hope, R. Johnsen, D. G. Moerman, A. L. Barabasi, D. Baillie and M. Vidal (2007).

"Genome-scale analysis of in vivo spatiotemporal promoter activity in Caenorhabditis elegans." Nat Biotechnol **25**(6): 663-668.

Durieux, J., S. Wolff and A. Dillin (2011). "The cell-non-autonomous nature of electron transport chain-mediated longevity." Cell **144**(1): 79-91.

Edwards, C. B., N. Copes, A. G. Brito, J. Canfield and P. C. Bradshaw (2013). "Malate and fumarate extend lifespan in Caenorhabditis elegans." PLoS One **8**(3): e58345.

Eide, D. J., J. T. Bridgham, Z. Zhao and J. R. Mattoon (1993). "The vacuolar H(+)-ATPase of Saccharomyces cerevisiae is required for efficient copper detoxification, mitochondrial function, and iron metabolism." Mol Gen Genet **241**(3-4): 447-456.

Eisenberg, T., H. Knauer, A. Schauer, S. Buttner, C. Ruckenstuhl, D. Carmona-Gutierrez, J. Ring, S. Schroeder, C. Magnes, L. Antonacci, H. Fussi, L. Deszcz, R. Hartl, E. Schraml, A. Criollo, E. Megalou, D. Weiskopf, P. Laun, G. Heeren, M. Breitenbach, B. Grubeck-Loebenstein, E. Herker, B. Fahrenkrog, K. U. Frohlich, F. Sinner, N. Tavernarakis, N. Minois, G. Kroemer and F. Madeo (2009). "Induction of autophagy by spermidine promotes longevity." Nat Cell Biol **11**(11): 1305-1314.

Engelen, E., J. H. Brandsma, M. J. Moen, L. Signorile, D. H. Dekkers, J. Demmers, C. E. Kockx, Z. Ozgur, I. W. F. van, D. L. van den Berg and R. A. Poot (2015). "Proteins that bind regulatory regions identified by histone modification chromatin immunoprecipitations and mass spectrometry." Nat Commun **6**: 7155.

Estes, K. A., T. L. Dunbar, J. R. Powell, F. M. Ausubel and E. R. Troemel (2010). "bZIP transcription factor zip-2 mediates an early response to Pseudomonas aeruginosa infection in Caenorhabditis elegans." Proc Natl Acad Sci U S A **107**(5): 2153-2158.

Evans, E. A., W. C. Chen and M. W. Tan (2008). "The DAF-2 insulin-like signaling pathway independently regulates aging and immunity in C. elegans." Aging Cell **7**(6): 879-893.

Feser, J., D. Truong, C. Das, J. J. Carson, J. Kieft, T. Harkness and J. K. Tyler (2010). "Elevated histone expression promotes life span extension." Mol Cell **39**(5): 724-735.

Fire, A., S. Xu, M. K. Montgomery, S. A. Kostas, S. E. Driver and C. C. Mello (1998). "Potent and specific genetic interference by double-stranded RNA in Caenorhabditis elegans." Nature **391**(6669): 806-811.

Fransen, M., M. Nordgren, B. Wang and O. Apanasets (2012). "Role of peroxisomes in ROS/RNS-metabolism: implications for human disease." Biochim Biophys Acta **1822**(9): 1363-1373.

Fraser, A. G., R. S. Kamath, P. Zipperlen, M. Martinez-Campos, M. Sohrmann and J. Ahringer (2000). "Functional genomic analysis of C. elegans chromosome I by

systematic RNA interference." Nature **408**(6810): 325-330.

Friedman, D. B. and T. E. Johnson (1988). "A mutation in the age-1 gene in Caenorhabditis elegans lengthens life and reduces hermaphrodite fertility." Genetics **118**(1): 75-86.

Fusaro, G., P. Dasgupta, S. Rastogi, B. Joshi and S. Chellappan (2003). "Prohibitin induces the transcriptional activity of p53 and is exported from the nucleus upon apoptotic signaling." J Biol Chem **278**(48): 47853-47861.

Gaiser, A. M., F. Brandt and K. Richter (2009). "The non-canonical Hop protein from Caenorhabditis elegans exerts essential functions and forms binary complexes with either Hsc70 or Hsp90." J Mol Biol **391**(3): 621-634.

Galdieri, L., T. Zhang, D. Rogerson and A. Vancura (2016). "Reduced Histone Expression or a Defect in Chromatin Assembly Induces Respiration." Mol Cell Biol **36**(7): 1064-1077.

Garcia-Martinez, J. M. and D. R. Alessi (2008). "mTOR complex 2 (mTORC2) controls hydrophobic motif phosphorylation and activation of serum- and glucocorticoid-induced protein kinase 1 (SGK1)." Biochem J **416**(3): 375-385.

Garsin, D. A., J. M. Villanueva, J. Begun, D. H. Kim, C. D. Sifri, S. B. Calderwood, G. Ruvkun and F. M. Ausubel (2003). "Long-lived C. elegans daf-2 mutants are resistant to bacterial pathogens." Science **300**(5627): 1921.

Gatsi, R., B. Schulze, M. J. Rodriguez-Palero, B. Hernando-Rodriguez, R. Baumeister and M. Artal-Sanz (2014). "Prohibitin-mediated lifespan and mitochondrial stress implicate SGK-1, insulin/IGF and mTORC2 in C. elegans." PLoS One **9**(9): e107671.

Gems, D. and L. Partridge (2013). "Genetics of longevity in model organisms: debates and paradigm shifts." Annu Rev Physiol **75**: 621-644.

Gems, D., A. J. Sutton, M. L. Sundermeyer, P. S. Albert, K. V. King, M. L. Edgley, P. L. Larsen and D. L. Riddle (1998). "Two pleiotropic classes of daf-2 mutation affect larval arrest, adult behavior, reproduction and longevity in Caenorhabditis elegans." Genetics **150**(1): 129-155.

Gershon, D. (1970). "Studies on aging in Nematodes. I. The nematode as a model organism for aging research." Exp Gerontol **5**(1): 7-12.

Gerstein, M. B., Z. J. Lu, E. L. Van Nostrand, C. Cheng, B. I. Arshinoff, T. Liu, K. Y. Yip, R. Robilotto, A. Rechtsteiner, K. Ikegami, P. Alves, A. Chateigner, M. Perry, M. Morris, R. K. Auerbach, X. Feng, J. Leng, A. Vielle, W. Niu, K. Rhrissorrakrai, A. Agarwal, R. P. Alexander, G. Barber, C. M. Brdlik, J. Brennan, J. J. Brouillet, A. Carr, M. S. Cheung, H. Clawson, S. Contrino, L. O. Dannenberg, A. F. Dernburg, A. Desai, L. Dick, A. C. Dose, J. Du, T. Egelhofer, S. Ercan, G. Euskirchen, B. Ewing, E. A. Feingold,

R. Gassmann, P. J. Good, P. Green, F. Gullier, M. Gutwein, M. S. Guyer, L. Habegger, T. Han, J. G. Henikoff, S. R. Henz, A. Hinrichs, H. Holster, T. Hyman, A. L. Iniguez, J. Janette, M. Jensen, M. Kato, W. J. Kent, E. Kephart, V. Khivansara, E. Khurana, J. K. Kim, P. Kolasinska-Zwierz, E. C. Lai, I. Latorre, A. Leahey, S. Lewis, P. Lloyd, L. Lochovsky, R. F. Lowdon, Y. Lubling, R. Lyne, M. MacCoss, S. D. Mackowiak, M. Mangone, S. McKay, D. Mecenas, G. Merrihew, D. M. Miller, 3rd, A. Muroyama, J. I. Murray, S. L. Ooi, H. Pham, T. Phippen, E. A. Preston, N. Rajewsky, G. Ratsch, H. Rosenbaum, J. Rozowsky, K. Rutherford, P. Ruzanov, M. Sarov, R. Sasidharan, A. Sboner, P. Scheid, E. Segal, H. Shin, C. Shou, F. J. Slack, C. Slightam, R. Smith, W. C. Spencer, E. O. Stinson, S. Taing, T. Takasaki, D. Vafeados, K. Voronina, G. Wang, N. L. Washington, C. M. Whittle, B. Wu, K. K. Yan, G. Zeller, Z. Zha, M. Zhong, X. Zhou, E. C. mod, J. Ahringer, S. Strome, K. C. Gunsalus, G. Micklem, X. S. Liu, V. Reinke, S. K. Kim, L. W. Hillier, S. Henikoff, F. Piano, M. Snyder, L. Stein, J. D. Lieb and R. H. Waterston (2010). “Integrative analysis of the Caenorhabditis elegans genome by the modENCODE project.” Science **330**(6012): 1775-1787.

Ghazi, A., S. Henis-Korenblit and C. Kenyon (2007). “Regulation of Caenorhabditis elegans lifespan by a proteasomal E3 ligase complex.” Proc Natl Acad Sci U S A **104**(14): 5947-5952.

Gosai, S. J., J. H. Kwak, C. J. Luke, O. S. Long, D. E. King, K. J. Kovatch, P. A. Johnston, T. Y. Shun, J. S. Lazo, D. H. Perlmutter, G. A. Silverman and S. C. Pak (2010). “Automated high-content live animal drug screening using C. elegans expressing the aggregation prone serpin alpha1-antitrypsin Z.” PLoS One **5**(11): e15460.

Gouda, K., Y. Matsunaga, T. Iwasaki and T. Kawano (2010). “An altered method of feeding RNAi that knocks down multiple genes simultaneously in the nematode Caenorhabditis elegans.” Biosci Biotechnol Biochem **74**(11): 2361-2365.

Guedouari, H., T. Daigle, L. Scorrano and E. Hebert-Chatelain (2017). “Sirtuin 5 protects mitochondria from fragmentation and degradation during starvation.” Biochim Biophys Acta **1864**(1): 169-176.

Halaschek-Wiener, J., J. S. Khattra, S. McKay, A. Pouzyrev, J. M. Stott, G. S. Yang, R. A. Holt, S. J. Jones, M. A. Marra, A. R. Brooks-Wilson and D. L. Riddle (2005). “Analysis of long-lived C. elegans daf-2 mutants using serial analysis of gene expression.” Genome Res **15**(5): 603-615.

Hamilton, B., Y. Dong, M. Shindo, W. Liu, I. Odell, G. Ruvkun and S. S. Lee (2005). “A systematic RNAi screen for longevity genes in C. elegans.” Genes Dev **19**(13): 1544-1555.

Hamilton, C. A., A. G. Good and G. J. Taylor (2001). “Vacuolar H+-ATPase, but not mitochondrial F1F0-ATPase, is required for aluminum resistance in Saccharomyces

cerevisiae." FEMS Microbiol Lett **205**(2): 231-236.

Han, J., C. Yu, R. F. Souza and A. L. Theiss (2014). "Prohibitin 1 modulates mitochondrial function of Stat3." Cell Signal **26**(10): 2086-2095.

Han, S. and A. Brunet (2012). "Histone methylation makes its mark on longevity." Trends Cell Biol **22**(1): 42-49.

Hansen, M., A. Chandra, L. L. Mitic, B. Onken, M. Driscoll and C. Kenyon (2008). "A role for autophagy in the extension of lifespan by dietary restriction in C. elegans." PLoS Genet **4**(2): e24.

Hansen, M., S. Taubert, D. Crawford, N. Libina, S. J. Lee and C. Kenyon (2007). "Lifespan extension by conditions that inhibit translation in Caenorhabditis elegans." Aging Cell **6**(1): 95-110.

Haynes, C. M., K. Petrova, C. Benedetti, Y. Yang and D. Ron (2007). "ClpP mediates activation of a mitochondrial unfolded protein response in C. elegans." Dev Cell **13**(4): 467-480.

Haynes, C. M., Y. Yang, S. P. Blais, T. A. Neubert and D. Ron (2010). "The matrix peptide exporter HAF-1 signals a mitochondrial UPR by activating the transcription factor ZC376.7 in C. elegans." Mol Cell **37**(4): 529-540.

He, B., Q. Feng, A. Mukherjee, D. M. Lonard, F. J. DeMayo, B. S. Katzenellenbogen, J. P. Lydon and B. W. O'Malley (2008). "A repressive role for prohibitin in estrogen signaling." Mol Endocrinol **22**(2): 344-360.

He, J., H. M. Cooper, A. Reyes, M. Di Re, H. Sembongi, T. R. Litwin, J. Gao, K. C. Neuman, I. M. Fearnley, A. Spinazzola, J. E. Walker and I. J. Holt (2012). "Mitochondrial nucleoid interacting proteins support mitochondrial protein synthesis." Nucleic Acids Res **40**(13): 6109-6121.

Heimbucher, T., Z. Liu, C. Bossard, R. McCloskey, A. C. Carrano, C. G. Riedel, B. Tanasa, C. Klammt, B. R. Fonslow, C. E. Riera, B. F. Lillemeier, K. Kemphues, J. R. Yates, 3rd, C. O'Shea, T. Hunter and A. Dillin (2015). "The Deubiquitylase MATH-33 Controls DAF-16 Stability and Function in Metabolism and Longevity." Cell Metab **22**(1): 151-163.

Hekimi, S., J. Lapointe and Y. Wen (2011). "Taking a "good" look at free radicals in the aging process." Trends Cell Biol **21**(10): 569-576.

Henis-Korenblit, S., P. Zhang, M. Hansen, M. McCormick, S. J. Lee, M. Cary and C. Kenyon (2010). "Insulin/IGF-1 signaling mutants reprogram ER stress response regulators to promote longevity." Proc Natl Acad Sci U S A **107**(21): 9730-9735.

Hernando-Rodriguez, B., A. P. Erinjeri, M. J. Rodriguez-Palero, V. Millar, S. Gonzalez-Hernandez, M. Olmedo, B. Schulze, R. Baumeister, M. J. Munoz, P. Askjaer and M. Artal-Sanz (2018). "Combined flow cytometry and high-throughput image

analysis for the study of essential genes in Caenorhabditis elegans." BMC Biol **16**(1): 36.

Hochberg, Y. and Y. Benjamini (1990). "More powerful procedures for multiple significance testing." Stat Med **9**(7): 811-818.

Honda, Y. and S. Honda (1999). "The daf-2 gene network for longevity regulates oxidative stress resistance and Mn-superoxide dismutase gene expression in Caenorhabditis elegans." FASEB J **13**(11): 1385-1393.

Houthoofd, K., B. P. Braeckman, I. Lenaerts, K. Brys, F. Matthijssens, A. De Vreese, S. Van Eygen and J. R. Vanfleteren (2005). "DAF-2 pathway mutations and food restriction in aging Caenorhabditis elegans differentially affect metabolism." Neurobiol Aging **26**(5): 689-696.

Houtkooper, R. H., L. Mouchiroud, D. Ryu, N. Moullan, E. Katsyuba, G. Knott, R. W. Williams and J. Auwerx (2013). "Mitonuclear protein imbalance as a conserved longevity mechanism." Nature **497**(7450): 451-457.

Hu, M., B. L. Pei, L. F. Zhang and Y. Z. Li (2014). "Histone H2B monoubiquitination is involved in regulating the dynamics of microtubules during the defense response to Verticillium dahliae toxins in Arabidopsis." Plant Physiol **164**(4): 1857-1865.

Huang da, W., B. T. Sherman and R. A. Lempicki (2009). "Systematic and integrative analysis of large gene lists using DAVID bioinformatics resources." Nat Protoc **4**(1): 44-57.

Huang, X., H. J. Cheng, M. Tessier-Lavigne and Y. Jin (2002). "MAX-1, a novel PH/MyTH4/FERM domain cytoplasmic protein implicated in netrin-mediated axon repulsion." Neuron **34**(4): 563-576.

Hughes, A. L. and D. E. Gottschling (2012). "An early age increase in vacuolar pH limits mitochondrial function and lifespan in yeast." Nature **492**(7428): 261-265.

Hung, J. H., I. J. Su, H. Y. Lei, H. C. Wang, W. C. Lin, W. T. Chang, W. Huang, W. C. Chang, Y. S. Chang, C. C. Chen and M. D. Lai (2004). "Endoplasmic reticulum stress stimulates the expression of cyclooxygenase-2 through activation of NF-kappaB and pp38 mitogen-activated protein kinase." J Biol Chem **279**(45): 46384-46392.

Iser, W. B. and C. A. Wolkow (2007). "DAF-2/insulin-like signaling in C. elegans modifies effects of dietary restriction and nutrient stress on aging, stress and growth." PLoS One **2**(11): e1240.

Ivashchenko, O., P. P. Van Veldhoven, C. Brees, Y. S. Ho, S. R. Terlecky and M. Fransen (2011). "Intraperoxisomal redox balance in mammalian cells: oxidative stress and interorganellar cross-talk." Mol Biol Cell **22**(9): 1440-1451.

Jadiya, P. and A. Nazir (2014). "A pre- and co-knockdown of RNAseT enzyme, Eri-1, enhances the efficiency of RNAi induced gene silencing in Caenorhabditis elegans." PLoS One **9**(1): e87635.

Jain, M., S. Rivera, E. A. Monclus, L. Synenki, A. Zirk, J. Eisenbart, C. Feghali-Bostwick, G. M. Mutlu, G. R. Budinger and N. S. Chandel (2013). "Mitochondrial reactive oxygen species regulate transforming growth factor-beta signaling." J Biol Chem **288**(2): 770-777.

Ji, X., D. B. Dadon, B. J. Abraham, T. I. Lee, R. Jaenisch, J. E. Bradner and R. A. Young (2015). "Chromatin proteomic profiling reveals novel proteins associated with histone-marked genomic regions." Proc Natl Acad Sci U S A **112**(12): 3841-3846.

Jia, K., D. Chen and D. L. Riddle (2004). "The TOR pathway interacts with the insulin signaling pathway to regulate C. elegans larval development, metabolism and life span." Development **131**(16): 3897-3906.

Jian, C., F. Xu, T. Hou, T. Sun, J. Li, H. Cheng and X. Wang (2017). "Deficiency of PHB complex impairs respiratory supercomplex formation and activates mitochondrial flashes." J Cell Sci **130**(15): 2620-2630.

Jin, C., J. Li, C. D. Green, X. Yu, X. Tang, D. Han, B. Xian, D. Wang, X. Huang, X. Cao, Z. Yan, L. Hou, J. Liu, N. Shukeir, P. Khaitovich, C. D. Chen, H. Zhang, T. Jenuwein and J. D. Han (2011). "Histone demethylase UTX-1 regulates C. elegans life span by targeting the insulin/IGF-1 signaling pathway." Cell Metab **14**(2): 161-172.

Johnson, S. C., P. S. Rabinovitch and M. Kaeberlein (2013). "mTOR is a key modulator of ageing and age-related disease." Nature **493**(7432): 338-345.

Jovaisaite, V. and J. Auwerx (2015). "The mitochondrial unfolded protein response-synchronizing genomes." Curr Opin Cell Biol **33**: 74-81.

Kaeberlein, M., R. W. Powers, 3rd, K. K. Steffen, E. A. Westman, D. Hu, N. Dang, E. O. Kerr, K. T. Kirkland, S. Fields and B. K. Kennedy (2005). "Regulation of yeast replicative life span by TOR and Sch9 in response to nutrients." Science **310**(5751): 1193-1196.

Kalb, R., S. Latwiel, H. I. Baymaz, P. W. Jansen, C. W. Muller, M. Vermeulen and J. Muller (2014). "Histone H2A monoubiquitination promotes histone H3 methylation in Polycomb repression." Nat Struct Mol Biol **21**(6): 569-571.

Kaletta, T. and M. O. Hengartner (2006). "Finding function in novel targets: C. elegans as a model organism." Nat Rev Drug Discov **5**(5): 387-398.

Kaltenbach, L., M. A. Horner, J. H. Rothman and S. E. Mango (2000). "The TBP-like factor CeTLF is required to activate RNA polymerase II transcription during C. elegans embryogenesis." Mol Cell **6**(3): 705-713.

Kamath, R. S., A. G. Fraser, Y. Dong, G. Poulin, R. Durbin, M. Gotta, A. Kanapin, N. Le Bot, S. Moreno, M. Sohrmann, D. P. Welchman, P. Zipperlen and J. Ahringer (2003). "Systematic functional analysis of the Caenorhabditis elegans genome using RNAi." Nature **421**(6920): 231-237.

Kamath, R. S., M. Martinez-Campos, P. Zipperlen, A. G. Fraser and J. Ahringer (2001). "Effectiveness of specific RNA-mediated interference through ingested double-stranded RNA in Caenorhabditis elegans." Genome Biol **2**(1): RESEARCH0002.

Kanehisa, M., Y. Sato, M. Kawashima, M. Furumichi and M. Tanabe (2016). "KEGG as a reference resource for gene and protein annotation." Nucleic Acids Res **44**(D1): D457-462.

Kapahi, P., B. M. Zid, T. Harper, D. Koslover, V. Sapin and S. Benzer (2004). "Regulation of lifespan in Drosophila by modulation of genes in the TOR signaling pathway." Curr Biol **14**(10): 885-890.

Kasashima, K., E. Ohta, Y. Kagawa and H. Endo (2006). "Mitochondrial functions and estrogen receptor-dependent nuclear translocation of pleiotropic human prohibitin 2." J Biol Chem **281**(47): 36401-36410.

Kasashima, K., M. Sumitani, M. Satoh and H. Endo (2008). "Human prohibitin 1 maintains the organization and stability of the mitochondrial nucleoids." Exp Cell Res **314**(5): 988-996.

Kashyap, L., S. Perera and A. L. Fisher (2012). "Identification of novel genes involved in sarcopenia through RNAi screening in Caenorhabditis elegans." J Gerontol A Biol Sci Med Sci **67**(1): 56-65.

Kathiria, A. S., L. D. Butcher, L. A. Feagins, R. F. Souza, C. R. Boland and A. L. Theiss (2012). "Prohibitin 1 modulates mitochondrial stress-related autophagy in human colonic epithelial cells." PLoS One **7**(2): e31231.

Kee, Y. and T. T. Huang (2016). "Role of Deubiquitinating Enzymes in DNA Repair." Mol Cell Biol **36**(4): 524-544.

Kennedy, S., D. Wang and G. Ruvkun (2004). "A conserved siRNA-degrading RNase negatively regulates RNA interference in C. elegans." Nature **427**(6975): 645-649.

Kenyon, C., J. Chang, E. Gensch, A. Rudner and R. Tabtiang (1993). "A C. elegans mutant that lives twice as long as wild type." Nature **366**(6454): 461-464.

Kim, H., K. Heo, J. Choi, K. Kim and W. An (2011). "Histone variant H3.3 stimulates HSP70 transcription through cooperation with HP1gamma." Nucleic Acids Res **39**(19): 8329-8341.

Kim, H. E., A. R. Grant, M. S. Simic, R. A. Kohnz, D. K. Nomura, J. Durieux, C. E. Riera, M. Sanchez, E. Kapernick, S. Wolff and A. Dillin (2016). "Lipid Biosynthesis Coordinates a Mitochondrial-to-Cytosolic Stress Response." Cell **166**(6): 1539-1552 e1516.

Kim, W., R. S. Underwood, I. Greenwald and D. D. Shaye (2018). "OrthoList 2:

A New Comparative Genomic Analysis of Human and Caenorhabditis elegans Genes." Genetics.

Klass, M. R. (1977). "Aging in the nematode Caenorhabditis elegans: major biological and environmental factors influencing life span." Mech Ageing Dev **6**(6): 413-429.

Klass, M. R. (1983). "A method for the isolation of longevity mutants in the nematode Caenorhabditis elegans and initial results." Mech Ageing Dev **22**(3-4): 279-286.

Koga, H., S. Kaushik and A. M. Cuervo (2011). "Protein homeostasis and aging: The importance of exquisite quality control." Ageing Res Rev **10**(2): 205-215.

Korvatska, O., N. S. Strand, J. D. Berndt, T. Strovas, D. H. Chen, J. B. Leverenz, K. Kiianitsa, I. F. Mata, E. Karakoc, J. L. Greenup, E. Bonkowski, J. Chuang, R. T. Moon, E. E. Eichler, D. A. Nickerson, C. P. Zabetian, B. C. Kraemer, T. D. Bird and W. H. Raskind (2013). "Altered splicing of ATP6AP2 causes X-linked parkinsonism with spasticity (XPDS)." Hum Mol Genet **22**(16): 3259-3268.

Kozlowski, L., S. Garvis, C. Bedet and F. Palladino (2014). "The Caenorhabditis elegans HP1 family protein HPL-2 maintains ER homeostasis through the UPR and hormesis." Proc Natl Acad Sci U S A **111**(16): 5956-5961.

Kruegel, U., B. Robison, T. Dange, G. Kahlert, J. R. Delaney, S. Kotireddy, M. Tsuchiya, S. Tsuchiyama, C. J. Murakami, J. Schleit, G. Sutphin, D. Carr, K. Tar, G. Dittmar, M. Kaeberlein, B. K. Kennedy and M. Schmidt (2011). "Elevated proteasome capacity extends replicative lifespan in Saccharomyces cerevisiae." PLoS Genet **7**(9): e1002253.

Labbadia, J. and R. I. Morimoto (2014). "Proteostasis and longevity: when does aging really begin?" F1000Prime Rep **6**: 7.

Labinskyy, N., A. Csiszar, Z. Orosz, K. Smith, A. Rivera, R. Buffenstein and Z. Ungvari (2006). "Comparison of endothelial function, O2-* and H2O2 production, and vascular oxidative stress resistance between the longest-living rodent, the naked mole rat, and mice." Am J Physiol Heart Circ Physiol **291**(6): H2698-2704.

Lamming, D. W., L. Ye, P. Katajisto, M. D. Goncalves, M. Saitoh, D. M. Stevens, J. G. Davis, A. B. Salmon, A. Richardson, R. S. Ahima, D. A. Guertin, D. M. Sabatini and J. A. Baur (2012). "Rapamycin-induced insulin resistance is mediated by mTORC2 loss and uncoupled from longevity." Science **335**(6076): 1638-1643.

Laplante, M. and D. M. Sabatini (2012). "mTOR signaling in growth control and disease." Cell **149**(2): 274-293.

Larsen, P. L., P. S. Albert and D. L. Riddle (1995). "Genes that regulate both development and longevity in Caenorhabditis elegans." Genetics **139**(4): 1567-1583.

Lee, S. S., R. Y. Lee, A. G. Fraser, R. S. Kamath, J. Ahringer and G. Ruvkun (2003). "A systematic RNAi screen identifies a critical role for mitochondria in C. elegans longevity." Nat Genet **33**(1): 40-48.

Lehner, B., C. Crombie, J. Tischler, A. Fortunato and A. G. Fraser (2006). "Systematic mapping of genetic interactions in Caenorhabditis elegans identifies common modifiers of diverse signaling pathways." Nat Genet **38**(8): 896-903.

Lehner, B., J. Tischler and A. G. Fraser (2006). "RNAi screens in Caenorhabditis elegans in a 96-well liquid format and their application to the systematic identification of genetic interactions." Nat Protoc **1**(3): 1617-1620.

Lenaz, G., A. Baracca, G. Barbero, C. Bergamini, M. E. Dalmonte, M. Del Sole, M. Faccioli, A. Falasca, R. Fato, M. L. Genova, G. Sgarbi and G. Solaini (2010). "Mitochondrial respiratory chain super-complex I-III in physiology and pathology." Biochim Biophys Acta **1797**(6-7): 633-640.

Leung, C. K., H. Empinado and K. P. Choe (2012). "Depletion of a nucleolar protein activates xenobiotic detoxification genes in Caenorhabditis elegans via Nrf /SKN-1 and p53/CEP-1." Free Radic Biol Med **52**(5): 937-950.

Lewis, J. A. and J. T. Fleming (1995). "Basic culture methods." Methods Cell Biol **48**: 3-29.

Li, J. and N. J. Holbrook (2004). "Elevated gadd153/chop expression and enhanced c-Jun N-terminal protein kinase activation sensitizes aged cells to ER stress." Exp Gerontol **39**(5): 735-744.

Li, J., Y. Wang, Y. Wang, X. Wen, X. N. Ma, W. Chen, F. Huang, J. Kou, L. W. Qi, B. Liu and K. Liu (2015). "Pharmacological activation of AMPK prevents Drp1-mediated mitochondrial fission and alleviates endoplasmic reticulum stress-associated endothelial dysfunction." J Mol Cell Cardiol **86**: 62-74.

Li, W., B. Gao, S. M. Lee, K. Bennett and D. Fang (2007). "RLE-1, an E3 ubiquitin ligase, regulates C. elegans aging by catalyzing DAF-16 polyubiquitination." Dev Cell **12**(2): 235-246.

Li, X., O. Matilainen, C. Jin, K. M. Glover-Cutter, C. I. Holmberg and T. K. Blackwell (2011). "Specific SKN-1/Nrf stress responses to perturbations in translation elongation and proteasome activity." PLoS Genet **7**(6): e1002119.

Li, X., C. Xu and P. Yang (2013). "c-Jun NH2-terminal kinase 1/2 and endoplasmic reticulum stress as interdependent and reciprocal causation in diabetic embryopathy." Diabetes **62**(2): 599-608.

Liang, B., M. Moussaif, C. J. Kuan, J. J. Gargus and J. Y. Sze (2006). "Serotonin targets the DAF-16/FOXO signaling pathway to modulate stress responses." Cell Metab **4**(6): 429-440.

Lithgow, G. J., T. M. White, S. Melov and T. E. Johnson (1995). "Thermotolerance and extended life-span conferred by single-gene mutations and induced by thermal stress." Proc Natl Acad Sci U S A **92**(16): 7540-7544.

Liu, H., G. Li, L. Liu and Y. Wan (2015). "Functional role of histone variant Htz1 in the stress response to oleate in Saccharomyces cerevisiae." Biosci Rep **35**(4).

Liu, J. L., D. Desjardins, R. Branicky, L. B. Agellon and S. Hekimi (2012). "Mitochondrial oxidative stress alters a pathway in Caenorhabditis elegans strongly resembling that of bile acid biosynthesis and secretion in vertebrates." PLoS Genet **8**(3): e1002553.

Liu, L., D. Feng, G. Chen, M. Chen, Q. Zheng, P. Song, Q. Ma, C. Zhu, R. Wang, W. Qi, L. Huang, P. Xue, B. Li, X. Wang, H. Jin, J. Wang, F. Yang, P. Liu, Y. Zhu, S. Sui and Q. Chen (2012). "Mitochondrial outer-membrane protein FUNDC1 mediates hypoxia-induced mitophagy in mammalian cells." Nat Cell Biol **14**(2): 177-185.

Liu, R. M. and L. P. Desai (2015). "Reciprocal regulation of TGF-beta and reactive oxygen species: A perverse cycle for fibrosis." Redox Biol **6**: 565-577.

Liu, S. and B. Lu (2010). "Reduction of protein translation and activation of autophagy protect against PINK1 pathogenesis in Drosophila melanogaster." PLoS Genet **6**(12): e1001237.

Liu, X., N. Jiang, B. Hughes, E. Bigras, E. Shoubridge and S. Hekimi (2005). "Evolutionary conservation of the clk-1-dependent mechanism of longevity: loss of mclk1 increases cellular fitness and lifespan in mice." Genes Dev **19**(20): 2424-2434.

Liu, X., Z. Ren, R. Zhan, X. Wang, X. Wang, Z. Zhang, X. Leng, Z. Yang and L. Qian (2009). "Prohibitin protects against oxidative stress-induced cell injury in cultured neonatal cardiomyocyte." Cell Stress Chaperones **14**(3): 311-319.

Liu, Y., B. S. Samuel, P. C. Breen and G. Ruvkun (2014). "Caenorhabditis elegans pathways that surveil and defend mitochondria." Nature **508**(7496): 406-410.

Lopez-Otin, C., M. A. Blasco, L. Partridge, M. Serrano and G. Kroemer (2013). "The hallmarks of aging." Cell **153**(6): 1194-1217.

Lord, C. J. and A. Ashworth (2012). "The DNA damage response and cancer therapy." Nature **481**(7381): 287-294.

Lourenco, A. B., C. Munoz-Jimenez, M. Venegas-Caleron and M. Artal-Sanz (2015). "Analysis of the effect of the mitochondrial prohibitin complex, a context-dependent modulator of longevity, on the C. elegans metabolome." Biochim Biophys Acta **1847**(11): 1457-1468.

Mabon, M. E., X. Mao, Y. Jiao, B. A. Scott and C. M. Crowder (2009). "Systematic identification of gene activities promoting hypoxic death." Genetics **181**(2): 483-496.

Magraner-Pardo, L., V. Pelechano, M. D. Coloma and V. Tordera (2014). "Dynamic remodeling of histone modifications in response to osmotic stress in Saccharomyces cerevisiae." BMC Genomics **15**: 247.

Maia, A. F., M. E. Tanenbaum, M. Galli, D. Lelieveld, D. A. Egan, R. Gassmann, C. E. Sunkel, S. van den Heuvel and R. H. Medema (2015). "Genome-wide RNAi screen for synthetic lethal interactions with the C. elegans kinesin-5 homolog BMK-1." Sci Data **2**: 150020.

Mair, W. and A. Dillin (2008). "Aging and survival: the genetics of life span extension by dietary restriction." Annu Rev Biochem **77**: 727-754.

Mair, W., I. Morantte, A. P. Rodrigues, G. Manning, M. Montminy, R. J. Shaw and A. Dillin (2011). "Lifespan extension induced by AMPK and calcineurin is mediated by CRTC-1 and CREB." Nature **470**(7334): 404-408.

Martianov, I., S. Brancorsini, A. Gansmuller, M. Parvinen, I. Davidson and P. Sassone-Corsi (2002). "Distinct functions of TBP and TLF/TRF2 during spermatogenesis: requirement of TLF for heterochromatic chromocenter formation in haploid round spermatids." Development **129**(4): 945-955.

Martianov, I., G. M. Fimia, A. Dierich, M. Parvinen, P. Sassone-Corsi and I. Davidson (2001). "Late arrest of spermiogenesis and germ cell apoptosis in mice lacking the TBP-like TLF/TRF2 gene." Mol Cell **7**(3): 509-515.

Marza, E., S. Taouji, K. Barroso, A. A. Raymond, L. Guignard, M. Bonneu, N. Pallares-Lupon, J. W. Dupuy, M. E. Fernandez-Zapico, J. Rosenbaum, F. Palladino, D. Dupuy and E. Chevet (2015). "Genome-wide screen identifies a novel p97/CDC-48-dependent pathway regulating ER-stress-induced gene transcription." EMBO Rep **16**(3): 332-340.

Matilainen, O., L. Arpalahti, V. Rantanen, S. Hautaniemi and C. I. Holmberg (2013). "Insulin/IGF-1 signaling regulates proteasome activity through the deubiquitinating enzyme UBH-4." Cell Rep **3**(6): 1980-1995.

Maures, T. J., E. L. Greer, A. G. Hauswirth and A. Brunet (2011). "The H3K27 demethylase UTX-1 regulates C. elegans lifespan in a germline-independent, insulin-dependent manner." Aging Cell **10**(6): 980-990.

McCay, C. M., M. F. Crowell and L. A. Maynard (1989). "The effect of retarded growth upon the length of life span and upon the ultimate body size. 1935." Nutrition **5**(3): 155-171; discussion 172.

McElwee, J. J., E. Schuster, E. Blanc, J. Thornton and D. Gems (2006). "Diapause-associated metabolic traits reiterated in long-lived daf-2 mutants in the nematode Caenorhabditis elegans." Mech Ageing Dev **127**(5): 458-472.

Meister, P., S. Schott, C. Bedet, Y. Xiao, S. Rohner, S. Bodennec, B. Hudry, L.

Molin, F. Solari, S. M. Gasser and F. Palladino (2011). "Caenorhabditis elegans Heterochromatin protein 1 (HPL-2) links developmental plasticity, longevity and lipid metabolism." Genome Biol **12**(12): R123.

Melendez, A., Z. Talloczy, M. Seaman, E. L. Eskelinen, D. H. Hall and B. Levine (2003). "Autophagy genes are essential for dauer development and life-span extension in C. elegans." Science **301**(5638): 1387-1391.

Melo, J. A. and G. Ruvkun (2012). "Inactivation of conserved C. elegans genes engages pathogen- and xenobiotic-associated defenses." Cell **149**(2): 452-466.

Merkwirth, C., S. Dargazanli, T. Tatsuta, S. Geimer, B. Lower, F. T. Wunderlich, J. C. von Kleist-Retzow, A. Waisman, B. Westermann and T. Langer (2008). "Prohibitins control cell proliferation and apoptosis by regulating OPA1-dependent cristae morphogenesis in mitochondria." Genes Dev **22**(4): 476-488.

Merkwirth, C., V. Jovaisaite, J. Durieux, O. Matilainen, S. D. Jordan, P. M. Quiros, K. K. Steffen, E. G. Williams, L. Mouchiroud, S. U. Tronnes, V. Murillo, S. C. Wolff, R. J. Shaw, J. Auwerx and A. Dillin (2016). "Two Conserved Histone Demethylases Regulate Mitochondrial Stress-Induced Longevity." Cell **165**(5): 1209-1223.

Merkwirth, C. and T. Langer (2009). "Prohibitin function within mitochondria: essential roles for cell proliferation and cristae morphogenesis." Biochim Biophys Acta **1793**(1): 27-32.

Merkwirth, C., P. Martinelli, A. Korwitz, M. Morbin, H. S. Bronneke, S. D. Jordan, E. I. Rugarli and T. Langer (2012). "Loss of prohibitin membrane scaffolds impairs mitochondrial architecture and leads to tau hyperphosphorylation and neurodegeneration." PLoS Genet **8**(11): e1003021.

Milgrom, E., H. Diab, F. Middleton and P. M. Kane (2007). "Loss of vacuolar proton-translocating ATPase activity in yeast results in chronic oxidative stress." J Biol Chem **282**(10): 7125-7136.

Min, K., J. Kang and J. Lee (2010). "A modified feeding RNAi method for simultaneous knock-down of more than one gene in Caenorhabditis elegans." Biotechniques **48**(3): 229-232.

Mishra, S. and B. G. Nyomba (2017). "Prohibitin - At the crossroads of obesity-linked diabetes and cancer." Exp Biol Med (Maywood) **242**(11): 1170-1177.

Mitsopoulos, P., Y. H. Chang, T. Wai, T. Konig, S. D. Dunn, T. Langer and J. Madrenas (2015). "Stomatin-like protein 2 is required for in vivo mitochondrial respiratory chain supercomplex formation and optimal cell function." Mol Cell Biol **35**(10): 1838-1847.

Miwa, S., H. Jow, K. Baty, A. Johnson, R. Czapiewski, G. Saretzki, A. Treumann and T. von Zglinicki (2014). "Low abundance of the matrix arm of complex I in mitochondria predicts longevity in mice." Nat Commun **5**: 3837.

Molin, M. and A. B. Demir (2014). "Linking Peroxiredoxin and Vacuolar-ATPase Functions in Calorie Restriction-Mediated Life Span Extension." Int J Cell Biol **2014**: 913071.

Monaghan, R. M., R. G. Barnes, K. Fisher, T. Andreou, N. Rooney, G. B. Poulin and A. J. Whitmarsh (2015). "A nuclear role for the respiratory enzyme CLK-1 in regulating mitochondrial stress responses and longevity." Nat Cell Biol **17**(6): 782-792.

Morley, J. F. and R. I. Morimoto (2004). "Regulation of longevity in Caenorhabditis elegans by heat shock factor and molecular chaperones." Mol Biol Cell **15**(2): 657-664.

Moy, T. I., A. L. Conery, J. Larkins-Ford, G. Wu, R. Mazitschek, G. Casadei, K. Lewis, A. E. Carpenter and F. M. Ausubel (2009). "High-throughput screen for novel antimicrobials using a whole animal infection model." ACS Chem Biol **4**(7): 527-533.

Muller, F., L. Lakatos, J. Dantonel, U. Strahle and L. Tora (2001). "TBP is not universally required for zygotic RNA polymerase II transcription in zebrafish." Curr Biol **11**(4): 282-287.

Munkacsy, E., M. H. Khan, R. K. Lane, M. B. Borror, J. H. Park, A. F. Bokov, A. L. Fisher, C. D. Link and S. L. Rea (2016). "DLK-1, SEK-3 and PMK-3 Are Required for the Life Extension Induced by Mitochondrial Bioenergetic Disruption in C. elegans." PLoS Genet **12**(7): e1006133.

Murakawa, T., O. Yamaguchi, A. Hashimoto, S. Hikoso, T. Takeda, T. Oka, H. Yasui, H. Ueda, Y. Akazawa, H. Nakayama, M. Taneike, T. Misaka, S. Omiya, A. M. Shah, A. Yamamoto, K. Nishida, Y. Ohsumi, K. Okamoto, Y. Sakata and K. Otsu (2015). "Bcl-2-like protein 13 is a mammalian Atg32 homologue that mediates mitophagy and mitochondrial fragmentation." Nat Commun **6**: 7527.

Murphy, C. T., S. A. McCarroll, C. I. Bargmann, A. Fraser, R. S. Kamath, J. Ahringer, H. Li and C. Kenyon (2003). "Genes that act downstream of DAF-16 to influence the lifespan of Caenorhabditis elegans." Nature **424**(6946): 277-283.

Narayan, V., T. Ly, E. Pourkarimi, A. B. Murillo, A. Gartner, A. I. Lamond and C. Kenyon (2016). "Deep Proteome Analysis Identifies Age-Related Processes in C. elegans." Cell Syst **3**(2): 144-159.

Nargund, A. M., C. J. Fiorese, M. W. Pellegrino, P. Deng and C. M. Haynes (2015). "Mitochondrial and nuclear accumulation of the transcription factor ATFS-1 promotes OXPHOS recovery during the UPR(mt)." Mol Cell **58**(1): 123-133.

Nargund, A. M., M. W. Pellegrino, C. J. Fiorese, B. M. Baker and C. M. Haynes (2012). "Mitochondrial import efficiency of ATFS-1 regulates mitochondrial UPR activation." Science **337**(6094): 587-590.

Ni, H. M., J. A. Williams and W. X. Ding (2015). "Mitochondrial dynamics and mitochondrial quality control." Redox Biol **4**: 6-13.

Nijtmans, L. G., S. M. Artal, L. A. Grivell and P. J. Coates (2002). "The mitochondrial PHB complex: roles in mitochondrial respiratory complex assembly, ageing and degenerative disease." Cell Mol Life Sci **59**(1): 143-155.

Nijtmans, L. G., L. de Jong, M. Artal Sanz, P. J. Coates, J. A. Berden, J. W. Back, A. O. Muijsers, H. van der Spek and L. A. Grivell (2000). "Prohibitins act as a membrane-bound chaperone for the stabilization of mitochondrial proteins." EMBO J **19**(11): 2444-2451.

Nishikawa, H., T. Miyazaki, H. Nakayama, A. Minematsu, S. Yamauchi, K. Yamashita, T. Takazono, S. Shimamura, S. Nakamura, K. Izumikawa, K. Yanagihara, S. Kohno and H. Mukae (2016). "Roles of vacuolar H+-ATPase in the oxidative stress response of Candida glabrata." FEMS Yeast Res **16**(5).

Nollen, E. A., S. M. Garcia, G. van Haaften, S. Kim, A. Chavez, R. I. Morimoto and R. H. Plasterk (2004). "Genome-wide RNA interference screen identifies previously undescribed regulators of polyglutamine aggregation." Proc Natl Acad Sci U S A **101**(17): 6403-6408.

Nordgren, M. and M. Fransen (2014). "Peroxisomal metabolism and oxidative stress." Biochimie **98**: 56-62.

Oeljeklaus, S., B. S. Reinartz, J. Wolf, S. Wiese, J. Tonillo, K. Podwojski, K. Kuhlmann, C. Stephan, H. E. Meyer, W. Schliebs, C. Brocard, R. Erdmann and B. Warscheid (2012). "Identification of core components and transient interactors of the peroxisomal importomer by dual-track stable isotope labeling with amino acids in cell culture analysis." J Proteome Res **11**(4): 2567-2580.

Oh, S., T. Suganuma, M. M. Gogol and J. L. Workman (2018). "Histone H3 threonine 11 phosphorylation by Sch9 and CK2 regulates chronological lifespan by controlling the nutritional stress response." Elife **7**.

Onken, B. and M. Driscoll (2010). "Metformin induces a dietary restriction-like state and the oxidative stress response to extend C. elegans Healthspan via AMPK, LKB1, and SKN-1." PLoS One **5**(1): e8758.

Osman, C., M. Haag, C. Potting, J. Rodenfels, P. V. Dip, F. T. Wieland, B. Brugger, B. Westermann and T. Langer (2009). "The genetic interactome of prohibitins: coordinated control of cardiolipin and phosphatidylethanolamine by conserved regulators in mitochondria." J Cell Biol **184**(4): 583-596.

Owusu-Ansah, E., W. Song and N. Perrimon (2013). "Muscle mitohormesis promotes longevity via systemic repression of insulin signaling." Cell **155**(3): 699-712.

Padmanabha, D., P. A. Padilla, Y. J. You and K. D. Baker (2015). "A HIF-independent mediator of transcriptional responses to oxygen deprivation in Caenorhabditis elegans." Genetics **199**(3): 739-748.

Pal, S. and J. K. Tyler (2016). “Epigenetics and aging.” Sci Adv **2**(7): e1600584.

Palikaras, K., E. Lionaki and N. Tavernarakis (2015). “Coordination of mitophagy and mitochondrial biogenesis during ageing in C. elegans.” Nature **521**(7553): 525-528.

Pan, K. Z., J. E. Palter, A. N. Rogers, A. Olsen, D. Chen, G. J. Lithgow and P. Kapahi (2007). “Inhibition of mRNA translation extends lifespan in Caenorhabditis elegans.” Aging Cell **6**(1): 111-119.

Park, S. and Y. K. Paik (2017). “Genetic deficiency in neuronal peroxisomal fatty acid beta-oxidation causes the interruption of dauer development in Caenorhabditis elegans.” Sci Rep **7**(1): 9358.

Pellegrino, M. W., A. M. Nargund, N. V. Kirienko, R. Gillis, C. J. Fiorese and C. M. Haynes (2014). “Mitochondrial UPR-regulated innate immunity provides resistance to pathogen infection.” Nature **516**(7531): 414-417.

Perez, V. I., R. Buffenstein, V. Masamsetti, S. Leonard, A. B. Salmon, J. Mele, B. Andziak, T. Yang, Y. Edrey, B. Friguet, W. Ward, A. Richardson and A. Chaudhuri (2009). “Protein stability and resistance to oxidative stress are determinants of longevity in the longest-living rodent, the naked mole-rat.” Proc Natl Acad Sci U S A **106**(9): 3059-3064.

Perumalsamy, L. R., M. Nagala and A. Sarin (2010). “Notch-activated signaling cascade interacts with mitochondrial remodeling proteins to regulate cell survival.” Proc Natl Acad Sci U S A **107**(15): 6882-6887.

Pfeiffer, K., V. Gohil, R. A. Stuart, C. Hunte, U. Brandt, M. L. Greenberg and H. Schagger (2003). “Cardiolipin stabilizes respiratory chain supercomplexes.” J Biol Chem **278**(52): 52873-52880.

Piper, P. W., G. W. Jones, D. Bringloe, N. Harris, M. MacLean and M. Mollapour (2002). “The shortened replicative life span of prohibitin mutants of yeast appears to be due to defective mitochondrial segregation in old mother cells.” Aging Cell **1**(2): 149-157.

Podshivalova, K., R. A. Kerr and C. Kenyon (2017). “How a Mutation that Slows Aging Can Also Disproportionately Extend End-of-Life Decrepitude.” Cell Rep **19**(3): 441-450.

Poole, R. J., E. Bashllari, L. Cochella, E. B. Flowers and O. Hobert (2011). “A Genome-Wide RNAi Screen for Factors Involved in Neuronal Specification in Caenorhabditis elegans.” PLoS Genet **7**(6): e1002109.

Price, N. L., A. P. Gomes, A. J. Ling, F. V. Duarte, A. Martin-Montalvo, B. J. North, B. Agarwal, L. Ye, G. Ramadori, J. S. Teodoro, B. P. Hubbard, A. T. Varela, J. G. Davis, B. Varamini, A. Hafner, R. Moaddel, A. P. Rolo, R. Coppari, C. M. Palmeira, R. de Cabo, J. A. Baur and D. A. Sinclair (2012). “SIRT1 is required for AMPK activation and the

beneficial effects of resveratrol on mitochondrial function." Cell Metab **15**(5): 675-690.

Qu, W., C. Ren, Y. Li, J. Shi, J. Zhang, X. Wang, X. Hang, Y. Lu, D. Zhao and C. Zhang (2011). "Reliability analysis of the Ahringer Caenorhabditis elegans RNAi feeding library: a guide for genome-wide screens." BMC Genomics **12**: 170.

Rea, S. and T. E. Johnson (2003). "A metabolic model for life span determination in Caenorhabditis elegans." Dev Cell **5**(2): 197-203.

Rea, S. L., N. Ventura and T. E. Johnson (2007). "Relationship between mitochondrial electron transport chain dysfunction, development, and life extension in Caenorhabditis elegans." PLoS Biol **5**(10): e259.

Richter-Dennerlein, R., A. Korwitz, M. Haag, T. Tatsuta, S. Dargazanli, M. Baker, T. Decker, T. Lamkemeyer, E. I. Rugarli and T. Langer (2014). "DNAJC19, a mitochondrial cochaperone associated with cardiomyopathy, forms a complex with prohibitins to regulate cardiolipin remodeling." Cell Metab **20**(1): 158-171.

Rieber, N., B. Knapp, R. Eils and L. Kaderali (2009). "RNAither, an automated pipeline for the statistical analysis of high-throughput RNAi screens." Bioinformatics **25**(5): 678-679.

Riedel, C. G., R. H. Dowen, G. F. Lourenco, N. V. Kirienko, T. Heimbucher, J. A. West, S. K. Bowman, R. E. Kingston, A. Dillin, J. M. Asara and G. Ruvkun (2013). "DAF-16 employs the chromatin remodeller SWI/SNF to promote stress resistance and longevity." Nat Cell Biol **15**(5): 491-501.

Ron, D. and P. Walter (2007). "Signal integration in the endoplasmic reticulum unfolded protein response." Nat Rev Mol Cell Biol **8**(7): 519-529.

Rottensteiner, H. and F. L. Theodoulou (2006). "The ins and outs of peroxisomes: co-ordination of membrane transport and peroxisomal metabolism." Biochim Biophys Acta **1763**(12): 1527-1540.

Rual, J. F., J. Ceron, J. Koreth, T. Hao, A. S. Nicot, T. Hirozane-Kishikawa, J. Vandenhaute, S. H. Orkin, D. E. Hill, S. van den Heuvel and M. Vidal (2004). "Toward improving Caenorhabditis elegans phenome mapping with an ORFeome-based RNAi library." Genome Res **14**(10B): 2162-2168.

Ruckenstuhl, C., C. Netzberger, I. Entfellner, D. Carmona-Gutierrez, T. Kickenweiz, S. Stekovic, C. Gleixner, C. Schmid, L. Klug, A. G. Sorgo, T. Eisenberg, S. Buttner, G. Marino, R. Koziel, P. Jansen-Durr, K. U. Frohlich, G. Kroemer and F. Madeo (2014). "Lifespan extension by methionine restriction requires autophagy-dependent vacuolar acidification." PLoS Genet **10**(5): e1004347.

Runkel, E. D., S. Liu, R. Baumeister and E. Schulze (2013). "Surveillance-activated defenses block the ROS-induced mitochondrial unfolded protein response." PLoS Genet **9**(3): e1003346.

Ruzanov, P., D. L. Riddle, M. A. Marra, S. J. McKay and S. M. Jones (2007). "Genes that may modulate longevity in C. elegans in both dauer larvae and long-lived daf-2 adults." Exp Gerontol **42**(8): 825-839.

Sakaki, K., S. Yoshina, X. Shen, J. Han, M. R. DeSantis, M. Xiong, S. Mitani and R. J. Kaufman (2012). "RNA surveillance is required for endoplasmic reticulum homeostasis." Proc Natl Acad Sci U S A **109**(21): 8079-8084.

Samuelson, A. V., C. E. Carr and G. Ruvkun (2007). "Gene activities that mediate increased life span of C. elegans insulin-like signaling mutants." Genes Dev **21**(22): 2976-2994.

Sarbassov, D. D., D. A. Guertin, S. M. Ali and D. M. Sabatini (2005). "Phosphorylation and regulation of Akt/PKB by the rictor-mTOR complex." Science **307**(5712): 1098-1101.

Saxton, R. A. and D. M. Sabatini (2017). "mTOR Signaling in Growth, Metabolism, and Disease." Cell **168**(6): 960-976.

Schleicher, M., B. R. Shepherd, Y. Suarez, C. Fernandez-Hernando, J. Yu, Y. Pan, L. M. Acevedo, G. S. Shadel and W. C. Sessa (2008). "Prohibitin-1 maintains the angiogenic capacity of endothelial cells by regulating mitochondrial function and senescence." J Cell Biol **180**(1): 101-112.

Schleit, J., S. C. Johnson, C. F. Bennett, M. Simko, N. Trongtham, A. Castanza, E. J. Hsieh, R. M. Moller, B. M. Wasko, J. R. Delaney, G. L. Sutphin, D. Carr, C. J. Murakami, A. Tocchi, B. Xian, W. Chen, T. Yu, S. Goswami, S. Higgins, M. Holmberg, K. S. Jeong, J. R. Kim, S. Klum, E. Liao, M. S. Lin, W. Lo, H. Miller, B. Olsen, Z. J. Peng, T. Pollard, P. Pradeep, D. Pruett, D. Rai, V. Ros, M. Singh, B. L. Spector, H. Vander Wende, E. H. An, M. Fletcher, M. Jelic, P. S. Rabinovitch, M. J. MacCoss, J. D. Han, B. K. Kennedy and M. Kaeberlein (2013). "Molecular mechanisms underlying genotype-dependent responses to dietary restriction." Aging Cell **12**(6): 1050-1061.

Schwartz, B. E. and K. Ahmad (2005). "Transcriptional activation triggers deposition and removal of the histone variant H3.3." Genes Dev **19**(7): 804-814.

Schweers, R. L., J. Zhang, M. S. Randall, M. R. Loyd, W. Li, F. C. Dorsey, M. Kundu, J. T. Opferman, J. L. Cleveland, J. L. Miller and P. A. Ney (2007). "NIX is required for programmed mitochondrial clearance during reticulocyte maturation." Proc Natl Acad Sci U S A **104**(49): 19500-19505.

Schweitzer, K. and M. Naumann (2015). "CSN-associated USP48 confers stability to nuclear NF-kappaB/RelA by trimming K48-linked Ub-chains." Biochim Biophys Acta **1853**(2): 453-469.

Scott, B. A., M. S. Avidan and C. M. Crowder (2002). "Regulation of hypoxic death in C. elegans by the insulin/IGF receptor homolog DAF-2." Science **296**(5577): 2388-

2391.

Sen, P., P. P. Shah, R. Nativio and S. L. Berger (2016). "Epigenetic Mechanisms of Longevity and Aging." Cell **166**(4): 822-839.

Senchuk, M. M., D. J. Dues, C. E. Schaar, B. K. Johnson, Z. B. Madaj, M. J. Bowman, M. E. Winn and J. M. Van Raamsdonk (2018). "Activation of DAF-16/FOXO by reactive oxygen species contributes to longevity in long-lived mitochondrial mutants in Caenorhabditis elegans." PLoS Genet **14**(3): e1007268.

Serricchio, M., A. Vissa, P. K. Kim, C. M. Yip and G. A. McQuibban (2018). "Cardiolipin synthesizing enzymes form a complex that interacts with cardiolipin-dependent membrane organizing proteins." Biochim Biophys Acta **1863**(4): 447-457.

Shammas, M. A. (2011). "Telomeres, lifestyle, cancer, and aging." Curr Opin Clin Nutr Metab Care **14**(1): 28-34.

Shao, L. W., R. Niu and Y. Liu (2016). "Neuropeptide signals cell non-autonomous mitochondrial unfolded protein response." Cell Res **26**(11): 1182-1196.

Shaye, D. D. and I. Greenwald (2011). "OrthoList: a compendium of C. elegans genes with human orthologs." PLoS One **6**(5): e20085.

Shirayama, M., W. Stanney, 3rd, W. Gu, M. Seth and C. C. Mello (2014). "The Vasa Homolog RDE-12 engages target mRNA and multiple argonaute proteins to promote RNAi in C. elegans." Curr Biol **24**(8): 845-851.

Shore, D. E., C. E. Carr and G. Ruvkun (2012). "Induction of cytoprotective pathways is central to the extension of lifespan conferred by multiple longevity pathways." PLoS Genet **8**(7): e1002792.

Simmer, F., M. Tijsterman, S. Parrish, S. P. Koushika, M. L. Nonet, A. Fire, J. Ahringer and R. H. Plasterk (2002). "Loss of the putative RNA-directed RNA polymerase RRF-3 makes C. elegans hypersensitive to RNAi." Curr Biol **12**(15): 1317-1319.

Song, H. O., W. Lee, K. An, H. S. Lee, J. H. Cho, Z. Y. Park and J. Ahnn (2009). "C. elegans STI-1, the homolog of Sti1/Hop, is involved in aging and stress response." J Mol Biol **390**(4): 604-617.

Squiban, B., J. Belougne, J. Ewbank and O. Zugasti (2012). "Quantitative and automated high-throughput genome-wide RNAi screens in C. elegans." J Vis Exp(60).

Steglich, G., W. Neupert and T. Langer (1999). "Prohibitins regulate membrane protein degradation by the m-AAA protease in mitochondria." Mol Cell Biol **19**(5): 3435-3442.

Stoldt, V., F. Rademacher, V. Kehren, J. F. Ernst, D. A. Pearce and F. Sherman (1996). "Review: the Cct eukaryotic chaperonin subunits of Saccharomyces cerevisiae and other yeasts." Yeast **12**(6): 523-529.

Stout, G. J., E. C. Stigter, P. B. Essers, K. W. Mulder, A. Kolkman, D. S. Snijders, N. J. van den Broek, M. C. Betist, H. C. Korswagen, A. W. Macinnes and A. B. Brenkman (2013). "Insulin/IGF-1-mediated longevity is marked by reduced protein metabolism." Mol Syst Biol **9**: 679.

Strub, G. M., M. Paillard, J. Liang, L. Gomez, J. C. Allegood, N. C. Hait, M. Maceyka, M. M. Price, Q. Chen, D. C. Simpson, T. Kordula, S. Milstien, E. J. Lesnefsky and S. Spiegel (2011). "Sphingosine-1-phosphate produced by sphingosine kinase 2 in mitochondria interacts with prohibitin 2 to regulate complex IV assembly and respiration." FASEB J **25**(2): 600-612.

Sulston, J. E. and H. R. Horvitz (1977). "Post-embryonic cell lineages of the nematode, Caenorhabditis elegans." Dev Biol **56**(1): 110-156.

Sulston, J. E., E. Schierenberg, J. G. White and J. N. Thomson (1983). "The embryonic cell lineage of the nematode Caenorhabditis elegans." Dev Biol **100**(1): 64-119.

Supek, F., M. Bosnjak, N. Skunca and T. Smuc (2011). "REVIGO summarizes and visualizes long lists of gene ontology terms." PLoS One **6**(7): e21800.

Syntichaki, P., K. Troulinaki and N. Tavernarakis (2007). "eIF4E function in somatic cells modulates ageing in Caenorhabditis elegans." Nature **445**(7130): 922-926.

Szklarczyk, D., J. H. Morris, H. Cook, M. Kuhn, S. Wyder, M. Simonovic, A. Santos, N. T. Doncheva, A. Roth, P. Bork, L. J. Jensen and C. von Mering (2017). "The STRING database in 2017: quality-controlled protein-protein association networks, made broadly accessible." Nucleic Acids Res **45**(D1): D362-D368.

Tabara, H., A. Grishok and C. C. Mello (1998). "RNAi in C. elegans: soaking in the genome sequence." Science **282**(5388): 430-431.

Tabrez, S. S., R. D. Sharma, V. Jain, A. A. Siddiqui and A. Mukhopadhyay (2017). "Differential alternative splicing coupled to nonsense-mediated decay of mRNA ensures dietary restriction-induced longevity." Nat Commun **8**(1): 306.

Tanji, T., K. Nishikori, S. Haga, Y. Kanno, Y. Kobayashi, M. Takaya, K. Gengyo-Ando, S. Mitani, H. Shiraishi and A. Ohashi-Kobayashi (2016). "Characterization of HAF-4- and HAF-9-localizing organelles as distinct organelles in Caenorhabditis elegans intestinal cells." BMC Cell Biol **17**: 4.

Tao, J., Q. Y. Wu, Y. C. Ma, Y. L. Chen and C. G. Zou (2017). "Antioxidant response is a protective mechanism against nutrient deprivation in C. elegans." Sci Rep **7**: 43547.

Tatar, M., A. Kopelman, D. Epstein, M. P. Tu, C. M. Yin and R. S. Garofalo (2001). "A mutant Drosophila insulin receptor homolog that extends life-span and impairs neuroendocrine function." Science **292**(5514): 107-110.

Tatsuta, T., K. Model and T. Langer (2005). "Formation of membrane-bound ring

complexes by prohibitins in mitochondria." Mol Biol Cell **16**(1): 248-259.

Tavernarakis, N., S. L. Wang, M. Dorovkov, A. Ryazanov and M. Driscoll (2000). "Heritable and inducible genetic interference by double-stranded RNA encoded by transgenes." Nat Genet **24**(2): 180-183.

Taylor, R. C., K. M. Berendzen and A. Dillin (2014). "Systemic stress signalling: understanding the cell non-autonomous control of proteostasis." Nat Rev Mol Cell Biol **15**(3): 211-217.

Taylor, R. C. and A. Dillin (2013). "XBP-1 is a cell-nonautonomous regulator of stress resistance and longevity." Cell **153**(7): 1435-1447.

Thieringer, H., B. Moellers, G. Dodt, W. H. Kunau and M. Driscoll (2003). "Modeling human peroxisome biogenesis disorders in the nematode Caenorhabditis elegans." J Cell Sci **116**(Pt 9): 1797-1804.

Thuaud, F., N. Ribeiro, C. G. Nebigil and L. Desaubry (2013). "Prohibitin ligands in cell death and survival: mode of action and therapeutic potential." Chem Biol **20**(3): 316-331.

Tian, Y., G. Garcia, Q. Bian, K. K. Steffen, L. Joe, S. Wolff, B. J. Meyer and A. Dillin (2016). "Mitochondrial Stress Induces Chromatin Reorganization to Promote Longevity and UPR(mt)." Cell **165**(5): 1197-1208.

Tijsterman, M., R. C. May, F. Simmer, K. L. Okihara and R. H. Plasterk (2004). "Genes required for systemic RNA interference in Caenorhabditis elegans." Curr Biol **14**(2): 111-116.

Timmons, L., D. L. Court and A. Fire (2001). "Ingestion of bacterially expressed dsRNAs can produce specific and potent genetic interference in Caenorhabditis elegans." Gene **263**(1-2): 103-112.

Timmons, L. and A. Fire (1998). "Specific interference by ingested dsRNA." Nature **395**(6705): 854.

Tischler, J., B. Lehner, N. Chen and A. G. Fraser (2006). "Combinatorial RNA interference in Caenorhabditis elegans reveals that redundancy between gene duplicates can be maintained for more than 80 million years of evolution." Genome Biol **7**(8): R69.

Tissenbaum, H. A. (2015). "Using C. elegans for aging research." Invertebr Reprod Dev **59**(sup1): 59-63.

Tortelli, T. C. J., L. M. F. de Godoy, G. A. de Souza, D. Bonatto, A. H. Otake, R. de Freitas Saito, J. C. Rosa, L. J. Greene and R. Chammas (2017). "Accumulation of prohibitin is a common cellular response to different stressing stimuli and protects melanoma cells from ER stress and chemotherapy-induced cell death." Oncotarget **8**(26): 43114-43129.

Toyama, E. Q., S. Herzig, J. Courchet, T. L. Lewis, Jr., O. C. Loson, K. Hellberg, N. P. Young, H. Chen, F. Polleux, D. C. Chan and R. J. Shaw (2016). "Metabolism. AMP-activated protein kinase mediates mitochondrial fission in response to energy stress." Science **351**(6270): 275-281.

Tullet, J. M., M. Hertweck, J. H. An, J. Baker, J. Y. Hwang, S. Liu, R. P. Oliveira, R. Baumeister and T. K. Blackwell (2008). "Direct inhibition of the longevity-promoting factor SKN-1 by insulin-like signaling in C. elegans." Cell **132**(6): 1025-1038.

Uckelmann, M., R. M. Densham, R. Baas, H. H. K. Winterwerp, A. Fish, T. K. Sixma and J. R. Morris (2018). "USP48 restrains resection by site-specific cleavage of the BRCA1 ubiquitin mark from H2A." Nat Commun **9**(1): 229.

Uno, M. and E. Nishida (2016). "Lifespan-regulating genes in C. elegans." NPJ Aging Mech Dis **2**: 16010.

van Haaften, G., N. L. Vastenhouw, E. A. Nollen, R. H. Plasterk and M. Tijsterman (2004). "Gene interactions in the DNA damage-response pathway identified by genome-wide RNA-interference analysis of synthetic lethality." Proc Natl Acad Sci U S A **101**(35): 12992-12996.

van Heemst, D. (2010). "Insulin, IGF-1 and longevity." Aging Dis **1**(2): 147-157.

Van Raamsdonk, J. M. and S. Hekimi (2009). "Deletion of the mitochondrial superoxide dismutase sod-2 extends lifespan in Caenorhabditis elegans." PLoS Genet **5**(2): e1000361.

Van Voorhies, W. A. and S. Ward (1999). "Genetic and environmental conditions that increase longevity in Caenorhabditis elegans decrease metabolic rate." Proc Natl Acad Sci U S A **96**(20): 11399-11403.

Veenstra, G. J., D. L. Weeks and A. P. Wolffe (2000). "Distinct roles for TBP and TBP-like factor in early embryonic gene transcription in Xenopus." Science **290**(5500): 2312-2315.

Velimezi, G., L. Robinson-Garcia, F. Munoz-Martinez, W. W. Wiegant, J. Ferreira da Silva, M. Owusu, M. Moder, M. Wiedner, S. B. Rosenthal, K. M. Fisch, J. Moffat, J. Menche, H. van Attikum, S. P. Jackson and J. I. Loizou (2018). "Map of synthetic rescue interactions for the Fanconi anemia DNA repair pathway identifies USP48." Nat Commun **9**(1): 2280.

Vellai, T., K. Takacs-Vellai, Y. Zhang, A. L. Kovacs, L. Orosz and F. Muller (2003). "Genetics: influence of TOR kinase on lifespan in C. elegans." Nature **426**(6967): 620.

Verma, G. and M. Datta (2010). "IL-1beta induces ER stress in a JNK dependent manner that determines cell death in human pancreatic epithelial MIA PaCa-2 cells." Apoptosis **15**(7): 864-876.

Wahlby, C., L. Kamentsky, Z. H. Liu, T. Riklin-Raviv, A. L. Conery, E. J. O'Rourke,

K. L. Sokolnicki, O. Visvikis, V. Ljosa, J. E. Irazoqui, P. Golland, G. Ruvkun, F. M. Ausubel and A. E. Carpenter (2012). "An image analysis toolbox for high-throughput C. elegans assays." Nat Methods **9**(7): 714-716.

Wang, D., S. Kennedy, D. Conte, Jr., J. K. Kim, H. W. Gabel, R. S. Kamath, C. C. Mello and G. Ruvkun (2005). "Somatic misexpression of germline P granules and enhanced RNA interference in retinoblastoma pathway mutants." Nature **436**(7050): 593-597.

Wang, D. and G. Ruvkun (2004). "Regulation of Caenorhabditis elegans RNA interference by the daf-2 insulin stress and longevity signaling pathway." Cold Spring Harb Symp Quant Biol **69**: 429-431.

Wang, J., S. Robida-Stubbs, J. M. Tullet, J. F. Rual, M. Vidal and T. K. Blackwell (2010). "RNAi screening implicates a SKN-1-dependent transcriptional response in stress resistance and longevity deriving from translation inhibition." PLoS Genet **6**(8).

Wang, S., G. Fusaro, J. Padmanabhan and S. P. Chellappan (2002). "Prohibitin co-localizes with Rb in the nucleus and recruits N-CoR and HDAC1 for transcriptional repression." Oncogene **21**(55): 8388-8396.

Wang, S., N. Nath, M. Adlam and S. Chellappan (1999). "Prohibitin, a potential tumor suppressor, interacts with RB and regulates E2F function." Oncogene **18**(23): 3501-3510.

Wang, X. and X. J. Chen (2015). "A cytosolic network suppressing mitochondria-mediated proteostatic stress and cell death." Nature **524**(7566): 481-484.

Wang, X., X. Zuo, B. Kucejova and X. J. Chen (2008). "Reduced cytosolic protein synthesis suppresses mitochondrial degeneration." Nat Cell Biol **10**(9): 1090-1097.

Watson, E., L. T. MacNeil, H. E. Arda, L. J. Zhu and A. J. M. Walhout (2013). "Integration of metabolic and gene regulatory networks modulates the C. elegans dietary response." Cell **153**(1): 253-266.

Wei, Y., W. C. Chiang, R. Sumpter, Jr., P. Mishra and B. Levine (2017). "Prohibitin 2 Is an Inner Mitochondrial Membrane Mitophagy Receptor." Cell **168**(1-2): 224-238 e210.

Weiner, A., H. V. Chen, C. L. Liu, A. Rahat, A. Klien, L. Soares, M. Gudipati, J. Pfeffner, A. Regev, S. Buratowski, J. A. Pleiss, N. Friedman and O. J. Rando (2012). "Systematic dissection of roles for chromatin regulators in a yeast stress response." PLoS Biol **10**(7): e1001369.

Weng, M., Y. Yang, H. Feng, Z. Pan, W. H. Shen, Y. Zhu and A. Dong (2014). "Histone chaperone ASF1 is involved in gene transcription activation in response to heat stress in Arabidopsis thaliana." Plant Cell Environ **37**(9): 2128-2138.

Williamson, W. R., D. Wang, A. S. Haberman and P. R. Hiesinger (2010). "A

dual function of V0-ATPase a1 provides an endolysosomal degradation mechanism in Drosophila melanogaster photoreceptors." J Cell Biol **189**(5): 885-899.

Winter, A., O. Kamarainen and A. Hofmann (2007). "Molecular modeling of prohibitin domains." Proteins **68**(1): 353-362.

Wong, A., P. Boutis and S. Hekimi (1995). "Mutations in the clk-1 gene of Caenorhabditis elegans affect developmental and behavioral timing." Genetics **139**(3): 1247-1259.

Wrobel, L., U. Topf, P. Bragoszewski, S. Wiese, M. E. Sztolsztener, S. Oeljeklaus, A. Varabyova, M. Lirski, P. Chroscicki, S. Mroczek, E. Januszewicz, A. Dziembowski, M. Koblowska, B. Warscheid and A. Chacinska (2015). "Mistargeted mitochondrial proteins activate a proteostatic response in the cytosol." Nature **524**(7566): 485-488.

Wu, C. W., A. Deonarine, A. Przybysz, K. Strange and K. P. Choe (2016). "The Skp1 Homologs SKR-1/2 Are Required for the Caenorhabditis elegans SKN-1 Antioxidant/ Detoxification Response Independently of p38 MAPK." PLoS Genet **12**(10): e1006361.

Wu, J. J., J. Liu, E. B. Chen, J. J. Wang, L. Cao, N. Narayan, M. M. Fergusson, Rovira, II, M. Allen, D. A. Springer, C. U. Lago, S. Zhang, W. DuBois, T. Ward, R. deCabo, O. Gavrilova, B. Mock and T. Finkel (2013). "Increased mammalian lifespan and a segmental and tissue-specific slowing of aging after genetic reduction of mTOR expression." Cell Rep **4**(5): 913-920.

Xu, J., F. Chi, T. Guo, V. Punj, W. N. Lee, S. W. French and H. Tsukamoto (2015). "NOTCH reprograms mitochondrial metabolism for proinflammatory macrophage activation." J Clin Invest **125**(4): 1579-1590.

Yoneda, T., C. Benedetti, F. Urano, S. G. Clark, H. P. Harding and D. Ron (2004). "Compartment-specific perturbation of protein handling activates genes encoding mitochondrial chaperones." J Cell Sci **117**(Pt 18): 4055-4066.

Yoon, J. C., A. Ng, B. H. Kim, A. Bianco, R. J. Xavier and S. J. Elledge (2010). "Wnt signaling regulates mitochondrial physiology and insulin sensitivity." Genes Dev **24**(14): 1507-1518.

Zanton, S. J. and B. F. Pugh (2006). "Full and partial genome-wide assembly and disassembly of the yeast transcription machinery in response to heat shock." Genes Dev **20**(16): 2250-2265.

Zhang, Q., X. Wu, P. Chen, L. Liu, N. Xin, Y. Tian and A. Dillin (2018). "The Mitochondrial Unfolded Protein Response Is Mediated Cell-Non-autonomously by Retromer-Dependent Wnt Signaling." Cell.

Zhang, S. O., A. C. Box, N. Xu, J. Le Men, J. Yu, F. Guo, R. Trimble and H. Y. Mak (2010). "Genetic and dietary regulation of lipid droplet expansion in Caenorhabditis elegans." Proc Natl Acad Sci U S A **107**(10): 4640-4645.

Zhang, X. D. (2007). “A pair of new statistical parameters for quality control in RNA interference high-throughput screening assays.” Genomics **89**(4): 552-561.

Zhou, P., L. Qian, M. D’Aurelio, S. Cho, G. Wang, G. Manfredi, V. Pickel and C. Iadecola (2012). “Prohibitin reduces mitochondrial free radical production and protects brain cells from different injury modalities.” J Neurosci **32**(2): 583-592.

Zhou, Z., H. Ai, K. Li, X. Yao, W. Zhu, L. Liu, C. Yu, Z. Song, Y. Bao, Y. Huang, Y. Wu, L. Zheng, Y. Sun, G. Wang, K. Ma, L. Sun and Y. Li (2018). “Prohibitin 2 localizes in nucleolus to regulate ribosomal RNA transcription and facilitate cell proliferation in RD cells.” Sci Rep **8**(1): 1479.

Zhu, B., J. Zhai, H. Zhu and N. Kyprianou (2010). “Prohibitin regulates TGF-beta induced apoptosis as a downstream effector of Smad-dependent and -independent signaling.” Prostate **70**(1): 17-26.

Zhu, Z., C. Li, Y. Zeng, J. Ding, Z. Qu, J. Gu, L. Ge, F. Tang, X. Huang, C. Zhou, P. Wang, D. Zheng and Y. Jin (2017). “PHB Associates with the HIRA Complex to Control an Epigenetic-Metabolic Circuit in Human ESCs.” Cell Stem Cell **20**(2): 274-289 e277.

Zi Xu, Y. X., S. R. Ande and S. Mishra (2018). “Prohibitin: A new player in immunometabolism and in linking obesity and inflammation with cancer.” Cancer Lett **415**: 208-216.


UNIVERSIDAD
PABLO DE OLAVIDE
SEVILLA
Centro
Andaluz
de Biología
del Desarrollo
CBDA